Computational Methods for Failure Analysis and Life Prediction

NASA
IN-39

Proceedings of a workshop held at
Research Center
Hampton, Virginia
1992

NASA
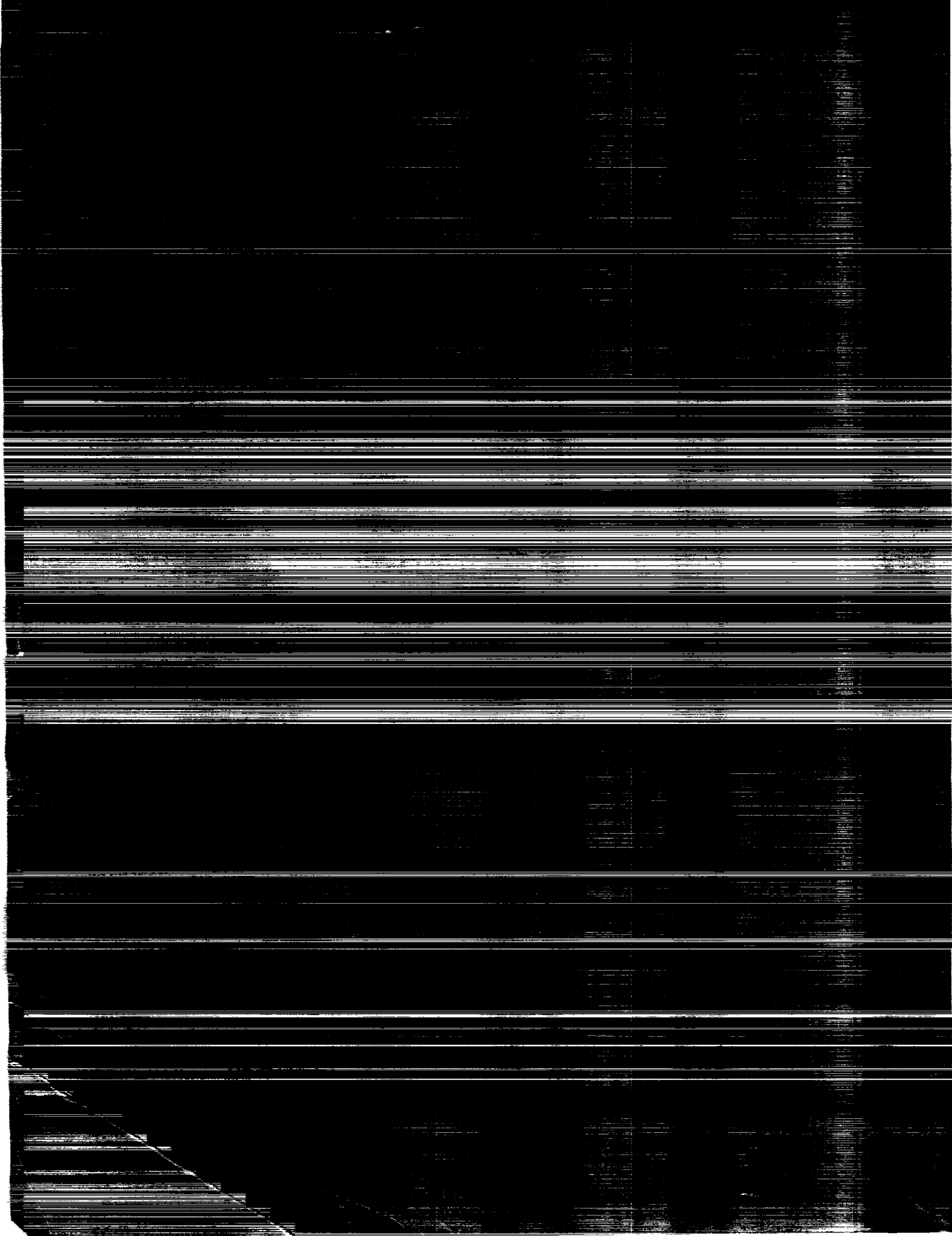
Computational Methods for Failure. Analysis and Life Prediction

Compiled by
Ahmed K. Noor
University of Virginia Center for
Computational Structures Technology
Hampton, Virginia

Charles E. Harris
and Jerrold M. Housner
Langley Research Center
Hampton, Virginia

Dale A. Hopkins
Lewis Research Center
Cleveland, Ohio

PREFACE

This document contains the proceedings of the Workshop on Computational Methods for Failure Analysis and Life Prediction held on October 14-15, 1992 at NASA Langley Research Center. The workshop was jointly sponsored by the University of Virginia Center for Computational Structures Technology and NASA. The attendees of the workshop came from government agencies, airframe and engine manufacturers and universities. The objectives of the workshop were to assess the state-of-technology in the numerical simulation of damage initiation and the prediction of safe operating life for flight vehicles, and to provide guidelines for future research leading to an enhanced capability for predicting failure and life of structures.

Certain materials and products are identified in this publication in order to specify adequately the materials and products that were investigated in the research effort. In no case does such identification imply recommendations or endorsement of products by NASA nor does it imply that the materials and products are the only ones or the best ones available for the purpose. In many cases equivalent materials and products are available and would probably produce equivalent results.

Ahmed K. Noor
University of Virginia Center for Computational Structures Technology
Hampton, Virginia

Charles E. Harris and Jerrold M. Housner
NASA Langley Research Center
Hampton, Virginia

Dale A. Hopkins
NASA Lewis Research Center
Cleveland, Ohio

INTRODUCTION

Performance requirements for future airframes and propulsion systems are rapidly increasing due to ambitious objectives of the U.S. civil and military aeronautics programs. Technology drivers for future aircraft include higher cruising speeds, altitudes, operating temperatures, and thrust-to-weight ratios; extended life; reduction in material, fabrication and maintenance costs; reduction in weight; and signature reduction.

To successfully achieve the performance requirements for planned and future aircraft, major advances are needed in a number of areas, including computational structures technology (CST). Specifically, there is a need for the accurate computational simulation of damage initiation and evolution, and quantitative prediction of safe operating cycles for airframes and propulsion systems.

The joint NASA/University of Virginia workshop held at NASA Langley Research Center, October 14-15, 1992 provided a forum for a wide spectrum of researchers and designers dealing with problems of damage, failure and life predictions of polymer-matrix composite structures. Both airframes and propulsion systems were considered and an attempt was made to

1) Assess the state-of-technology in the numerical simulation of damage initiation and evolution, and the prediction of safe operating life cycles for airframes and propulsion systems.

2) Identify technology needs and provide guidelines for focused research leading to verifiable failure and life prediction capabilities.

The list of technology needs given in this introduction was compiled from a number of participants and can be grouped into the following five major headings: 1) understanding the physical phenomena associated with damage and failure; 2) development of a framework for modeling material and structural damage; 3) efficient computational strategies; 4) test methods, measurement techniques and scaling laws; and 5) validation of numerical simulations. The five major technology needs are described subsequently.

1. Understanding Physical Phenomena Associated with Damage and Failure

Developing a fundamental understanding of the material-level damage mechanisms (including local damage at the interfaces of the composite), damage growth, and the subsequent structural failure modes is crucial to the development of computational methods to predict residual strength and fatigue life of structures. This fundamental understanding can only be established through a strong coupling between experimental characterization and the development of the associated mathematical and computational models that describe the physical phenomena. Computational models guide the testing, while the test results refine the computational-model assumptions. The major factors affecting damage initiation and propagation need to be identified. These include stress and strain levels, load history, thermal gradients, material toughness, laminate layup, residual stresses, component configuration and environmental interactions.

An essential component of the experimental program must be the performance of representative experiments that clearly establish the cause-and-effect relationships between the characteristics of the material in the service environment and their effect on structural performance. The service environment may include thermomechanical, multiaxial and cyclic loadings, moisture changes and jet propulsion fuel.

2. Framework for Characterization and Modeling of Material and Structural Damage

The mechanics framework for characterizing material damage and structural failure needs to be developed in an interdisciplinary setting, which relates the material-level damage to the structural failure modes. Two of the key tasks of research in this area are

a) Development of physically based, design-oriented damage and fatigue models

b) Accurate long-term extrapolation from shorter-time databases

The models developed must include damage characterization and description approaches (e.g., micromechanical, internal state variable description, phenomenological description). The parameters used in these models need to be characterized by a series of relatively inexpensive experiments. Also, it is desirable to develop simple models for specific structural applications in order to allow for trade-off design studies to be carried out early in the design process. For example, a structure designed on the basis of a safe-life philosophy must account for damage initiation and damage growth. By contrast, a structure designed to a damage tolerance philosophy does not require the prediction of crack initiation because damage is assumed to exist below the limits of detectability.

3. Efficient Computational Strategies

The effective use of numerical simulations for predicting damage initiation and propagation requires strategies for treating phenomena occurring at disparate spatial and time scales, using reasonable computer resources. The efficiency of the numerical simulations enables the many complex analyses and design studies to be performed in order to resolve the structural integrity issues. The key tasks of the research in this area include the following:

a) Simplified damage models (e.g., debonding and delamination models)

b) Integrated numerical simulation strategies (hierarchical multiscale/multimodel approaches which attempt to relate local damage effects to global response)

c) Probabilistic methods for the accurate quantification of the reliability and risk, convex modeling of uncertainty to deal with mostly encountered situations when insufficient data is available to justify use of probabilistic methods, and fuzzy subset-based analysis when the input information is vaguely presented

4. Test Methods, Measurement Techniques and Scaling Laws

The effective coupling of numerical simulations and experiments requires a high degree of interaction between the computational analysts and the experimentalists. This is done at three different levels, namely: 1) laboratory tests on small specimens to understand the material-level damage mechanisms and to obtain material data; 2) component tests to understand the progression from material-level damage to component failure; to verify the computational models; and to determine semi-empirical structural properties which can be used in hybrid experimental/numerical models for life predictions; and 3) full-scale (or scale model) tasks to validate the computational model and assess the need for model improvement.

New test methods and non-intrusive measurement techniques are needed to establish the cause-and-effect relationships between the characteristics of composite materials in the service environment and their effect on structural performance. The influence of specimen size or scale factor on structural response is not well understood. Thus, testing of geometrically similar sub-scale models can only be

useful after the scaling laws governing the damage phenomena are understood. The scaling laws must account for the material response, damage initiation and propagation, structural and topological details, and loading characteristics.

5. Validation of Numerical Simulations

In addition to validating the numerical simulations by component and full-scale tests, a number of carefully selected benchmark tests are needed for assessing new computational strategies and numerical algorithms. These standardized benchmark tests would provide a measure of confidence in new codes or add functional capabilities to existing codes. They could also serve as a basis of code comparisons for efficiency and accuracy in predicting damage initiation and propagation, as well as for safe operating life cycles of structures.

CONTENTS

ATTENDEES

Professor David H. Allen
Center for Mechanics of Composites
Texas Engineering Experiment Station
Texas A&M University
College Station, TX 77843
PH: (409) 845-1669
FAX: (409) 845-6051

Mr. Steven M. Arnold
NASA Lewis Research Center
Mail Stop 49-7
21000 Brookpark Road
Cleveland, OH 44135
PH: (216) 433-3334
FAX: (216) 433-8011

Dr. Vinod K. Arya
Mail Stop SVR-2
Sverdrup Technology, Inc.
2001 Aerospace Parkway
Brook Park, OH 44142
PH: (216) 433-2816
FAX:

Dr. John G. Bakuckas, Jr.
NASA Langley Research Center
Mail Stop 188E
Hampton, VA 23681-1000
PH: (804) 864-3486
FAX:

Dr. Charles L. Blackburn
NASA Langley Research Center
Mail Stop 396
Hampton, VA 23681-1000
PH: (804) 864-2987
FAX:

Dr. Charles P. Blankenship
NASA Langley Research Center
Mail Stop 118
Hampton, VA 23681-1000
PH: (804) 864-6005
FAX:

Ms. Vicki Britt
NASA Langley Research Center
Mail Stop 190
Hampton, VA 23681-1000
PH: (804) 864-8030
FAX:

Mr. Frederick Brust
Battelle Columbus Labs
505 King St.
Columbus, OH 43201-2693
PH: (614) 424-4458
FAX:

Dr. Charles J. Camarda
NASA Langley Research Center
Mail Stop 396
Hampton, VA 23681-1000
PH: (804) 864-5436
FAX:

Mr. Jeffrey A. Cerro
NASA Langley Research Center
Mail Stop 396
Hampton, VA 23681-1000
PH: (804) 864-5425
FAX:

Dr. Christos C. Chamis
NASA Lewis Research Center
Mail Stop 49-8
21000 Brookpark Road
Cleveland, OH 44135
PH: (216) 433-3252
FAX: (216) 433-5033

Professor Fu-Kuo Chang
Department of Aeronautics and Astronautics
Stanford University
Stanford, CA 94035
PH: (415) 723-3466
FAX: (415) 725-3377

Dr. Susan E. Cunningham
Pratt and Whitney
710 Beeline Hwy
P. O. Box 109600
West Palm Beach, FL 33410
PH: (407) 796-7945
FAX: (407) 796-3687

Mr. D. Dale Davis, Jr.
NASA Langley Research Center
MS 240
Hampton, VA 23681-1000
PH:
FAX:

Mr. Bernhard Dopker
Boeing Airplane Company
Advanced Composites Stress Group
Mail Stop 7L/46
P. O. Box 3707
Seattle, WA 98124
PH: (206) 234-1108
FAX: (206) 234-4543

Professor Isaac Elishakoff
Center for Applied Stochastics Research
Florida Atlantic University
P. O. Box 3091
Boca Raton, FL 33431-0991
PH: (407) 367-3449
FAX: (407) 367-2868

Mr. Rod Ellis
NASA Lewis Research Center
Mail Stop 49-7
21000 Brookpark Road
Cleveland, OH 44135
PH: (216) 433-3340
FAX: (216) 433-8011

Mr. Mark Feldman
NASA Langley Research Center
Mail Stop 188E
Hampton, VA 23681-1000
PH: (804) 864-3472
FAX: (804) 864-7729

Mr. Mark Finefield
McDonnell Douglas Aircraft Company
Mail Code 1021322
P. O. Box 516
St. Louis, MO 63166-0516
PH: (314) 234-1301
FAX: (314) 777-1171

Dr. Tom Gates
NASA Langley Research Center
Mail Stop 188E
Hampton, VA 23681-1000
PH: (804) 864-3400
FAX: (804) 864-7729

Dr. David E. Glass
NASA Langley Research Center
Mail Stop 396
Hampton, VA 23681-1000
PH: (804) 864-5423
FAX:

Mr. John P. Gyekenyesi
NASA Lewis Research Center
Mail Stop 6-1
21000 Brookpark Road
Cleveland, OH 44135
PH: (216) 433-8184
FAX: (216) 433-8300

Mr. Gary R. Halford
NASA Lewis Research Center
Mail Stop 49-7
21000 Brookpark Road
Cleveland, OH 44135
PH: (216) 433-3265
FAX: (216) 433-8011

Dr. Charles E. Harris
NASA Langley Research Center
Mail Stop 188E
Hampton, VA 23681-1000
PH: (804) 864-3449
FAX: (804) 864-7729

Mr. Marvin H. Hirschberg
NASA Lewis Research Center
Mail Stop 49-6
21000 Brookpark Road
Cleveland, OH 44135
PH: (216) 433-3206
FAX: (216) 433-8011

Mr. Dale A. Hopkins
NASA Lewis Research Center
Mail Stop 49-8
21000 Brookpark Road
Cleveland, OH 44135
PH: (216) 433-3260
FAX: (216) 433-8011

Dr. Jerrold Housner
NASA Langley Research Center
MS 240
Hampton, VA 23665
PH: (804) 864-2906
FAX: (804) 864-8318

Dr. W. Steven Johnson
NASA Langley Research Center
MS 188E
Hampton, VA 23681-0001
PH: (804) 864-3463
FAX: (804) 864-7729

Dr. Wolfgang G. Knauss
Graduate Aeronautical Laboratories
Mail Code 105-50
Cal Tech
Pasadena, CA 91125
PH: (818) 356-4524
FAX: (818) 449-2677

Dr. James Lee
George Washington University
Dept. of Civil, Engineering & Environmental
Engineering
Washington, D. C. 20052
PH: (202) 994-5971
FAX: (202) 994-0238

Dr. Michael A. McGaw
NASA Lewis Research Center
Mail Stop 49-7
21000 Brookpark Road
Cleveland, OH 44135
PH: (216) 433-3308
FAX: (216) 433-8011

Mr. Dan Murphy
Boeing Airplane Company
Advanced Composites Stress Group
Mail Stop 7L/46
P. O. Box 3707
Seattle, WA 98124
PH: (206) 234-1108
FAX: (206) 234-4543

Mr. Noel N. Nemeth
NASA Lewis Research Center
Mail Stop 6-1
21000 Brookpark Road
Cleveland, OH 44135
PH: (216) 433-3215
FAX: (216) 433-8300

Professor Ahmed K. Noor
NASA Langley Research Center
Mail Stop 210
Hampton, VA 23681-1000
PH: (804) 864-1978
FAX: (804) 864-8089

Dr. Kevin O'Brien
NASA Langley Research Center
Mail Stop 188E
Hampton, VA 23681-1000
PH: (804) 864-3465
FAX: (804) 864-7729

Dr. Michael J. Pereira
NASA Lewis Research Center
Mail Stop 49-8
21000 Brookpark Road
Cleveland, OH 44135
PH: (216) 433-6738
FAX:

Mr. Clarence C. Poe, Jr.
NASA Langley Research Center
Mail Stop 188E
Hampton, VA 23681-1000
PH: (804) 864-3467
FAX: (804) 864-7729

Mr. Ivatury S. Raju
NASA Langley Research Center
MS 240
Hampton, VA 23681-1000
PH: (804) 864-2928
FAX: (804) 864-8318

Dr. B. Walter Rosen
Materials Sciences Corporation
930 Harvest Drive
Suite 300
Union Meeting Corporate Center
Blue Bell, PA 19422
PH: (215) 542-8400
FAX: (215) 542-8401

Dr. James Wayne Sawyer
NASA Langley Research Center
Mail Stop 396
Hampton, VA 23681-1000
PH: (804) 864-5432
FAX:

Dr. George P. Sendeckyj
WL/FIBEC
Wright Patterson Air Force Base, OH 45433

PH: (513) 255-6104
FAX: (513) 476-4999

Mr. Phil Shore
NASA Langley Research Center
Mail Stop 396
Hampton, VA 23681-1000
PH: (804) 864-5429
FAX:

Dr. Mark J. Shuart
NASA Langley Research Center
Mail Stop 244
Hampton, VA 23681-1000
PH: (804) 864-3170
FAX: (804) 864-7791

Mr. David W. Sleight
NASA Langley Research Center
MS 240
Hampton, VA 23681-1000
PH: (804) 864-8427
FAX: (804) 864-8318

Dr. W. Jefferson Stroud
NASA Langley Research Center
MS 240
Hampton, VA 23681-1000
PH: (804) 864-2928
FAX: (804) 864-8318

Dr. Alex Tessler
NASA Langley Research Center
MS 240
Hampton, VA 23681-1000
PH: (804) 864-3178
FAX: (804) 864-8318

Dr. Ben H. Thacker
Southwest Research Institute
P. O. Drawer 28510
San Antonio, TX 78228
PH: (512) 684-5111
FAX: (512) 522-5122

Dr. Mark Tuttle
University of Washington
Department of Mechanical Engineering
FU10
Seattle, WA 98195
PH: (206) 543-0299
FAX:

Dr. Tom Walker
Boeing Airplane Company
Advanced Composites Stress Group
Mail Stop 6H/CF
P. O. Box 3707
Seattle, WA 98124
PH: (206) 234-1108
FAX: (206) 234-4543

Dr. John T. Wang
NASA Langley Research Center
MS 240
Hampton, VA 23681-1000
PH: (804) 864-8185
FAX: (804) 864-8318

Mr. Erwin V. Zaretsky
NASA Lewis Research Center
Mail Stop 49-6
21000 Brookpark Road
Cleveland, OH 44135
PH: (216) 433-3241
FAX:

Highlights of the Workshop

Ahmed K. Noor
Center for Computational Structures Technology
University of Virginia

Objectives and Format

The study of damage and failure of materials and structures has attracted considerable attention in recent years and is manifested by, among other things, the number of monographs and conference proceedings devoted to the subject (see, for example, Refs. 1-11). Despite these efforts, major advances are needed in a number of different areas before accurate numerical simulations of damage initiation, evolution and quantitative predictions of safe operating cycles for aerospace systems can be achieved. The objectives of the present workshop (Fig. 1) are to assess the state-of-technology in the computational simulation of damage initiation and evolution, to predict safe operating cycles for airframes and propulsion systems, and to identify current and future needs to achieve verifiable failure and life prediction capabilities for polymer-matrix composite structures.

The workshop includes presentations and two panels. The presentations are included in the proceedings to illuminate some of the diverse issues and to provide fresh ideas for future research and development.

Objectives

- ## To assess the state-of-technology in the numerical simulation of damage initiation and evolution, and the prediction of safe operating life cycles for airframes and propulsion systems

- ## To identify future directions of research

Format

- ## Presentations
- ## Panels

  - ### Panel 1 - *Computational Needs for Failure Prediction* Moderators: Jerry Housner/Kevin O'Brien
  - ### Panel 2 - *Computational Needs for Life Prediction* Moderator: Charlie Harris

- ## Proceedings

Figure 1

Assessment of the State-of-Technology

The first aspect of assessing the state-of-technology is to assess our understanding of the physical phenomena associated with damage and failure. Some of the issues that affect these physical phenomena are listed in Fig. 2. These are damage mechanisms and failure modes for both isothermal and thermomechanical loading conditions; range of applicability and limitations of phenomenological continuum damage theories, which employ internal (damage) state variable concept; major factors affecting damage initiation and propagation; the length scale and level of detail required to capture important phenomena; and the influence of specimen size or scale factor on structural response and damage.

Understanding of Physical Phenomena Associated with Crash

- Damage mechanisms and failure modes (isothermal and thermomechanical)

- Continuous state variables to describe macroscopic effects of damage - continuum damage mechanics

- Major factors affecting damage initiation and propagation (nonlinear, history-dependent and time-dependent response, local damage at the interfaces, damage degradation, environmental interactions, stress and strain levels, nonhomogeneities - e.g., effect of environment on crack formation and growth)

- Length scale and level of detail required to capture important phenomena

- Scale effects and scaling laws

Figure 2

4

Assessment of the State-of-Technology (Cont'd.)
Current Capabilities

The second aspect of assessment of technology is that of current capabilities for numerical simulation of damage and life prediction (Fig. 3). These capabilities include damage models and fatigue life prediction models. Continuum damage mechanics and fracture mechanics models are among the currently-used damage models. A number of complex phenomena are not fully represented by these models. An example of these phenomena is the interaction between creep, fatigue and oxidation for high-temperature applications. A large number of fatigue life prediction models have been proposed over the years, some of these models are reviewed in a survey paper (Ref. 4) and are discussed in the succeeding presentations.

- **Damage Models**

  - Continuum damage mechanics models, fracture mechanics models, ...

  - Damage initiation criteria and propagation modeling

  - Interaction between creep, fatigue and oxidation (or oxidation protective coating)

- **Fatigue Life Prediction Models**

  - Material models, structural models

  - Performance simulation (predicting remaining strength and life), strainrange partitioning approach, ...

Figure 3

Assessment of the State-of-Technology (Cont'd.)

Assessment of current capabilities (Fig. 4) also includes currently used computational strategies and software systems, specifically, the effectiveness of using hierarchical and adaptive strategies for simulating damage evolution, the accurate simulation of the effect of local damage or global response, and the facilities available in current software systems for handling failure analysis and life prediction.

Current Capabilities

- **Computational Strategies**

  - **Hierarchical, global-local, multiscale, multilevel and adaptive strategies**

  - **Interaction between local damage (including inteface damage) and global response**

- **Capabilities of Current Software Systems for Handling Failure Analysis and Life Prediction**

  - **MSC NASTRAN, ANSYS, ABAQUS, Langley and Lewis programs**

Figure 4

Future Directions of Research

Three factors should be taken into account in identifying future directions for research (Fig. 5):

1) Characteristics of future aircraft and their operating environment (e.g., higher speeds, operating temperatures and thrust-to-weight ratios), and the need for accurate quantitative predictions of damage initiation, evolution and safe operating life cycles

2) Future computing environment and computing paradigm

3) Recent and future developments in other fields of computational technology, which can be adapted to numerical simulation of damage and failure.

- ## Characteristics of future airframes and propulsion systems and their implications on design requirements

    - ### Higher (speeds, operating temperatures, thrust-to-weight ratios)

    - ### Need for accurate quantitative predictions of damage initiation, evolution and safe operating life cycles.

- ## Impact of emerging and future computing environment (high-performance computers, advanced visualization technology)

- ## Impact of developments in other fields of computational technology (e.g., CFD, computational mathematics)

Figure 5

Research Areas

Three of the important research tasks are listed in Fig. 6:

1) Computational models for damage and fatigue

2) Computational strategies. These include integrated numerical simulation strategies which relate local effects to global response, progressive failure methodologies, and probabilistic methods for the accurate quantification of reliability and risk.

3) Validation and certification tools, which include effective coupling between numerical simulations and experiments, and selection of benchmark tests for assessing new models, computational strategies and numerical algorithms. The standardized tests would provide a measure of confidence in added functional capabilities to existing codes, or in new codes.

Computational Models
- *Hierarchy of thermomechanical damage and fatigue models*
  - Damage initiation criteria and propagation modeling
  - Creep - fatigue - oxidation interactions
  - Effect of temperature gradients
  - Accurate long-term extrapolation from shorter-time data bases
  - Design-oriented simplified fatigue models

Computational Strategies
- *Integrated numerical simulation strategies*
  - Multiscale/multimodel approaches (relating local effects to global response)
  - Progressive failure methodologies
- *Probabilistic methods* (accurate quantification of reliability and risk)

Validation and Certification Tools
- Effective coupling of numerical simulations and experiments
- Benchmarks

Figure 6

REFERENCES

1. Allen, D. H. and Lagoudas, D. C. (eds.), Damage Mechanics in Composites, AMD Vol. 150, AD Vol. 32, American Society of Mechanical Engineers, NY, 1992.

2. Dvorak, G. J. and Lagoudas, D. C. (eds.), Microcracking - Induced Damage in Composites, AMD Vol. 111, MD Vol. 22, American Society of Mechanical Engineers, NY, 1990.

3. Folias, E. S. (ed.), *Structural Integrity - Theory and Experiment*, Kluwer Academic Publishers, Boston, 1989.

4. Halford, G. R., "Evolution of Creep-Fatigue Life Prediction Models," in Creep-Fatigue Interaction at High Temperature, Haritos, G. K. and Ochoa, O. O. (eds.), AD Vol. 21, American Society of Mechanical Engineers, NY, 1991, pp. 43-58.

5. Haritos, G. K. and Ochoa, O. O. (eds.), Creep-Fatigue Interaction at High Temperature, AD Vol. 21, American Society of Mechanical Engineers, NY, 1991.

6. Haritos, G. K. and Ochoa, O. O. (eds.), Damage and Oxidation Protection in High Temperature Composites, AD Vol. 25-1, American Society of Mechanical Engineers, NY, 1991.

7. Haritos, G. K., Newaz, G. and Mall, S. (eds.), Failure Mechanism in High Temperature Composite Materials, AMD Vol. 122, AD Vol. 22, AMD Vol. 122, American Society of Mechanical Engineers, NY, 1991.

8. Ju, J. W., Krajcinovic, D. and Schreyer, H. L. (eds.), Damage Mechanics in Engineering Materials, AMD Vol. 109, MD Vol. 24, American Society of Mechanical Engineers, NY, 1990.

9. Lindberg, H. E. (ed.), Failure Criteria and Analysis in Dynamic Response, AMD Vol. 107, American Society of Mechanical Engineers, NY, 1990.

10. Nagar, A. (ed.), Fracture and Damage, AD Vol. 27, American Society of Mechanical Engineers, NY, 1992.

11. Viswanathan, R. (tech. advisor), *Damage Mechanisms and Life Assessment of High-Temperature Components*, ASM International, Metals, Park, OH, 1990.

Nonlinear and Progressive Failure Aspects of Transport Composite Fuselage Damage Tolerance

T. Walker, L. Ilcewicz
Boeing Commercial Airplane Group
Seattle, WA

D. Murphy, B. Dopker
Boeing Computer Services
Seattle, WA

PAGE _____ INTENTIONALLY BLANK

INTRODUCTION

The purpose of this paper is to provide an end-user's perspective on the state of the art in life prediction and failure analysis by focusing on subsonic transport fuselage issues being addressed in the NASA/Boeing Advanced Technology Composite Aircraft Structure (ATCAS) contract and a related task-order contract. First, some discrepancies between the ATCAS tension-fracture test database and classical prediction methods will be discussed, followed by an overview of material modeling work aimed at explaining some of these discrepancies. Finally, analysis efforts associated with a pressure-box test fixture will be addressed, as an illustration of modeling complexities required to model and interpret tests.
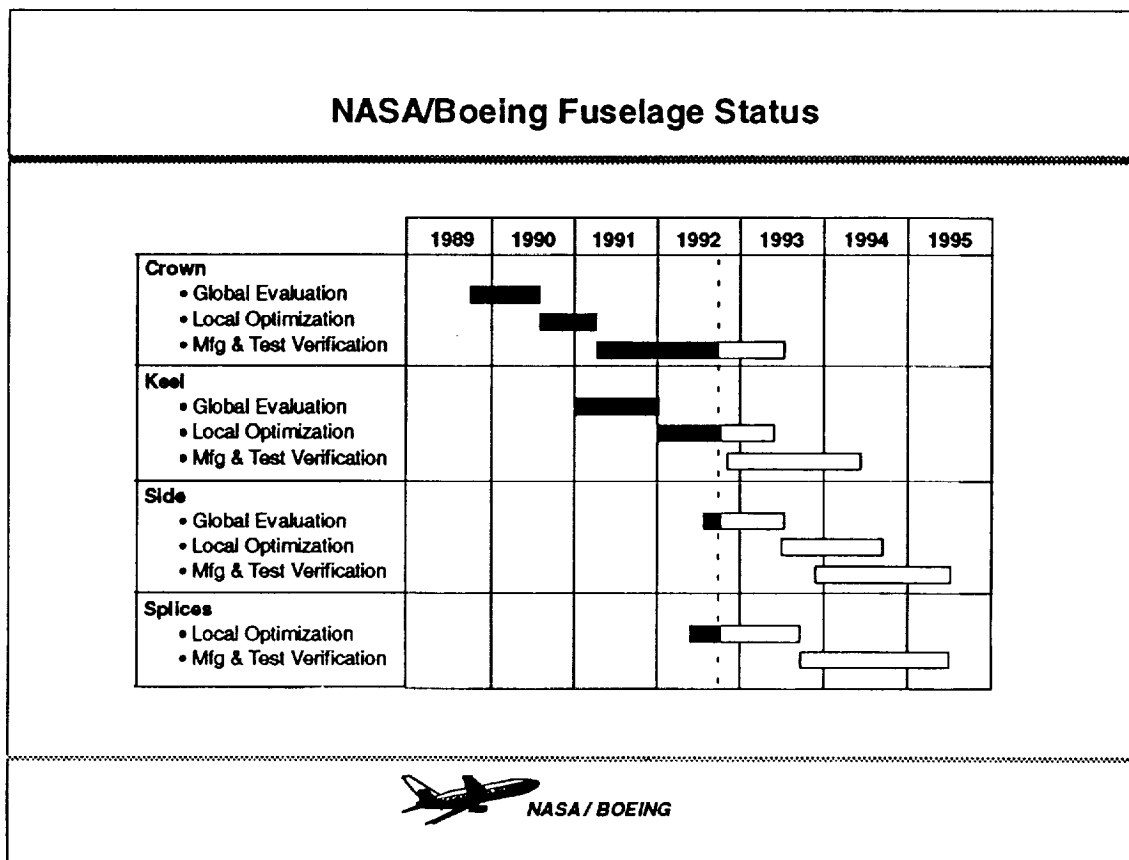
Fuselage loading is complex, with combined loads in all regions. ATCAS has divided the cylinder into four quadrants based on primary loading considerations. The internal pressure is reacted primarily as hoop tension, and is effective in all quadrants. Critical axial loads are primarily tension in the crown and compression in the keel, with shear being dominant in the side. The upper and lower portions of the side panel have significant regions of combined tension-shear and compression-shear, respectively. The lower side has the additional issue of major load redistribution around cargo door and wheel-well cutouts.

Load levels are necessarily coupled with damage states. Ultimate load levels must be sustained with undetectable damage, the upper limit of which is often "barely-visible damage." Limit loads must be sustained with large damage levels, often represented in tests with element and/or skin saw-cuts. The prediction of strength with damage caused by realistic threats is complicated by the limitations of current non-destructive inspection methods to accurately quantify existing damage states.

Critical Fuselage Loading Conditions

NASA / BOEING
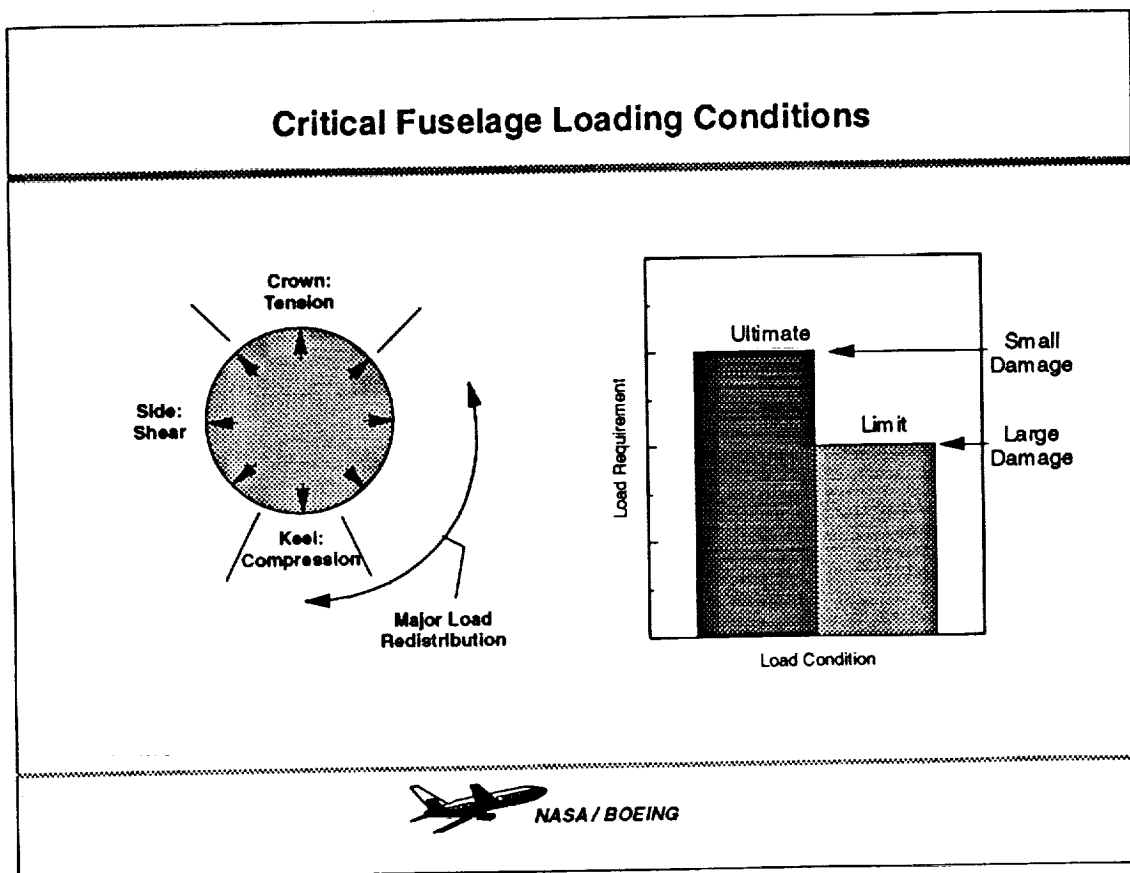
The ATCAS schedule indicates the current status. Crown activities are nearing completion, with only component tests remaining. The keel and splice activities are in the technology development stage, and the side efforts are addressing design trade studies. Further discussions will focus on the crown region since it is the farthest along. The problems raised are representative of what has been found, and have some general applicability. Additional issues are likely to be uncovered as the keel, side, and splice regions are addressed in more detail.

NASA/Boeing Fuselage Status

	1989	1990	1991	1992	1993	1994	1995
Crown							
• Global Evaluation							
• Local Optimization							
• Mfg & Test Verification							
Keel							
• Global Evaluation							
• Local Optimization							
• Mfg & Test Verification							
Side							
• Global Evaluation							
• Local Optimization							
• Mfg & Test Verification							
Splices							
• Local Optimization							
• Mfg & Test Verification							

NASA / BOEING

15

CROWN PANEL TESTS VERSUS EXISTING THEORIES

The topic of the following discussions will be limited to tension damage tolerance, which is a critical design driver in the crown region. Several competing failure modes contribute to this issue, including skin fracture, stiffener strength, and skin/stiffener attachment. Each is affected by several variables. In addition, behavioral characteristics of composite materials that must be contained in predictions include damage growth simulation, trade-offs between strength and toughness for laminate/material variations, and load redistribution. The competing failure modes interact through load redistribution. For example, as stable damage growth occurs in the skin, additional load is projected towards the stiffener, requiring additional load-transfer capability in the skin/stiffener attachment and additional load-carrying capability in the stiffener. Similarly, limited amounts of debonding or fastener yielding along a skin/stiffener interface as major damage approaches provide a structural benefit, shielding the stiffening element from the sharp stress concentration in the skin. More severe debonding or fastener yielding, however, is detrimental, removing the stiffening element from the structural load paths. Understanding and having predictive capabilities for these complex interactions are essential to developing balanced structural designs.

Crown Panel Damage Tolerance Example

Competing failure modes

- Skin fracture
  - Layup
  - Material
  - Manufacturing process
  - Load rate
  - Environment
- Stiffener strength
  - Layup
  - Material
  - Load rate
  - Environment
  - Damage state
- Skin/stiffener attachment
  - Nonlinear shear stiffness
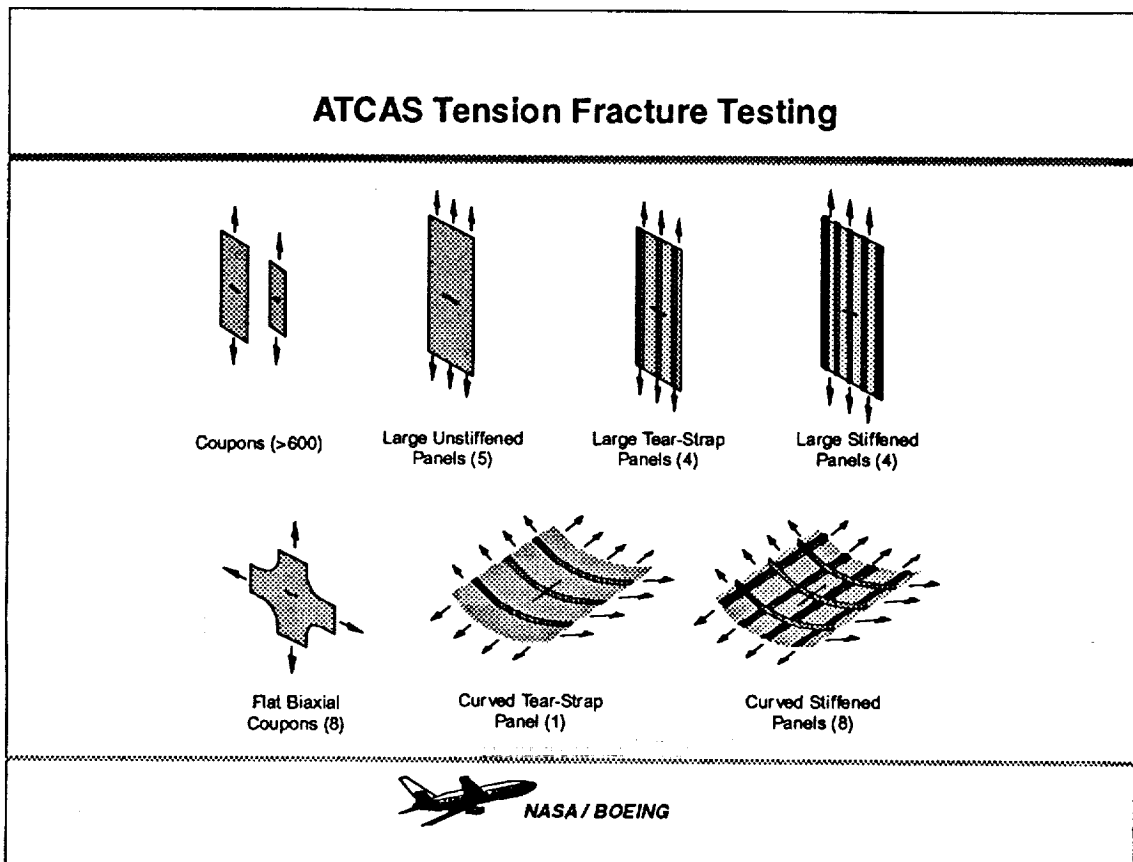 - Load sharing
  - Fastener flexibility
  - Bondline strength

Unique characteristics of composite materials

- Damage growth simulation
- Strength versus toughness
- Load redistribution

NASA / BOEING

ATCAS has obtained a large tension-fracture database, ranging from small coupons to 5' x 6' fully configured panels. The wide range of variables included in the testing have proven to be extremely valuable in understanding analytical limitations. The database is being thoroughly documented, and is available for verification of predictive techniques. The following discussions focus on the relationships between simpler specimen geometries and analyses. Any difficulties encountered at this simple level will be magnified as more complex structure is addressed.

ATCAS Tension Fracture Testing

Coupons (>600)

Large Unstiffened
Panels (5)

Large Tear-Strap
Panels (4)

Large Stiffened
Panels (4)

Flat Biaxial
Coupons (8)

Curved Tear-Strap
Panel (1)

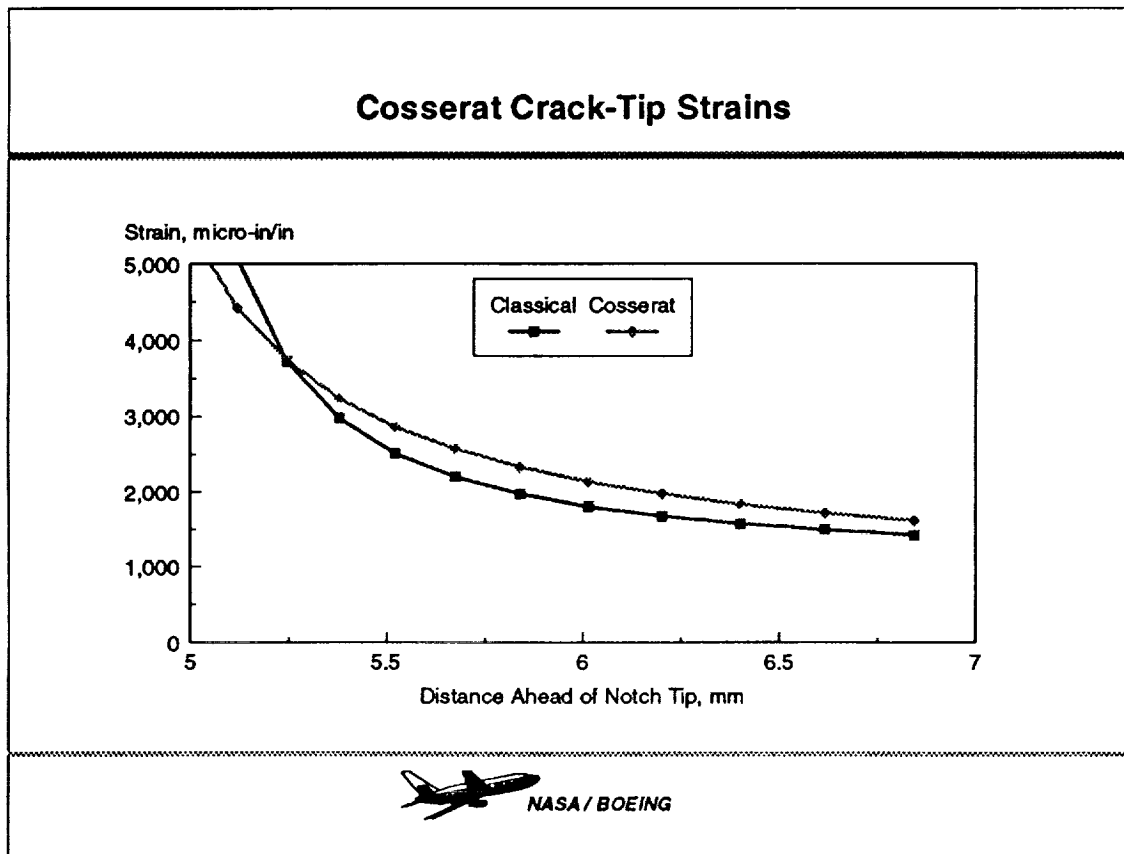Curved Stiffened
Panels (8)

NASA / BOEING

Classical methods have been found to underpredict the effects of specimen geometry. The figure contains two sets of data, each with a different specimen-width-to-notch-length ratio (w/2a). Both data sets have been corrected for finite width using classical finite width correction factors (FWCF), and should fall on a single curve if the FWCFs accurately predict the geometry effects. The two distinct curves indicate the inaccuracies of classical FWCFs. Similar results were observed for other laminates, materials, and less severe specimen geometries (i.e., between w/2a = 4 and w/2a = 8). The inaccuracies are caused by larger-than-expected projections of stresses towards the specimen edge. This projection is likely caused by a combination of (a) prefailure damage progression, (b) transverse buckling of the notch, (c) repeatable material inhomogeneities, and (d) point-rotation degrees-of-freedom in the material.
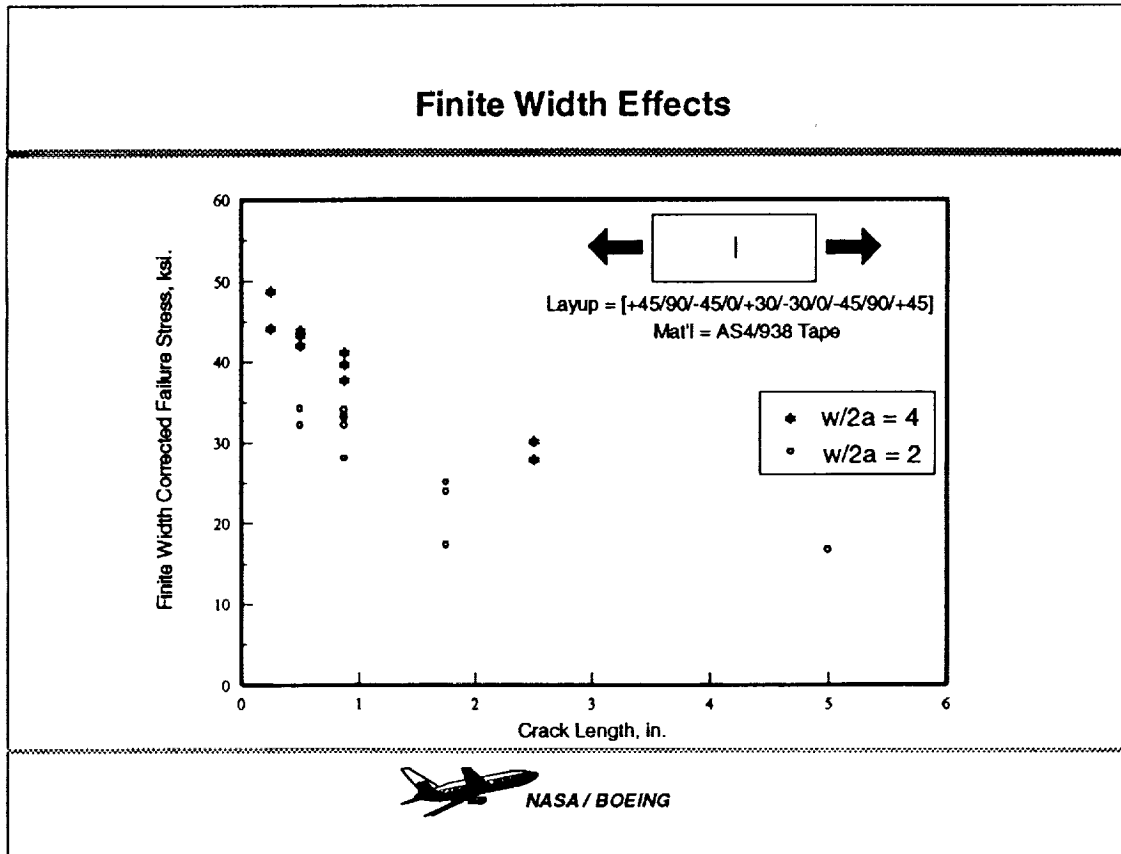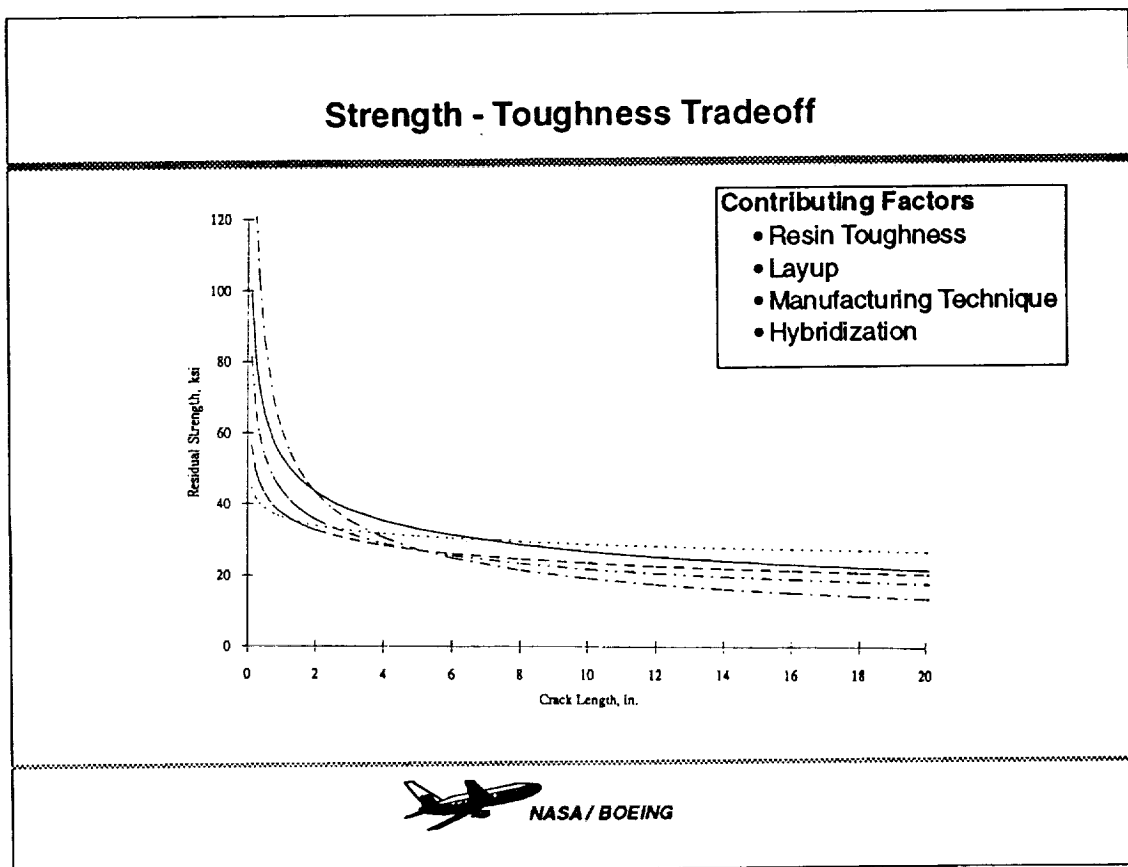
In large notched specimens, a projection of strains towards the specimen edge was observed prior to any damage growth from the notch tip. For this particular laminate/material combination, classical square-root-singularity methods underpredict the actual strains by approximately 25%. Similar trends, with similar or smaller differences between predicted and measure strains, were observed for a variety of other laminate/material combinations.

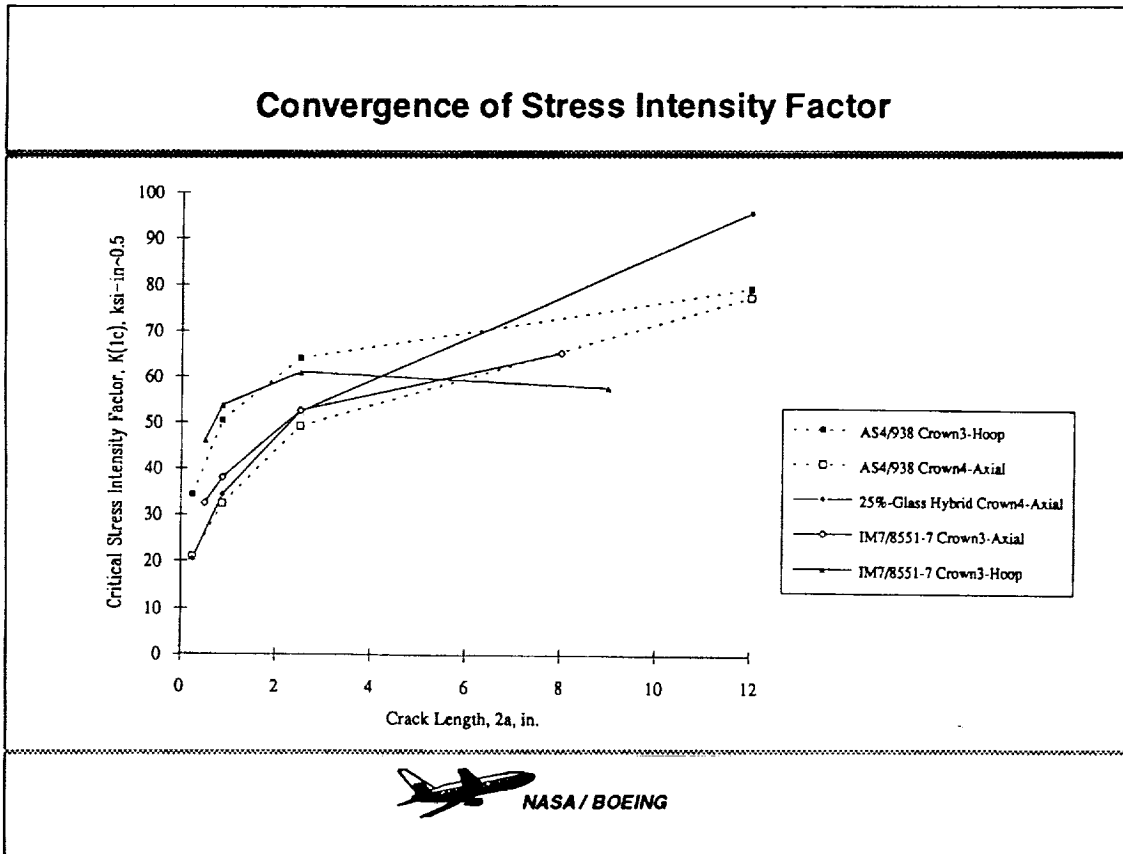## Pre-damage Notch-Tip Strains

NASA / BOEING
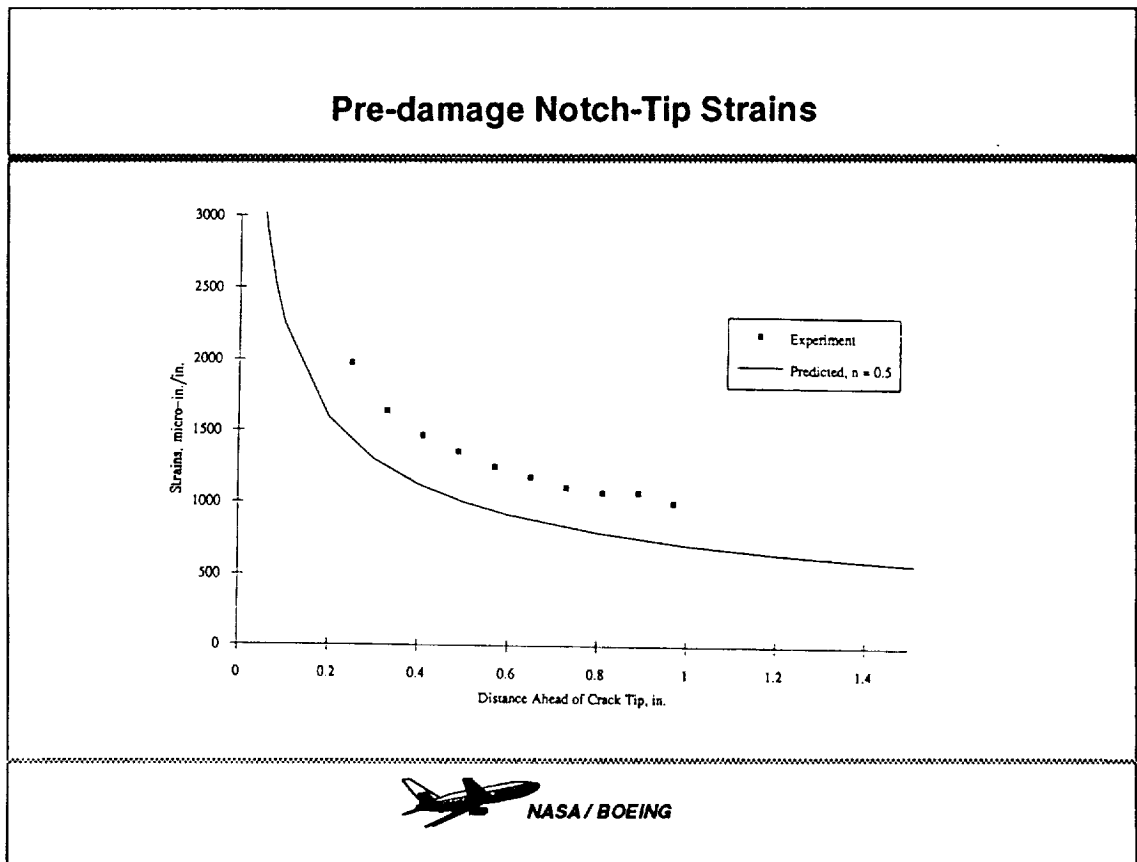
Dr. Roderick Lakes, on sabbatical to Boeing from the University of Iowa, illustrated similar strain projection using Cosserat material models. These models allow for point-rotation degrees of freedom in the continuum. It should be emphasized that it is important to accurately predict strains prior to damage growth, since load distribution is critical in predicting both structural response and local failures. Models that do not predict initial distributions will not accurately follow the redistribution as damage progresses, and will therefore be unable to predict each of the competing failure mechanisms. Note that the distributions, and therefore effects of specimen geometry, for Cosserat theory differ as a function of the material length parameters.

Cosserat Crack-Tip Strains

Strain, micro-in/in

Classical	Cosserat

Distance Ahead of Notch Tip, mm

NASA / BOEING

Significantly different residual strength curves were observed in the ATCAS tension fracture testing. Variables in this behavior include resin toughness, layup, manufacturing technique, and hybridization. The differences imply that a trade-off between strength (small-notch strengths) and toughness (large-notch strength) exists, as is the case with aluminum alloys (e.g., 7075 vs. 2024). Tough resins, hard layups, and small scales of repeatable material inhomogeneities result in higher strengths but lower toughnesses. Conversely, brittle resins, soft layups and large scales of repeatable material inhomogeneities result in lower strengths and higher toughnesses. The higher-strength, lower-toughness laminate/material combinations tend to follow classical predictions more closely. The lower-strength, higher-toughness materials respond as would be predicted for a reduced-singularity stress field.

Strength - Toughness Tradeoff

Contributing Factors
- Resin Toughness
- Layup
- Manufacturing Technique
- Hybridization

NASA / BOEING

In fact, the higher-strength, lower-toughness combinations converge to their classical mode 1 stress intensity factor (K_{1c}) at smaller notch sizes than do the lower-strength, higher-toughness combinations. It should be noted that the toughest laminate/material combinations, which are most attractive for skin applications, do not converge until well into the crack-size range of interest. Classical fracture mechanics properly predicts failure of a particular laminate/material combination for all notch sizes within the converged-K_{1c} range. For notch sizes below the converged-K_{1c} range, prediction of specimen failure becomes analogous to an elastic collapse problem.

Convergence of Stress Intensity Factor

Legend:
- AS4/938 Crown3-Hoop
- AS4/938 Crown4-Axial
- 25%-Glass Hybrid Crown4-Axial
- IM7/8551-7 Crown3-Axial
- IM7/8551-7 Crown3-Hoop

Y-axis: Critical Stress Intensity Factor, K(1c), ksi-in^0.5
X-axis: Crack Length, 2a, in.

NASA / BOEING

22

STRAIN SOFTENING MODEL DEVELOPMENT

After careful review of many previous efforts to analytically simulate and predict the fracture characteristics of laminated composite materials, a sophisticated nonlinear finite element implementation of the cohesive stress crack theory has been undertaken. Relative to metallic structure, the nonlinear softening behavior that occurs in the vicinity of a crack in multidirectional composite laminates involves a much larger area. Experimental observation suggests that the damage zone at a crack tip in composite laminates is large enough to be represented by several finite elements in a model that can be economically and quickly processed.

Extensive experimental study strongly suggests that a comparatively large damage zone develops around cracks in laminates and that a number of physical phenomena contribute to a strain softening effect

- Fiber breaks
- Matrix cracking
- "Scissoring" of angle plies
- Crack bridging, fiber bundle pull-out

By introducing a local, non-monotonic load capability (elastic, yield, unload) to a finite element model, a damage zone of finite size is represented and stable crack growth can be simulated

The resulting problem is extremely nonlinear, both locally and globally, and has been solved using the ABAQUS analysis system

NASA / BOEING

23

A flat, center crack tension coupon is modeled using two planes of symmetry. Initial studies assumed self-similar crack growth, allowing the loading, yielding, and unloading along the crack line in the model to be precisely prescribed with individual spring elements. The load-displacement relationships for these springs are derived from the measured stiffness and failure strengths of the laminate/material combinations being studied.

Problem Formulation

sym.

Applied Stress

10.0"

3.75"

5.0"
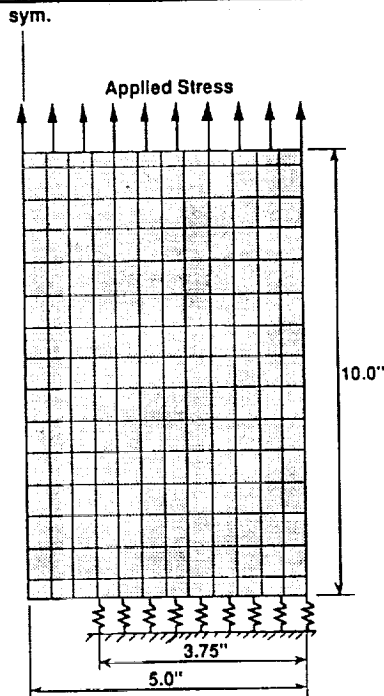
A detailed analytical study using design-of-experiments principles was conducted to evaluate the sensitivity of the specimen response to each of the parameters which define the strain softening law. The most dominant parameter affecting residual strength for a given notch size was found to be the maximum stress for elastic laminate behavior, σ_{max}. Other factors tended to control the shape of the residual strength curve (i.e., change in residual strength as a function of notch length).

Strain Softening Law
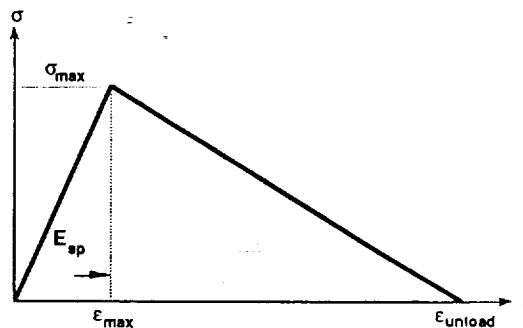
$$F = \sigma \cdot A$$

A = element thickness · distance between springs

σ = stress within spring

E_{sp} = spring modulus

ε_{max} = failure strain

ε_{unload} = strain at total unload

These models were exercised to determine if the proper degrees-of-freedom exist to predict the strength-toughness trade-off observed in the ATCAS test data. As shown in the figure, a softening law with a relatively short but steep unloading segment predicts a steeper residual strength curve than a law with a longer, less-steep unloading segment. Since classical materials instantaneously unload at a single strain, the steeper unloading curve is more representative of classical response, and does, in fact, result in a residual strength curve closer to that predicted by classical fracture mechanics. In addition, steep unloading curves also tend to drive a classical response in the finite element models whereby a more dense mesh is needed to facilitate failure prediction. These findings illustrate that the proper degrees-of-freedom required to predict the observed response are present, and there appears to be a physical basis for the observed predictions.

Influence of Strain Softening Laws

Boeing Computer Services
**Technology**

Crack Length, 2a, in.
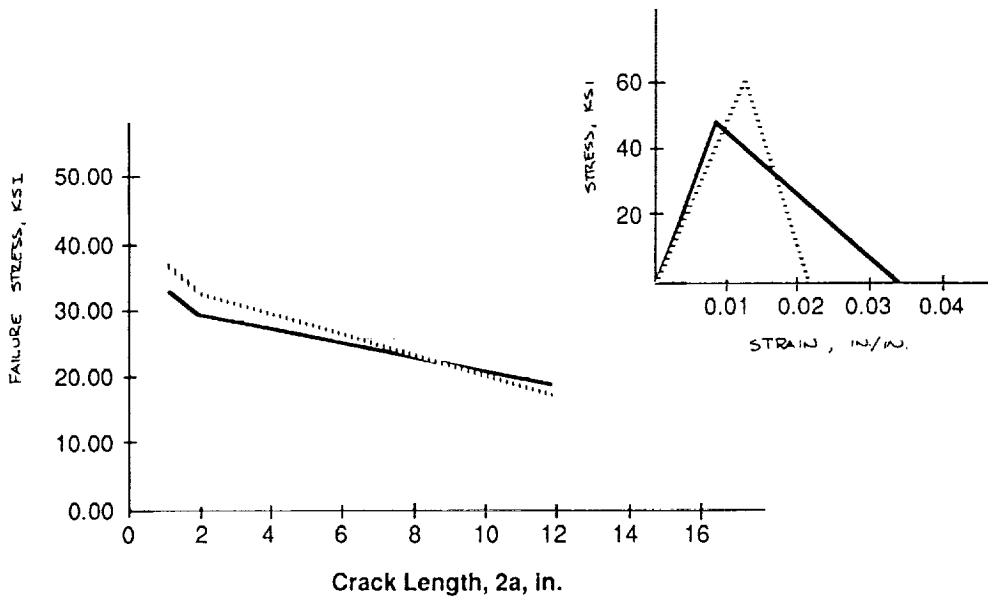
The specific laminate/material combinations tested in ATCAS were analyzed using this strain-softening approach to evaluate the accuracy of predicting their residual strength curves. As this figure illustrates, linear elastic fracture mechanics (LEFM), calibrated to 2.5" crack test results, grossly overpredicts fracture strength for smaller cracks, and underpredicts test data by 40% at larger crack lengths. Applying the damage zone model (also calibrated at the 2.5" crack test results) results in significantly improved predictions of actual response.

With large-damage conditions controlling much of the crown design, any conservatism in the anticipated strengths at these notch sizes translates directly into additional design cost and weight. Minimizing the conservatism can be accomplished either by testing the large notch sizes (a costly proposition) or predicting the large-notch strengths by analytically extending the small-notch strengths. The strain-softening models clearly provide superior extrapolation capability, and also predict the load redistribution resulting from damage growth that is required for accurate structural analysis.

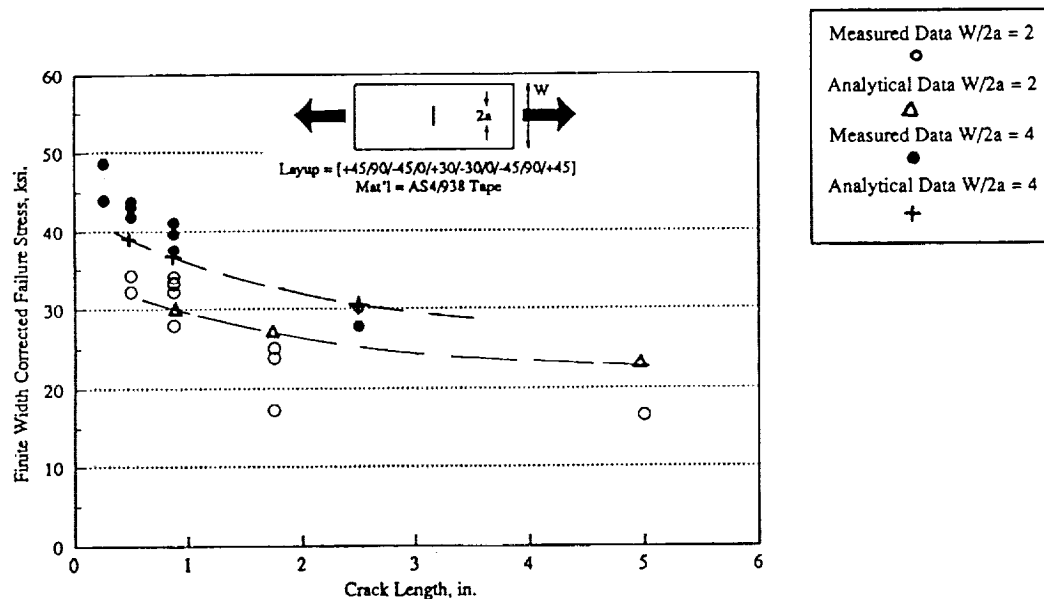## Comparison of AS4/938, Crown4 Laminate – Axial Data

Boeing Computer Services
Technology
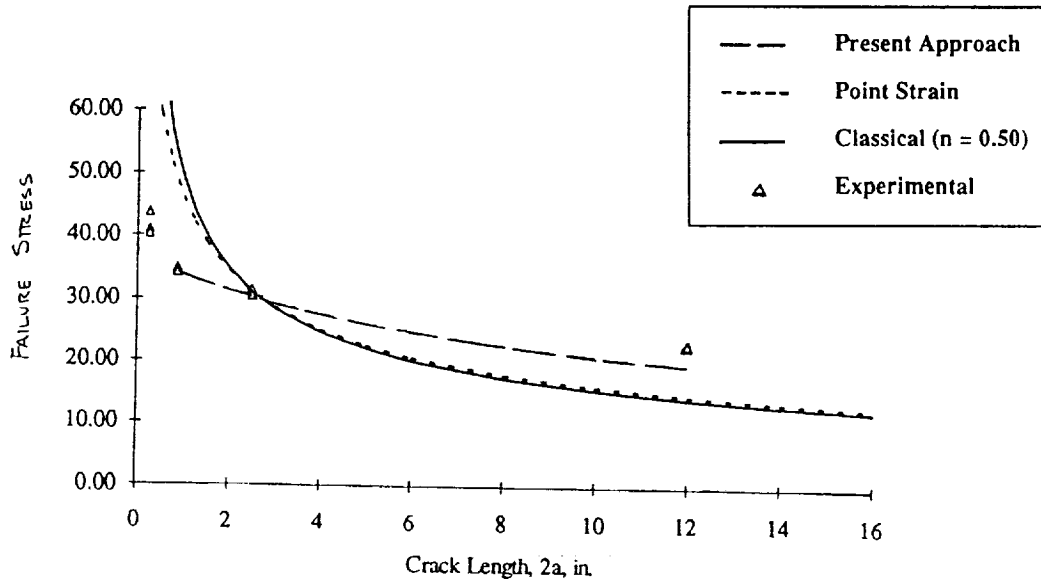
Another significant predictive ability demonstrated by the damage zone model is the sensitivity of center crack test specimens to the width of a coupon relative to the crack size (w/2a). A single strain-softening law was obtained by calibrating at a single specimen geometry, and used for all other geometries. As can be clearly seen, the strain-softening law predicts differing trends between the two data sets. This initial attempt at predicting the experimentally-observed differences resulted in surprisingly good correlation with the data. Further understanding of the effects of the law parameters on the response would likely lead to improved correlation.

Comparison of Finite Width Correlated Strength

Boeing Computer Services
Technology

Measured Data W/2a = 2
O

Analytical Data W/2a = 2
Δ

Measured Data W/2a = 4
●

Analytical Data W/2a = 4
+

Layup = [+45/90/-45/0/+30/-30/0/-45/90/+45]
Mat'l = AS4/938 Tape

ANALYSIS REQUIREMENTS FOR COMBINED LOAD TEST FIXTURE

The purpose of the pressure-box test apparatus is to simulate the structural response of a portion of a 122-inch radius aircraft fuselage. The tests specimen is a 72 in. x 63 in. graphite/epoxy skin panel with the curvature along the 63 in. edge. The test fixture permits the inclusion of longitudinal stiffeners and circumferential frames. The heart of the test fixture is the pressure box, which permits the simulation of a pressurized fuselage. Pressure loads act on the skin panel and are reacted in the hoop direction by large plates attached to the skin panel and by truss elements attached to the frames. Axial loads arising from internal pressure and/or fuselage bending are introduced by hydraulic cylinders attached to axial loading plates. The test specimen, the loading plates, and the various reacting trusses and actuators are free to float on the pressurized air.
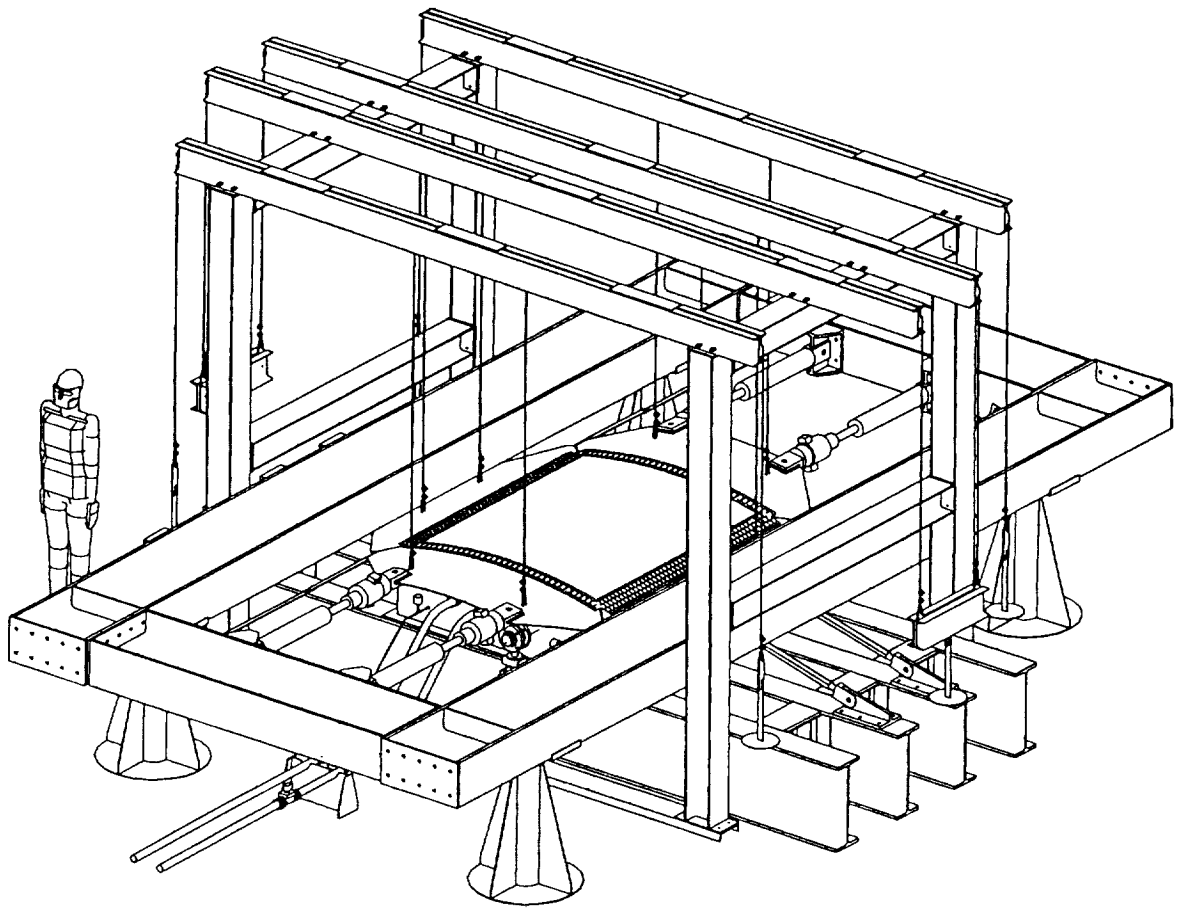
Finite element analysis of the pressure-box test apparatus has played an ongoing role in its design and development. Initial analyses were focused on sizing and locating the test fixturing to most accurately represent the remainder of the fuselage. These items included the loading plates, the pairs of grips which transmit load between the test specimen and the loading plates, the actuators, and the load reaction members. As the design has matured, more detail has been incorporated in the finite element model in efforts to finalize the panel doubler configurations to minimize interactions between the test fixturing and the panel response. The predictions may also serve to identify and quantify any discrepancies which might be unavoidable.

Objectives

Boeing Computer Services
Technology

Geometrically nonlinear (large deflection) finite element simulations of the pressure box test fixture have been performed using ABAQUS. The objectives of these analyses are

1. Identify and understand the interactions between the test fixture and the stringer and frame stiffened test panels. This task is critical in relating pressure box test data to full fuselage analyses, and to larger scale tests. (Scaling)

2. Support the detailed design of the pressure box test apparatus

3. Generate pretest predictions and recommend sensor locations

4. Evaluate the effects of damage to pressure box test panels subjected to biaxial loading. Compare to test results and complete fuselage assessments. (Damage scaling)

The current finite element model represents one quarter of the test specimen, as shown in the figure. It consists of 2260 node points, 238 beam elements, and 1911 shell elements. This model requires approximately 90 seconds of CPU time to run a static, large deflection analysis on the Boeing CRAY YMP. When damage is represented in the model, local deflections are much larger, and run times increase to approximately 175 seconds.

Detailed Finite Element Model

Boeing Computer Services
Technology
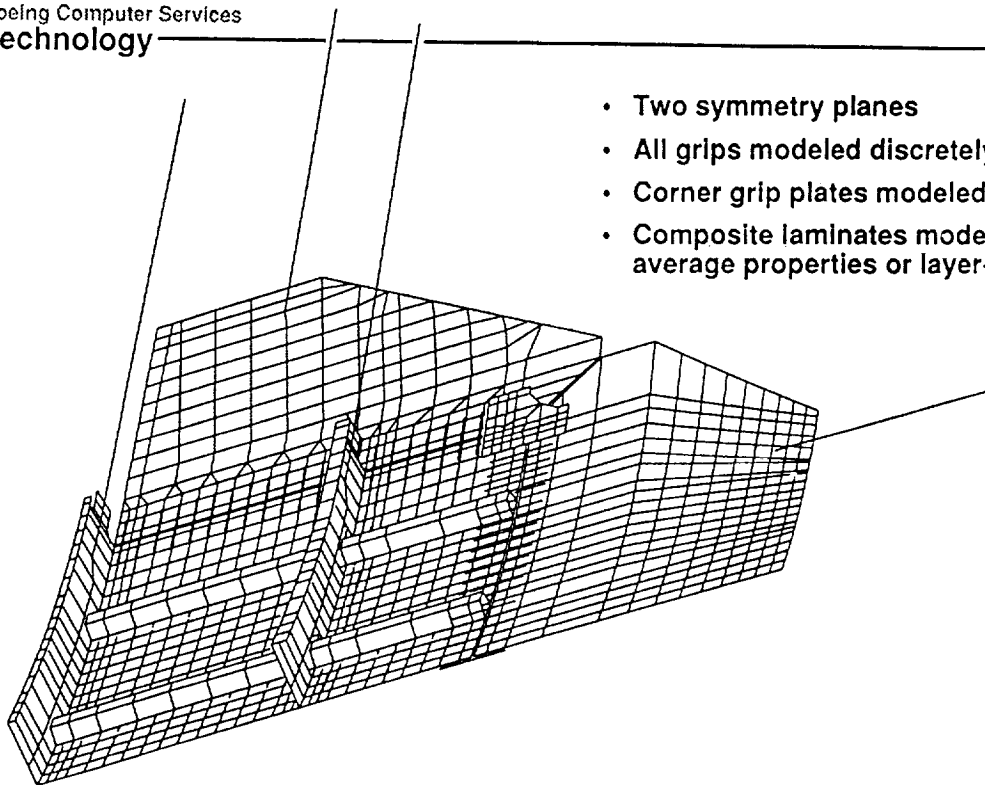
- Two symmetry planes
- All grips modeled discretely
- Corner grip plates modeled in detail
- Composite laminates modeled with average properties or layer-by-layer

A great deal of effort has been devoted to a more detailed representation of the pairs of grips and the corner plates which transfer loads between the test specimen and the loading plates. To permit the grips and plates to be modeled at their proper radii relative to the plates and test specimen, and to duplicate the slotted attachments of the hoop grips, the beams representing the grips must be joined to the model via multiple constraint laws and special equations. This has permitted a more accurate assessment of the "as built" test hardware.

The finite element models have evolved with and supported the detailed design of the pressure box test apparatus. Simulations of various load cases have been used to assess and verify:

- Grip design and resulting load distributions

- Location of axial load application

- The effectiveness of "slotted" hoop grips and corner grip plate design

- Grip fastener loads – led to the step-tapered, "scalloped" doubler design for introducing axial loads

- The impact of grip and doubler design on the response of panels with central damage

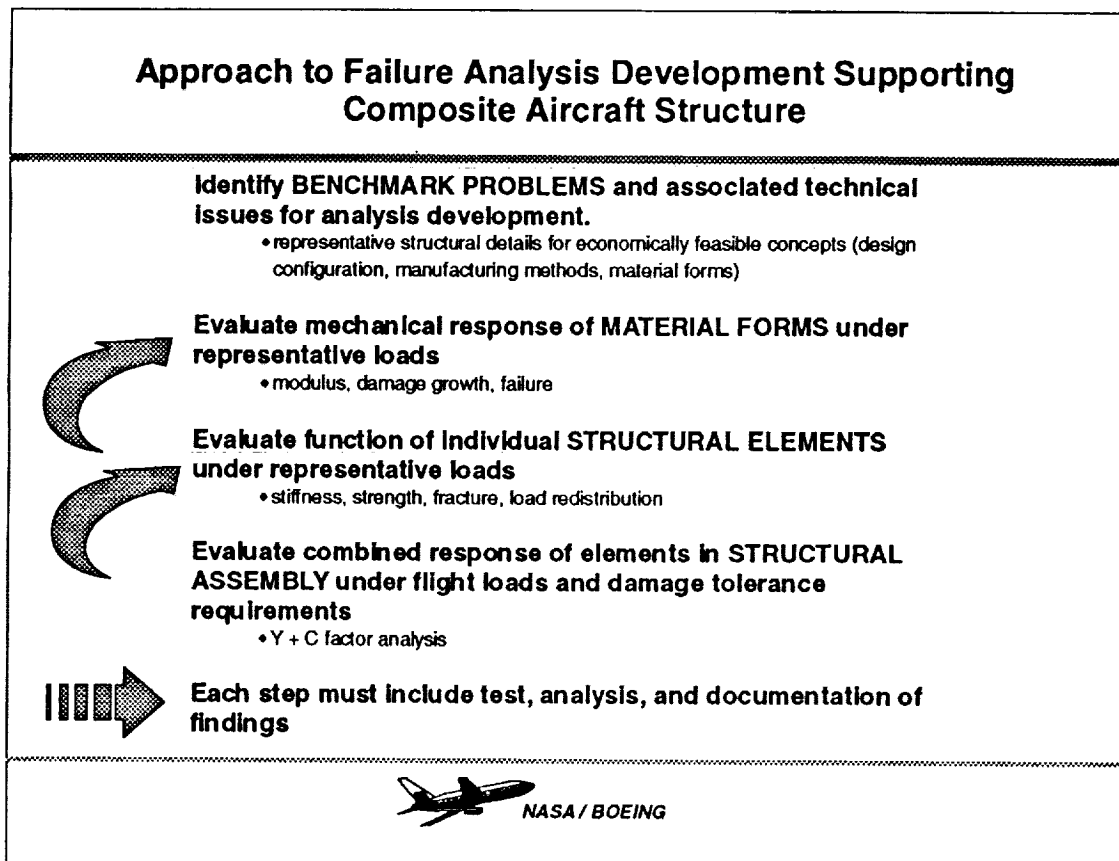{Approximately 8 man-month support effort}

32

SUMMARY

NASA/Boeing programs are generating a large structural database and supporting analysis methods for composite fuselage damage tolerance. Crown test results indicate that advanced analysis methods are needed to simulate composite failure. Strain-softening models have been successfully implemented in an existing nonlinear finite element code (ABAQUS), and have predicted several important experimentally-observed trends that were not properly addressed by classical fracture mechanics methods. Evaluation of the pressure-box test fixture have indicated that detailed analyses of the panels, attachments, and test fixtures are required to properly interpret test results.

RECOMMENDATIONS

At Boeing, the goal of composite materials research is the critical assessment of the cost- and weight-efficiency of using advanced composite materials in commercial aircraft primary structure while ensuring structural integrity. To guarantee competitiveness, it is essential that the assessment and subsequent application of attractive concepts be accomplished as expeditiously as possible. This is most efficiently accomplished with a combination of test and analysis. Test data is currently essential for real-world engineering problems that include built-up structure, major load redistribution (e.g., around cutouts), combined loads, and damage tolerance. Analysis can play a role in extending element and subcomponent panel test data to structural design problems. Analytical developments over the next five to ten years should be dominated by these concerns, since the prohibitively high costs associated with a test-only certification approach are the large scale tests for multiple load, damage, and environmental conditions.

Analysis methods can also be used to (a) reduce testing requirements and hence developmental, verification and certification costs; (b) reduce response time in the resolution of field problems and identify sites for periodic inspection; (c) support concurrent engineering problems in which manufacturing desires design details that require comprehensive analysis to ensure performance is not compromised; and (d) support composite material development through a basic understanding of failure mechanisms and their sensitivity to design variations. These applications should be longer-term goals for analysis method development.

To develop methods for extending element and subcomponent test results to fully configured structure, it is important to focus efforts to real-world problems, including layups, structural configurations, loading conditions, and damage requirements. A method to accomplish this is shown in the figure. The thrust of this approach is to identify "benchmark" problems to identify the configurations, loading, and associated technical issues. Attractive material forms would then be evaluated under loading conditions representative of their structural usage. Next, the structural role of each of the elements should be evaluated under representative loading conditions. Finally, the response of the structural assembly under flight loads and damage tolerance conditions would be assessed. With the knowledge gained in each step, the evaluations in the previous steps would be revisited, and modification made where required. Each step must include a combination of test, analysis, and documentation of the findings. Analytical capabilities must be assessed by their ability not only to predict failure, but to predict structural response throughout the loading regime.

Approach to Failure Analysis Development Supporting Composite Aircraft Structure

Identify BENCHMARK PROBLEMS and associated technical issues for analysis development.
- representative structural details for economically feasible concepts (design configuration, manufacturing methods, material forms)

Evaluate mechanical response of MATERIAL FORMS under representative loads
- modulus, damage growth, failure

Evaluate function of Individual STRUCTURAL ELEMENTS under representative loads
- stiffness, strength, fracture, load redistribution

Evaluate combined response of elements in STRUCTURAL ASSEMBLY under flight loads and damage tolerance requirements
- Y + C factor analysis

Each step must include test, analysis, and documentation of findings

NASA / BOEING

From the work conducted to date at Boeing on tension fracture of fuselage crown structure, several detailed recommendations can be made. Non-destructive evaluation methods should be developed for quantifying composite material response and damage states. Lamb-wave dispersion has proved attractive in measuring damage levels near impact locations and in progressive damage zones. Methods for determining operative generalized constitutive laws (e.g., non-local, Cosserat) and their necessary material constants are also required.

Further work should be pursued on extending strain softening models for composite structural analysis. This activity includes addressing an orthotropic plate element, including membrane, shear and bending laws. Inclusion of Cosserat material behavior might be necessary. Other issues include (a) development of softening laws for compression and combined loads, (b) environmental and dynamic effects, and (c) analysis and test schemes for multidirectional material characterization.

Needs exist for development of a larger element and subcomponent test database, including shear lag, combined loads, and major load redistribution. Further analysis of subcomponent combined load tests (i.e., pressure-box tests) is required, including a range of panel design details and damage states. An analysis of the full-scale fuselage subjected to the full range of loading conditions and damage states is necessary to allow evaluation of the subscale tests.

Projections on Structures and Material Strength in the Computational Context

Wolfgang G. Knauss
California Institute of Technology
Pasadena, CA

INTRODUCTION

This text summarizes the ideas associated with the subsequent viewgraphs. The primary motivation behind this presentation is to observe that certain macroscopic, microscopic and sub-microscopic phenomena are being understood that have basic influence on understanding the durability and high temperature sensitivity of polymers and polymer-based composites. This understanding covers important issues of long term stability with respect to residual stresses and deformations which can have very deleterious effects on structures used for long periods of time as a result of the heat-involving manufacturing process. Beyond this, important progress is being made in understanding the nonlinear material response of polymers in the fracture context, because the nonlinear mechanics of the material at the tip of a crack, either propagating or ready to do so, is being understood with increasing precision.

Projections on

STRUCTURES AND MATERIAL STRENGTH

in the computational context

Motivation:

MANUFACTURING PROCESSES INVOLVING

Effects of long term stability as in

Residual stresses   (failure)

Residual deformations   (space mirrors
& antennas)

DEFORMATION PROCESSES

Non-linear mechanics

Non-linear material response   (Rheology)

OUTLINE OF PRESENTATION

This understanding is necessarily coupled to extensive use of computers, but should not be separated from the physical understanding that must precede computer analysis if realistic advances are to be made in engineering. Three examples are to be presented that progress from the macroscopic to the increasingly microscopic domain, with attendant increase in computational need for adding understanding to the present state of affairs.

Needs:

Computer support

Experimental/physical phenomena
(not necessarily in that order)

1) Structural size scale   (m)

2) Macroscopic material size scale (mm)

3) Microscopic/molecular size scale (mm,μ)

Examples:

1) Structural computational

2) Macroscopic/microscopic

3) Molecular aspects

2) and 3) as examples of the
### Evolution of Computational Material Description

An example of a case for which the computational methods are fairly well understood but for which the analysis needs to be demonstrated as an incentive for design understanding relative to long term stability of structures is that of buckling under the influence of not only temperature, but thermal gradients. The effect of the thermal gradient is twofold: First, because of the different thermal expansion of the panel according to the local temperature the panel or column will bend, thus introducing an initial imperfection. In addition, it changes the time-dependent response of the polymer through the thickness of the panel and generates thus a time-dependent material structure that possesses inhomogeneous properties through the panel thickness. The solution to this problem is likely to be possible only in numerical rather than closed-form analytical terms.
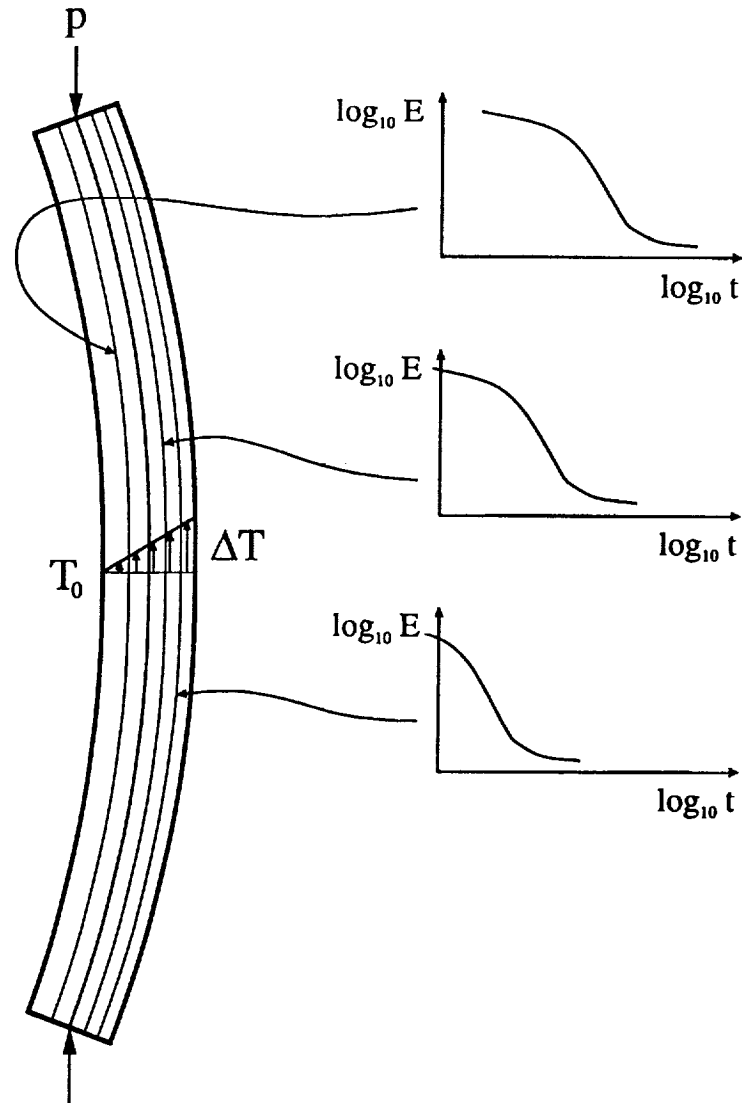
Compression of a Thermoviscoelastic Column/Plate
under a Transverse Thermal Gradient

COMPUTATIONAL MATERIAL MECHANICS

There are many materials which at the microscale are composite solids. Examples are multiphase polymer blends with co-polymers for which different components are joined in order to render properties that are superior to the individual phases alone. Although the individual phases possess thermo-rheologically simple behavior, their combination does not, so that a simple test scheme for accelerated testing is questionable or not possible. It turns out that a relatively straightforward analysis procedure based on numerical modeling can provide a framework for accelerated determination for long-range properties which is only limited by the assumption of even phase distribution and by the precision of finite element analysis. The problem with more than two viscoelastic phases is treated with ease typical of numerical methods.
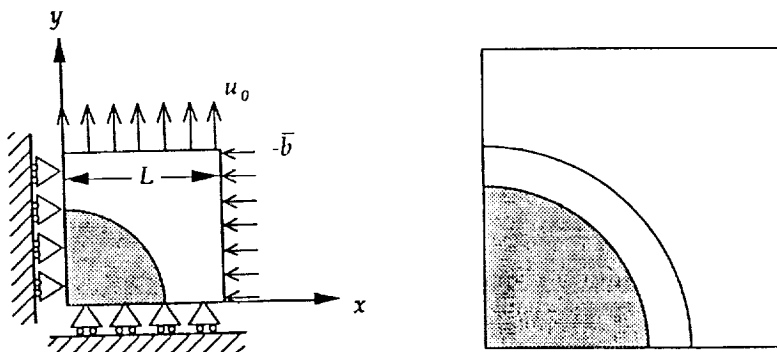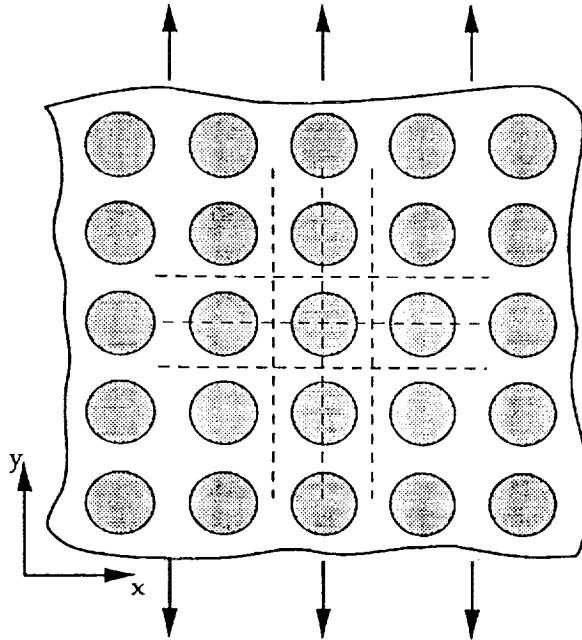
ANALYTICALLY DERIVED COMPLEX NATURAL BEHAVIOR

An example is shown of the complex modulus data assuming that only two discrete phases of the two basic building blocks exist. Note that the viscoelastic composite exhibits properties that are closer to those of the matrix material rather than following a rule of mixtures.
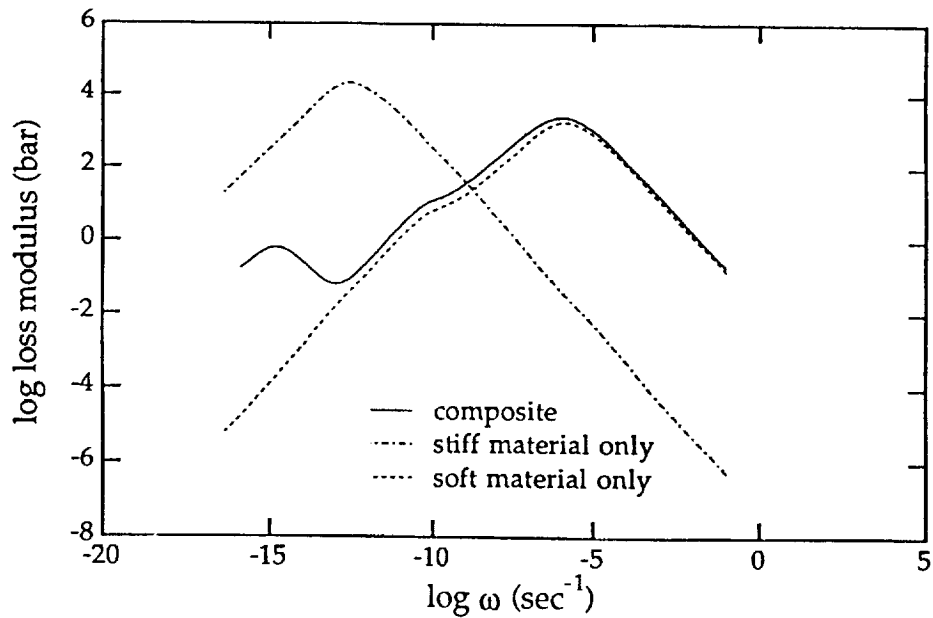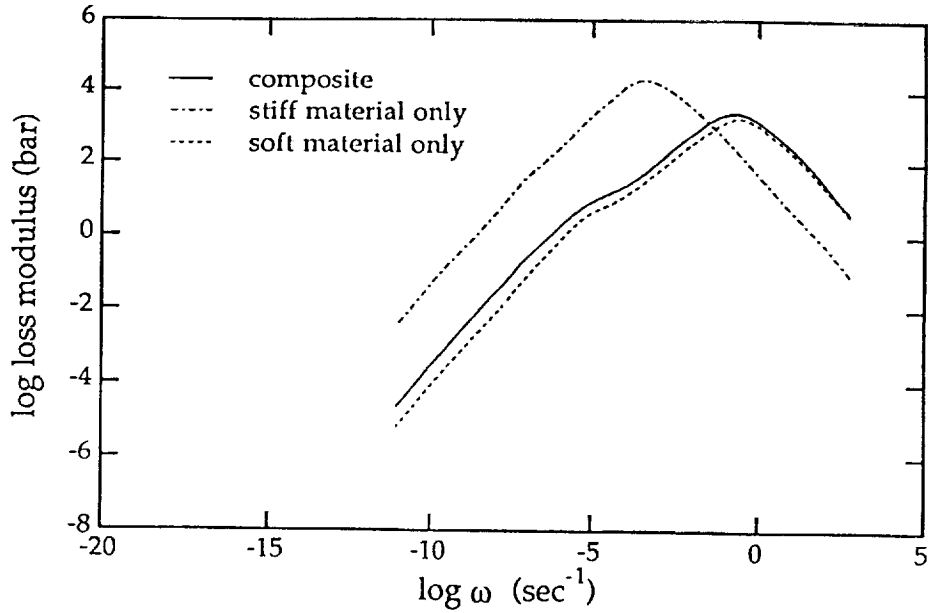
LOSS MODULUS FOR A TWO-PHASE MATERIAL MODEL

Upon comparing the computations to experiments for a Styrene-Butadiene-Styrene block co-polymer, one finds that the agreement with the experiment is not satisfactory for a two-phase solid. However, by considering a third phase surrounding the hard inclusions, the properties of which can be initially estimated roughly, the agreement between analysis and experiment is rather good.
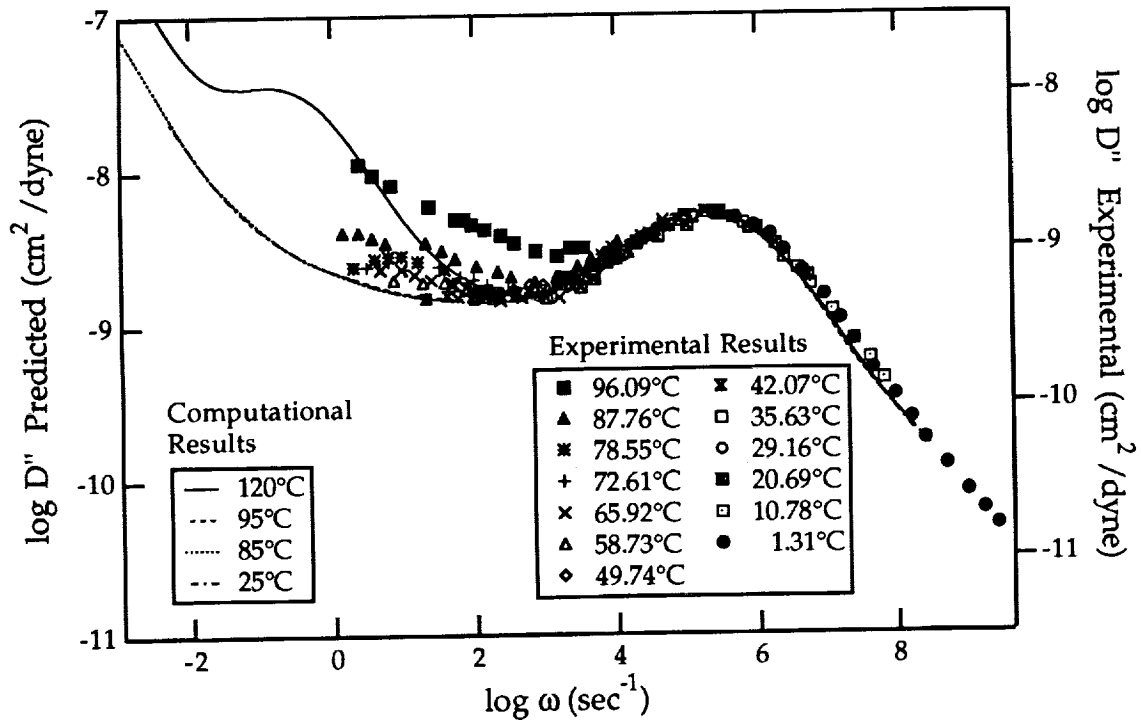
VISCOELASTIC (DYNAMIC) PROPERTIES INCORPORATING VISCOELASTIC PHASE BOUNDARIES INTO COMPOSITE

One can then refine that initial estimate and "back-fit" a three-phase model to the experimental data without violating the boundaries imposed from fundamental but less detailed analysis by fine-tuning the computational model. The resulting material properties have thus been determined experimentally with the aid of a fairly refined material model. The computations also point out the range of frequency measurements one needs to perform in order to improve on the precision with which such phase property determinations can be performed.

This description concludes the example of how computations can assist in refined analyses of property domains that are difficult to access by direct physical test procedures, although such procedures are now being developed. It is of interest to point out that although the model is conceived on the macroscopic scale, its application is made here to the sub-micron range of inclusion sizes.
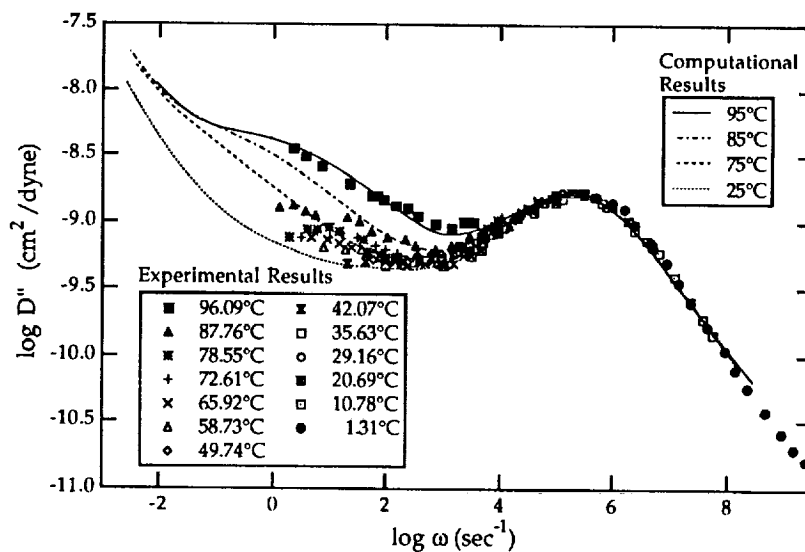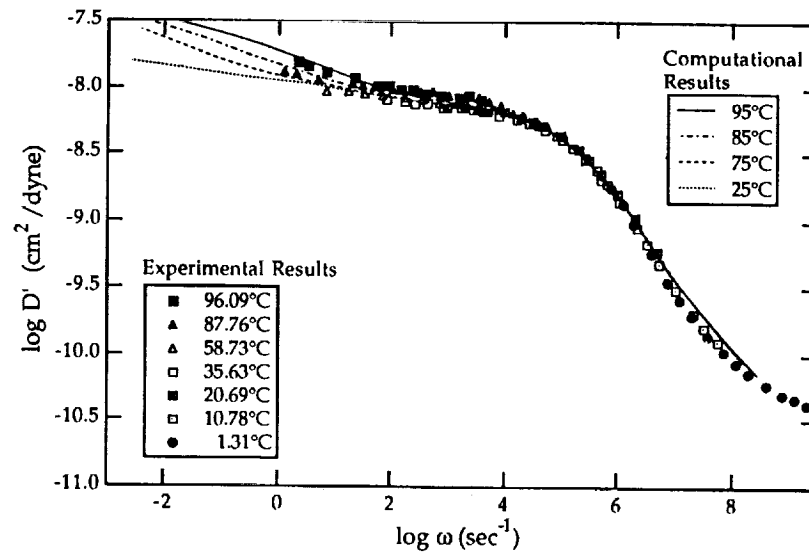
THE NONLINEARLY VISCOELASTIC CONSTITUTION
OF STRUCTURAL POLYMERS

A third example leading to the need for still smaller size scales is illustrated next. The motivation for this work is the need to better understand the time-dependent behavior of polymers (durability), their long-term fracture behavior, how it is to be studied in accelerated tests, as well as a host of problems related to composite manufacturing. It is of basic interest to generate constitutive behavior that incorporates the material behavior of the matrix material as it progresses through the manufacturing process, as it ages physically, as it is stressed to moderate and high levels, as, for example, at the tip of a crack. It appears that we meet here a (temporary) limit of continuum mechanics, because the parameters which govern the dominant microscopic (molecular) details and their definite influence on the macroscopic constitutive response are not yet known.

The model starts from linear viscoelasticity, but includes the effect of small volume changes that result from either thermal expansion, solvent diffusion or mechanically induced dilatation, as it influences the time-dependent behavior of the polymer. In contrast to the linearity assumption, this material description couples shear and dilatational behavior, and renders a large effect of small volume changes on the time scale of the material response.

NONLINEARLY VISCOELASTIC BEHAVIOR

$$s_{ij} = \int_{-\infty}^{t} 2\mu\left(t*(t) - \xi*(\xi)\right) \frac{\partial e_{ij}\left(\underset{\sim}{x},\xi\right)}{\partial \xi} d\xi$$

$$\tau_{kk}\left(\underset{\sim}{x},t\right) = 3\int_{-\infty}^{t} K\left(t*(t) - \xi*(\xi)\right) \frac{\partial \varepsilon_{kk}\left(\underset{\sim}{x},\xi\right)}{\partial \xi} d\xi$$

INTERNAL TIME
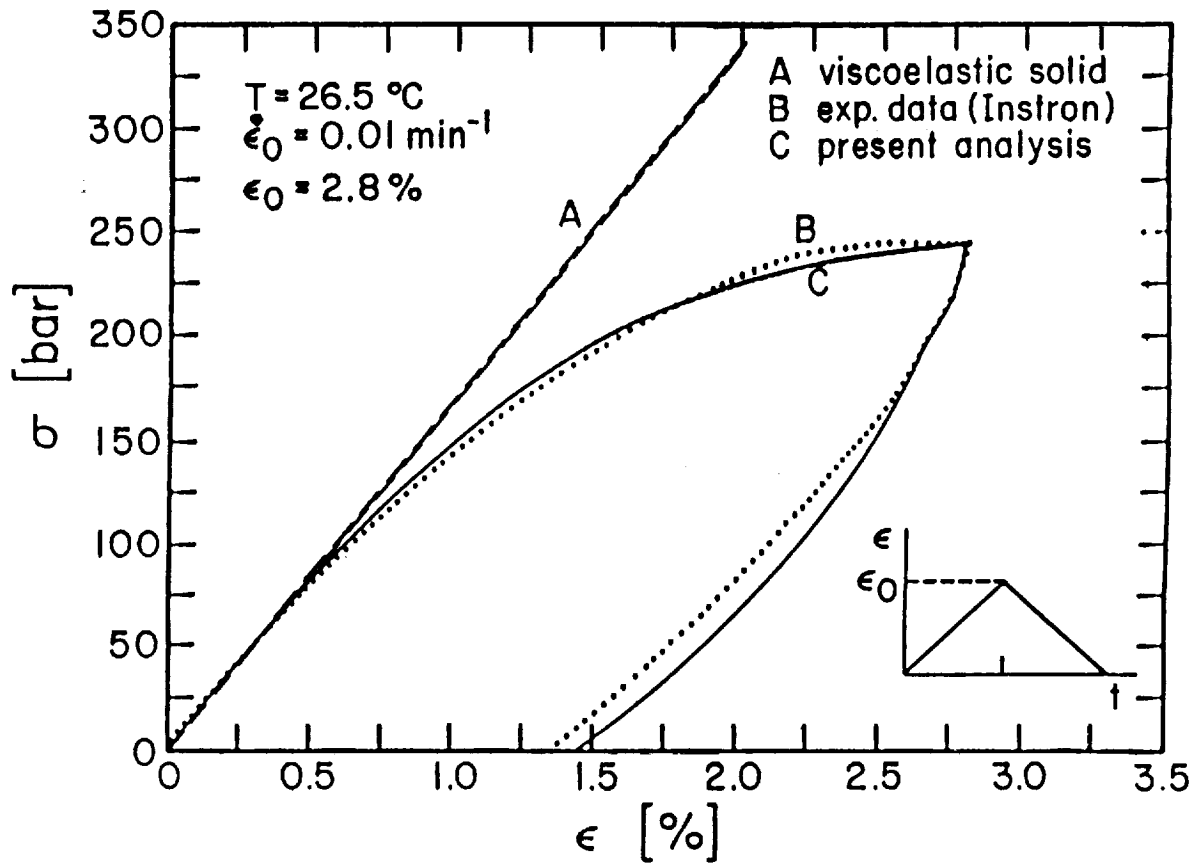
$$dt* = \frac{dt}{a\left[T\left(\underset{\sim}{x},t\right), \varepsilon_{kk}\left(\underset{\sim}{x},t\right)\right]}$$

$$\log_{10}(a) = \frac{B}{2.3}\left[\frac{1}{f} - \frac{1}{f_0}\right]$$

$$f = f_0 + A_1\alpha*dT + A_2K^{-1}*d\tau_{kk}$$

NONLINEAR MATERIAL MODEL: CONSTANT STRAIN
RATE LOADING AND UNLOADING

Illustrated below is an example of the model characterizing a loading-unloading sequence as compared with a) linearly viscoelastic prediction, and b) experiments.

NONLINEAR MATERIAL MODEL: PHYSICAL (PRESSURE) AGING

An example of the model illustrates how time-dependent solidification of the material influences the subsequent stress strain behavior in a constant strain rate test: As the material solidifies more and more (curves A -> F), a yield behavior emerges which is the result of delayed viscous response as the stress level increases.
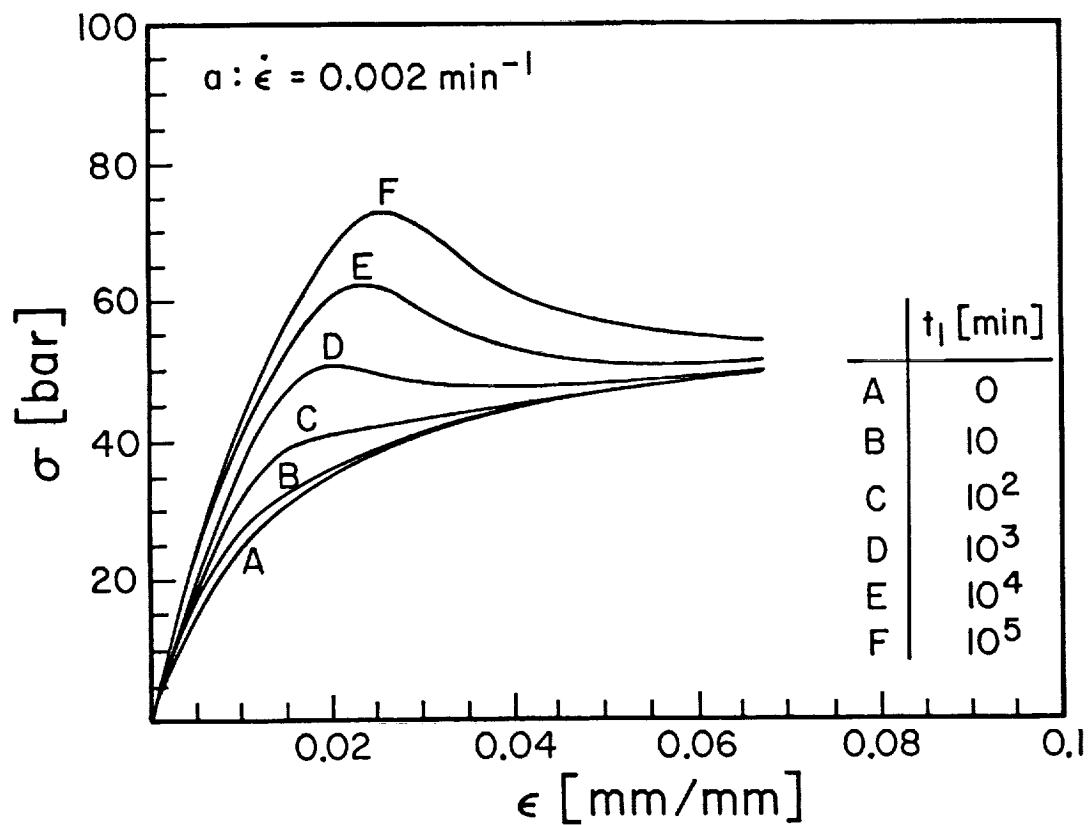
NONLINEAR MATERIAL RESPONSE: EXAMPLE OF COOLING THROUGH THE GLASS TRANSITION

Another example and comparison with experiments of the time-dependent change in volume of a material quenched suddenly from above and below the glass temperature is illustrated. Considering that the detailed properties of the material for the test configuration were not available to us and needed to be estimated (especially the important bulk modulus in its time dependency), the agreement is better than merely qualitative.
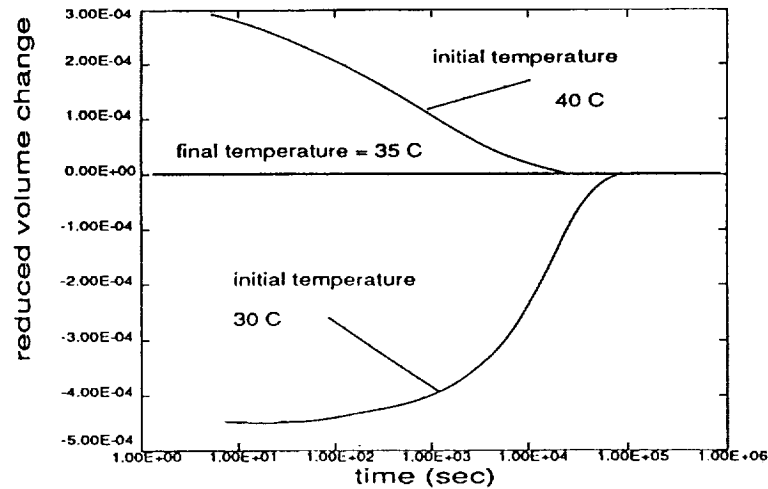

Reduced volume change $\frac{V-V_\infty}{V_\infty|\Delta T|}$ of PVAc, plotted vs. time; data obtained by Kovacs (1963).
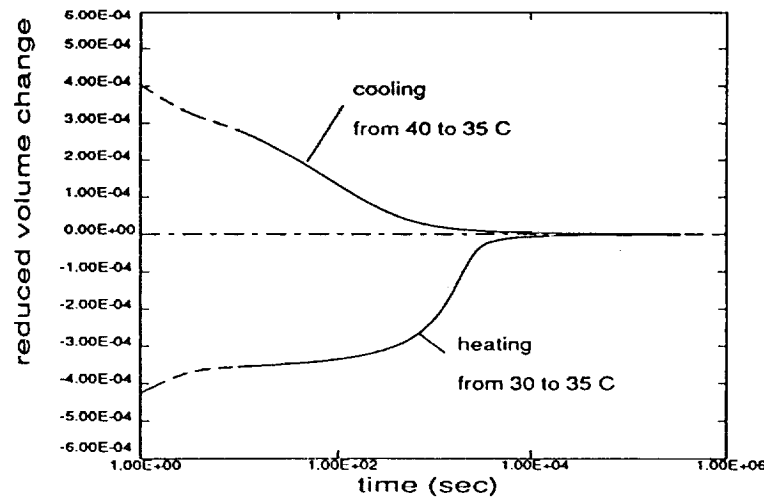
Reduced volume change $\frac{V-V_\infty}{V_\infty|\Delta T|}$ for the 1 mm radius sphere cooled from 40 to 35 C and heated from 30 to 35 C (thermorheological model, "modified" bulk modulus).

COMPLEX COOLING HISTORIES NEAR THE GLASS TRANSITION
AND THEIR EFFECT ON VOLUME BEHAVIOR

A final comparison addresses more complex temperature histories as outlined in the insert to the figure on the left. The qualitative comparison to the experiments supplied by Kovacs is shown in the figure on the right.
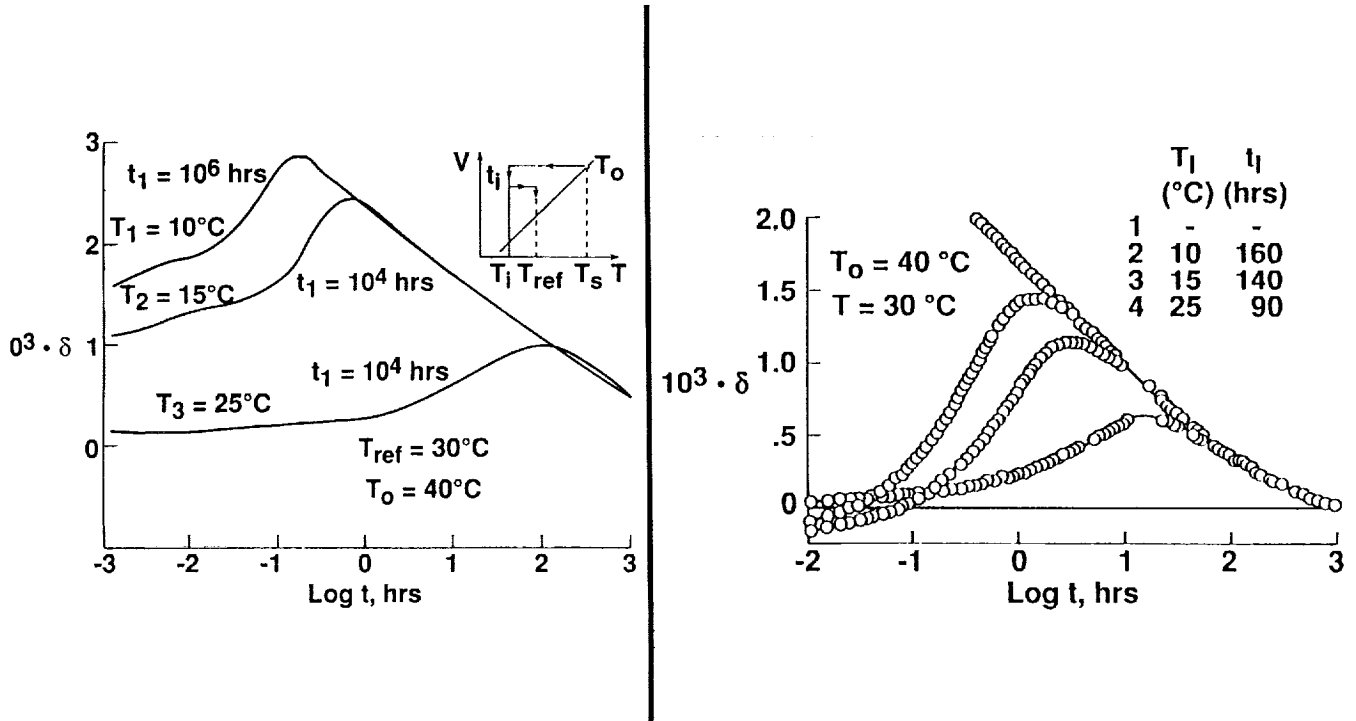
CONCLUSIONS

Progress is being made in understanding the thermorheological behavior of polymers with respect to:

a) complex temperature histories of interest in high-temperature applications and manufacturing processes;

b) elevated stresses and nonlinear material behavior of vital importance in understanding the material behavior at the tip of cracks and how that influences their evolution and growth in a time-dependent manner, giving rise to improved understanding of what governs the long-range durability of these materials. Moreover, this understanding makes it increasingly possible to evolve acceleration test schemes because the physics underlying these schemes are becoming clear.

It is also becoming clear that mere continuum concepts are insufficient to characterize the diversity of material behavior at the molecular level and how that diversity influences the macroscopic behavior. As a consequence it becomes increasingly important to devote computational efforts to molecular and supramolecular domains in an effort to better understand the influence of molecular parameters on the mechanical continuum behavior of these materials. With the arrival of supercomputers, significant advances can be established from this perspective to provide guidance on what improvements can be made, if any, in the macroscopic and phenomenological description of matrix material constitutive behavior.

A Thermodynamic Analysis of Propagating Subcritical Cracks with Cohesive Zones

David H. Allen
Center for Mechanics of Composites
Texas A&M University
College Station, TX

INTRODUCTION

The results of the so-called energetic approach to fracture with particular attention to the issue of energy dissipation due to crack propagation are applied to the case of a crack with cohesive zone. The thermodynamic admissibility of subcritical crack growth (SCG) is discussed together with some hypotheses that lead to the derivation of SCG laws. A two-phase cohesive zone model for discontinuous crack growth is presented and its thermodynamics analyzed, followed by an example of its possible application.

INTRODUCTION

Subcritical crack growth (SCG), under both general and cyclic loading, is a phenomenon that has been receiving more and more attention during the last forty years. Starting with early investigations mainly on fatigue in metals (Refs. 1-9), current research covers a wide variety of materials, especially those such as polymers (Refs. 9-13), and ceramics (Ref. 14), that are becoming important in the fabrication of composites. From a theoretical standpoint, the problem is that of relating crack growth to the load history. In this sense, fundamental understanding has been provided by the energetic approach to fracture (Refs. 15-32), that showed (Refs. 15-19) how SCG is strictly related to the rate of dissipation in the vicinity of the crack front.

OBJECTIVE:

TO RELATE CRACK GROWTH TO THE LOAD HISTORY

A CRACK GROWTH LAW AND/OR CRITERION IS NEEDED

56

APPROACHES TO THE PROBLEM

Several theoretical studies in the continuum thermodynamics of fracture have shown that independently of the global or local (around the crack tip) constitutive assumptions, a sharp crack with no cohesive zone is constrained to evolve according to the Griffith criterion (Ref. 20). Unfortunately, SCG cannot be described in terms of the Griffith criterion. In the case of SCG, mainly in fatigue, a number of growth laws are available, although the great majority of them are based on phenomenological observation only.

● **GRIFFITH CRITERION (1920)**

$$\dot{l} \geq 0 \quad IF \quad G \geq G_{CR}$$

ORIGINALLY FORMULATED USING AN ENERGY BALANCE APPROACH (FIRST LAW) FOR BRITTLE SYSTEMS.

● **FATIGUE GROWTH LAWS (SINCE EARLY 1950's)**

- CYCLIC LOADING

- SUBCRITICAL CONDITIONS
  (GRIFFITH CRITERION DOES NOT APPLY)

- MOST OF THEM ARE ONLY
  PHENOMENOLOGICALLY BASED

CURRENT STATE OF RESEARCH

Modern continuum thermodynamics sees crack propagation like an internal dissipation mechanism. In this sense the propagation of fracture can be described by the evolution of a set of convenient kinematic state variables, e.g., crack length, whose driving force can be computed directly from the total free energy of the body. The application of the thermodynamics with ISV's is immediate. One of the important outcomes of such an approach is the interpretation of a moving crack tip as a moving heat source and the subsequent determination of the corresponding near crack tip temperature field.

- **ENERGETIC APPROACH AS A UNIFIED APPROACH:**

  - **FRACTURE STUDIED WITHIN THE FRAMEWORK OF CONTINUUM THERMODYNAMICS**

  - **CRACK SURFACE CONSIDERED AN <u>INTERNAL STATE VARIABLE</u>;**

$$G = -\frac{\partial \psi}{\partial l}$$

  - **CRACK PROPAGATION IS AN INTERNAL DISSIPATION MECHANISM. IT CAN BE INCLUDED IN CONSTITUTIVE THEORIES WITH I.S.V.**

  - **FORM OF TEMPERATURE SINGULARITY AT THE TIP OF A RUNNING CRACK**

58

The present research effort employs many of the results of the modern thermodynamics approach to fracture. We therefore list some of the most important contributions of this approach.

THERMODYNAMIC APPROACH
TO FRACTURE

- GRIFFITH (1920): CRACK GROWTH CRITERION USING THE FIRST LAW OF THERMODYNAMICS

- CHEREPANOV, G.A. (1967): APPLICATION OF CONTINUUM MECHANICS & CONSIDERATIONS BASED ON THE SECOND LAW

- RICE, J.R. (1968): PATH INDEPENDENT INTEGRALS IN ELASTICITY; ENERGY RELEASE RATE AS CRACK LENGTH CONJUGATE FORCE

- GURTIN (1979): APPLICATION OF RATIONAL THERMODYNAMICS TO A THERMOELASTIC SYSTEM WITH A SHARP CRACK

- NGUYEN (1980-1985): GLOBAL THERMODYNAMIC AND DISSIPATION ANALYSIS TO FRACTURE

GENERALIZATION OF THE GRIFFITH CRITERION DERIVED BY A DISSIPATION POTENTIAL THERMOMECHANICAL SINGULARITY ANALYSIS

MAJOR PROBLEMS WITH CURRENT METHODS

The thermodynamic approach to fracture, in the absence of a cohesive zone, derives the Griffith criterion as the only possible consequence of the second law. This result is fatigue since fatigue is an example of SCG. Another problem in the analysis of cracks with no C.Z. is the loss of weaving of the fracture parameter G for almost all material behaviors except the thermoelastic one, thus including special behaviors like that of a process zone around a sharp crack.

- SOME RESEARCHERS HAVE DERIVED SUBCRITICAL CRACK PROPAGATION LAWS FROM THE FIRST LAW ALONE: THERMODYNAMIC ADMISSIBILITY IS DISREGARDED.

- WHEN THE SECOND LAW IS CONSIDERED SUBCRITICAL CRACK PROPAGATION HAS BEEN SHOWN TO BE THERMODYNAMICALLY INADMISSIBLE

- FOR THE RUNNING CRACK PROBLEM, SINGULARITY ANALYSES SHOW THAT G IS MEANINGLESS FOR PLASTICITY AND VISCOPLASTICITY AND FOR CERTAIN VISCOELASTIC MODELS

- MODELS THAT INCLUDE PROCESS ZONES AROUND SHARP CRACKS DO NOT NECESSARILY REMOVE THE THERMOMECHANICAL SINGULARITY AT THE TIP, NOR SOLVE THE ABOVE PROBLEMS.

APPROACH USED IN THIS RESEARCH

The present research effort introduces a cohesive zone into a continuum mechanics model for SCG in order to allow for a thermodynamically consistent description of the problem. After postulating the presence of a C.Z. ahead of the crack tip, the circumstances under which SCG is thermodynamically admissible will be discussed. The assumption leading to the derivation of the traditional form of fatigue growth laws is also discussed and a similar form for discontinuous crack growth laws will be obtained.

- **CONTINUUM THERMODYNAMIC FRAMEWORK**
  - **CLASSICAL FIELD THEORY CAN BE USED INSTEAD OF NON-LOCAL MODELS**

- **COHESIVE ZONE**
  - **ALL THERMOMECHANICAL SINGULARITIES ARE REMOVED**
  - **CRACK TIP HAS A FINITE SIZE**

- **SUBCRITICAL CONDITIONS**
  - **THERMODYNAMICALLY ADMISSIBLE**
  - **UNIFIED APPROACH TO STUDY FATIGUE AND DISCONTINUOUS CRACK PROPAGATION.**

BASIC EQUATIONS AND DEFINITIONS

The analysis prosecuted is basically a global thermodynamic analysis. It consists of deriving global thermodynamic statements for the entire structure by interpreting the pointwise governing equations over the whole body.

POINTWISE GOVERNING EQUATIONS

$$\rho \dot{u} = \sigma_{ij} \dot{\varepsilon}_{ij} - q_{i,i} + \rho r \tag{1}$$

$$\rho \dot{s} + \left(\frac{q_i}{T} \right)_{,i} - \rho \frac{r}{T} \geq 0 \tag{2}$$

$$\sigma_{ji,j} + \rho f_i = 0 \tag{3}$$

$$\varepsilon_{ij} = \frac{1}{2} (u_{i,j} + u_{j,i}) \tag{4}$$

$$
\begin{aligned}
\sigma_{ij} &= \sigma_{ij}(\varepsilon_{kl}, T, \alpha^n) \\
q_i &= q_i(\varepsilon_{kl}, T, T_{,k}, \alpha^n) \\
u &= u(\varepsilon_{kl}, T, \alpha^n) \\
s &= s(\varepsilon_{kl}, T, \alpha^n)
\end{aligned}
\tag{5}
$$

62

Note that the constitutive behavior is assumed to be as general as possible through the use of interval state variables (at the pointwise level) together with their correspondent solution equations.

such that

$$\sigma_{ij} = \rho \frac{\partial h}{\partial \varepsilon_{ij}} \ ; \ s = -\frac{\partial h}{\partial T} \tag{6}$$

where $h = h(\vec{x}, t)$ is the Helmholtz free energy:

$$h \equiv u - Ts \tag{7}$$

$$\dot{\alpha}^n = \Omega^n(\varepsilon_{kl}, T, \alpha^m) \ ; \ n, m = 1, \dots, N \tag{8}$$

$$q_i = -kT_{,i} \tag{9}$$

ALSO LET

$$\rho \eta_I = \rho \eta_{mic} - \frac{q_i T_{,i}}{T^2} \tag{10}$$

STRONG FORM OF THE SECOND LAW

$$\rho \eta_{mic} \geq 0 \ ; \ -\frac{q_i T_{,i}}{T^2} \geq 0 \tag{11}$$

In Figure 1 we have a schematic representation of the system analyzed. The body contains a single edge crack which teminates with a cohesive zone characterized by the points α and β.
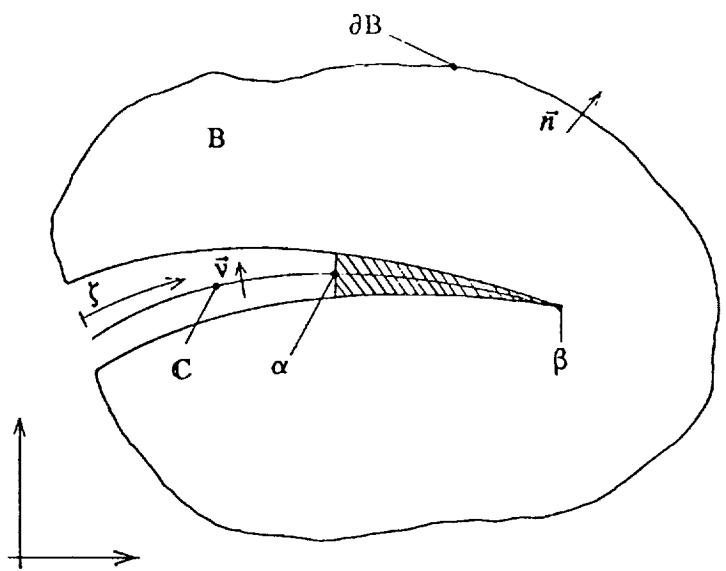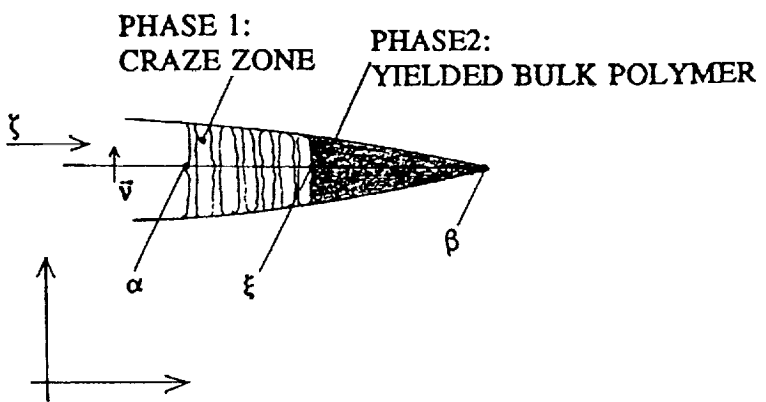

Figure 1 - Crack with a cohesive zone

Figure 2 - Two-phase cohesive zone model

DEFINITION OF A CRACK WITH A COHESIVE ZONE

From a mathematical viewpoint a crack is represented by a line (surface) of discontinuity for the various field variables. The cohesive zone is a portion of the crack line (surface) along which a system of cohesive forces σ_i is acting, and that is also characterized by its own opening displacement δ_i. A quantity in brackets represents the jump of that quantity across the cohesive zone. At this point it is possible to derive global statements for the first and second law and for the dissipation equation.

$$C(t) = \{\vec{x}(\zeta) : 0 \leq \zeta \leq \beta(t)\}$$
$$c.z. = \{\vec{x}(\zeta) : \alpha(t) \leq \zeta \leq \beta(t)\} \tag{12}$$

$$\sigma_i(\zeta,t) \equiv \sigma_{ji}^+ v_j = \sigma_{ji}^- v_j$$
$$\delta_i(\zeta,t) = [u_i] \ ; \ \delta_i(\beta(t),t) = 0 \tag{13}$$

GLOBAL FORMS OF THE LAWS OF THERMODYNAMICS

$$\frac{d}{dt}\int_B \rho u \ dA - \int_S (\sigma_{ji} n_j \dot{u}_i - q_i n_i) \ dS = - \int_{\alpha(t)}^{\beta(t)} (\sigma_i \dot{\delta}_i - [q_i] v_i) \ d\zeta \tag{14}$$

$$\frac{d}{dt}\int_B \rho s \ dA + \int_S q_i n_i \ dS - \int_{\alpha(t)}^{\beta(t)} [q_i] v_i \ d\zeta \geq 0 \tag{15}$$

$$\int_B \rho \eta_{mic} T \ dA = \int_B \rho \dot{s} T \ dA + \int_S q_i n_i \ dS - \int_{\alpha(t)}^{\beta(t)} [q_i] v_i \ d\zeta \tag{16}$$

WHERE

$$S \equiv \partial B \cup C^*$$
$$C^* \equiv C - c.z. \tag{17}$$

DEFINITION OF THE THERMODYNAMIC
QUANTITIES FOR THE C.Z.

The cohesive zone is considered a thermodynamic system with its own characteristics. In order to discuss such characteristics and write the two laws of thermodynamics for the cohesive zone above, it is necessary to define the C.Z. internal energy ε, entrophy φ, temperature ϑ and free energy ψ.

$$\varepsilon = \begin{cases} 2\gamma_o = const, & 0 \leq \zeta \leq \alpha(t) \\ \varepsilon(\zeta,t), & \alpha(t) \leq \zeta \leq \beta(t) \\ 0, & \zeta = \beta(t) \end{cases} \tag{18}$$

$$\varphi = \begin{cases} \varphi_o = const, & 0 \leq \zeta \leq \alpha(t) \\ \varphi(\zeta,t), & \alpha(t) < \zeta < \beta(t) \\ 0, & \zeta = \beta(t) \end{cases} \tag{19}$$

$$\vartheta = T^+ = T^- \\ \forall \zeta: \ \zeta \in c.z. \tag{20}$$

$$\psi = \varepsilon - \varphi \vartheta \tag{21}$$

FIRST LAW FOR THE C.Z. FROM THE GLOBAL
STATEMENT AND ABOVE DEFINITIONS

$$\int_{\alpha(t)}^{\beta(t)} \dot{\varepsilon} \ d\zeta = \int_{\alpha(t)}^{\beta(t)} (\sigma_i \dot{\delta}_i - [q_i] v_i) \ d\zeta \tag{22}$$

$$\frac{d}{dt} \int_{\alpha(t)}^{\beta(t)} \varepsilon \ d\zeta + 2\gamma_o \dot{\alpha} = \int_{\alpha(t)}^{\beta(t)} (\sigma_i \dot{\delta}_i - [q_i] v_i) \ d\zeta \tag{23}$$

LOCAL FORM

$$\dot{\varepsilon} = \sigma_i \dot{\delta}_i - [q_i] v_i \tag{24}$$

DISCUSSION ABOUT SECOND LAW AS POSTULATED BY GURTIN

The formulation of the second law for the cohesive zone is not a trivial matter. We therefore adopt the statement given by Gurtin in Ref. 26. We then impose a further restriction on the C.Z. behavior so as to restrain the C.Z. to act, as a whole, like an actual dissipative system.

GLOBAL STATEMENT (COHESIVE ZONE ALONE)

$$\int_{\alpha(t)}^{\beta(t)} (\dot{\varphi} + \frac{[q_i]v_i}{\vartheta}) \, d\zeta \geq 0 \qquad (25)$$

LOCAL STATEMENT

$$\dot{\lambda} = \dot{\varphi} + \frac{[q_i]v_i}{\vartheta} \geq 0 \qquad (26)$$

FURTHER RESTRICTIONS

$$\int_{\alpha(t)}^{\beta(t)} [q_i]v_i \, d\zeta \geq 0 \qquad (27)$$

THE ABOVE EXPRESSION IS THE DISSIPATION DUE TO THE EVOLUTION OF THE COHESIVE ZONE.

In order to properly discuss the dissipation associated with the C.Z. evolution, i.e., crack propagation and C.Z. deformation, the thermodynamic force (G-R) work conjugate of the global state variable α must be properly characterized.

BEING α A GLOBAL INDEPENDENT STATE VARIABLE, WE CAN WRITE:

$$\phi(x_k,t) = \phi(x_k,\alpha(t),t) \qquad (28)$$

$$\dot{\phi} = \frac{\partial \phi}{\partial \alpha}\dot{\alpha} + \frac{\partial \phi}{\partial t}\bigg|_{\alpha = const.} \qquad (29)$$

FIRST LAW:

$$\int_{\alpha(t)}^{\beta(t)} (\sigma_i \frac{\partial \delta_i}{\partial t} - \frac{\partial \varepsilon}{\partial t})\ d\zeta + (G-R)\dot{\alpha} = \int_{\alpha(t)}^{\beta(t)} [q_i]v_i\ d\zeta \qquad (30)$$

where

$$G = \int_{\alpha(t)}^{\beta(t)} \sigma_i \frac{\partial \delta_i}{\partial \alpha}\ d\zeta \ ; \ R = \int_{\alpha(t)}^{\beta(t)} \frac{\partial \varepsilon}{\partial \alpha}\ d\zeta \qquad (31)$$

CRACK ADVANCEMENT RESISTANCE IS A FUNCTION OF THE C.Z. THERMODYNAMIC STATE.

DISSIPATION ANALYSIS (Case 1)

We will now consider a special type of C.Z. evolution: crack growth with pure translation of the cohesive zone. The above assumption is certainly restrictive, but it yields results analogous to that obtained in the study of a crack without a cohesive zone. This leads to the following interpretation: a running crack with no cohesive zone behaves like a crack with a cohesive zone when the C.Z. is constrained to simply translate with the crack tip.

CASE 1: - **PURE TRANSLATION**
  - **BARENBLATT ASSUMPTIONS**

$$\Delta = \beta(t) - \alpha(t) \tag{32}$$

$$\dot{\phi} = -\frac{\partial \phi}{\partial \zeta} \qquad \dot{\alpha} = \frac{\partial \phi}{\partial \alpha} \tag{33}$$

  - **PURELY ELASTIC COHESIVE ZONE**

RESULTS:

$$(G - 2\gamma_s)\dot{\alpha} = \int_{\alpha(t)}^{\beta(t)} [q_i]v_i \ d\zeta \geq 0 \tag{34}$$

$$G = \int_{\delta(\beta)=0}^{\delta(\alpha)} \sigma_i \ d\delta_i \tag{35}$$

RESULTS ANALOGOUS TO THOSE FOR THE CASE OF A CRACK WITHOUT COHESIVE ZONE

When a cohesive zone with general behavior, thus with some being of dissipation mechanism, is left to evolve without special constraints, we see from the first and second law for the C.Z. that subcritical crack propagation, that is $\alpha > 0$ when $G < R$, is an admissible phenomenon.

CASE 2: - ELASTO-PLASTIC COHESIVE ZONE
- GENERAL DEFORMATION

$$\frac{\partial \psi}{\partial \delta_i^e} = \sigma_i \; ; \; -\frac{\partial \psi}{\partial \vartheta} = \varphi \tag{36}$$

$$\vartheta \dot{\lambda} = \sigma_i \dot{\delta}_i^P \geq 0 \tag{37}$$

$$\dot{\delta}_i^P = \frac{\partial \omega}{\partial \sigma_i} \tag{38}$$

FIRST LAW BECOMES

$$\int_{\alpha(t)}^{\beta(t)} [\tilde{q}_i]v_i \; d\zeta + (G-R)\dot{\alpha} = \int_{\alpha(t)}^{\beta(t)} [q_i]v_i \; d\zeta \geq 0 \tag{39}$$

WHERE

$$[\tilde{q}_i]v_i \equiv \sigma \frac{\partial \delta_i^P}{\partial t} - \vartheta \frac{\partial \varphi}{\partial t} = \sigma \frac{\partial \delta_i}{\partial t} - \frac{\partial \varepsilon}{\partial t} \tag{40}$$

SUBCRITICAL CRACK GROWTH ADMISSIBLE WHEN

$$\int_{\alpha(t)}^{\beta(t)} [\tilde{q}_i]v_i \; d\zeta > (R-G)\dot{\alpha} \tag{41}$$

WHEN $\dot{\alpha} = 0$ WE HAVE EVOLUTION OF THE C.Z. INTERNAL STATE VARIABLES

In general, thermodynamics does not allow to derive evolution laws for the internal state variables, thus for the kinematic variables that describe crack propagation and fatigue, some special assumptions can be made that allow us to derive a crack evolution law strictly from the first law of thermodynamics. For some cases of slow crack propagation, the principle of the minimum entropy production can be evoked, thus leading to a certain form of crack growth law.

CASE 3 - SLOW CRACK GROWTH
- DISSIPATIVE COHESIVE ZONE (ELASTO-PLASTIC)

ASSUME PRINCIPLE OF MINIMUM ENTROPY PRODUCTION HOLDS

$$\int_{\alpha(t)}^{\beta(t)} [q_i]v_i \, d\zeta = 0 \tag{42}$$

FROM FIRST LAW:

$$\dot{\alpha} = \frac{\int_\alpha^\beta \left(\sigma_i \frac{\partial \delta_i^T}{\partial t} - \vartheta \frac{\partial \varphi}{\partial t} \right) d\zeta}{R - G} \tag{43}$$

● CYCLIC LOADING

INTEGRATE OVER A CYCLE

$$\Delta\alpha = \frac{\Delta\Lambda - \Delta Q}{2\gamma_o - G_M} \tag{44}$$

SIMPLIFIED FORM

$$\Delta\alpha = \frac{\Delta\Lambda}{2\gamma_o - G_{Max}} \tag{45}$$

DISCONTINUOUS CRACK GROWTH

The analysis presented so far can be easily extended to describe discontinuous crack propagation (DCP). With reference to Fig. 2, we present a two-phase cohesive zone model inspired by the experimental work by Hertzberg, et al (Ref. 33). Proceeding as in the case of a single phase C.Z. model, assuming that the principle of minimum entropy production holds, we obtain an evolution equation for the phase separation coordinate ξ that allows to study DCP.

A VERY SIMPLE 2-PHASE MODEL (HERTZBERG, ET AL., 1979)

$$\int_{\alpha(t)}^{\beta(t)} (\sigma_i \frac{\partial \delta_i}{\partial t} - \frac{\partial \varepsilon}{\partial t})\ d\zeta + (G_\alpha - R_\alpha)\dot{\alpha} + (G_\xi - R_\xi)\dot{\xi} = \int_{\alpha(t)}^{\beta(t)} [q_i]v_i\ d\zeta \qquad (46)$$

where

$$G_\xi = \int_{\alpha(t)}^{\beta(t)} \sigma_i \frac{\partial \delta_i}{\partial \xi}\ d\zeta \ ; \ R_\xi = \int_{\alpha(t)}^{\beta(t)} \frac{\partial \varepsilon}{\partial \xi}\ d\zeta \qquad (47)$$

ASSUME
$$\dot{\alpha} = 0$$

$$\dot{\xi} > 0 \ ; \ 0 < G_\xi < R_\xi \qquad (48)$$

UNDER CYCLIC LOADING

$$\Delta \xi = \frac{\Delta\Lambda - \Delta Q}{R_{\xi M} - G_{\xi M}} \qquad (49)$$

SIMPLIFIED

$$\Delta \xi = \frac{\Delta\Lambda}{R_{\xi M} - G_{\xi M}} \qquad (50)$$

OTHER DISCONTINUOUS CRACK GROWTH MODELS

Very few models of DCP have been presented in the open literature. The ones mentioned below are those in Refs. 12 and 34. Further study of the thermodynamics of the process is certainly needed.

- **J.G. WILLIAMS, 1977**

  - **TWO PHASES**

  - **NOT THERMODYNAMICALLY BASED**

- **K. KADOTA & A. CHUDNOVSKY, 1992**

  - **SINGLE PHASE**

  - **BASED ON THE PREDICTION OF A PROCESS ZONE CRACK RESISTANCE DEGRADATION**

A very simple example of application of the DCP model presented is given. We have assumed that $G\xi_m = G\xi_{m_{max}}$ and $R\xi_m = X$ where X is the phase transformation energy per unit lengths of transformed material. The cohesive zone has been modeled as a two-phase Dugdale zone.

GEOMETRY:
- STRAIGHT CRACK IN UNBOUNDED MEDIUM

LOAD:
- UNIFORM TENSILE STRESS APPLIED AT INFINITY
- CYCLIC, FROM 0 TO T_0
  CASE1: $T_0 = 0.1$MPa
  CASE2: $T_0 = 0.2$MPa
- PLANE STRESS

MATERIAL SYSTEM:
- PS

PROPERTIES[*]:
- $E = 2.2$GPa
- $\sigma_{c.z.} = 18.0$MPa
- $f = 2.0$
- $\chi = 30.0$J/m^2

[*]Botsis et Al, Int. J. Fract., v.33, 1987, pp.263-276.

In Figs. 3 and 4 we have a schematic of the geometry, load conditions and detailed view of the cohesive zone.
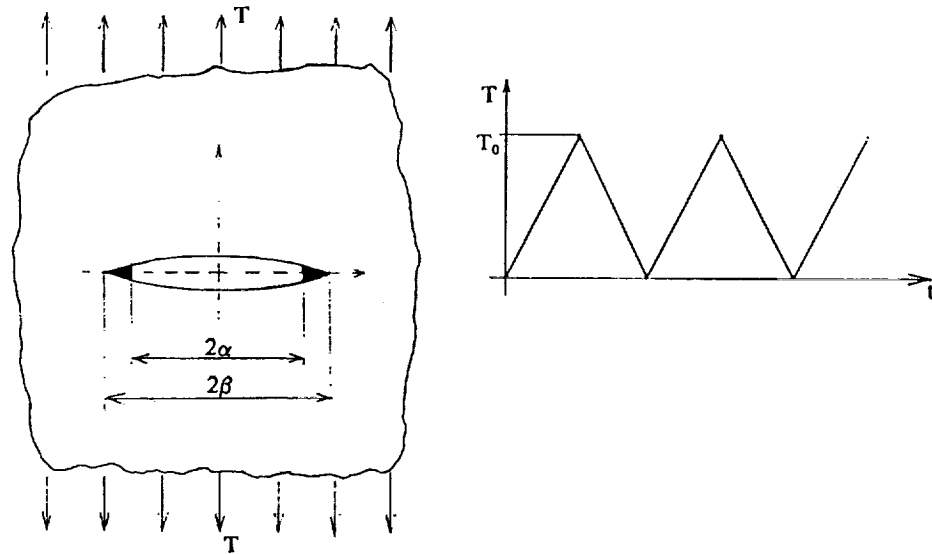
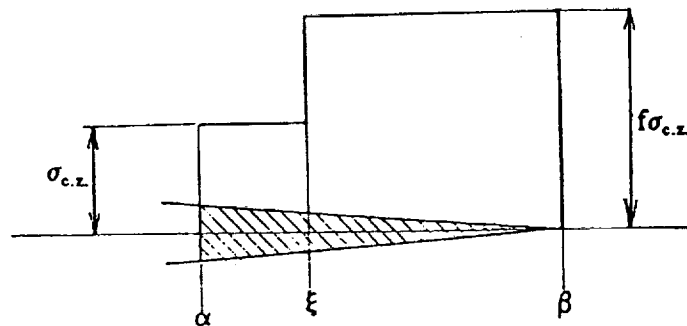

Figure 3 - Example geometry and load conditions

Figure 4 - Two-phase Dugdale model

FIGURE 5

The trend of C.Z. evolution obtained is shown in Fig. 5. It is easy to recognize the discontinuous crack growth pattern.
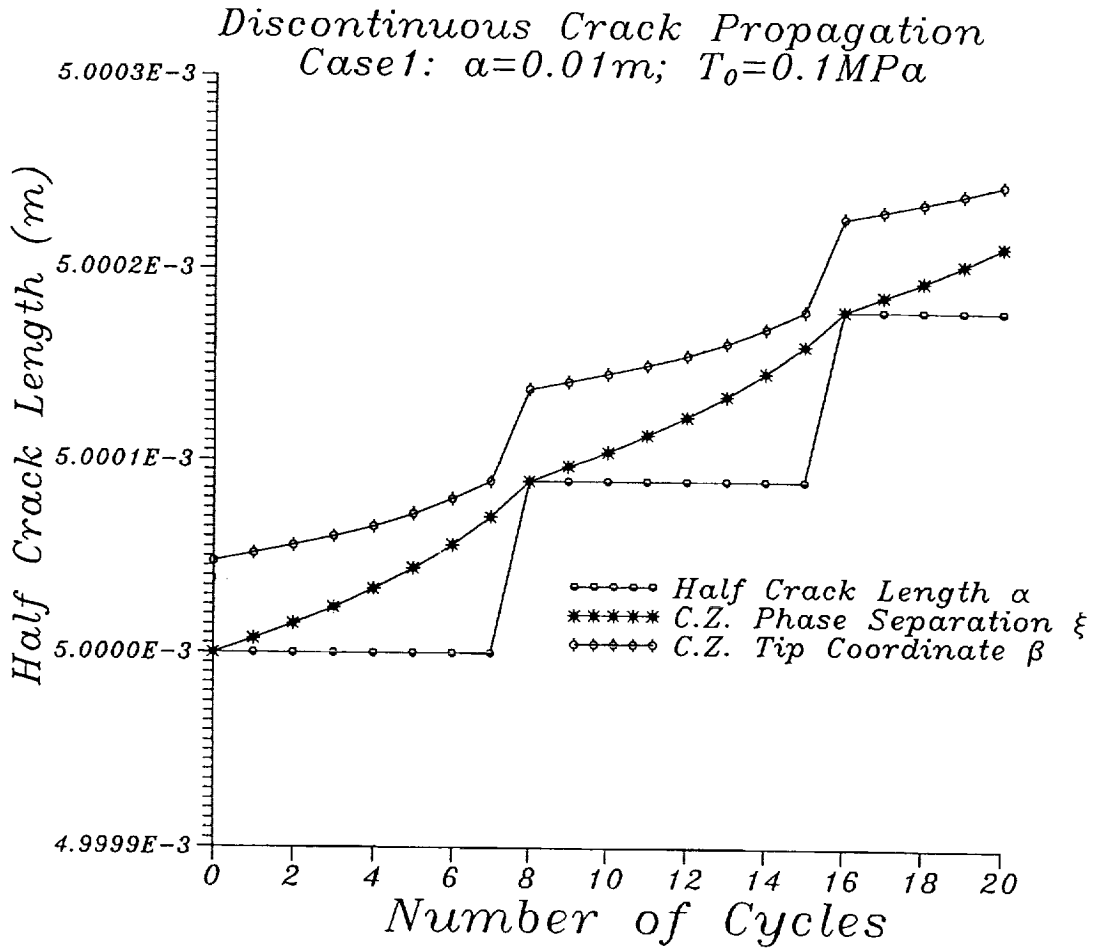

Figure 5 - C.Z. Evolution during DCP

FIGURE 6

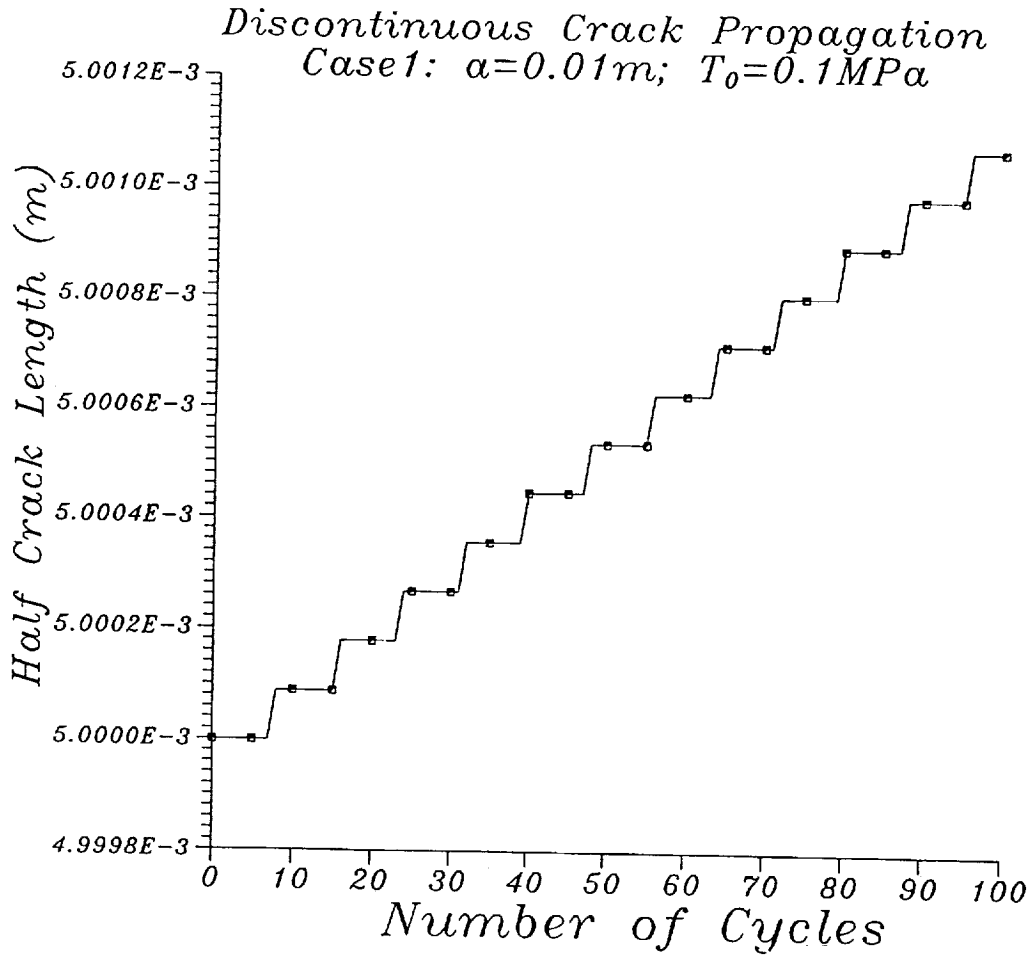Figure 6 shows the trend of the growth of α only.

Figure 6 - Discontinuous crack propagation

CONCLUSIONS

In this work a continuum thermodynamic analysis of a crack with a cohesive zone has been presented. In particular, the issue of thermodynamic admissibility of subcritical crack growth has been addressed. The theory espoused has been applied to the study of DCP and an approximated DCP law has been obtained. An example of application of the DCP law is provided.

- **APPLICATION OF THE CONTINUUM THERMODYNAMICS APPROACH TO THE CASE OF A CRACK WITH A COHESIVE ZONE**

- **DISCUSSION OF THE ADMISSIBILITY OF SUBCRITICAL CRACK GROWTH**

- **SUBCRITICAL GROWTH LAWS OBTAINED USING THE DISSIPATION EQUATION FOR FATIGUE AND DISCONTINUOUS CRACK PROPAGATION**

- **SIMPLE EXAMPLE OF APPLICATION OF THE DISCONTINUOUS CRACK GROWTH LAW**

FUTURE WORK

Further study is certainly necessary, especially toward a better characterization of the constitutive equations for the cohesive zone. Also necessary is the coupling of the presented thermodynamic analysis with elements of the kinetic theory of fracture in order to obtain more general crack advancement laws. A more accurate analysis is needed for the study of DCP together with a stability analysis. Possible applications of the theory include the study of delamination in laminated composites, R-toughening in ceramics and problems of matrix-fiber interface degradation in fiber reinforced composites.

- OBTAIN MORE REALISTIC C.Z. CONSTITUTIVE EQUATIONS

- STABILITY ANALYSIS OF THE CRACK PROPAGATION EVENT DURING DISCONTINUOUS CRACK GROWTH AND TRANSITION FROM D.C.P. TO STANDARD (SUBCRITICAL) CRACK GROWTH

- COMPARISON AND COUPLING OF THE PRESENT THEORY WITH THE LATEST RESULTS OF THE KINETIC THEORY OF FRACTURE (SUBCRITICAL CRACK GROWTH IN QUASI-PERFECTLY BRITTLE SYSTEMS)

- POSSIBLE APPLICATIONS:
  - FRACTURE OF POLYMERS
  - DELAMINATION IN LAMINATED COMPOSITES
  - FRACTURE OF FIBER-MATRIX INTERFACES IN MMC

REFERENCES

1. Paris, P. C., "Twenty Years of Reflection on Questions Involving Fatigue Crack Growth. Part I: Historical Observations and Perspectives," *Fatigue Thresholds*, J. Backlund, A. F. Blom, C. J. Beevers (eds.), Chemelem, London, Vol. 1, 1982, pp. 3-10.

2. Paris, P. C., *The Growth of Cracks Due to the Variations in Loads*, Ph.D. Thesis, Lehigh University, Bethlehem, Pennsylvania, 1962.

3. Paris, P. C., "The Fracture Mechanics Approach to Fatigue," *Fatigue - An Interdisciplinary Approach*, Syracuse University Press, Syracuse, New York, 1964.

4. Head, A. K., "The Growth of Fatigue Cracks," *Philosophical Magazine*, Vol. 44, Series 7, 1953.

5. McClintock, F. A., "On the Plasticity of the Growth of Fatigue Cracks," *Fracture of Solids*, John Wiley & Sons, 1963.

6. Rice, J. R., "Mechanics of Crack Tip Deformation and Extension by Fatigue," *Fatigue Crack Propagation*, ASTP STP 415, American Society for Testing and Materials, 1967, pp. 247-309.

7. Frost, N. E., Dixon, J. R., "A Theory of Fatigue Crack Growth," *International Journal of Fracture Mechanics*, Vol. 3, 1967, pp. 301-306.

8. Hertzberg, R. W., *Deformation and Fracture Mechanics of Engineering Materials*, John Wiley & Sons, 1976.

9. Kanninen, M. F. and Popelar, C. H., *Advanced Fracture Mechanics*, Oxford University Press, 1985.

10. Andrews, E. H., *Fracture in Polymers*, Aberdeen University Press, 1968.

11. Hertzberg, R. W. and Mason, J. A., *Fatigue of Engineering Plastics*, Academic Press, 1980.

12. Williams, J. G., *Fracture Mechanics of Polymers*, Ellis Horwood, Ltd., 1987.

13. Kinloch, A. J. and Young, R. J., *Fracture Behavior of Polymers*, Elsevier Applied Science, 1983.

14. Masaki, K., "Life Prediction and Fatigue," *Superalloy, Supercomposites and Superceramics*, J. K. Tien and T. Canfield (eds.), Academic Press, 1989, pp. 413-437.

15. Cherepanov, G. R., "Cracks in Solids," *International Journal of Solids and Structures*, Vol. 4, 1968, pp. 811-831.

16. Izumi, Y., Fine, M. E. and Mura, T., "Energy Considerations in Fatigue Crack Propagation," *International Journal of Fracture*, Vol. 17, 1981, pp. 15-25.

17. Chudnovsky, A., Dunaevsky, V. and Khandogin, V., "On the Quasistatic Growth of Cracks," *Archives of Mechanics*, Vol. 30, 1978, pp. 165-174.

18. Chudnovsky, A., *Crack Layer Theory*, NASA CR-174634, 1984.

19. Short, J. S., Hoeppner, D. W., "A Global/Local Theory of Fatigue Crack Propagation," *Engineering Fracture Mechanics*, Vol. 33, 1989, pp. 175-184.

20. Griffith, A. A., "The Phenomena of Rupture and Flow in Solids," *Philosophical Transaction of the Royal Society of London*, A221, 1921, pp. 163-197.

21. Cherepanov, G. P., *Mechanics of Brittle Fracture*, McGraw-Hill, 1979.

22. Rice, J. R., "Mathematical Analysis in the Mechanics of Fracture," *Fracture*, Vol. 2, Academic Press, 1968, pp. 191-311.

23. Rice, J. R., "Thermodynamics of the Quasi-Static Growth of Griffith Cracks," *Journal of Mechanics and Physics of Solids*, Vol. 26, 1978, pp. 61-78.

24. Gurtin, M. E., "On the Energy Release Rate in Quasi-Static Elastic Crack Propagation," *Journal of Elasticity*, Vol. 9, 1979, pp. 187-195.

25. Gurtin, M. E., "Thermodynamics and the Griffith Criterion for Brittle Fracture," *International Journal of Solids and Structures*, Vol. 15, 1979, pp. 553-560.

26. Gurtin, M. E., "Thermodynamics and the Cohesive Zone in Fracture," *Zeitschirift fur Angewandte Mathematik und Physik (ZAMP)*, Vol. 30, 1979, pp. 991-1003.

27. Nguyen, Q. S., "Normal Dissipativity and Energy Criteria in Fracture," *Variational Methods in the Mechanics of Solids*, IUTAM Symposium, Evanston, Pergamon Press, 1980, pp. 254-259.

28. Nguyen, Q. S., "Methodes Energetiques en Mecanique de La Rupture," *Journal de Mecanique*, Vol. 19, 1980, pp. 363-386.

29. Nguyen, Q. S., "A Thermodynamic Description of the Running Crack Problem," *Three-Dimensional Constitutive Relations and Ductile Fracture*, IUTAM Symposium, Dourdan, North Holland, 1980, pp. 315-330.

30. Nguyen, Q. S., "Bifurcation et Stabilite des Systemes Irreversibles Obeisant au Principe de Dissipation Maximale," Journal de Mecanique Theorique Applique, Vol. 3, 1984, pp. 41-61.

31. Nguyen, Q. S., "Bifurcation et Analyse Post-Critique en Rupture Fragile et en Plasticite," C.R. Acad. Sci. Paris, Vol. 300, Serie II, 1985, pp. 191-194.

32. Nguyen, Q. S., "Critere de Propagation en Rupture Ductile," C.R. Acad. Sci. Paris, Vol. 301, Serie II, 1985, pp. 567-570.

33. Hertzberg, R. W., Skibo, M. D., Manson, J. A., "Fatigue Fracture Micromechanisms in Engineering Plastics," Fatigue Mechanisms, J. T. Fond (ed.), ASTM STP-675, 1979, pp. 471-500.

34. Kadota, K. and Chudnovsky, A., "Constitutive Equations of Crack Layer Growth," Recent Advances in Damage Mechanics and Plasticity, AMD Vol. 132/MD Vol. 30, J. W. Ju (ed.), ASME, NY, 1992, pp. 115-130.

35. Botsis, J., Chudnovsky, A. and Moet, A., "Fatigue Crack Layer Propagation in Polystyrene - Part I," International Journal of Fracture, Vol. 33, 1987, pp. 263-276.

36. Botsis, J., Chudnovsky, A. and Moet, A., "Fatigue Crack Layer Propagation in Polystyrene - Part II," International Journal of Fracture, Vol. 33, 1987, pp. 277-284.

N94-22612

Modeling of Failure and Response to Laminated Composites Subjected to In-Plane Loads

Iqbal Shahid and Fu-Kuo Chang
Stanford University
Stanford, CA

CURRENT STATUS

An analytical model has been developed for predicting the response of laminated composites with or without a cutout and subjected to in-plane tensile and shear loads. Material damage resulting from the loads in terms of matrix cracking, fiber-matrix shearing, and fiber breakage was considered in the model. Delamination, an out-of-plane failure mode, was excluded from the model.
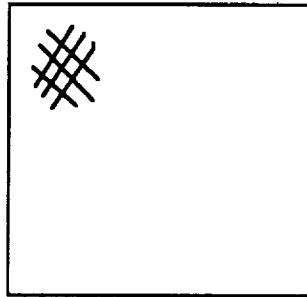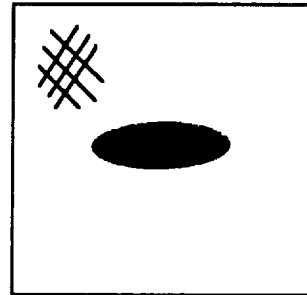
TENSION   SHEAR

GIVEN : GEOMETRY, LAYUP, LOADS

PREDICT: ° DAMAGE IN COMPOSITES

MATRIX CRACKING

FIBER-MATRIX SHEARING

FIBER BREAKAGE

° RESIDUAL STIFFNESS

## ° RESPONSE AS A FUNCTION OF LOADS

° FAILURE

WHAT DO WE NEED?

In order to accurately predict the response of the laminates, the model must be capable of predicting the state of damage as a function of the applied load, relating the damage state to the loss of material properties, and calculating stresses and strains everywhere inside the materials. Accordingly, the proposed analytical model consists of three parts: constitutive modeling, failure analysis and stress analysis.

LOAD

↓

```
┌─────────────────────────────────┐
│ DAMAGE STATE                    │
│       ° FAILURE MODE            │
│       ° EXTENT OF DAMAGE        │
└─────────────────────────────────┘
```

```
┌─────────────────────────────────┐
│ CONSTITUTIVE EQUATIONS          │
│       ° DAMAGE STATE            │
└─────────────────────────────────┘
```

```
┌─────────────────────────────────┐
│ STRESS ANALYSIS                 │
└─────────────────────────────────┘
```
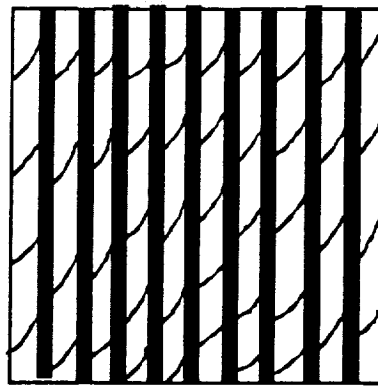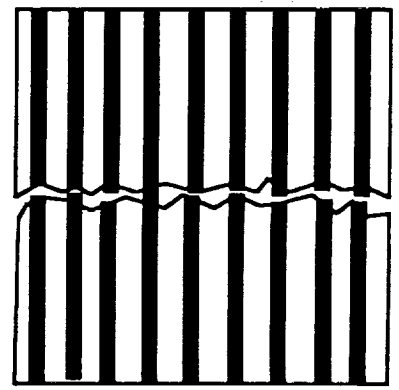
↓

RESPONSE
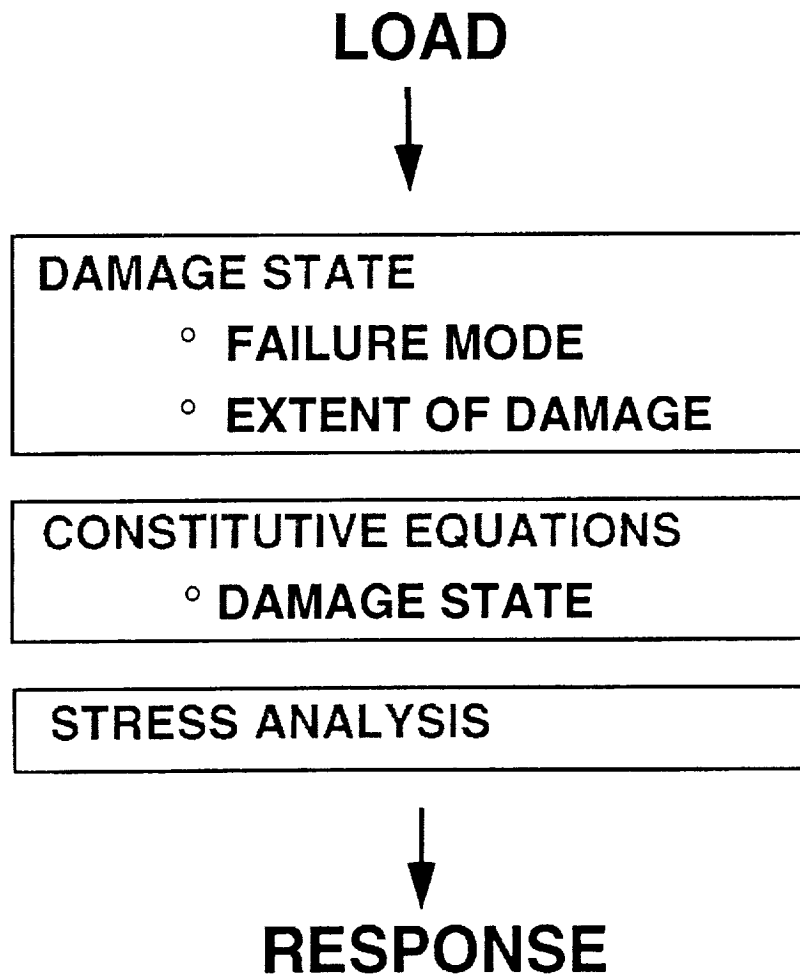
FAILURE MODES

The three basic in-plane failure modes of a single unidirectional ply considered in the model are matrix cracking, fiber-matrix shearing, and fiber breakage.
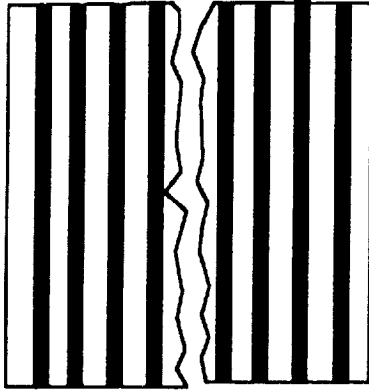
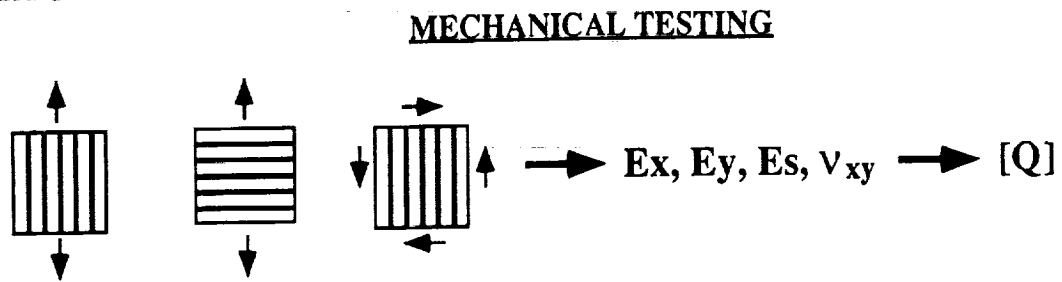**MATRIX CRACKING**

FIBER-MATRIX SHEAR-OUT

FIBER BREAKAGE

CONSTITUTIVE MODELING

The constitutive equations of a unidirectional ply in an undamaged state can be characterized by standard mechanical testing. However, once damage occurs in a ply within a multidirectional laminate, the material properties of the ply need to be determined in order to construct the constitutive equations for the damaged laminate. Therefore, the proposed model was based on continuum mechanics whereby the damaged ply in a laminate was treated as a continuous body with degraded material properties.

PLY STIFFNESS (UNDAMAGED STIFFNESS, DAMAGE STATE)

## UNDAMAGED PLY:

MECHANICAL TESTING

$E_x, E_y, E_s, \nu_{xy} \longrightarrow [Q]$

DAMAGED PLY: (IN LAMINATE)

O MATRIX CRACKING

O FIBER-MATRIX SHEAR-OUT

O FIBER BREAKAGE

$E_x^D, E_y^D, E_s^D, \nu_{xy}^D \longrightarrow [Q^D] = ?$

MATRIX CRACKING

In order to determine the effect of matrix cracking on the reduction of the stiffness of a unidirectional ply in a laminate, crack density was selected as the damage parameter for characterizing the damage state of matrix cracking.
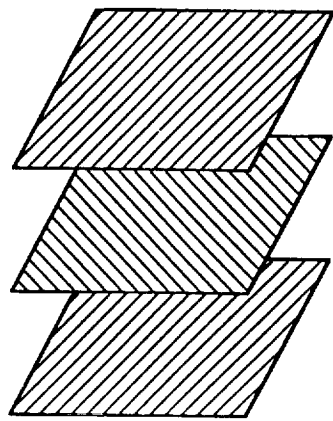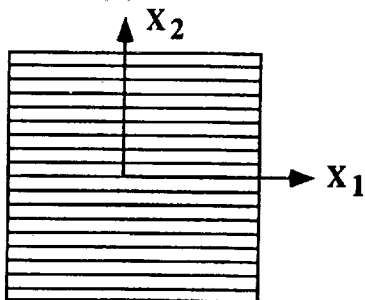
LAMINATION EFFECT

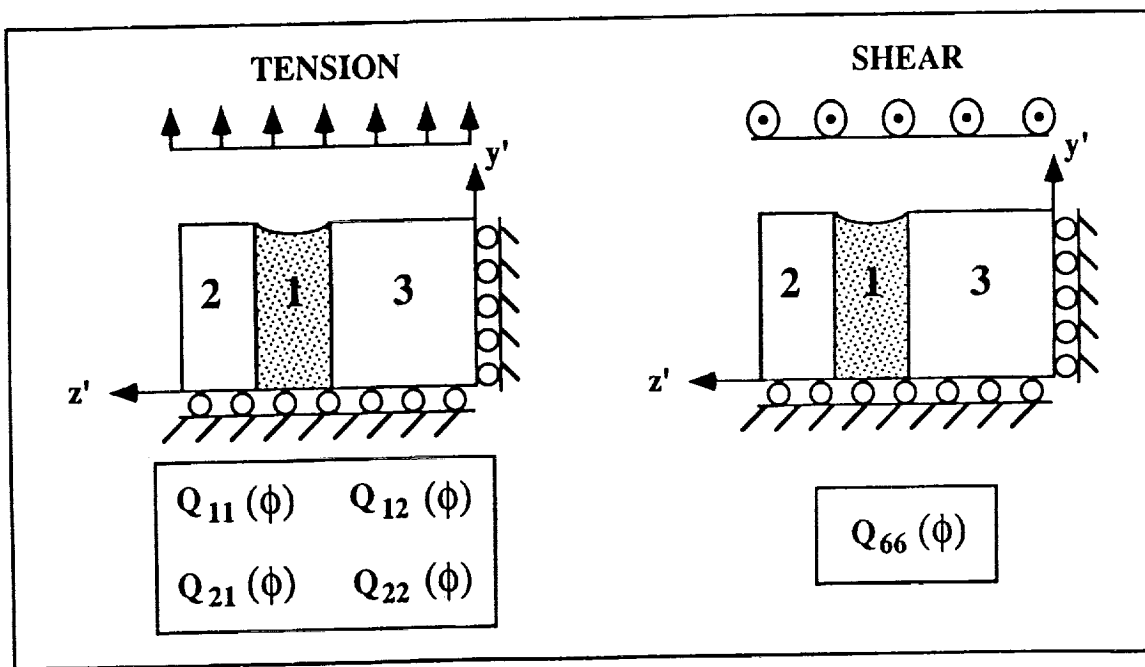MATRIX CRACK DENSITY

(ϕ)

FOR EACH PLY

X_2

X_1

EFFECTIVE PLY STIFFNESS

$$[Q^D] = \begin{bmatrix} Q_{11}(\phi) & Q_{12}(\phi) & 0 \\ Q_{21}(\phi) & Q_{22}(\phi) & 0 \\ 0 & 0 & Q_{66}(\phi) \end{bmatrix}$$

C1-2

A constitutive model was developed for characterizing the material properties of a ply in a symmetric laminate as a function of its own crack density. For a given crack density in a ply whose fiber direction may not be parallel to the global x-axis, the model first rotates the laminate such that the fiber direction of the cracked ply is aligned with the x-axis. It is then assumed that all the matrix cracks in the ply are uniformly distributed. As a result, a unit-cell of the laminate can be selected as a representative volume of the cracked laminate. The representative volume may be comprised of up to three sublaminates labeled as 1, 2 and 3 in the figure.

- **ORTHOTROPIC SUBLAMINATES ASSUMPTION**
- **2-D ELASTICITY ANALYSIS**

- **REPEAT PROCEDURE FOR ALL PLIES OF THE LAMINATE**

MATRIX CRACKING

In the constitutive model it was further assumed that the sublaminates 2 and 3 could be treated as homogeneous and orthotropic materials. Accordingly, the three-dimensional volume could be reduced to a two-dimensional element. By applying a far-field tensile or shear load, the material properties of the cracked ply (sublaminate 1) as a function of the crack density could be calculated from a two-dimensional elasticity theory. The aforementioned procedure was then applied to each of the plies in a laminate for any given crack density.

APPROACH

REPRESENTATIVE ELEMENT
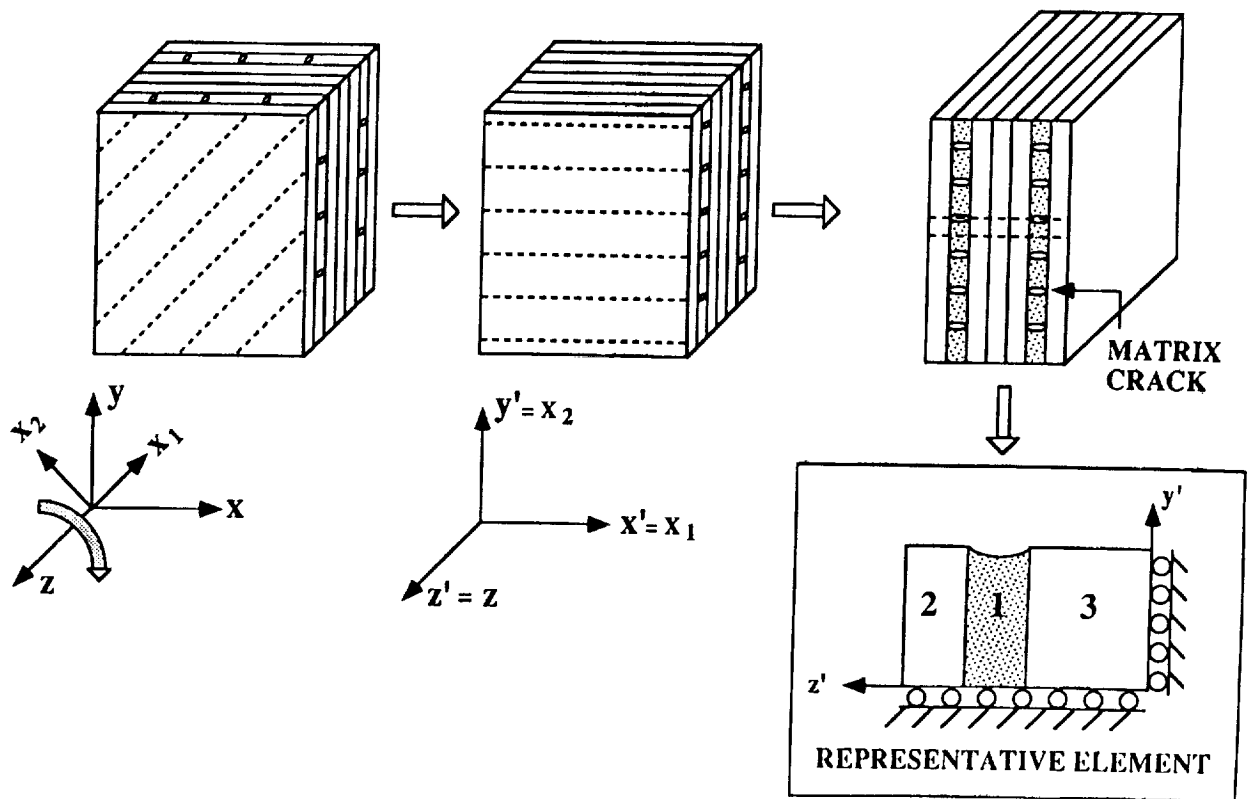
FIBER-MATRIX SHEAR-OUT

Once the applied load continued to increase, the plies in the laminate may have failed due to either fiber-matrix shearing or fiber breakage, leading to catastrophic failure of the laminate. Fiber-matrix shear-out failure could be attributed to interfacial debonding and slipping or nonlinear elasticity of the material. The aforementioned elasticity theory for matrix cracks could not be applied to characterize the reduction of material properties resulting from the shear-out failure. To account for interfacial debonding and slipping, continuum damage mechanics was adopted based on the concept proposed by Krajcinovic and Fonseka. Nonlinear material response was considered in the model through the shear stress-shear strain relationship.

HIGH SHEAR DEFORMATION

$\downarrow$

● FIBER-MATRIX INTERFACE DEBONDING, SLIP ETC.

● NONLINEAR SHEAR DEFORMATION
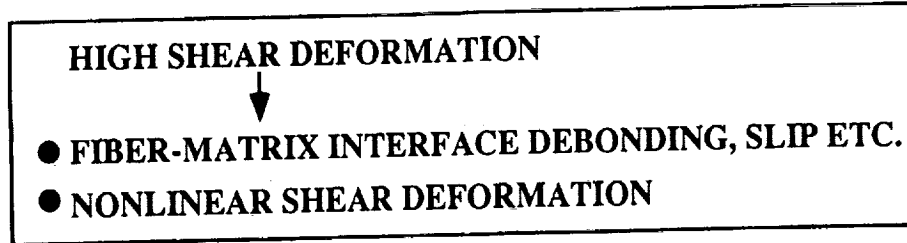
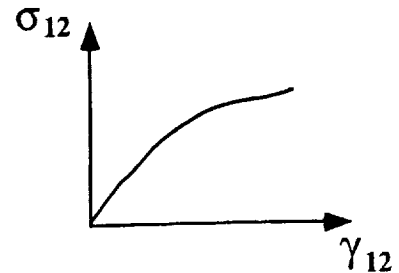● **CONTINUUM DAMAGE MECHANICS:** (Krajcinovic and Fonseka, 1981)

$$Q_{66}^{D} = Q_{66}(\phi)\, d_s \qquad d_s = e^{-\left(\frac{\phi}{\phi_0}\right)^{\eta}}$$

ϕ_0 = SATURATION CRACK DENSITY

η = SHAPE PARAMETER

● **PLY SHEAR STRESS-SHEAR STRAIN:**

Hahn: $\gamma_{12} = \dfrac{\sigma_{12}}{Q_{66}^{D}} + \alpha\left(\dfrac{\sigma_{12}}{Q_{66}^{D}}\right)^{3}$

92

Based on Rosen's cumulative weakening failure theory, failure of a unidirectional ply under tension occurs only when there are enough fiber breaks that occur within a critical area characterized by the fiber interaction distance δ, which is the maximum distance within which one fiber break would affect the stresses of the neighboring fibers. Accordingly, not only stresses but also the area within which fiber breaks occur are essential for characterizing fiber failure of a unidirectional composite.

UNIDIRECTIONAL COMPOSITE:

CUMULATIVE WEAKENING FAILURE (Rosen, 1964)

FAILURE OF UNIDIRECTIONAL PLY OCCURS AT THE WEAKEST CROSS SECTION

$\delta \longleftarrow$ FIBER INTERACTION ZONE
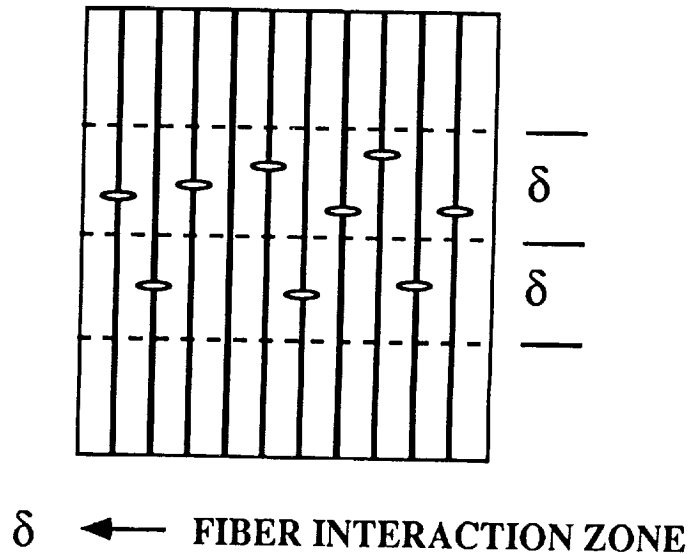
FIBER BREAKAGE

A hypothesis was postulated that stiffness reduction of a unidirectional composite due to fiber breakage is related to the extent of the area in which fiber breakage occurs.

NOTCHED COMPOSITE:
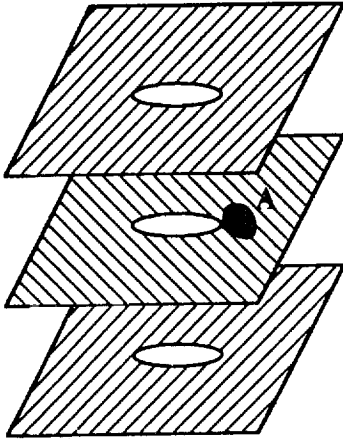
HYPOTHESIS:

STIFFNESS REDUCTION IS FUNCTION OF FIBER BREAKAGE AREA (A)

$$d_f = e^{-\left(\frac{A}{\delta^2}\right)^{\beta}}$$

A = FIBER BREAKAGE AREA

β = SHAPE PARAMETER

$$[Q^D] = \begin{bmatrix} Q_{11} & Q_{12} & 0 \\ Q_{21} & Q_{22} & 0 \\ 0 & 0 & Q_{66} \end{bmatrix} \begin{bmatrix} d_f & 0 & 0 \\ 0 & d_f & 0 \\ 0 & 0 & d_f \end{bmatrix}$$

CONSTITUTIVE MODEL

The effective material properties of a single ply within a symmetric laminate can be related to undamaged material properties and damage state with three different failure modes.

- ## WITHOUT SHEAR NON-LINEARITY

$$\{\sigma\} = [Q^D]\{\varepsilon\}$$

<div align="center">

MATRIX CRACKING   FIBER-MATRIX SHEAR-OUT   FIBER BREAKAGE

</div>

$$[Q^D] = \begin{bmatrix} Q_{11}(\phi) & Q_{12}(\phi) & 0 \\ Q_{21}(\phi) & Q_{22}(\phi) & 0 \\ 0 & 0 & Q_{66}(\phi) \end{bmatrix} \begin{bmatrix} 1 & 0 & 0 \\ 0 & 1 & 0 \\ 0 & 0 & d_s \end{bmatrix} \begin{bmatrix} d_f & 0 & 0 \\ 0 & d_f & 0 \\ 0 & 0 & d_f \end{bmatrix}$$

- ## WITH SHEAR NON-LINEARITY

$$\{d\sigma\} = [Q^D]^t\{d\varepsilon\}$$

DAMAGE GROWTH CRITERIA

Modified Hashin Failure Criteria were adopted for predicting the mode and state of damage of a ply in a laminate. The stresses used in the criteria are the effective stresses obtained from the effective properties. The effective strengths of the ply are no longer treated as constants, but may vary as a function of crack density (damage state).

PREDICT MODE OF FAILURE AND DAMAGE STATE

MATRIX CRACKING
$$\left(\frac{\sigma_{22}}{Y_t(\phi)}\right)^2 + \left(\frac{\sigma_{12}}{S(\phi)}\right)^2 \geqq 1$$

FIBER-MATRIX SHEAR-OUT
$$\left(\frac{\sigma_{11}}{X_t}\right)^2 + \left(\frac{\sigma_{12}}{S(\phi)}\right)^2 \geqq 1$$

FIBER BREAKAGE
$$\left(\frac{\sigma_{11}}{X_t}\right)^2 \geqq 1$$

$$\boxed{Y_t(\phi) = ? \qquad S(\phi) = ?}$$

EFFECTIVE STRENGTHS

The effective transverse tensile and shear strengths at crack density ϕ are defined as the minimum stresses that are required to generate crack density ϕ in the ply. A model was proposed based on the elasticity theory and fracture mechanics to characterize the effective strengths as a function of crack density.

$Y_t (\phi)$ = MINIMUM TRANSVERSE STRESS REQUIRED TO GENERATE CRACK DENSITY ϕ

$S (\phi)$ = MINIMUM SHEAR STRESS REQUIRED TO GENERATE CRACK DENSITY ϕ
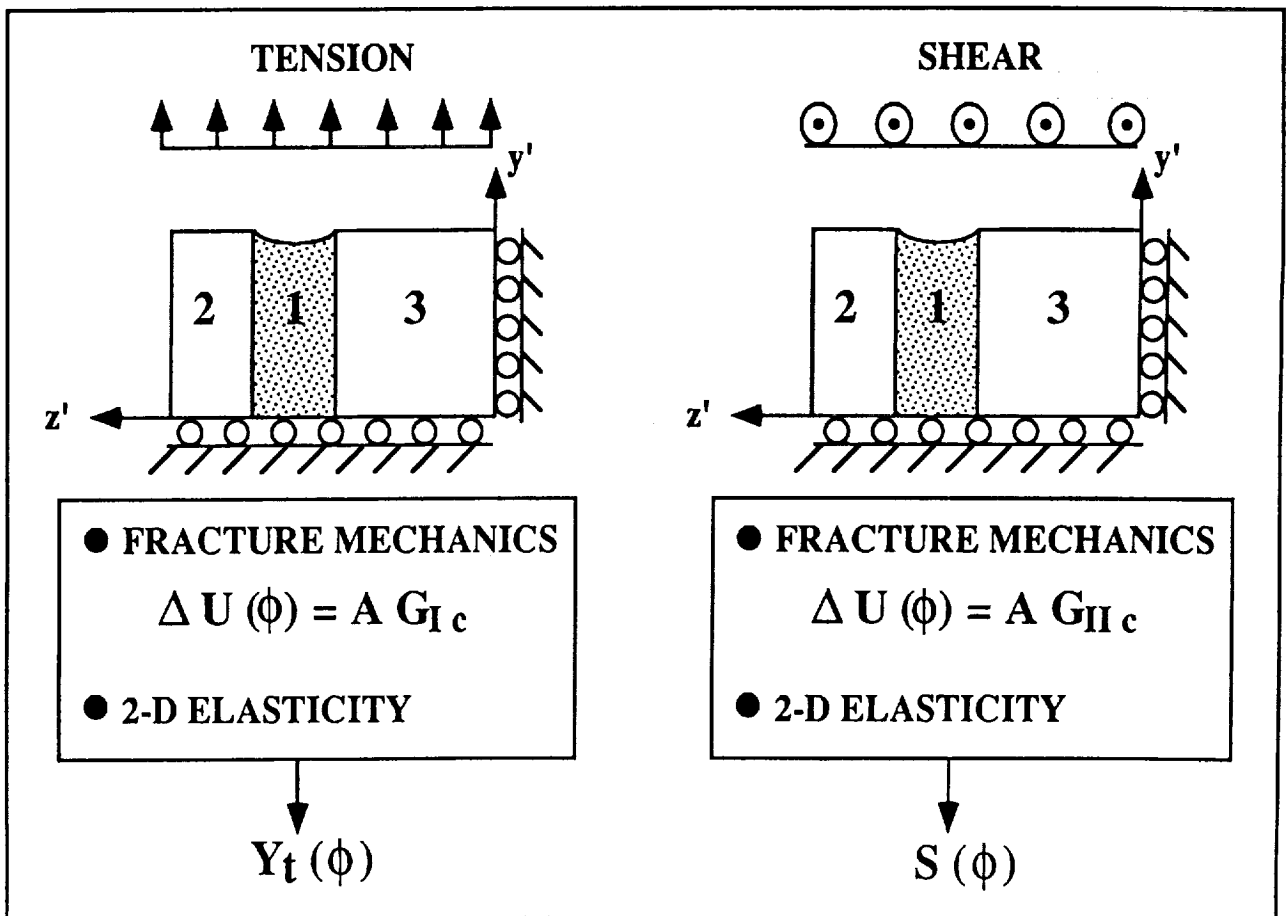
FLOWCHART

A finite element analysis has been developed based on the proposed model. The flowchart of the analysis is presented.

```
                    ┌──────────────────────────┐
                    │  GEOMETRY                │
                    │  MATERIAL AND LAYUP      │
                    │  LOADING                 │
                    └──────────────────────────┘
                                │
                                ▼
        ┌──────────────►  STRESS ANALYSIS  ◄──────────────┐
        │                       │                          │
┌───────────────────┐          │              ┌──────────────────────────┐
│     UPDATE         │          │              │       INCREASE           │
│ CONSTITUTIVE       │          │              │  LOAD    │ CYCLE   │     │
│ RELATION           │          │              │ (STATIC) │(FATIGUE)│     │
│ UPDATE STRESSES    │          │              └──────────────────────────┘
└───────────────────┘          ▼                          ▲
        ▲            ┌──────────────────────┐             │
        │            │ GROWTH CRITERIA      │             │
        │            │ MATRIX CRACKING      │    NO        │
   FAILURE           │ SHEAR-OUT            │  FAILURE     │
        │            │ FIBER BREAKAGE       │             │
     MODE            │                      │             │
     STATE           │  ┌────────────────┐  │             │
                     │  │ DELAMINATION   │  │             │
                     │  └────────────────┘  │             │
                     └──────────────────────┘
                                │
                                ▼
                     ┌──────────────────────┐
                     │  ULTIMATE FAILURE    │
                     └──────────────────────┘
```
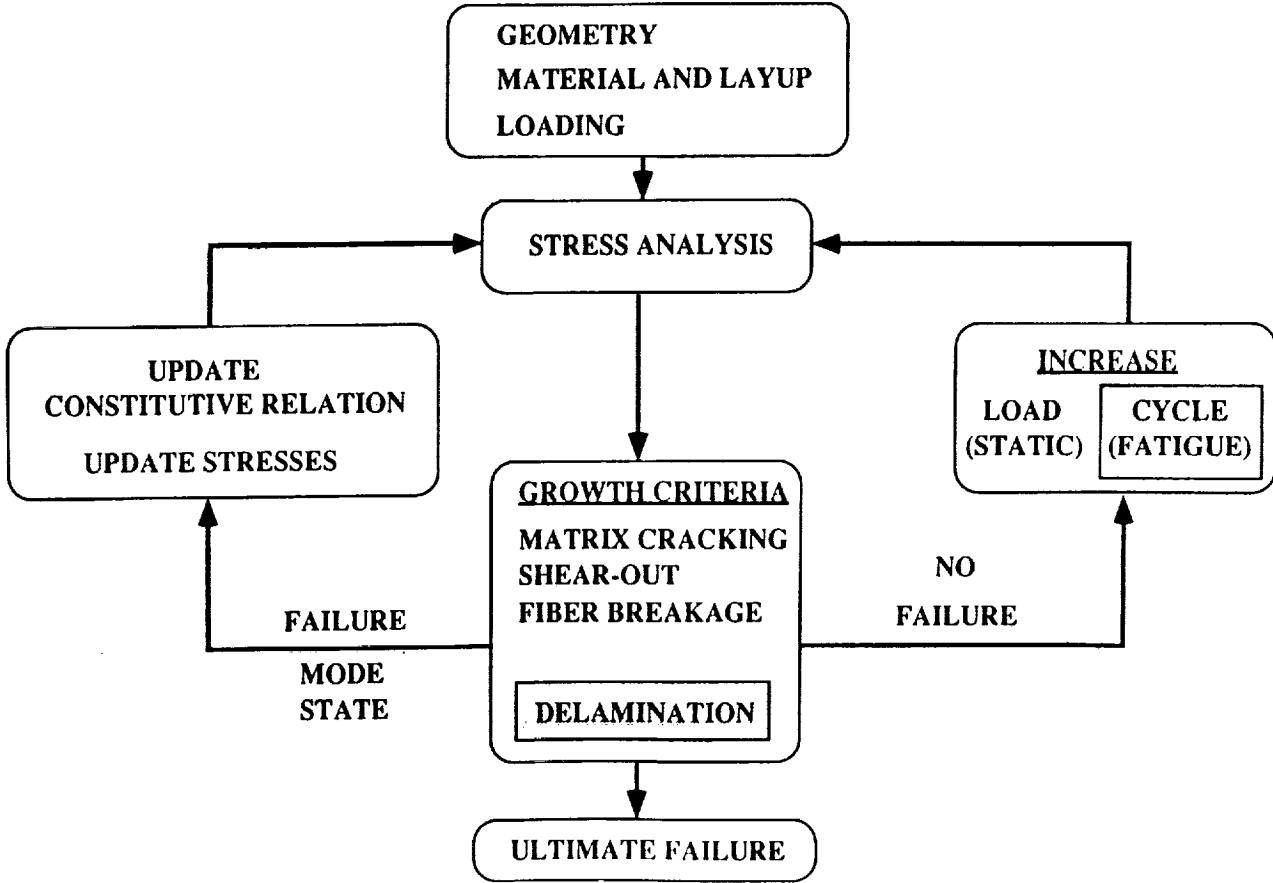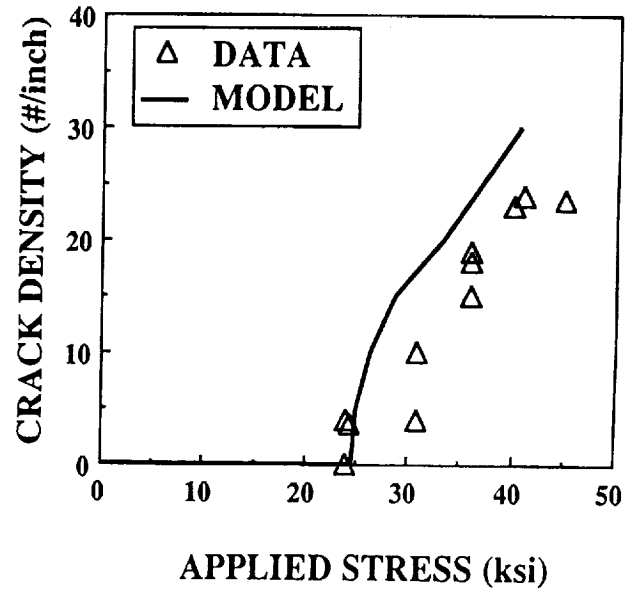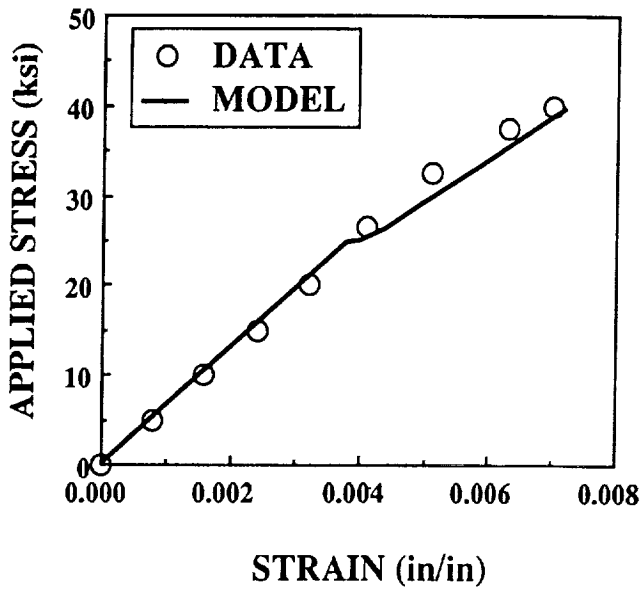
Comparison between the model prediction and the test data. A $[0/90_2]_s$ composite subjected to a $10°$ off axis uniaxial tensile load.
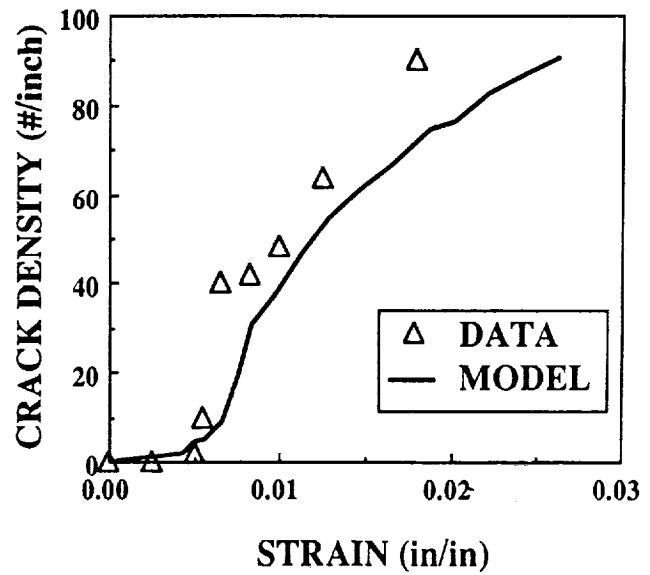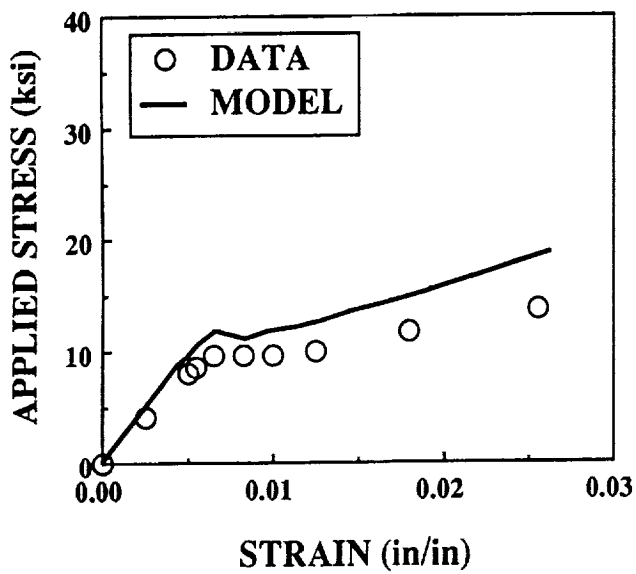
AS4/3501-6

$[0/90_2]_s$

$10°$ Off-Axis Tensile Loading

(Daniel and tsai, 1991)

Comparison between the model prediction and the test data. A [60/90/-60/60/90/-60/90]ₛ composite subjected to a uniaxial tensile load.

AS4/3502

$[60/90/-60/90/60/90/-60/\overline{90}]_S$

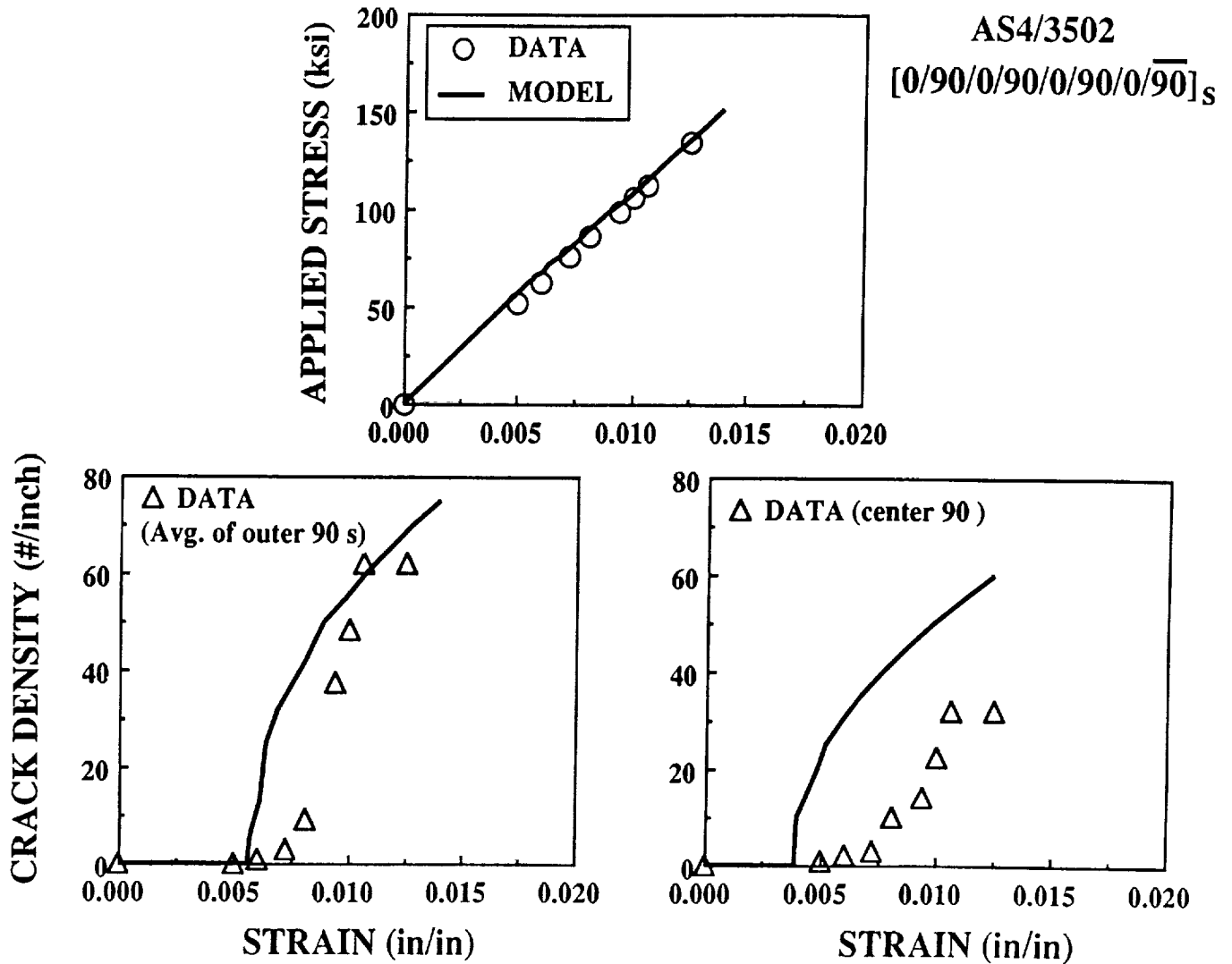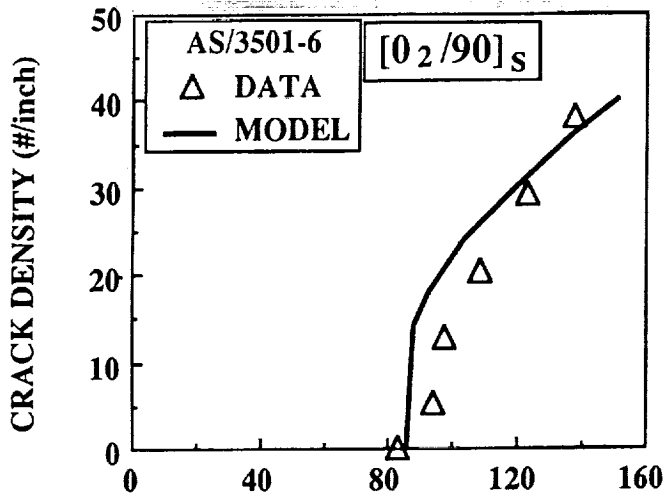(Kistner et al., 1985)

AS4/3502 [0/90/0/90/0/90/0/90]s

Comparison between the model prediction and the test data. A [0/90/0/90/0/90/0/90]s composite subjected to a uniaxial tensile load.

AS4/3502
[0/90/0/90/0/90/0/$\overline{90}$]$_S$

Comparison between the model prediction and the test data. Cross-ply composites subjected to a uniaxial tensile load.

Comparison between the model prediction and the test data. A [45/90/-45/90/45/90/-45/90]ₛ composite subjected to a uniaxial tensile load.
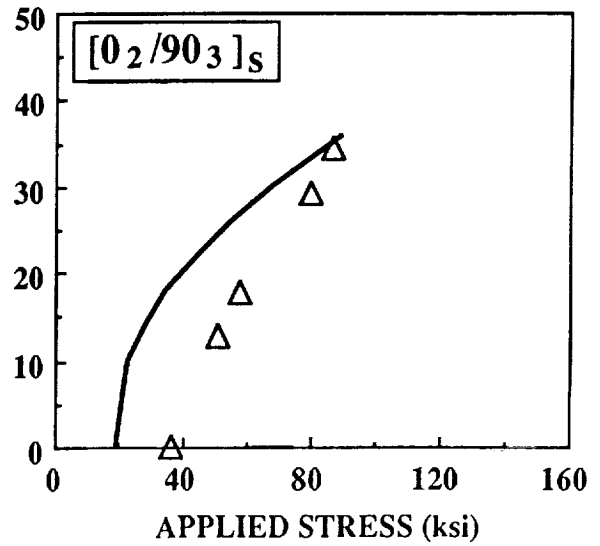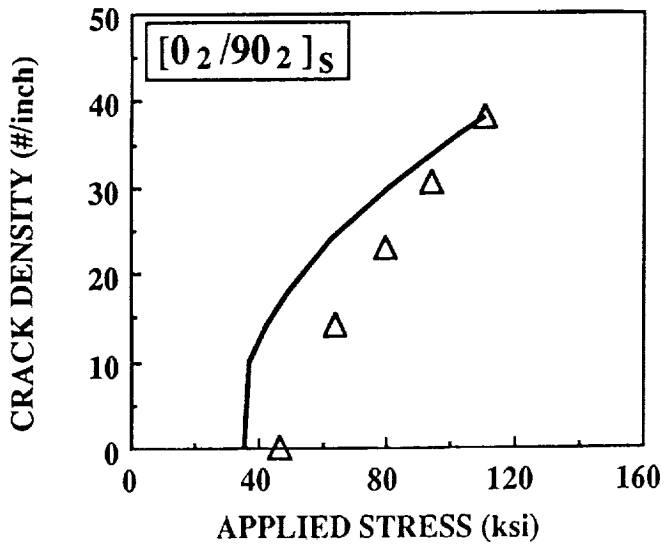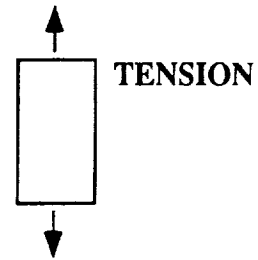
AS4/3502

[45/90/-45/90/45/90/-45/$\overline{90}$]ₛ

(Kistner et al., 1985)
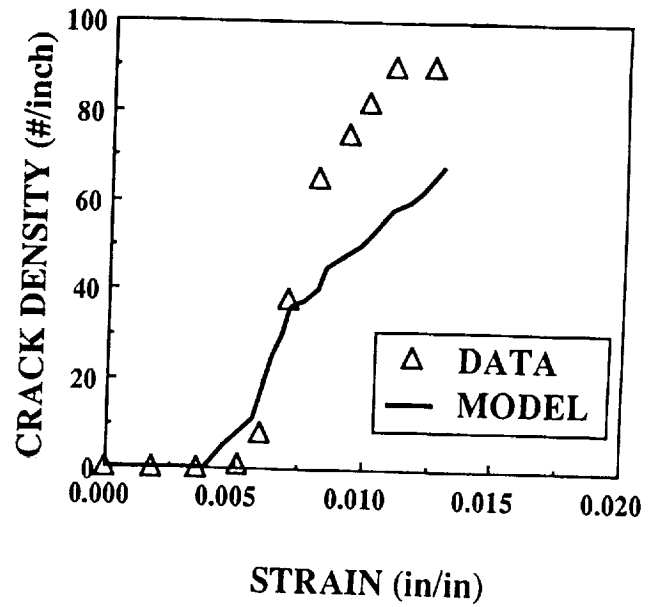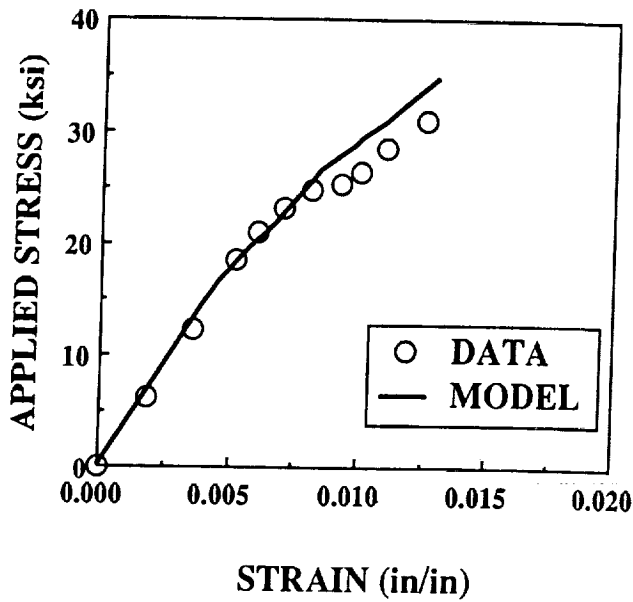
RAIL SHEAR SPECIMEN

A typical finite element mesh used in the calculation for rail shear specimens.
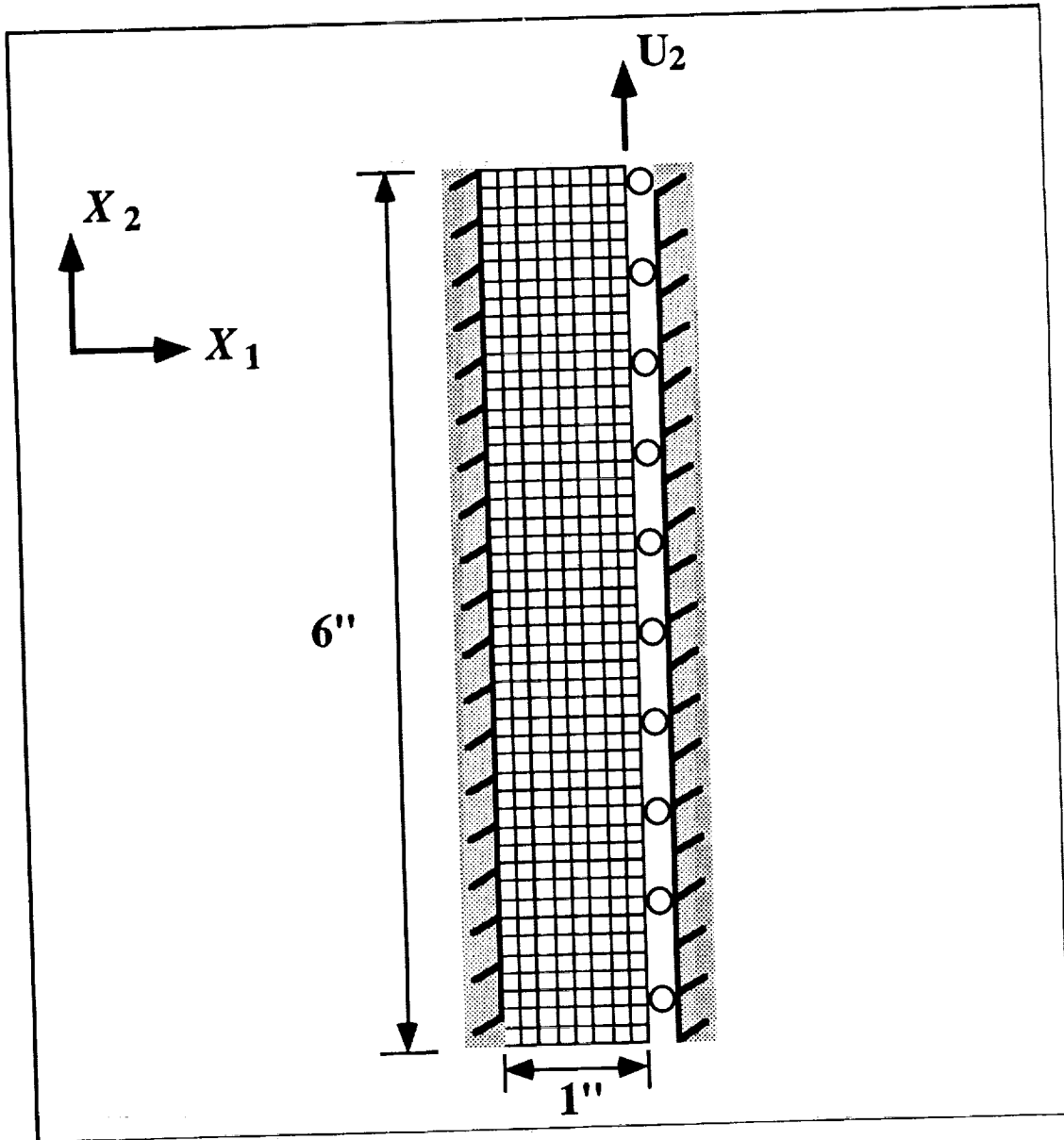
IN-PLANE SHEAR STRENGTH

Comparison between the prediction of rail shear strength and the measurement.
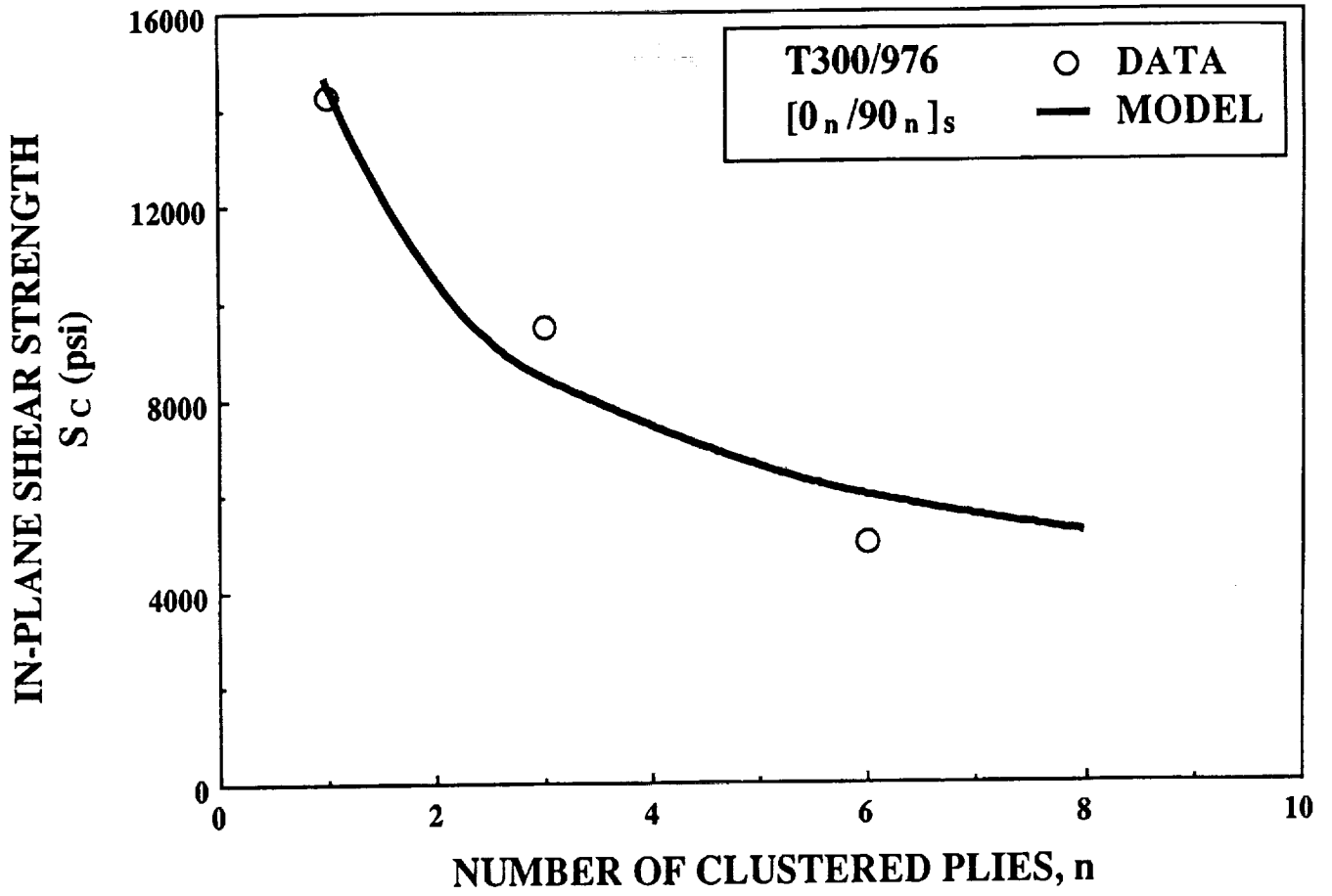
RAIL SHEAR TEST SIMULATION

The predicted matrix crack density distribution in a $[0_4/90_2]_s$ shear specimen near 90% of the final failure load.

MATRIX CRACK DENSITY DISTRIBUTION

T300/976
$[0_4/90_2]_s$

$0 <= CD < 5$
$5 <= CD < 10$
$10 <= CD < 20$
$20 <= CD < 25$
$CD > 25$
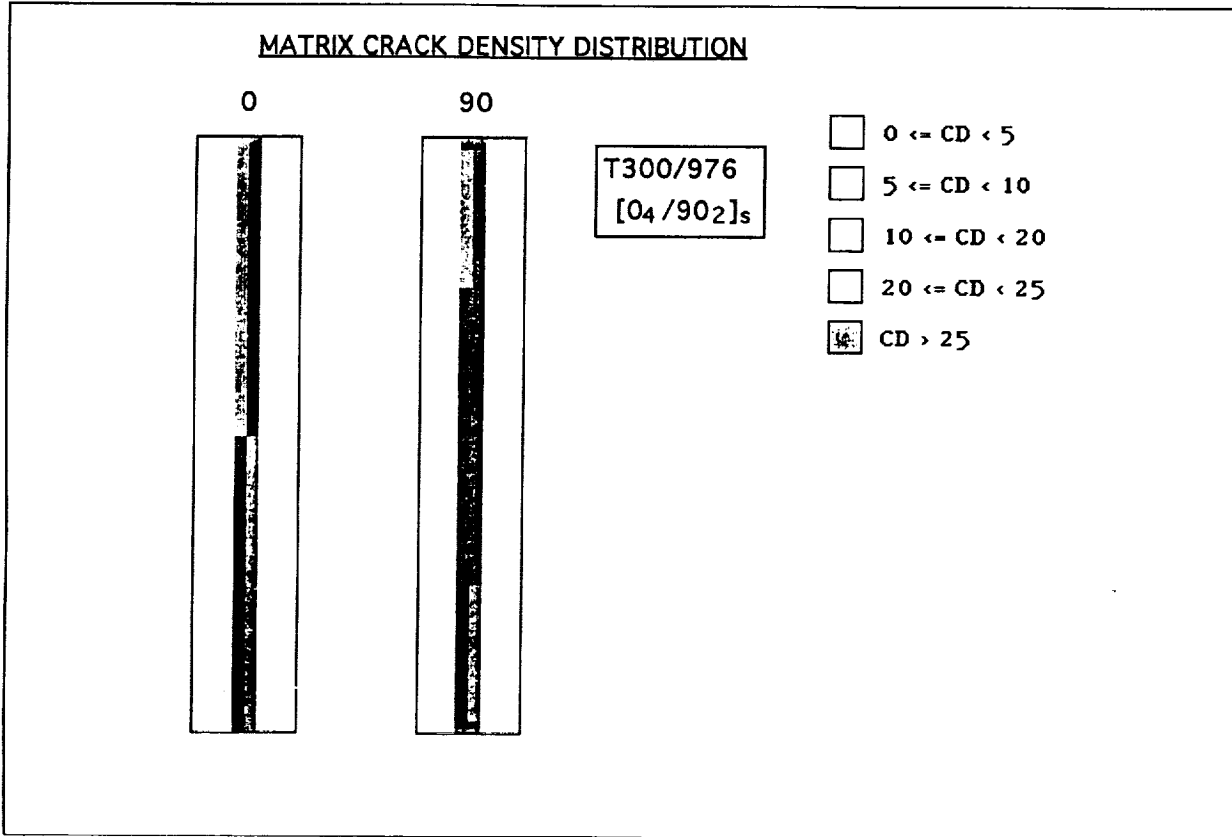
SHEAR LOAD

The predicted load-deflection response of cross-ply rail shear specimens.
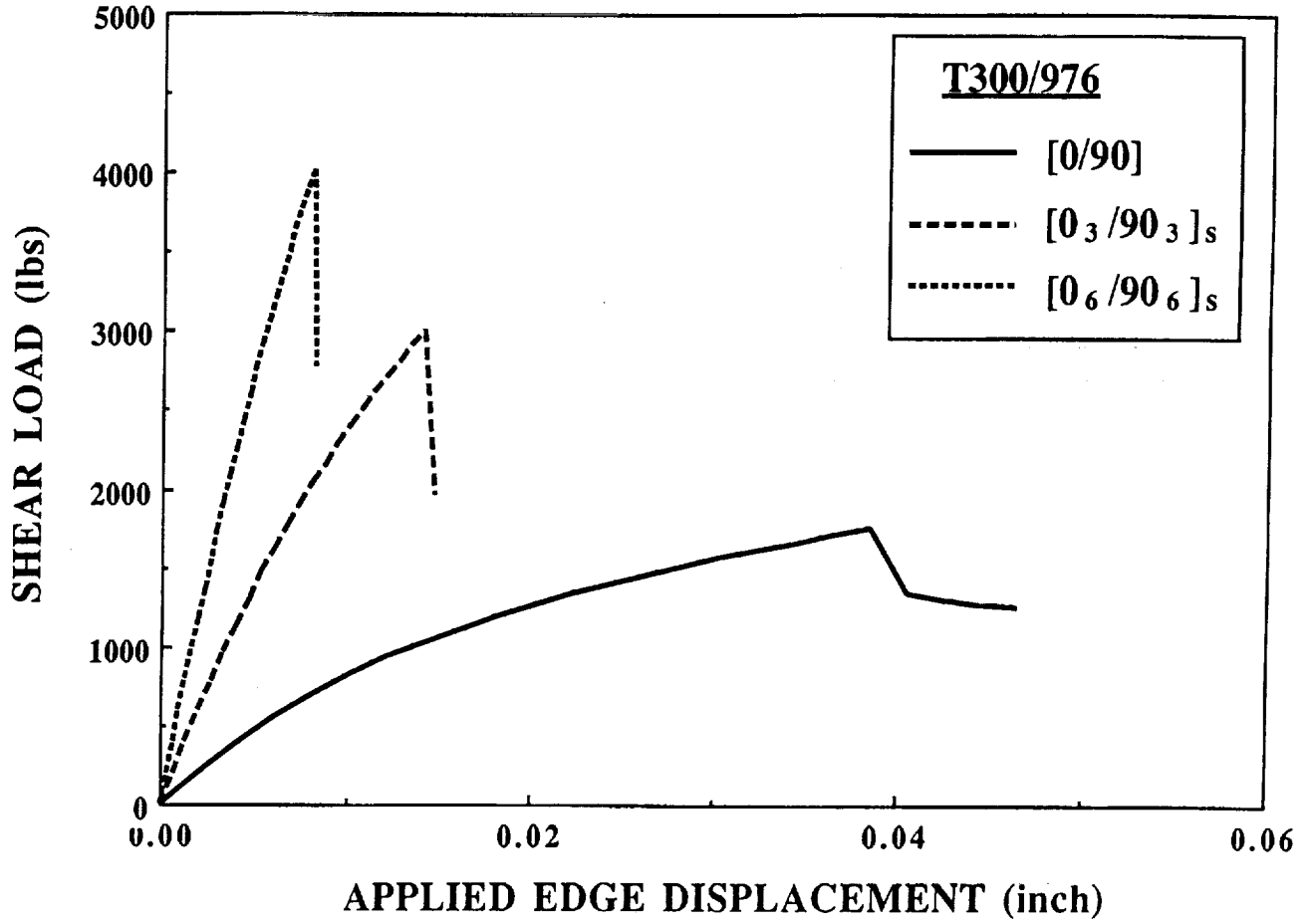
PROGRESSIVE FAILURE PREDICTION (VERIFICATION - NOTCHED LAMINATE)

Numerical simulation of damaged extension of notched laminated composites as a function of applied load under uniaxial tension.
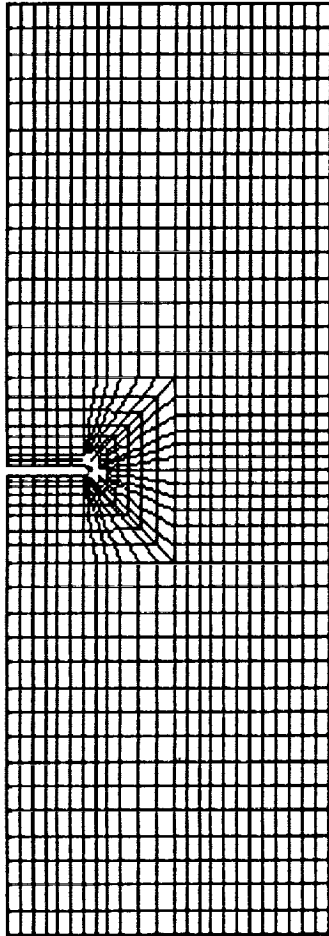
MATERIAL: AS4/3501-6
LAYUP: [45/90/-45/0]s
D= 0.872(in)
W/D= 4.0

LOAD =   5328(lbs)

DAMAGE MODE
■ Fiber Breakage
■ Fiber-Matrix Shear-Out
▨ Matrix Cracking

108

PROGRESSIVE FAILURE PREDICTION

Numerical simulation of damaged extension of notched laminated composites as a function of applied load under uniaxial tension.

MATERIAL: AS4/3501-6
LAYUP: [45/90/-45/0]s
D= 0.872(in)
W/D= 4.0

LOAD = 6720(lbs)

DAMAGE MODE
■ Fiber Breakage
■ Fiber-Matrix Shear-Out
▓ Matrix Cracking

PROGRESSIVE FAILURE PREDICTION

Numerical simulation of damaged extension of notched laminated composites as a function of applied load under uniaxial tension.

MATERIAL: AS4/3501-6
LAYUP: [45/90/-45/0]s
D= 0.872(in)
W/D= 4.0

LOAD =   7447(lbs)

DAMAGE MODE
Fiber Breakage
Fiber-Matrix Shear-Out
Matrix Cracking

PROGRESSIVE FAILURE PREDICTION

Numerical simulation of damaged extension of notched laminated composites as a function of applied load under uniaxial tension.

MATERIAL: AS4/3501-6
LAYUP: [45/90/-45/0]s
D= 0.872(in)
W/D= 4.0

LOAD = 3847(lbs)

DAMAGE MODE
■ Fiber Breakage
■ Fiber-Matrix Shear-Out
▨ Matrix Cracking

111

RESIDUAL STRENGTH

The residual strength distribution of notched [45/90/-45/0]$_s$ composites as a function of laminate width. Comparison between the prediction and the test data.
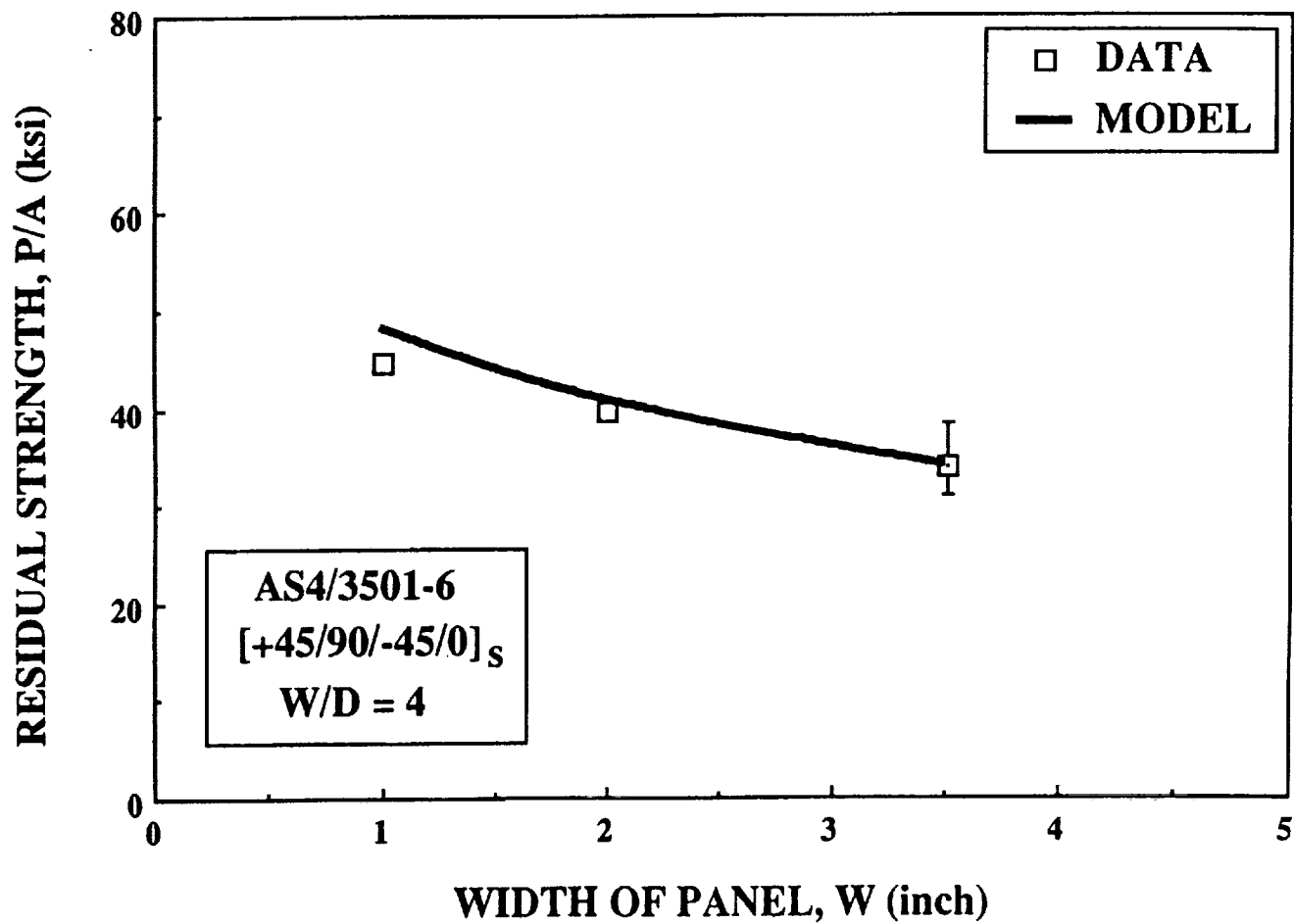
RESIDUAL STRENGTH

The residual strength distribution of notched [Crown-1] composites as a function of laminate width. Comparison between the predictions based on the model and the existing methods and the test data.
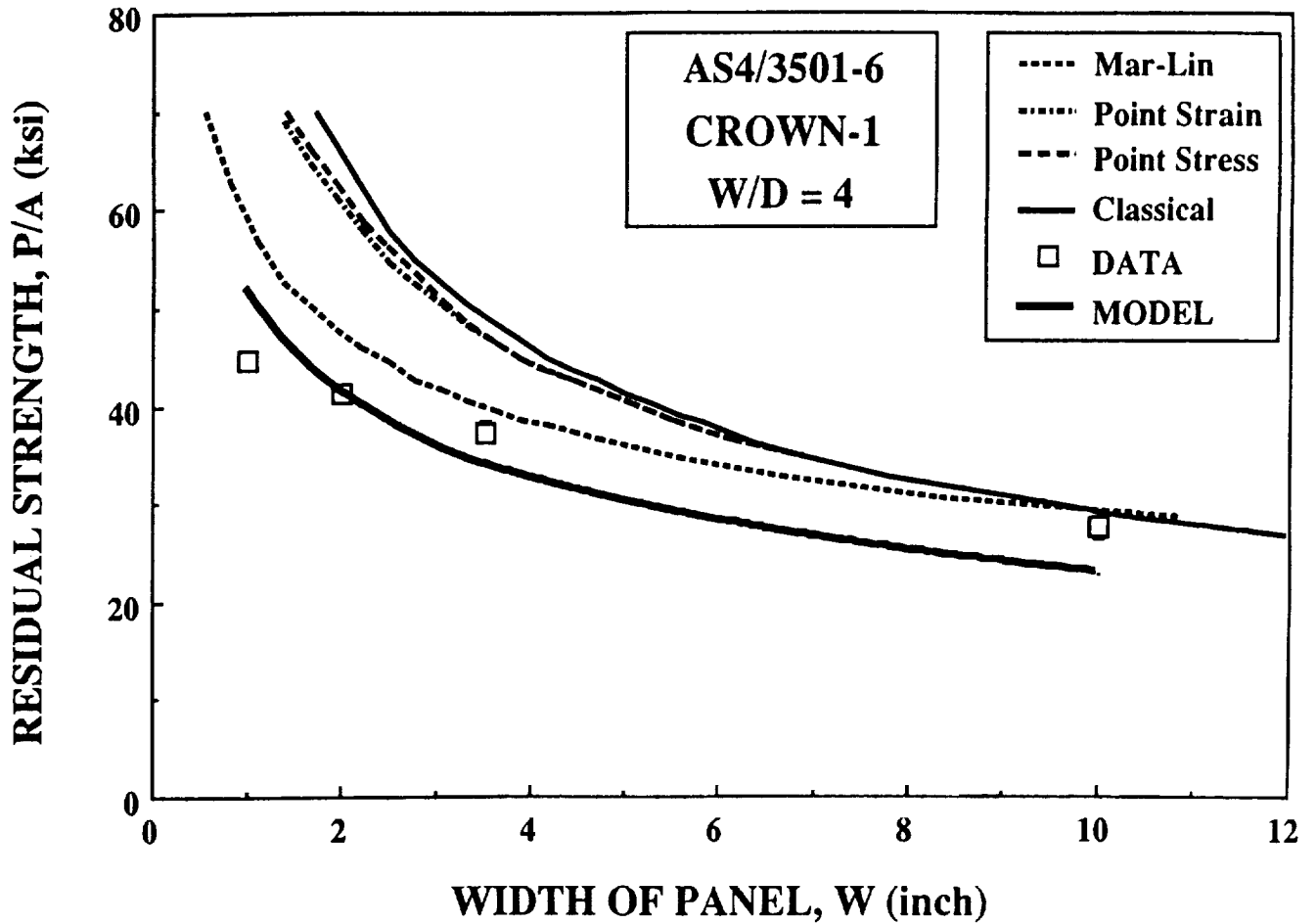
RESIDUAL STRENGTH

The residual strength distribution of notched [0/90/0/90]$_s$ composites as a function of laminate width. Comparison between the prediction and the test data.
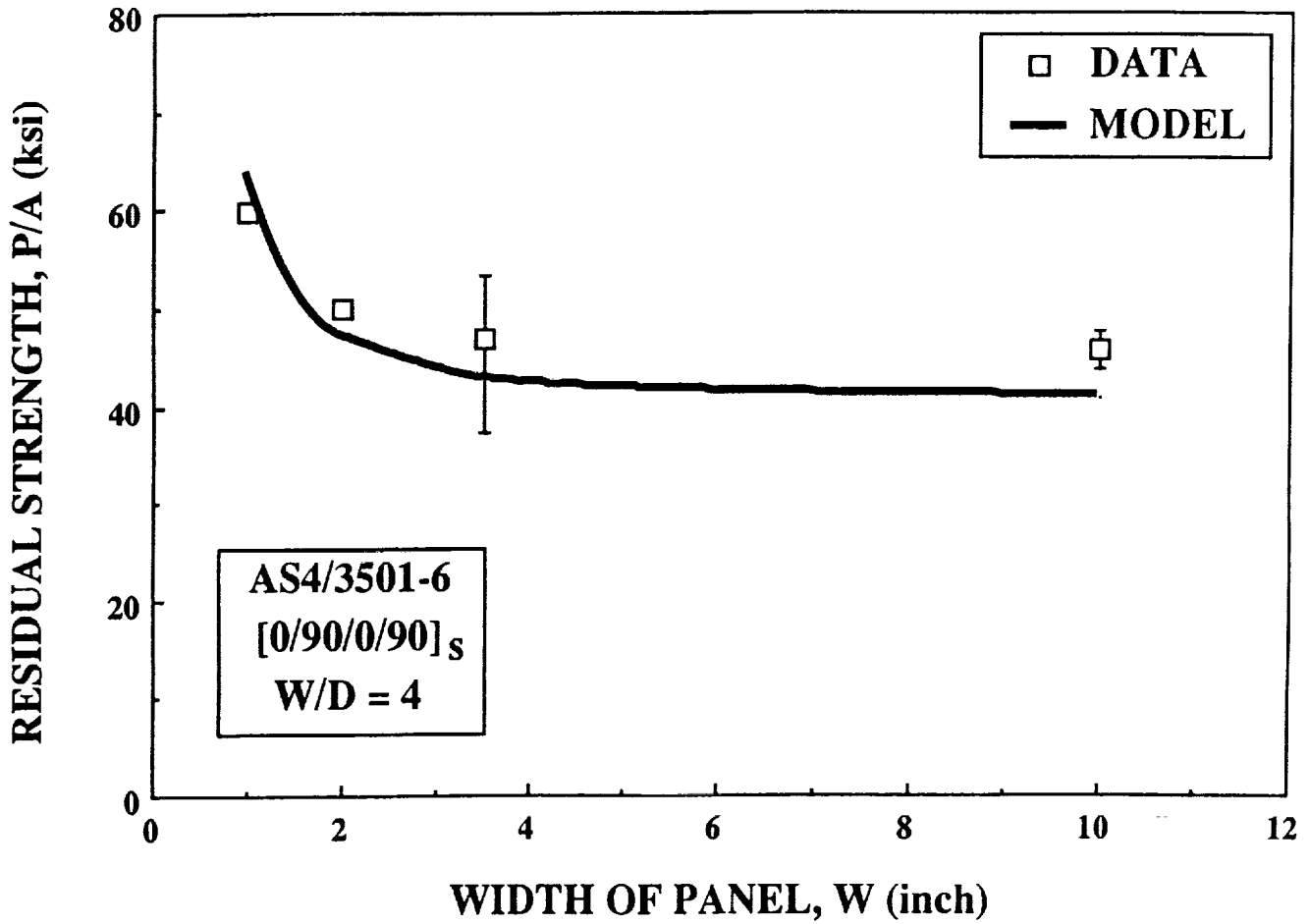
RESIDUAL STRENGTH

The residual strength distribution of notched [Crown-1] tow-composites as a function of laminate width. Comparison between the predictions based on the present model and the Mar-Lin model and the test data.
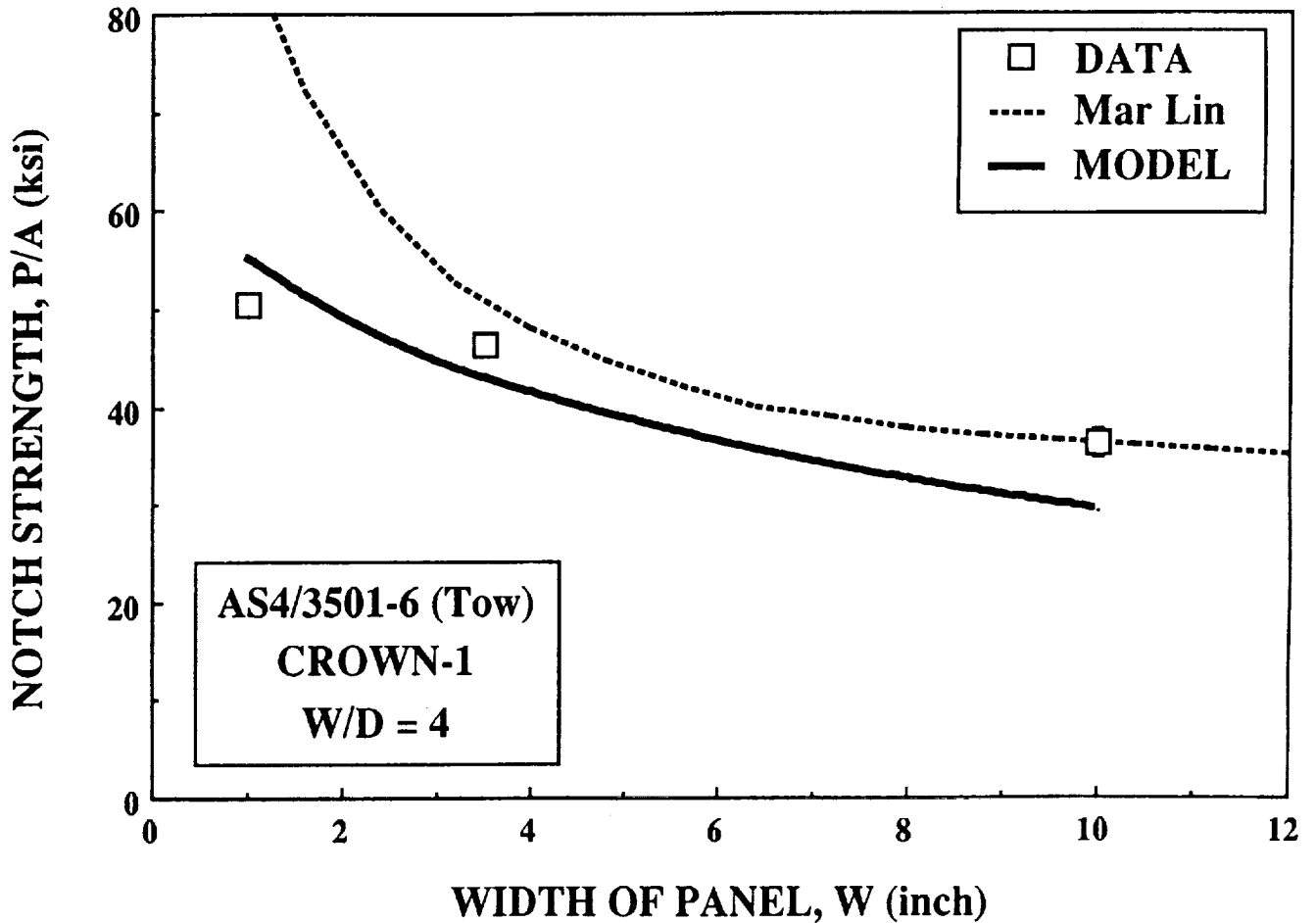
PROGRESSIVE FAILURE PREDICTION

Numerical simulation of damaged extension of notched laminated composites as a function of applied load under uniaxial tension.
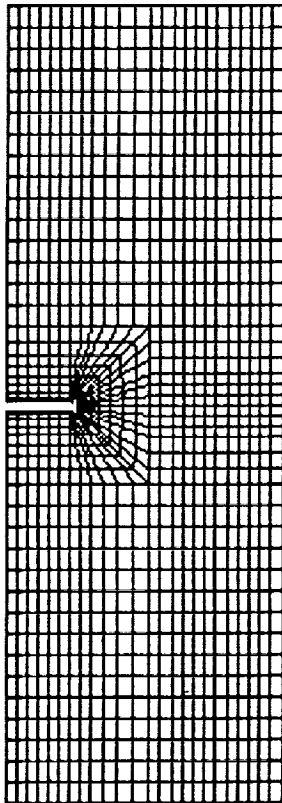
MATERIAL: AS4/3501-6 (TOW)
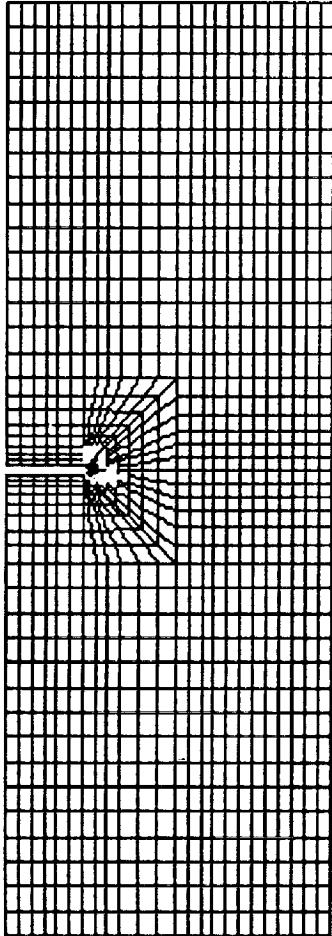LAYUP: CROWN-1
D= 0.872(in)
W/D= 4.0

LOAD =   3612(lbs)

DAMAGE MODE
■ Fiber Breakage
■ Fiber-Matrix Shear-Out
▨ Matrix Cracking

PROGRESSIVE FAILURE PREDICTION

Numerical simulation of damaged extension of notched laminated composites as a function of applied load under uniaxial tension.
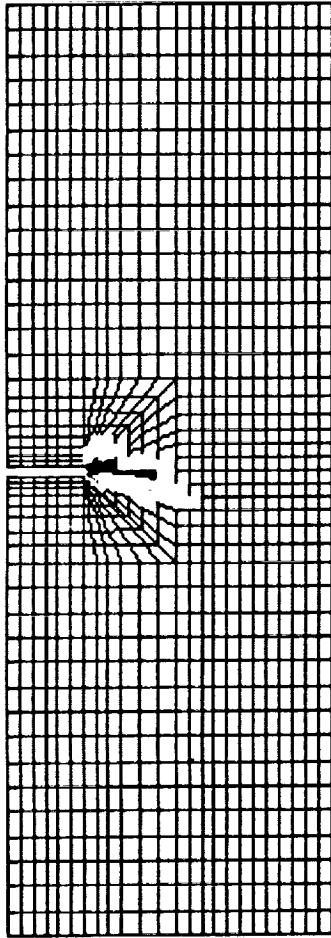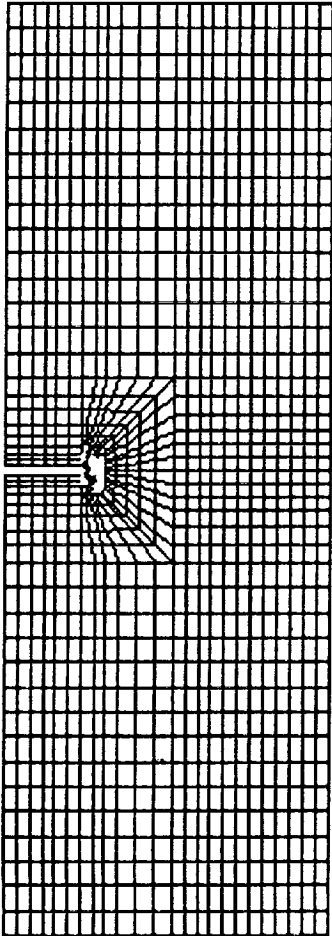
MATERIAL: AS4/3501-6 (TOW)
LAYUP: CROWN-1
D= 0.872(in)
W/D= 4.0

LOAD = 7771(lbs)

DAMAGE MODE
■ Fiber Breakage
■ Fiber-Matrix Shear-Out
▨ Matrix Cracking

PROGRESSIVE FAILURE PREDICTION

Numerical simulation of damaged extension of notched laminated composites as a function of applied load under uniaxial tension.
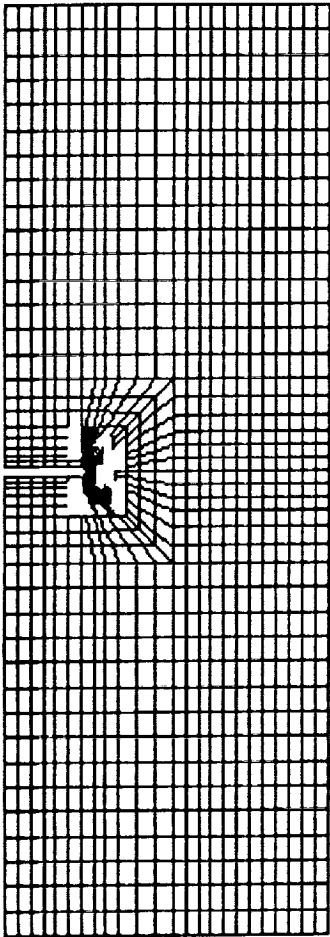
MATERIAL: AS4/3501-6 (TOW)
LAYUP: CROWN-1
D= 0.872(in)
W/D= 4.0

LOAD = 10202(lbs)
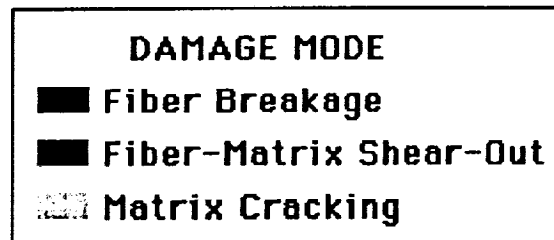
DAMAGE MODE
■ Fiber Breakage
■ Fiber-Matrix Shear-Out
▨ Matrix Cracking

PROGRESSIVE FAILURE PREDICTION

Numerical simulation of damaged extension of notched laminated composites as a function of applied load under uniaxial tension.
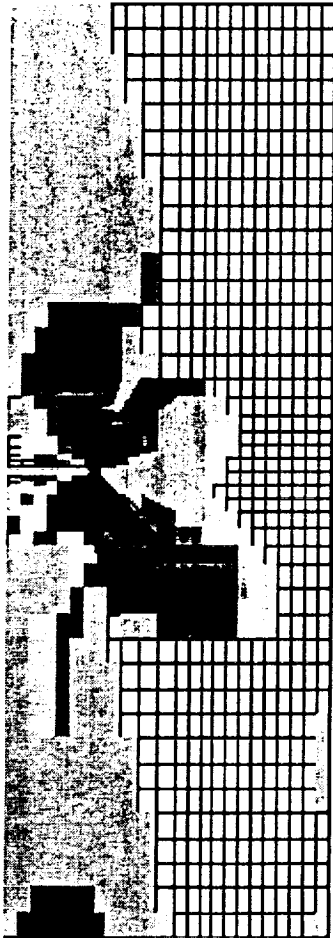
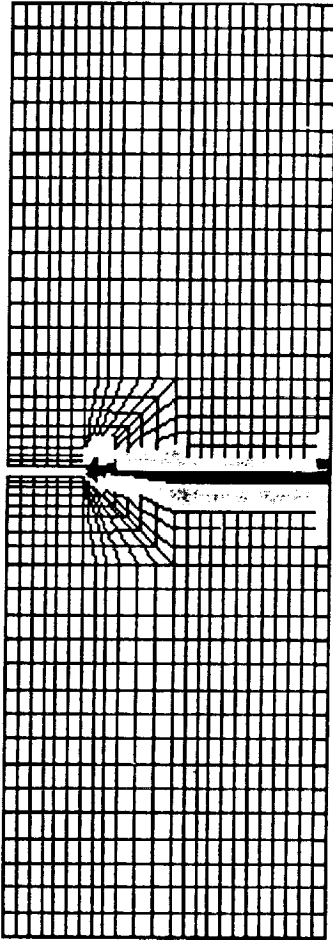MATERIAL: AS4/3501-6 (TOW)
LAYUP: CROWN-1
D= 0.872(in)
W/D= 4.0

LOAD = 8612(lbs)

DAMAGE MODE
■ Fiber Breakage
■ Fiber-Matrix Shear-Out
▨ Matrix Cracking

I. IMPLEMENTATION

1. IMPLEMENTATION OF THE CURRENT MODEL TO EXISTING FEM CODES

II. DAMAGE MODELLING

1. CRACK GROWTH MODEL
2. DELAMINATION INITIATION AND GROWTH MODEL
3. FATIGUE MODEL

III. COMPUTATIONAL MECHANICS

1. MESH SENSITIVITY
2. DAMAGE SIMULATION
3. GLOBAL-LOCAL FEM
4. PARALLEL PROCESSING

Brief Summary of the Evolution of High-Temperature Creep-Fatigue Life Prediction Models for Crack Initiation

Gary R. Halford
NASA Lewis Research Center
Cleveland, OH

PAGE _____ INTENTIONALLY BLANK

INTRODUCTION

The evolution of high-temperature, creep-fatigue, life-prediction methods used for cyclic crack initiation is traced from inception in the late 1940's. The methods reviewed are material models as opposed to structural life prediction models. Material life models are used by both structural durability analysts and by material scientists. The latter use micromechanistic models as guidance to improve a material's crack initiation resistance. Nearly one hundred approaches and their variations have been proposed to date. This proliferation poses a problem in deciding which method is most appropriate for a given application. Approaches have been identified as being combinations of thirteen different classifications. This review is intended to aid both developers and users of high-temperature fatigue life prediction methods by providing a background from which choices can be made.

The need for high-temperature, fatigue-life prediction methods followed immediately on the heels of the development of large, costly, high-technology industrial and aerospace equipment immediately following the second world war. Major advances were made in the design and manufacture of high-temperature, high-pressure boilers and steam turbines, nuclear reactors, high-temperature forming dies, high-performance poppet valves, aeronautical gas turbine engines, reusable rocket engines, etc. These advances could no longer be accomplished simply by trial and error using the "build-em and bust-em" approach. Development lead times were too great and costs too prohibitive to retain such an approach. Analytic assessments of anticipated performance, cost, and durability were introduced to cut costs and shorten lead times. The analytic tools were quite primitive at first and out of necessity evolved in parallel with hardware development.

After forty years we are actively developing more descriptive, more accurate, and more efficient analytic tools. These include thermal-structural finite element and boundary element analyses, advanced constitutive stress-strain-temperature-time relations, and creep-fatigue-environmental models for crack initiation and propagation. This paper is concerned with the high-temperature durability methods that have evolved for calculating high-temperature fatigue crack initiation lives of structural engineering materials. Only a few of the methods have been refined to the point of being directly useable in design. Recently, two of the methods have been transcribed into computer software for use with personal computers (McGaw and Saltsman (1991) and Nelson, et al (1992)).

PAGE 122 INTENTIONALLY BLANK

CONCEPT OF FATIGUE CRACK INITIATION

The high-temperature, life-prediction models considered in this review have been developed for fatigue crack initiation. They are material models rather than structural models. Development has been based on the behavior of smooth, axially-loaded specimens with uniform stresses, strains and temperatures. Influences of structural shape, size, and function are lacking intentionally to permit determination of underlying material rather than structural behavior.

Structural life prediction procedures utilize material life models in direct conjunction with thermal and structural analyses to quantify material response in identified local crack initiation-prone regions of a structure. The tacit assumption being that if a material's response is accurately known under well-controlled laboratory conditions, it will respond similarly within a small region of a loaded structure provided the local conditions are identical. For example, if a smooth axially-loaded laboratory specimen initiates a crack of prescribed size after 1000 cycles of repetition of a 1% axial strainrange, a structural element will also initiate the same size crack in the same number of cycles provided the local range of cyclic strain is the equivalent of the 1% axial strainrange. If the structure can tolerate appreciably longer cracks without loss of structural integrity, the additional crack propagation life cannot be estimated on the basis of knowledge from small, smooth, axially-loaded laboratory crack "initiation" specimens. Computation of the rate of cyclic crack progression at these larger crack lengths must be dealt with using the principals of fracture mechanics. However, the field of fracture mechanics has not as yet progressed to the same level of engineering utility for high-temperature, time-dependent creep-fatigue as has the field of cyclic crack initiation. High-temperature fracture mechanics methods are beyond the scope of this manuscript. The reader is referred to recent literature on the subject; see, for example, Anon. (1989).
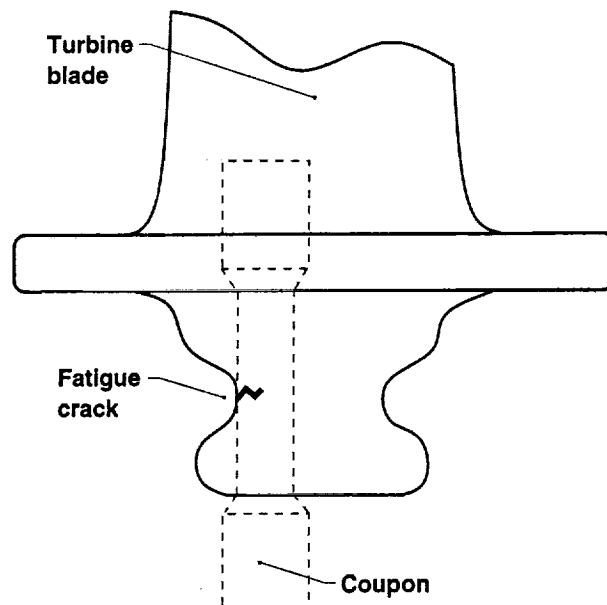
Figure 1 - Crack initiation in structural element modeled
by laboratory coupon

ENGINEERING CRACK INITIATION

While the validity of fatigue crack initiation as a basic physical concept is debatable, it is, nevertheless, a powerful engineering assumption that has permitted the economic life assessment of countless structural components over the years. It is likely to remain that way for the foreseeable future, as dire needs remain for accurate engineering durability assessment of newly proposed, high-performance industrial and aerospace equipment.

The term fatigue crack initiation has considerable meaning at the engineering level. It loses this meaning as the scale of observation becomes more microscopic. The term, unless specifically defined by a crack size (depth, length), normally implies the appearance of a small crack, readily identifiable with the unaided eye, that because of its current size, has begun to influence the macroscopic engineering stress-strain response of an otherwise smooth, axially-loaded, laboratory fatigue specimen. Often there is little fatigue life remaining to complete specimen separation once the initiated crack becomes noticeable. Many investigations of the low-cycle fatigue resistance of engineering alloys utilize complete separation as the definition of fatigue life. This life is referred to as the crack initiation life. Close examination of the fatigue fractured surface would reveal distinct striations marking nearly every cycle of microscopic fatigue crack propagation that would then account for the majority of the specimen life. This is especially so in low-cycle fatigue testing. Models that accurately deal with the propagation of microscopic sized cracks, especially under high-temperature creep-fatigue-environmental interaction conditions (McDowell and Miller (1991)) are still under development. Such models are used in the establishment of engineering fatigue crack initiation behavior and are thus included in this review.
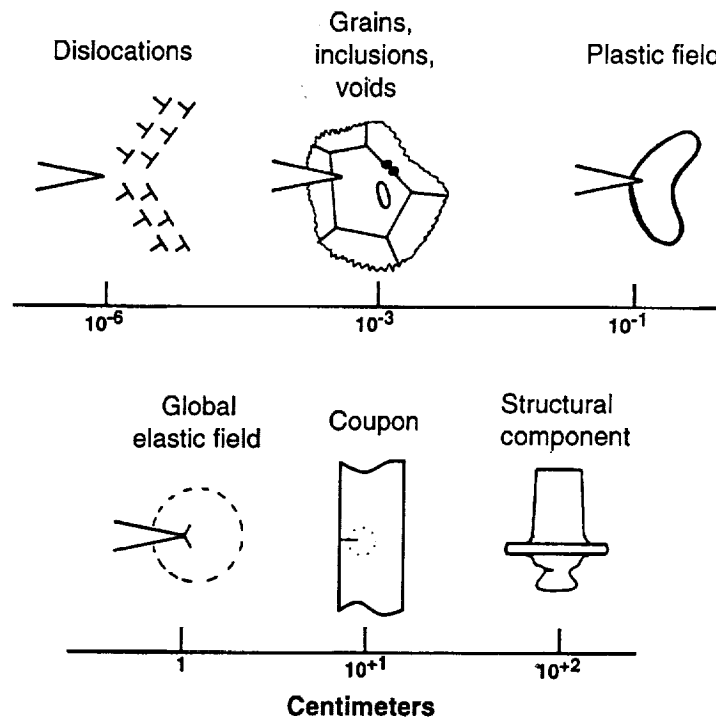
Figure 2 - Observational scales for cracking

MODEL EVOLUTION

In the earliest years of high-temperature structural durability prediction, the only concern with fatigue was for endurance limits in the very high cycles-to-failure regime (greater than about one million). Only mechanical fatigue loading at rather high frequencies was of concern, and efforts were devoted to reducing the magnitude of the excitations. Prior to the 1950's, there was no attempt to predict fatigue life -- only a concern that high-cycle fatigue may or may not occur. This greatly simplified the task of predicting structural life. Durability lifetimes, however, were calculated on the basis of time to failure as a result of creep-rupture phenomena. For this reason, creep-rupture became a commonly accepted means of inexpensively testing and judging a material's resistance to high-temperature operation. Simple, conservative procedures evolved that assumed, for pressure vessel design, for example, that the internal pressure acted continuously at its maximum value at maximum temperature for the entire duration of high-temperature usage. No credit was taken for operational time at lower temperatures or lower pressures (the time-fraction rule of Robinson (1952) was the first attempt to refine this simplistic approach). This simple bounding procedure was easy to put into practice using elastic strength of materials analyses. So long as designs could be built and operated economically while meeting these stringent requirements, there was little concern for developing more realistic life assessment methods. This simplistic view was accompanied by necessarily large factors of safety. However, durability problems persisted.

Pressure vessels did rupture prematurely and for a variety of reasons: poor quality control over material and fabrication techniques; intervention of corrosion and oxidation not considered in the original durability calculations; improper usage of the equipment by poorly trained operators; poor structural analysis procedures; intervention of thermal stresses and thermal fatigue; and a host of other parasitic causes about which the designer was ignorant or had little control. In addition, there was the continual desire to extend the useful lifetime of expensive equipment. There was virtually no acknowledgement of the complex technological problems of thermal stresses and thermal fatigue. No consideration was given to cyclic creep, creep-fatigue interactions, or attendant complex interaction with an active, aggressive environment.

126

It was nearly a decade after the identification (Manson (1953) and Coffin (1954)) of the plastic strain range power law for low-cycle fatigue that proposals were made for predicting structural lives in terms of both creep-rupture and cyclic strain fatigue, i.e., creep-fatigue (Taira (1962)). In the decade of the 1970's, there was rapid expansion of the number of creep-fatigue-environmental life assessment models being proposed. Although the rate of proposals declined in the 1980's, the degree of sophistication increased to keep pace with advancements in structural analysis techniques and corresponding increases in understanding of basic micromechanisms. The vast majority of the methods, once proposed, have seen little or no followup. From the standpoint of effort put forth toward their development, three basic methods stand out: 1) the time- and cycle-fraction rule as used in ASME Nuclear Code Case N-47; 2) the continuum damage mechanics approach of ONERA in France; and 3) the Strainrange Partitioning method of NASA Lewis. Each has sustained continual refinement owing to the support and continuity of the sponsoring organizations. The latter two have received the greatest attention during the last decade.

0 - VIRTUALLY NON-EXISTENT BEFORE WWII

0 - THE SECOND INDUSTRIAL REVOLUTION
    - RAILROAD BRAKING
    - PRESSURE VESSELS & PIPING
    - IC ENGINE POPPET VALVES
    - HIGH-TEMPERATURE FORMING DIES
    - AERONAUTICAL GAS TURBINES
    - NUCLEAR REACTORS
    - REUSABLE ROCKET ENGINES
    - SOLDERED LEAD-LESS CHIPS

0 - "BUILD-EM & BUST-EM" TOO EXPENSIVE (TIME & DOLLARS)

0 - STRUCTURAL ANALYSIS TECHNIQUES NOW AVAILABLE TO SUPPORT LOCAL
    STRESS-STRAIN KNOWLEDGE REQUIRED OF LIFE PREDICTION MODELS

0 - CRACK INITIATION "VALID" FOR DESIGN CALCULATIONS

Figure 3 - The drivers in historic evolution of high-temperature
fatigue life prediction models

CLASSIFICATION OF METHODS

The large number of life prediction methods are classified in the following somewhat arbitrary categories. The thirteen categories are listed A through M below. Many methods fall into more than one category. The early linear damage (LDR) rules for fatigue are listed because they formed an important base for subsequent high-temperature life prediction methods. In Figs. 5-17 the first column refers to the categories appropriate to each method and the second column lists a three-letter shorthand notation for each method.

A - LIFE OR DAMAGE FRACTION RULES

B - STRESS-LIFE DIAGRAMS

C - FREQUENCY EFFECT EQUATIONS

D - STRAINRANGE - LIFE MODELS

E - DAMAGE MECHANICS

F - HYSTERESIS ENERGY MODELS

G - DUCTILITY EXHAUSTION

H - MICROCRACK GROWTH

I - STRAINRANGE PARTITIONING

J - MACRO-PHENOMENOLOGICAL MODELS

K - DAMAGE RATE MODELS

L - CYCLIC DAMAGE ACCUMULATION MODELS

M - MICROMECHANISTIC MODELS

Figure 4 - Classification of fatigue life prediction methods into thirteen overlapping categories

A - LIFE OR DAMAGE FRACTION RULES

The life- or damage-fraction rules are perhaps the most basic of all life prediction models. These rules simply state that when the fraction sums to a critical value, a crack or cracks instantaneously appear and failure has occurred. Earliest rules were linear in their summation of fractions to a value of unity at failure. Taira (1962) was the first to add time fractions (creep damage) to cycle fractions (fatigue damage) to represent creep-fatigue interaction. Wood (1966) proposed one of the first nonlinear summations of life fractions to obtain a nonlinear creep-fatigue interaction. A number of different fractional rules evolved as a result of using a different parameter (stress, strain, energy, etc.) to correlate with life (cycles-to-failure, time-to-rupture, etc.). The most widely used models listed below are the linear damage rule (Palmgren-Langer-Miner) for fatigue and the ASME Boiler and Pressure Vessel Code Case 1331 (currently updated and designated N-47) for high-temperature creep-fatigue interaction. In the latter, the damage is summed in a bi-linear fashion to a value of 1.0 or less, depending upon alloy and relative amounts of creep and fatigue fractions. Over half of the models below are listed under additional categories.

A	LDR	Linear Damage Rule/Palmgren (1924)
A	LDR	Linear Damage Rule/Langer (1937)
A	LDR	Linear Damage Rule/Miner (1945)
A	LCR	Linear Creep Rupture Damage Rule/Robinson (1952)
A	LCF	Linear Creep Damage/Berkovits (1961)
A	TCF	Time + Cycle Fraction Rule/Taira (1962)
A	LFA	Life Fraction Approach/D. S. Wood (1966)
AD	TPR	Ten Percent Rule/Manson & Halford (1967)
ABD	LCD	Linear Creep Damage for Thermal Fatigue/Spera (1968)
ABD	MLF	Modified Life Fraction Rule/Manson, Halford & Spera (1971)
ABD	LFR	Life Fraction Rule/ASME Code Case 1331 (pre-N-47) (1971)
ABD	TCD	Turbine Component Design/Timo (1971)
ABD	ITC	Interactive Time-Cycle Frac/Lagneborg & Attermo (1971)
ABD	RCF	Relaxation Creep Fatigue/Marshall & Cook (1971)
A	TCD	Time-Cycle Diagram/Esztergar & Ellis (1971)
ABE	CDC	Cumulative Damage Under Creep/Bui-Quoc (1979)
ABDE	PFC	Phenomenological Fatigue Creep/Bui-Quoc & Biron (1982)
AE	FCD	Fatigue + Creep Damage Mechs./Plumtree & Lemaitre (1982)
A	FNC	French Nuclear Code/Anon. (1985)
ABDM	FCE	Fatigue-Creep-Env Model/Neu & Sehitoglu (1989a & 1989b)
ABE	DDM	Differential Damage Mechanics/Arnold & Kruch (1991)

Figure 5 - Life prediction models based on life-fraction
or damage-fraction concepts

B - STRESS-LIFE DIAGRAMS

The very first fatigue equations were written in terms of applied cyclic stresses, an approach well suited for classical high-cycle fatigue wherein the material responds in a nominally elastic manner. Since stress was also the primary parameter used to measure creep-rupture resistance, it was only natural that the first attempts to represent creep-fatigue damage were done on what came to be known as stress range diagrams. These plots related fatigue strength on one axis, creep-rupture strength on the other, with connecting families of lines each representing a different time to failure. Fatigue cycling frequencies associated with these diagrams were rather high. Cyclic lives were determined from knowledge of the time-to-failure and the frequency. Many years passed before these approaches fell into disuse and were replaced with models of a more general nature. Application of stress-based creep-rupture curves to the computation of creep damage during low-cycle isothermal and thermal fatigue began to appear in the late 1960s and early 1970s. In fact, the ASME Boiler and Pressure Vessel Code Case N-47 utilizes this approach for computation of creep damage during creep-fatigue loading under isothermal and thermal fatigue conditions. The damage mechanics approaches utilize stress-life diagrams for both creep and fatigue as the basic material failure diagrams for use in assessing damage during creep-fatigue cycling. Because of the very strong dependency of time-to-rupture on applied stress, computed lives are highly sensitive to the accuracy of magnitudes of the stresses computed from structural analyses. This excess sensitivity provided impetus to examine strain-based life prediction models.

B	SRD	Stress Range Diagrams/Lazan (1949)
B	SRD	Stress Range Diagrams/Forrest (1950)
ABD	LCD	Linear Creep Damage for Thermal Fatigue/Spera (1968)
ABD	MLF	Modified Life Fraction Rule/Manson, Halford & Spera (1971)
ABD	LFR	Life Fraction Rule/ASME Code Case 1331 (pre-N-47) (1971)
ABD	TCD	Turbine Component Design/Timo (1971)
ABD	ITC	Interactive Time-Cycle Frac/Lagneborg & Attermo (1971)
ABD	RCF	Relaxation Creep Fatigue/Marshall & Cook (1971)
ABE	CDC	Cumulative Damage Under Creep/Bui-Quoc (1979)
ABDE	PFC	Phenomenological Fatigue Creep/Bui-Quoc & Biron (1982)
ABDM	FCE	Fatigue-Creep-Environment Model/Neu & Sehitoglu (1989)
ABE	DDM	Differential Damage Mechanics/Arnold & Kruch (1991)

Figure 6 - Life prediction models based on stress-life diagrams

130

C - FREQUENCY EFFECT EQUATIONS

A common way to represent the amount of time under active stressing at temperature during fatigue cycling is through the frequency of cycling. Frequency-dependent fatigue lives of lead cable sheathing tested at room temperature were noted by Eckel as the decade of the 1950's began. While a number of different models have been proposed that utilize frequency as a principal parameter, the most famous have been the contributions of Dr. Coffin in association with the General Electric R&D Center. Rather complex equations resulted when attempts were made to use frequency as a means of capturing creep-fatigue effects during thermomechanical fatigue cycling. Ad hoc rules were developed to cover the widely varying creep-fatigue response of different alloy systems. Despite the attractiveness of using frequency as a simple metric for assessing the time-dependent complex interactions of fatigue with creep and oxidation, frequency-effect high-temperature fatigue models have not seen widespread usage.

C	FEE	Frequency Effect Equation/Eckel (1951)
C	TTF	Time To Failure Model/Coles & Skinner (1965)
CD	MCS	Method of Characteristic Slopes/Berling & Conway (1969)
CD	FMF	Frequency Modified Fatigue/Coffin (1970)
C	HTE	Hold Time Effects Model/Wellinger & Sautter (1973)
C	FSM	Frequency Separation Method/Coffin (1976)
CF	THE	Tensile Hysteresis Energy Model/Ostergren (1976a & 1976b)
CF	MTE	Mod Tensile Hyst Energy Model/Ostergren & Krempl (1979)
C	EFE	Endochronic Frequency Equation/Valanis (1981)

Figure 7 - Life prediction models based on frequency as
a primary variable

D - STRAINRANGE - LIFE MODELS

In the early 1950's, high-performance industrial applications demanded attention from the design community. Electric power generation plants were being designed for higher use temperatures and efficiencies, aeronautical gas turbine engines had to have high performance and low weight, and such equipment did not have to have a nominally infinite design life. These circumstances set the stage for interest in high-strain, low-cycle fatigue. Stress no longer correlated well with fatigue life in the nonlinear, low-cycle, finite-life regime. The historically and physically significant plastic strain power law of low-cycle fatigue was proposed in 1953 and was developed subsequently into what is now known as the Manson-Coffin Law of low-cycle fatigue. For room temperature fatigue, it was soon recognized that plastic strain, while an excellent physically correct parameter, was not a convenient entity for designers to use. At the time, inelastic structural analysis was just in its infancy. To overcome this limitation, the total mechanical strain range (plastic plus inelastic) was correlated with low-cycle fatigue life in the early 1960's. A particularly significant model incorporating total strain range was the Method of Universal Slopes (MUS) that resulted from the intensive low-cycle fatigue research at the Lewis Research Center of the National Aeronautics and Space Administration. This method, published in 1965, is widely used for estimating the low-cycle fatigue resistance of materials in the absence of cyclic data. The fatigue properties used in the design of the Space Shuttle main engines were, for the most part, estimated by the method of universal slopes. Many models, even for high-temperature conditions wherein creep and environmental interaction are influential, are now based on total strain range versus life equations.

D	PSF	Plastic Strain Fatigue Law/Manson (1953)
D	PSF	Plastic Strain Fatigue Law/Coffin (1954)
D	TSR	Total Strain Range - Life Model/Manson & Hirschberg (1964)
D	MUS	Method of Universal Slopes/Manson (1965)
AD	TPR	Ten Percent Rule/Manson & Halford (1967)
D	TSR	Total Strain Range - Life Model/Morrow (1968)
ABD	LCD	Linear Creep Damage for Thermal Fatigue/Spera (1968)
D	PST	Plastic Strainrange Time Model/Berling & Conway (1969)
CD	FMF	Frequency Modified Fatigue/Coffin (1970)
CD	MCS	Method of Characteristic Slopes/Berling & Conway (1970)
DJ	TCE	Thermal Cycling Equation/Udoguchi & Wada (1971)
ABD	MLF	Modified Life Fraction Rule/Manson, Halford & Spera (1971)
ABD	LFR	Life Fraction Rule/ASME Code Case 1331 (pre-N-47) (1971)
ABD	TCD	Turbine Component Design/Timo (1971)
ABD	ITC	Interactive Time-Cycle Frac/Lagneborg & Attermo (1971)
ABD	RCF	Relaxation Creep Fatigue/Marshall & Cook (1971)
D	MSE	Modified Strainrange Equation/Sunamoto et al (1974)
D	TDE	Time Dependent Exponent of Strain/Udoguchi et al (1974)
ABDE	PFC	Phenomenological Fatigue Creep/Bui-Quoc & Biron (1982)
DF	OCF	Overstress Concept of Creep-Fatigue/Morishita et al (1988)
ABDM	FCE	Fatigue-Creep-Environment Model/Neu & Sehitoglu (1989)

Figure 8 - Models based on strain range as dominant
cyclic variable

E - DAMAGE MECHANICS

Continuum Damage Mechanics has gained considerable interest over the past two decades through the aggressive efforts of Dr. Louis Chaboche and numerous colleagues at the French Space Agency (ONERA). The listing below represents but a small fraction of the large number of publications on the subject (numbering in the hundreds). Through personnel exchanges between ONERA and the NASA Lewis Research Center, NASA also has been contributing to the development of this powerful mathematical representation of fatigue damage, creep damage, and their manner of accumulation. A summary of the numerous significant contributions in the area of continuum damage mechanics has been published recently (Arnold and Kruch (1991)).

In the most basic of terms, the approach views damage as being volumetrically distributed in a uniform, homogeneous manner (hence the description, continuum mechanics). Its influence is to reduce the effective cross-sectional area available for carrying applied load, hence, steadily increasing the average stresses as damage increases. Failure is calculated to occur when a critical damage is reached. The method treats fatigue damage and creep damage on a common basis so that the two types of damage can be added directly.

E	DMC	Damage Mechanics for Creep/Kachanov (1958)
E	CDM	Continuum Damage Model/Lemaitre & Chaboche (1973)
E	CDM	Cyclic Damage Model/Lemaitre & Plumtree (1978)
ABE	CDC	Cumulative Damage Under Creep/Bui-Quoc (1979)
AE	FCD	Fatigue + Creep Damage Mechs./Plumtree & Lemaitre (1982)
ABDE	PFC	Phenomenological Fatigue Creep/Bui-Quoc & Biron (1982)
ABE	DDM	Differential Damage Mechanics/Arnold & Kruch (1991)

Figure 9 - Life prediction models based on classical damage mechanics

F - HYSTERESIS ENERGY MODELS

A logical extension of stress-based and strain-based low-cycle fatigue life prediction models is to examine the product of these two correlating variables, i.e., strain energy. The product of the stress and the plastic strain ranges is proportional to the plastic strain hysteresis energy that is expended per unit volume of material during a complete cycle. This is a scalar quantity that, upon initial consideration, might be deemed useful in correlating fatigue lives under states of multiaxial stresses and strains. This concept, however, has not fulfilled its promise, and little is gained by using this slightly more complex parameter over a strain-based parameter. Each is related to cyclic life in about the same manner. Whatever fatigue lives can be correlated with hysteresis energy can also be correlated with a simpler strain range parameter to within the same degree of accuracy. The vast majority (greater than 99.9%) of the plastic strain hysteresis energy imposed upon a volume of material during its fatigue life is converted to heat energy which in turn is dissipated to the surroundings. The dissipation process is akin to the heat generated by the friction of two sliding solids. Hysteresis energy models have been adapted for high-temperature creep-fatigue conditions. Again, however, they do not seem to offer any advantage above and beyond what can be obtained with strain range-based approaches.

F	HEA	Hysteresis Energy Approach/Morrow (1960)
CF	THE	Tensile Hysteresis Energy Model/Ostergren (1976a & 1976b)
FI	PEM	Partitioned Energy Model/Leis (1977)
CF	MTE	Mod Tensile Hyst Energy Model/Ostergren & Krempl (1979)
FH	CTE	Crack Tip Energy Model/Radhakrishnan (1980 & 1982)
F	CEG	Constant Enthalpy Gain Approach/Whaley (1983)
FI	SEP	Strain Energy Partitioning/He et al (1983)
DF	OCF	Overstress Concept of Creep-Fatigue/Morishita et al (1988)
F	CAB	Coated Anisotropic Blade Model/Nissley et al (1991)

Figure 10 - Life prediction models based on concept of
hysteresis energy

134

G - DUCTILITY EXHAUSTION

Following on the heels of the Manson-Coffin equation for plastic strain low-cycle fatigue, ductility exhaustion models were proposed for both time-independent plasticity and time-dependent creep strains. The models are rather basic and are easy to understand at the layman level. They do require the ability to calculate small incremental amounts of inelastic deformation, a task that was not possible with any degree of accuracy for the early structural analysis computer codes. Even today, the reliability of computations of small ratcheting increments leaves a lot to be desired. The latest unified viscoplastic constitutive models do an excellent job of qualitative description, but require calibration to be able to match specific problems and achieve quantitative accuracy. None of the ductility exhaustion models have been used in any extensive way for calculating lifetimes of structural components.

G	DEM	Ductility Exhaustion Model/Manson (1960)
G	LDE	Linear Creep Ductility Exhaustion/Edmunds & White (1966)
G	DET	Ductility Exh for Thermal Fatigue/Polhemus et al (1973)
G	CPE	Creep-Plasticity Ductility Exh./Priest & Ellison (1981)
G	LPC	Linear Plastic-Creep Strain Exh./D.A. Miller et al (1982)
G	CPE	Creep-Plastic Exh/Priest, Beauchamp & Ellison (1983)
G	MDE	Modified Ductility Exhaustion Model/Hales (1983)

Figure 11 - Life prediction models based on concept
of ductility exhaustion

H - CRACK GROWTH

It may at first appear contradictory that cyclic crack growth is listed as a category under fatigue crack initiation. However, it must be recognized that cracks associated with macrocrack initiation do not instantaneously appear. Rather, these short cracks physically grow to their size through a somewhat continuous microcrack growth process. On rare occasions, macrocrack growth behavior, as measured on specimens with long cracks, has been extrapolated into the small crack regime with acceptable results. In general, however, such extrapolation has not been satisfactory. The impetus for development of crack growth models is based on the desire to treat the problem in a more physically-correct manner. Indeed, cracks are generated from initial microscopic atomic level defects in metallic crystalline structures, and these cracks grow in size on a cycle-by-cycle evolutionary basis. The models considered herein are ones proposed for use in predicting fatigue lives of what are best referred to as crack initiation specimens. They were not intended for use in prediction of macroscopic, large crack growth behavior of structural components. A considerable number of these models have been proposed on a continuing basis since the Tompkins model of 1968. The listing below notes many such models, but it should not be considered as thorough and complete. To the best of the author's knowledge, none of the models have been adopted for use in structural engineering design.

H	CGM	Crack Growth Model/Tomkins (1968)
H	HCG	High Temp Crack Growth/Wareing, Tomkins & Sumner (1973)
H	CPM	Crack Propagation Model/Carden (1973)
H	CGA	Crack Growth Approach/Solomon (1973)
H	ETC	Elevated Temperature Crack Propagation/Tomkins (1975)
H	CCT	Creep Crack Tip Model/Wareing (1977)
H	CCD	Cyclic Creep Damage Model/Franklin (1978)
H	CIM	Crack Interaction Model/Janson (1979)
DH	MCI	Macro Crack Init, Fracture Mechs/Taira et al (1979)
HM	LCT	Local Crack Tip Model/Saxena (1981)
FH	CTE	Crack Tip Energy Model/Radhakrishnan (1982 & 1983)
HJM	FAM	FATIGMOD/A. Miller (1983)
H	CFC	Creep Fatigue Cracks Model/Riedel (1983)
H	SCC	Short Crack Creep Fatigue/Renner et al (1989)
HM	MMM	Microcracking, Creep-Fat-Envir/McDowell & Miller (1991)

Figure 12 - Life prediction models based on crack growth concepts

136

I - STRAINRANGE PARTITIONING

The Strainrange Partitioning (SRP) concept for representing high-temperature creep-fatigue interaction and life prediction has evolved into a comprehensive, workable engineering approach. From its revolutionary introduction in 1971 by Manson, Halford, and Hirschberg, the approach has been developed on a continuing basis through the uninterrupted sponsorship and efforts of the Lewis Research Center of the National Aeronautics and Space Administration (NASA). The titles of the major advances in the method's development are listed below and are good brief descriptors of these sub-elements of the SRP method. As seen from a cursory examination, the SRP method has been developed to deal with all of the major conditions expected during elevated temperature usage. These entail environmental interactions, mean stress effects, multiaxiality of stress and strain, thermal cycling, nonlinear cumulative damage, statistical representations, and representation in terms of total strain range rather than just the inelastic strain. Various industrial design usage has been made of the model, including the design of aeronautical gas turbine engine combustor liners. Software for implementation of the Total Strain Version of SRP is being made available to the general public through the COSMIC organization. The method is currently being evaluated for use in predicting thermal fatigue lives of thermally loaded structural components of the National Aero Space Plane (NASP). Aspects of the method are also being applied to advanced fiber-reinforced metal and intermetallic matrix composites for high-temperature aerospace structural components.

I	SRP	Strainrange Part/Manson, Halford & Hirschberg (1971)
Ia	IDR-SRP	Interaction Damage Rule, SRP/Manson (1973)
Ib	PDR-SRP	Product Damage Rule, SRP/Annis et al (1976)
Ic	ITF-SRP	Inelastic Thermal Fat, SRP/Halford & Manson (1976)
Id	DEX-SRP	Linear Ductility Exh., SRP/Manson & Halford (1976)
Ie	PWA-SRP	Pratt & Whitney Combustor, SRP/Vogel et al (1976)
If	MAF-SRP	Multiaxiality Factor, SRP/Manson & Halford (1977)
Ig	DNE-SRP	Ductility Normalized Eqs, SRP/Halford et al (1977)
Ih	SRC-SRP	Strainrange Conversion Prin, SRP/Manson (1979 & 1983)
Ii	MSE-SRP	Mean Stress Effects, SRP/Halford & Nachtigall (1980)
Ij	CEP-SRP	Combustion Engineering Model, SRP/Lawton (1982)
Ik	TSV-SRP	Total Strain Version of SRP/Halford & Saltsman (1983)
Il	DEP-SRP	Diesel Engine Piston, SRP/Saugerud (1983)
Im	NDR-SRP	Nonlinear Damage Rule, SRP/Hoffelner et al (1983)
In	SDA-SRP	Statistical Data Analysis, SRP/Wirsching (1984)
Io	SRL-SRP	Statistically Refined Life, SRP/Bicego (1984)
Ip	ETM-SRP	Exposure Time Modified, SRP/Kalluri & Manson (1985)
Iq	SSC-SRP	Steady-State Creep Rate, SRP/Kalluri et al (1987)
Ir	TFM-SRP	Time To Failure Modified SRP/Solomon (1988)
Is	TMF-SRP	Thermomech Fatigue, TSV-SRP/Saltsman & Halford (1988)
It	FMB-SRP	Fracture Mechs Basis of SRP/Kitamura & Halford (1989)
FI	PEM	Partitioned Energy Model/Leis (1977)
FI	SEP	Strain Energy Partitioning/He et al (1983)

Figure 13 - Life Prediction models based on variations
of the method of strainrange partitioning

J - MACRO-PHENOMENOLOGICAL MODELS

This category represents those high-temperature fatigue crack initiation models that utilize phenomenological descriptors at the macroscopic level. While there are guiding reasons for selection of the phenomenological variables, some of the models assembled the variables in an empirically driven manner, i.e., what combination of the phenomenological variables will give the "best fit" to the available experimental results. A notable exception to this philosophy is the FATIGMOD of Miller (1983). The Miller model, which underwent considerable development, follows a highly rational approach that was based on considerable understanding of the sequences in the fatigue process. In this category, FATIGMOD and the CDA models are the most highly developed and would stand the greatest chance of being implemented into engineering design and use for structural life prediction.

DJ	TCE	Thermal Cycling Equation/Udoguchi & Wada (1971)
J	PHF	Parametric High Temperature Fatigue/Krempl (1971)
J	SST	Stress-Strain-Temperature Empirical Model/Bernstein (1979)
HJM	FAM	FATIGMOD/A. Miller (1983)
JL	PDA	Preliminary Cyclic Damage Accumulation/Moreno (1985)
J	ICC	Internal Cracking, Coated Single Xtal/Miner et al (1988)
JL	CDA	Cyclic Damage Accumulation/Nelson et al (1992)

Figure 14 - Life prediction models based on macro-phenomenological considerations

K - DAMAGE RATE MODELS

This category of high-temperature fatigue crack initiation life prediction models adopts an interesting perspective for dealing with time-dependent damage accumulation. The basic premise is that if time-dependent damage is being done, and it is more damaging than time-independent damage, then the slower is the rate of application of damage, the greater is the net affect of the damage. In other words, the slower the rate of application of the damaging parameter (inelastic strain, stress, energy, etc.) the greater will be the damage per cycle, and hence the lower will be the cyclic life. Considerable effort went into the development of the Majumdar and Maiya (1976 and 1980) approach at the Argonne National Laboratories. The driver for the research and development efforts was the requirement for life assessment, in advance of construction and usage, of nuclear power plants for electricity generation. The author is unaware of any current application of the listed damage rate models to engineering structural design.

K	DRM	Damage Rate Model/Majumdar & Maiya (1976)
K	MDR	Modified Damage Rate Model/Majumdar & Maiya (1980)
K	ILP	Incremental Life Prediction Law/Satoh & Krempl (1982)
K	TSM	Temp. & Strain Rate Model/Zhang et al (1990)

Figure 15 - Life prediction models based on
damage rate concepts

L - CYCLIC DAMAGE ACCUMULATION MODELS

This category is limited because of the uniqueness of the assumptions that originally went into the development of the first cyclic damage accumulation model. The reader is referred to Moreno's 1985 account for a full justification of the assumptions. Beyond the original assumptions, however, the model takes on more of the character of the MACRO PHENOMENOLOGICAL MODELS described earlier. The model was developed by engineers at the Pratt & Whitney Commercial Engineering Division of United Technologies Corporation, East Hartford, CT, under sponsorship of the NASA Lewis Research Center's Hot Section Turbine Engine Technology Program (HOST). The method has been transcribed into a PC-compatible computer code and is being made commercially available through the COSMIC organization. It is one of only two high-temperature creep-fatigue life prediction computer programs being made available to the general public through COSMIC. The other is the Total Strain Version of Strain Range Partitioning.

JL PDA Preliminary Cyclic Damage Accumulation/Moreno (1985)
JL CDA Cyclic Damage Accumulation/Nelson et al (1992)

Figure 16 - Life prediction models based on a unique assumption
of cyclic damage accumulation

M - MICROMECHANISTIC MODELS

As the micromechanisms of high-temperature cyclic deformation and damage become more widely known and documented through use of advanced metallurgical investigative tools, the more models will be created to describe these physical effects. For the most part, the models proposed to date are highly specific to the alloy systems and cyclic circumstances studied. The most generalized of the models are those of Miller (1983), Neu and Sehitoglu (1989a and 1989b), and McDowell and Miller (1991). The two Millers are unrelated.

M	GBS	Grain Boundary Sliding Model/McLean & Pineau (1978)
M	RVG	R-Void Growth Model/Min & Raj (1978)
M	OCC	Oxide Cracking/Challenger et al (1981a & 1981b)
M	SOC	Stress-Oxidation Crack Tip Model/Antolovich et al (1981)
HM	LCT	Local Crack Tip Model/Saxena (1981)
M	GBV	Grain Boundary Void Model/Weertman (1982)
M	IGW	Init and Growth of Wedge Cracks/Baik & Raj (1982a & 1982b)
M	OFI	Oxidation Fatigue Interaction Model/Reuchet & Remy (1983)
M	ARN	Anelastic Recovery, ODS Alloys/Nardone (1983)
HJM	FAM	FATIGMOD/A. Miller (1983)
M	CCC	Critical Cavity Criteria Model/Rie et al (1988)
M	CBS	Cohesive Boundary Strength Model/Romanoski et al (1988)
M	GBO	Grain Boundary Oxidation Model/Oshida & Liu (1988)
ABDM	FCE	Fatigue-Creep-Envir Model/Neu & Sehitoglu (1989a & 1989b)
HM	MMM	Microcracking, Creep-Fat.-Envir./McDowell & Miller (1991)

Figure 17 - Life prediction models based on micromechanistic
observations and descriptions

MOST HIGHLY DEVELOPED MODELS

The vast majority of the methods, once proposed, have seen little or no followup. From the standpoint of effort put forth toward their development, three basic methods stand out: 1) the time- and cycle-fraction rule as used in ASME Nuclear Code Case N-47; 2) the continuum damage mechanics approach of ONERA in France; and 3) the Strainrange Partitioning Method of NASA Lewis. Each has sustained continual refinement owing to the support and continuity of the sponsoring organizations. The latter two have received the greatest attention during the last decade. The review presented is a severe condensation of a more extensive review being prepared by the author for a monograph on the topic of high-temperature fatigue life prediction methodology for cyclic crack initiation of materials.

0 - TIME-FRACTION + CYCLE-FRACTION
   - ASME CODE, USA

0 - CONTINUUM DAMAGE MECHANICS
   - ONERA, FRANCE
   - NASA-LEWIS, USA

0 - STRAINRANGE PARTITIONING
   - NASA-LEWIS, USA

Figure 18 - Three models are the most highly developed

REFERENCES

Annis, C. G., VanWanderham, M. C. and Wallace, R. M., Strainrange Partitioning Behavior of an Automotive Turbine Alloy, NASA CR-134974, 1976.

Anon., Section III ASME Boiler and Pressure Vessel Code Case 1331-5 (predecessor of current Code Case N-47), 1971.

Anon., Design and Construction Rules for Mechanical Components of Fast Breeder Reactor Nuclear Islands, RCC-MR. Association Francaise pour les regles de conception et de construction des materiels des chaudieres electro-nucleaires, France, 1985.

Antolovich, S. D., Liu, S. and Baur, R., "Low Cycle Fatigue Behavior of Rene' 80 at Elevated Temperature," Metallurgical Transactions A, Vol. 12A, 1981, pp. 473-481.

Arnold, S. M. and Kruch, S., Differential Continuum Damage Mechanics Models for Creep and Fatigue of Unidirectional Metal Matrix Composites, NASA TM-105213, 1991.

Baik, S. and Raj, R., "Wedge Type Creep Damage in Low Cycle Fatigue," Metallurgical Transactions A, Vol. 13A, 1982, pp. 1207-1214.

Baik, S. and Raj, R., "Mechanisms of Creep-Fatigue Interactions," Metallurgical Transactions A, Vol. 13A, 1982, pp. 1215-1221.

Berkovits, A., Investigation of Three Analytical Hypotheses for Determining Material Creep Behavior Under Varied Loads, NASA TN-D-799, 1961.

Berling, J. T. and Conway, J. B., "A Proposed Method for Predicting Low-Cycle Fatigue Behavior of 304 and 316 Stainless Steel," Transactions of the Metallurgical Society, AIME, Vol. 245, 1969, pp. 1137-1140.

Berling, J. T. and Conway, J. B., "A New Approach to the Prediction of Low-Cycle Fatigue Data," Metallurgical Transactions, Vol. 1, 1970, pp. 805-809.

Bernstein, H., "A Stress-Strain-Time Model (SST) for High Temperature Low Cycle Fatigue," in Methods for Predicting Material Life in Fatigue, W. J. Ostergren and J. R. Whitehead (eds.), ASME, NY, 1979, pp. 89-100.

Bicego, V., "A Nonstandard Technique for the Evaluation of the Basic Laws of the Strain Range Partitioning Method in Creep-Fatigue Life Prediction," in Proceedings, Second International Conference on Fatigue and Fatigue Thresholds (Fatigue 84), C. J. Beevers (ed.), Engineering Materials Advisory Services, Ltd., Cradley Heath, Warley, U.K., Vol. 3, 1984, pp. 1257-1268.

Bui-Quoc, T., "An Engineering Approach for Cumulative Damage in Metals Under Creep Loading," Transactions, ASME, Journal of Pressure Vessel Technology, Vol. 101, 1979, pp. 337-343.

Bui-Quoc, T. and Biron, A., "A Phenomenological Approach for the Analysis of Combined Fatigue and Creep," Nuclear Engineering Design, Vol. 71, 1982, pp. 89-102.

Carden, A. E., "Parametric Analysis of Fatigue Crack Growth," in Proceedings, Conference on Creep and Fatigue in Elevated Temperature Environment, Philadelphia, PA, Sept. 1973 (Sheffield, England, April 1974). Sponsored by the American Society for Testing and Materials, Philadelphia, and the Institute of Mechanical Engineers, London, 1974.

Challenger, K. D., Miller, A. K. and Brinkman, C. R., "An Explanation for the Effects of Hold Periods on the Elevated Temperature Fatigue Behavior of 2 1/4Cr-1Mo Steel," Journal of Engineering Materials and Technology, ASME, Vol. 103, 1981, pp. 7-14.

Challenger, K. D., Miller, A. K. and Langdon, R. L., Journal of Materials and Energy Systems, Vol. 3, 1981, pp. 51-61.

Chan, K. S. and Miller, A. K., "FATIGMOD: A Unified Phenomenological Model for Predicting Fatigue Crack Initiation and Propagation," ASME International Conference on Advances in Life Prediction Methods, 1983, pp. 1-16.

Coffin, L. F., "A Study of the Effects of Cyclic Thermal Stresses on a Ductile Metal," Transactions, ASME, Vol. 76, 1954, pp. 931-950.

Coffin, L. F., "The Effect of Frequency on High-Temperature, Low-Cycle Fatigue," in Proceedings, Air Force Conference on Fracture and Fatigue of Aircraft Structures, AFDL-TR-70-144, 1970, pp. 301-312.

Coffin, L. F., "The Concept of Frequency Separation in Life Prediction for Time-Dependent Fatigue," ASME-MPC Symposium on Creep-Fatigue Interaction, MPC-3, 1976, pp. 349-363.

Coles, A. and Skinner, D., "Assessment of Thermal-Fatigue Resistance of High Temperature Alloys," Journal of the Royal Aeronautical Society of London, Vol. 69, 1965, pp. 53-55.

Eckel, J. F., "Influence of Frequency on the Repeated Bending Life of Acid Lead," Proceedings, American Society for Testing and Materials, Vol. 51, 1951, pp. 745-756.

Edmunds, H. G. and White, D. J., "Observations of the Effect of Creep Relaxation on High-Strain Fatigue," Journal of Mechanical Engineering Science, Vol. 8, No. 3, 1966, pp. 310-321.

Esztergar, E. P. and Ellis, J. R., "Cumulative Fatigue Damage Concepts in Creep-Fatigue Life Predictions," in Proceedings, International Conference on Thermal Stresses and Thermal Fatigue, D. J. Littler (ed.), The Butterworth Group, London, 1969, pp. 128-156.

Franklin, C. J., High-Temperature Alloys for Gas Turbines, D. Coutsouradis, P. Felix, H. Fischmeister, L. Habraken, Y. Lindblom and M. O. Speidel (eds.), Applied Science, London, 1978, pp. 513-547.

Hales, R., "A Method of Creep Damage Summation Based on Accumulated Strain for the Assessment of Creep-Fatigue Endurance," Fatigue of Engineering Materials and Structures, Vol. 6, No. 2, 1983, pp. 121-135.

Halford, G. R. and Manson, S. S., "Life Prediction of Thermal-Mechanical Fatigue Using Strainrange Partitioning," in Thermal Fatigue of Materials and Components, ASTM STP 612, D. A. Spera and D. F. Mowbray (eds.), 1976, pp. 239-254.

Halford, G. R., Saltsman, J. F. and Hirschberg, M. H., "Ductility Normalized-Strainrange Partitioning Life Relations for Creep-Fatigue Life Prediction," in Proceedings, Conference on Environmental Degradation of Engineering Materials, Virginia Polytechnic Institute and State University, Blacksburg, VA, 1977, pp. 599-612.

Halford, G. R. and Nachtigall, A. J., "The Strainrange Partitioning Behavior of an Advanced Gas Turbine Disk Alloy, AF2-1DA," Journal of Aircraft, Vol. 17, No. 8, 1980, pp. 598-604.

Halford, G. R. and Saltsman, J. F., "Strainrange Partitioning - A Total Strainrange Version," ASME International Conference on Advances in Life Prediction, D. A. Woodford and J. R. Whitehead (eds.), 1983, pp. 17-26.

He, J., Duan, Z., Ning, Y. and Zhao, D., "Strain Energy Partitioning and Its Application to GH33A Nickel-Base Superalloy and 1Cr18Ni9Ti Stainless Steel," in Advances in Life Prediction Methods, D. A. Woodford and J. R. Whitehead (eds.), ASME, NY, 1983, pp. 27-32.

Hoffelner, W., Melton, K. N. and Wuthrich, C., "On Life Time Predictions with the Strain Range Partitioning Method," Fatigue of Engineering Materials and Structures, Vol. 6, No. 1, 1983, pp. 77-87.

Janson, J., "Damage Model of Creep-Fatigue Interaction," Engineering Fracture Mechanics, Vol. 11, 1979, pp. 397-403.

Kachanov, L. M., "Time of the Rupture Process Under Creep Conditions," Izvestiia Akademii Nauk, SSSR, Otdelenie Tekhnicheskikh Nauk., No. 8, 1958, pp. 26-31.

Kalluri, S. and Manson, S. S., Time Dependency of SRP Life Relationships, NASA CR-174946, 1985.

Kalluri, S., Manson, S. S. and Halford, G. R., "Environmental Degradation of 316 Stainless Steel in High Temperature Low Cycle Fatigue," in Third International Conference on Environmental Degradation of Engineering Materials, R. P. McNitt and M. R. Louthan, Jr. (eds.), Pennsylvania State University, University Park, PA, 1987, pp. 503-519.

Kalluri, S., Manson, S. S. and Halford, G. R., "Exposure Time Considerations in High Temperature Low Cycle Fatigue," in Proceedings, Fifth International Conference on Mechanical Behavior of Materials (ICM-5, Beijing), M. G. Yan, S. H. Zhang and Z. M. Zheng (eds.), Pergamon Press, Vol. 2, 1987, pp. 1029-1036.

Kitamura, T. and Halford, G. R., High Temperature Fracture Mechanics Basis for Strainrange Partitioning, NASA TM-4133, 1989.

Krempl, E., "The Temperature Dependence of High-Strain Fatigue Life at Elevated Temperature in Parameter Representation," in Proceedings, International Conference on Thermal Stresses and Thermal Fatigue, D. J. Littler (ed.), The Butterworth Group, London, 1971, pp. 36-46.

Lagneborg, R. and Attermo, R., "The Effect of Combined Low-Cycle Fatigue and Creep on the Life of Austenitic Stainless Steels," Metallurgical Transactions, Vol. 2, 1971, pp. 1821-1827.

Langer, B. F., "Fatigue Failure From Stress Cycles of Varying Amplitude," Transactions, ASME, Vol. 59, 1937, pp. A160-A162.

Lawton, C. W., "Use of Low-Cycle Fatigue Data for Pressure Vessel Design Low-Cycle Fatigue and Life Prediction," ASTM STP-770, C. Amzallag, B. N. Leis, P. Rabbe (eds.), 1982, pp. 585-599.

Lazan, B. J., "Dynamic Creep and Rupture Properties Under Tensile Fatigue Stress," in Proceedings, American Society for Testing and Materials, Vol. 49, 1949, p. 757.

Leis, B. N., "An Energy-Based Fatigue and Creep-Fatigue Damage Parameter," Transactions, ASME, Journal of Pressure Vessel Technology, Vol. 99, 1977, pp. 524-533.

Lemaitre, J., Chaboche, J. L. and Munakata, Y., "Method of Metal Characterization for Creep and Low Cycle Fatigue Prediction in Structures - Example of Udimet 700," in Proceedings, Symposium on Mechanical Behavior of Materials, Kyoto, Japan, 1973, pp. 239-249.

Lemaitre, J. and Plumtree, A., Joint ASME/CSME PVP Conference, Montreal, 1978.

Levaillant, C., Rezgui, B. and Pineau, A., Proceedings, Third International Conference on Mechanical Behavior of Materials, Cambridge, England, Miller and Smith (eds.), Vol. 2, 1979, pp. 163-173.

Majumdar, S. and Maiya, P. S., "A Damage Equation for Creep-Fatigue Interaction," 1976 ASME-MPC Symposium on Creep-Fatigue Interaction, MPC-3, ASME, NY, 1976, pp. 323-336.

Majumdar, S. and Maiya, P. S., "A Mechanistic Model for Time-Dependent Fatigue," Journal of Engineering Materials and Technology, ASME, Vol. 102, 1980, pp. 159-167.

Manson, S. S., Behavior of Materials Under Conditions of Thermal Stress, NACA TN-2933, 1954.

Manson, S. S., "Thermal Stress in Design, Part 19, Cyclic Life of Ductile Materials," Machine Design, Vol. 32, 1960, pp. 139-144.

Manson, S. S. and Hirschberg, M. H., "Fatigue Behavior in Strain Cycling in the Low- and Intermediate-Cycle Range," in Fatigue - An Interdisciplinary Approach, Burke, Reed and Weiss (eds.), Syracuse University Press, NY, 1964, pp. 133-178.

Manson, S. S., "Fatigue: A Complex Subject - Some Simple Approximations," Experimental Mechanics, Vol. 5, No. 7, 1965, pp. 193-226.

Manson, S. S. and Halford, G. R., "A Method of Estimating High-Temperature Low-Cycle Fatigue Behavior of Materials," in Proceedings, International Conference on Thermal and High-Strain Fatigue, Metals and Metallurgy Trust, London, 1967, pp. 154-170.

Manson, S. S., Halford, G. R. and Hirschberg, M. H., "Creep-Fatigue Analysis by Strain-Range Partitioning," Symposium on Design for Elevated Temperature Environment, ASME, NY, 1971, pp. 12-28.

Manson, S. S., Halford, G. R. and Spera, D. A., "The Role of Creep in High Temperature Low-Cycle Fatigue," Chapter 12, Advances in Creep Design, A. I. Smith and A. M. Nicolson (eds.), Halsted Press, 1971, pp. 229-249.

Manson, S. S., "The Challenge to Unify Treatment of High Temperature Fatigue - A Partisan Proposal Based on Strainrange Partitioning," in Fatigue at Elevated Temperatures, ASTM STP-520, A. E. Carden, A. J. McEvily and C. H. Wells (eds.), 1973, pp. 744-782.

Manson, S. S. and Halford, G. R., "Treatment of Multiaxial Creep-Fatigue by Strainrange Partitioning," 1976 MPC Symposium on Creep-Fatigue Interaction, MPC-3, R. M. Curran (ed.), 1976, pp. 299-322.

Manson, S. S. and Halford, G. R., Discussion to paper by J. J. Blass and S. Y. Zamrik entitled, Multiaxial Low-Cycle Fatigue of Type 304 Stainless Steel in 1976 ASME-MPC Symposium on Creep-Fatigue Interaction, ASME, NY, pp. 129-159. Journal of Engineering Materials and Technology, ASME, Vol. 99, 1977, pp. 283-286.

Manson, S. S., "Some Useful Concepts for the Designer in Treating Cumulative Fatigue Damage at Elevated Temperatures," Third International Conference on Mechanical Behavior of Materials, Cambridge, England, Vol. I, 1979, pp. 13-45.

Manson, S. S., "The Strainrange Conversion Principle for Treating Cumulative Fatigue Damage in the Creep Range," in Random Fatigue Life Prediction, Y. S. Shin and M. K. Au-Yang (eds.), PVP Vol. 72, ASME, NY, 1983, pp. 1-30.

Marshall, P. and Cook, T. R., "Prediction of Failure of Materials Under Cyclic Loading," in Proceedings, International Conference on Thermal Stresses and Thermal Fatigue, D. J. Littler (ed.), The Butterworth Group, London, 1971, pp. 81-88.

McDowell, D. L. and Miller, M. P., "Physically Based Microcrack Propagation Laws for Creep-Fatigue-Environment Interaction," presented at the ASME Winter Annual Meeting, Atlanta, GA, 1991.

McLean, D. and Pineau, A., "Grain-Boundary Sliding as a Correlating Concept for Fatigue Hold-Times," Metal Science, Vol. 12, 1978, pp. 313-316.

Miller, D. A., Hamm, C. D. and Phillips, J. L., "A Mechanistic Approach to the Prediction of Creep-Dominated Failure During Simulated Creep-Fatigue," Material Science and Engineering, Vol. 53, 1982, pp. 233-244.

Min, B. K. and Raj, R., "Hold-Time Effects in High Temperature Fatigue," Acta Metallurgica, Vol. 26, 1978, pp. 1007-1022.

Miner, M. A., "Cumulative Damage in Fatigue," Transactions, ASME, Journal of Applied Mechanics, Vol. 67, 1945, pp. A159-A167.

Miner, R. V., Gayda, J., Hebsur, M. G., "Creep-Fatigue Behavior of Ni-Co-Cr-Al-Y Coated PWA 1480 Superalloy Single Crystals," in Low Cycle Fatigue - Directions for the Future, ASTM STP-942, H. D. Solomon, G. R. Halford, L. R. Kaisand and B. N. Leis (eds.), 1988, pp. 371-384.

Morishita, M., Taguchi, K., Asayama, T., Ishikawa, A. and Asada, Y., "Application of the Overstress Concept for Creep-Fatigue Evaluation," in Low Cycle Fatigue - Directions for the Future, ASTM STP-942, H. D. Solomon, G. R. Halford, L. R. Kaisand and B. N. Leis (eds.), 1988, pp. 487-499.

Morrow, J., An Investigation of Plastic Strain Energy as a Criterion for Finite Fatigue Life, Report to the Garrett Corp., 1960.

Nelson, R. S., Levan, G. W. and Harvey, P. R., Creep Fatigue Life Prediction for Engine Hot Section Materials (Isotropic), NASA CR-189221, August 1992.

Neu, R. W. and Sehitoglu, H., "Thermomechanical Fatigue, Oxidation, and Creep: Part I. Damage Mechanisms," Metallurgical Transactions A, Vol. 20A, 1989, pp. 1755-1767.

Neu, R. W. and Sehitoglu, H., "Thermomechanical Fatigue, Oxidation, and Creep: Part II. Life Prediction," Metallurgical Transactions A, Vol. 20A, 1989, pp. 1769-1783.

Nissley, D. M., Meyer, T. G. and Walker, K. P., "Life Prediction and Constitutive Models for Engine Hot Section Anisotropic Materials Program," Final Report, NASA CR-189223, Sept. 1992.

Nordone, V. C., Doctoral Dissertation, Columbia University, NY, 1983.

Oshida, Y. and Liu, H. W., "Grain Boundary Oxidation and an Analysis of the Effects of Oxidation on Fatigue Crack Nucleation Life," in Low Cycle Fatigue - Directions for the Future, ASTM STP-942, H. D. Solomon, G. R. Halford, L. R. Kaisand and B. N. Leis (eds.), 1988, pp. 1199-1217.

Ostergren, W. J., "A Damage Function and Associated Failure Equations for Predicting Hold Time and Frequency Effects in Elevated Temperature, Low Cycle Fatigue," Journal of Testing and Evaluation, Vol. 4, No. 5, 1976, pp. 327-339.

Ostergren, W. J., "Correlation of Hold Time Effects in Elevated Temperature Low Cycle Fatigue Using a Frequency Modified Damage Function," 1976 ASME MPC Symposium on Creep-Fatigue Interaction, MPC-3, 1976, pp. 179-202.

Ostergren, W. J. and Krempl, E., "A Uniaxial Damage Accumulation Law for Time-Varying Loading Including Creep-Fatigue Interaction," Transactions, ASME, Journal of Pressure Vessel Technology, Vol. 101, 1979, pp. 118-124.

Palmgren, A., "Die Lebensdauer von Kugellagern," Z.V.D.I., Vol. 68, No. 14, 1924, pp. 339-341.

Plumtree, A. and Lemaitre, J., Advances in Fracture Research, D. Francois (ed.), Pergamon Press, NY, 1982, p. 2379.

Polhemous, J. F., Spaeth, C. E. and Vogel, W. H., "Ductility Exhaustion for Prediction of Thermal Fatigue and Creep Interaction," in Fatigue at Elevated Temperatures, ASTM STP-520, A. E. Carden, A. J. McEvily and C. H. Wells (eds.), 1973, pp. 625-636.

Priest, R. H. and Ellison, E. G., "A Combined Deformation Map - Ductility Exhaustion Approach to Creep-Fatigue Analysis," Materials Science and Engineering, Vol. 49, 1981, pp. 7-17.

Priest, R. H., Beauchamp, D. J. and Ellison, E. G., "Damage During Creep-Fatigue," in Advances in Life Prediction Methods, D. A. Woodford and J. R. Whitehead (eds.), ASME, NY, 1983, pp. 115-122.

Radhakrishnan, V. M., "Damage Accumulation and Fracture Life in High-Temperature Low-Cycle Fatigue," in Low-Cycle Fatigue and Life Prediction, ASTM STP-770, D. Amzallag, B. N. Leis and P. Rabbe (eds.), 1982, pp. 135-151.

Radhakrishnan, V. M., "Life Prediction in Time Dependent Fatigue," in Advances in Life Prediction Methods, D. A. Woodford and J. R. Whitehead (eds.), ASME, NY, 1983, pp. 143-150.

Renner, E., Vehoff, H. and Neumann, P., "Prediction for Creep-Fatigue Based on the Growth of Short Cracks," Fatigue and Fracture of Engineering Materials and Structures, Vol. 12, No. 6, 1989, pp. 569-584.

Reuchet, J. and Remy, L., "Fatigue Oxidation Interaction in a Superalloy - Application to Life Prediction in High Temperature Low Cycle Fatigue," Metallurgical Transactions A, Vol. 14A, 1983, pp. 141-149.

Rie, K. T., Schmidt, R. M., Ilschner, B. and Nam, S. W., "A Model for Predicting Low Cycle Fatigue Life Under Creep-Fatigue Interaction," in Low Cycle Fatigue - Directions for the Future, ASTM STP-942, H. D. Solomon, G. R. Halford, L. R. Kaisand and B. N. Leis (eds.), 1988, pp. 313-328.

Riedel, H., "Crack-Tip Stress Fields and Crack Growth Under Creep-Fatigue Conditions," in Elastic-Plastic Fracture, Second Symposium, Vol. 1, Inelastic Crack Analysis, ASTM STP-803, C. F. Shih and J. P. Guda (eds.), 1983, pp. 505-520.

148

Robinson, E. L., "Effect of Temperature Variation on the Long-Time Rupture Strength of Steels," Transactions, ASME, Vol. 74, No. 5, 1952, pp. 777-780.

Romanoski, G. R., Antolovich, S. D. and Pelloux, R. M., "A Model for Life Predictions of Nickel-Base Superalloys in High-Temperature Low Cycle Fatigue," in Low Cycle Fatigue - Directions for the Future, ASTM STP-942, H. D. Solomon, G. R. Halford, L. R. Kaisand and B. N. Leis (eds.), 1988, pp. 456-467.

Saltsman, J. F. and Halford, G. R., A Model for Life Prediction of Thermomechanical Fatigue Using the Total Strain Version of Strainrange Partitioning (SRP) - A Proposal, NASA TP-2779, 1988.

Satoh, M. and Krempl, E., "An Incremental Life Prediction Law for Creep-Fatigue Interaction," Pressure Vessels and Piping, Vol. 60, ASME, NY, 1982, pp. 71-79.

Saugerud, O. T., "Advances in Life Prediction of Thermally-Loaded Diesel Engine Components," in Advances in Life Prediction Methods, D. A. Woodford and J. R. Whitehead (eds.), ASME, NY, 1983, pp. 229-240.

Saxena, A., "A Model for Predicting the Effect of Frequency on Fatigue Crack Growth Behavior at Elevated Temperature," Fatigue of Engineering Materials and Structures, Vol. 3, No. 3, 1981, pp. 247-255.

Saxena, A., Landes, J. D. and Bassani, J. L. (eds.), Nonlinear Fracture Mechanics: Vol. I - Time-Dependent Fracture, ASTM STP-995, 1989.

Solomon, H. D., "Frequency Modified Low Cycle Fatigue Crack Propagation," Metallurgical Transactions, Vol. 4, 1973, pp. 341-347.

Solomon, H. D., "Low-Frequency, High-Temperature Low Cycle Fatigue of 60Sn-40Pb Solder," in Low Cycle Fatigue - Directions for the Future, ASTM STP-942, H. D. Solomon, G. R. Halford, L. R. Kaisand and B. N. Leis (eds.), 1988, pp. 342-370.

Spera, D. A., A Linear Creep Damage Theory for Thermal Fatigue of Materials, Doctoral Thesis, University of Wisconsin, Madison, WI, 1968.

Sunamoto, D., Endo, T. and Fujihara, M., "Hold Time Effects in High Temperature, Low Cycle Fatigue of Low Alloy Steels," in Creep and Fatigue in Elevated Temperature Applications, Institution of Mechanical Engineers, Vol. 1, 1974, C252.

Taira, S., "Lifetime of Structures Subjected to Varying Load and Temperature," Colloquium on Creep in Structures, Stanford University, Stanford, CA. International Union of Theoretical and Applied Mechanics (IUTAM), N. J. Hoff (ed.), Springer-Verlag, 1962, pp. 96-119.

Taira, S., Ohtani, R. and Komatsu, T., "Application of J - Integral to High-Temperature Crack Propagation, Part 1: Creep Crack Propagation," Transactions of ASME, Journal of Engineering Materials Technology, Vol. 101, 1979, pp. 154-161.

Tapsell, H. J., Forrest, P. G. and Tremain, G. R., "Creep Due to Fluctuating Stresses at Elevated Temperatures," Engineering, Vol. 170, 1950, p. 189.

Timo, D. P., "Designing Turbine Components for Low-Cycle Fatigue," Proceedings, International Conference on Thermal Stresses and Thermal Fatigue, D. J. Littler (ed.), The Butterworth Group, London, 1971, pp. 453-469.

Tomkins, B., "Fatigue Crack Propagation - An Analysis," Philosophical Magazine, Vol. 18, 1968, pp. 1041-1066.

Tomkins, B., "The Development of Fatigue Crack Propagation Models for Engineering Applications at Elevated Temperatures," ASME Journal of Engineering Materials and Design, Vol. 97, 1975, pp. 289-297.

Udoguchi, T. and Wada, T., "Thermal Effect on Low-Cycle Fatigue Strength of Steels," Proceedings, International Conference on Thermal Stresses and Thermal Fatigue, D. J. Littler (ed.), The Butterworth Group, London, 1971, pp. 109-123.

Udoguchi, T., Asada, Y. and Ichino, I., "A Frequency Interpretation of Hold-Time Experiments on High Temperature Low-Cycle Fatigue of Steels for LMFBR," Creep and Fatigue in Elevated Temperature Applications, Institution of Mechanical Engineers, Vol. 1, 1974, C211.

Valanis, K. C., "On the Effect of Frequency on Fatigue Life," Mechanics of Fatigue, AMD Vol. 47, Proceedings of a Symposium on Mechanics in Fatigue, Washington, D.C., T. Mura (ed.), ASME, NY, 1981, pp. 21-32.

Vogel, W. H., Soderquist, R. W. and Schlein, B. C., "Application of Creep-LCF Cracking Model to Combustor Durability Prediction," in Fatigue Life Technology, T. A. Cruse and J. P. Gallagher (eds.), ASME, NY, 1977, pp. 22-31.

Wareing, J., Tomkins, B. and Sumner, G., "Extent to Which Material Properties Control Fatigue Failure at Elevated Temperatures," in Fatigue at Elevated Temperatures, ASTM STP-520, American Society for Testing and Materials, Philadelphia, PA, 1973, pp. 123-138.

Wareing, J., "Creep-Fatigue Interactions in Austenitic Stainless Steels," Metallurgical Transactions A, Vol. 8A, 1977, pp. 711-721.

Weertman, J. R., "A Study of the Role of Grain Boundary Cavitation in the Creep-Fatigue Interaction in High Temperature Fatigue," Final Technical Report, Northwestern University, Evanston, IL, 1982.

Wellinger, K. and Sautter, S., "Der Einfluss von Tempertur, Dehnungsgeschwindigkeit and Haltezeit auf das Zeitfestigkeitsverhalten von Stahlen," Arck. Eisenhuttenwes, Vol. 44, 1973, pp. 47-55.

Whaley, P. W., "A Thermodynamic Approach to Material Fatigue," in Advances in Life Prediction Methods, D. A. Woodford and J. R. Whitehead (eds.), ASME, NY, 1983, pp. 41-50.

Wirsching, P. H. and Wu, Y. T., Reliability Considerations for the Total Strainrange Version of Strainrange Partitioning, NASA CR-174757, 1984.

Wood, D. S., "The Effect of Creep on the High-Strain Fatigue Behavior of a Pressure Vessel Steel," Welding Research Supplement, Vol. 45, 1966, pp. 90s-96s.

Zhang, A., Bui-Quoc, T. and Gomuc, R., "A Procedure for Low Cycle Fatigue Life Prediction for Various Temperatures and Strain Rates," submitted to Journal of Engineering Materials and Technology, 1990.

Life Assessment of Structural Components Using Inelastic Finite Element Analyses

Vinod K. Arya
University of Toledo
Toledo, OH

and

Gary R. Halford
NASA Lewis Research Center
Cleveland, OH

PAGE _____ INTENTIONALLY BLANK

INTRODUCTION

The need for enhanced and improved performance of structural components subject to severe cyclic thermal/mechanical loadings, such as in the aerospace industry, requires development of appropriate solution technologies involving time-dependent inelastic analyses. Such analyses are mandatory to predict local stress-strain response and to assess more accurately the cyclic life time of structural components. The NASA-Lewis Research Center is cognizant of this need. As a result of concerted efforts at Lewis during the last few years, several such finite element solution technologies (in conjunction with the finite element program MARC (Ref. 1)) have been developed and successfully applied to numerous uniaxial and multiaxial problems. These solution technologies, although developed for use with MARC program, are general in nature and can easily be extended for adaptation with other finite element programs such as ABAQUS, ANSYS, etc.

This paper presents the description and results obtained from two such inelastic finite element solution technologies. The first employs a classical (non-unified) creep-plasticity model. An application of this technology is presented for a hypersonic inlet cowl-lip problem. The second of these technologies uses a unified creep-plasticity model put forth by Freed (Ref. 2). The structural component for which this finite element solution technology is illustrated, is a cylindrical rocket engine thrust chamber. The paper also demonstrates the advantages of employing a viscoplastic model for nonlinear time-dependent structural analyses.

The life analyses for cowl-lip and cylindrical thrust chambers are presented. These analyses are conducted by using the stress-strain response of these components obtained from the corresponding finite element analyses.

It is believed that the results from the present work will encourage other researchers to perform such finite element analyses to assess more accurately the deformation behavior and cyclic life time of structural components.

COWL LIP
(Classical Creep-Plasticity Analysis)

A three-dimensional finite element model of the cowl lip, Fig. 1, was constructed by Melis and Gladden (Ref. 3). The model consists of 3294 eight-noded, solid, isoparametric elements and 4760 nodes. A considerably large number of elements was required to handle the steep temperature gradient produced by the severe thermal loading imposed on the component. The steady-state temperature distributions in the cowl lip were obtained from Ref. 3. A linear interpolation technique was then employed to calculate the temperatures during the transient state. The simplified thermal loading cycle used to perform the time-dependent non-unified creep-plasticity analysis is shown in Fig. 2.
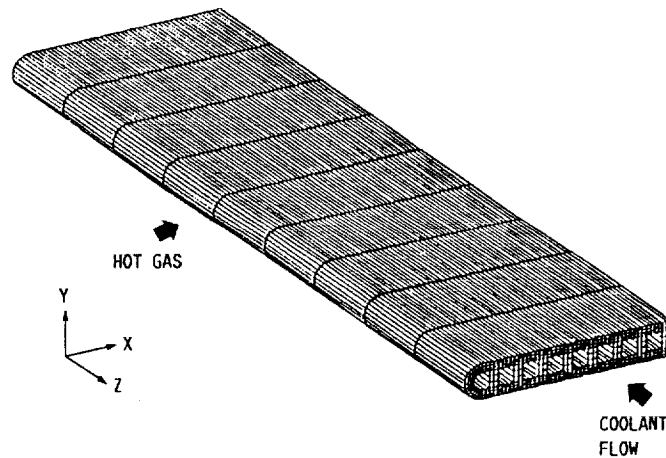
Figure 1 - Cowl lip finite element model
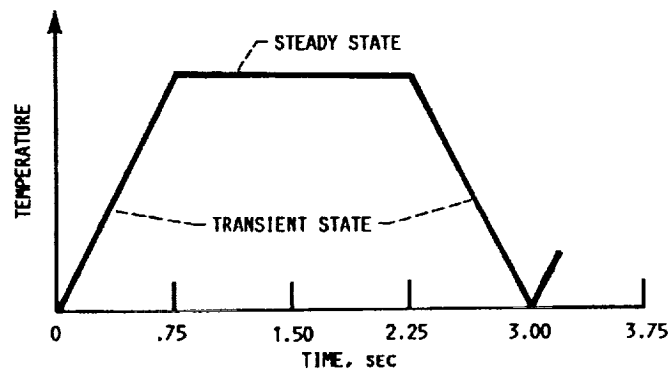
Figure 2 - Simulated thermal response used in structural analyses

STRUCTURAL ANALYSES

Linear elastic, nonlinear elastic-plastic and elastic-plastic-creep analyses were performed using the finite element program MARC. The values of material constants and the description of creep law used in the analysis are given in Arya, et al (Ref. 4). Figure 3 depicts the elastically calculated stress along a cross section of the cowl lip at thermal steady state. The magnitude of the largest stress predicted from this analysis is much higher than the yield strength for copper (the material of cowl lip). This shows that an elastic analysis for this severely thermally driven problem is inadequate. The stress values from an elastic-plastic analysis are exhibited in Fig. 4. The figure shows the reduction of maximum compressive stress (from about 554.3 MPa) to a more reasonable value (of about 196.5 MPa). The effect of time on stress distribution is obtained by conducting an elastic-plastic-creep analysis and it is shown in Fig. 5. The maximum compressive stress still occurs at the leading edge but with a further reduced magnitude of about 131.0 MPa.
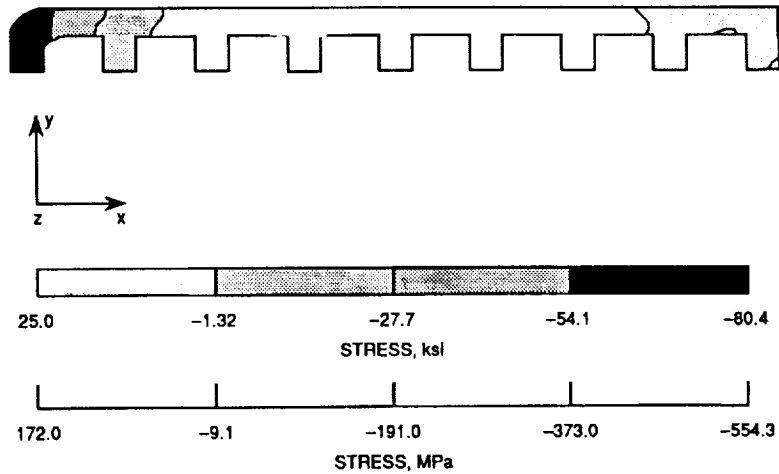
Figure 3 - Elastic analysis
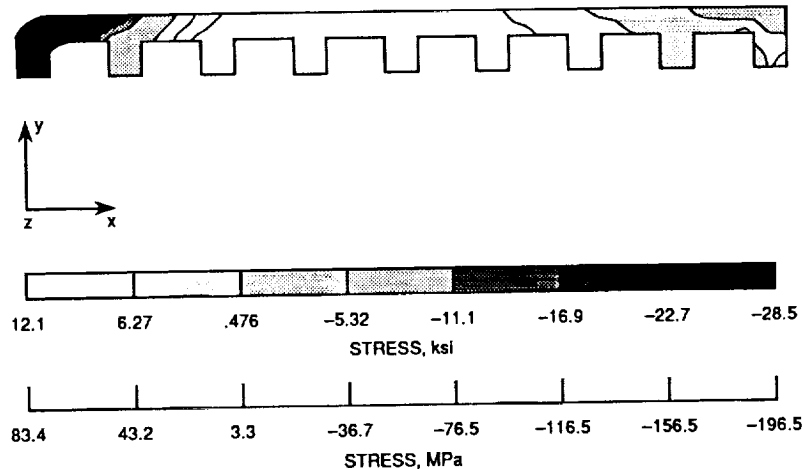
Figure 4 - Elastic-plastic analysis
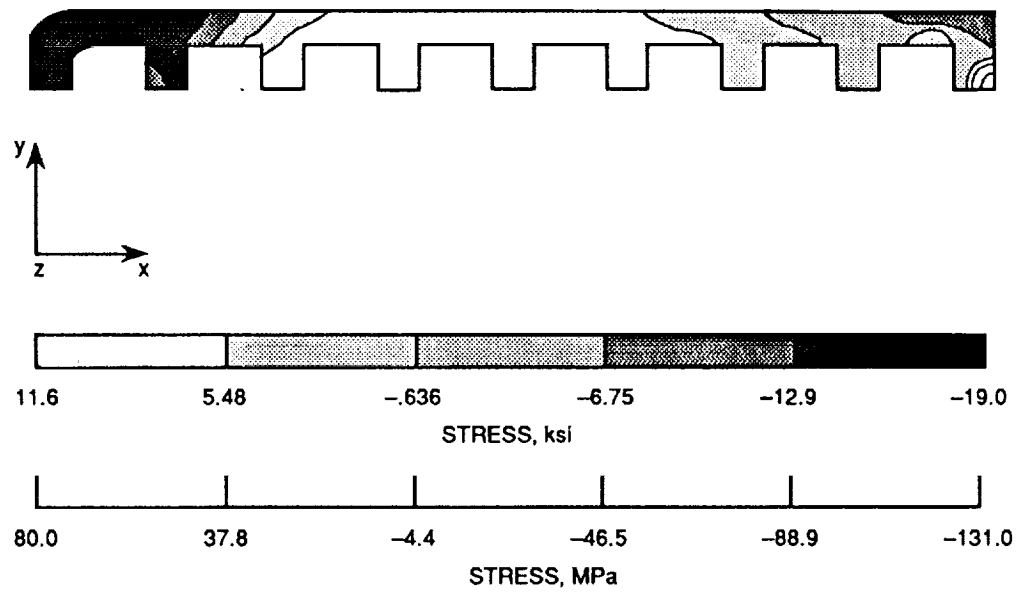
Figure 5 - Elastic-plastic-creep analysis

LIFE ANALYSIS OF COWL LIP

The stress-strain results from the structural analyses were used in estimating the cyclic crack initiation life of the cowl lip. The thermo-mechanical fatigue (TMF) loops calculated at the 'critical' cowl lip location are shown in Fig. 6. The critical location is defined as the location with largest total strain range. Using this total strain range and the fatigue curve of Fig. 7, the cyclic crack initiation lives from different structural analyses can be estimated. The fatigue curve of Fig. 7 is obtained by Conway, et al (Ref. 5). The details of life analyses and justification for using data of Fig. 7 for current life analyses may be found in Arya, et al (Ref. 4).
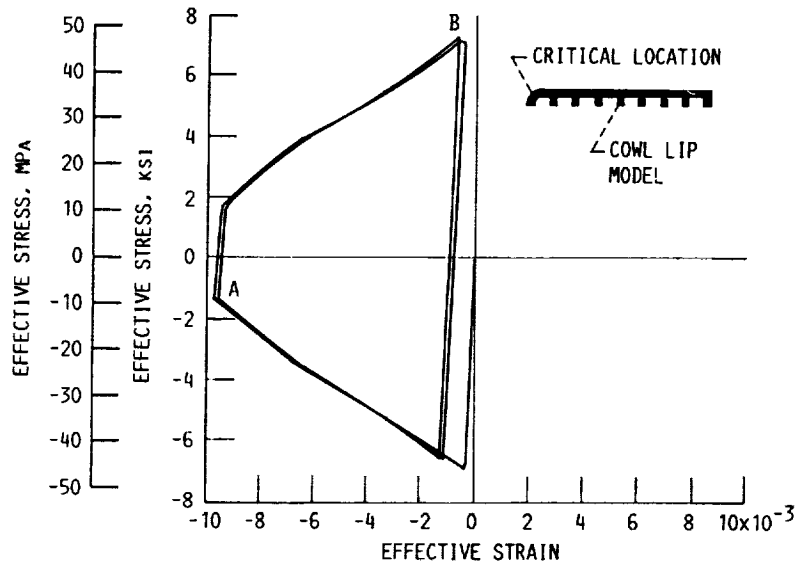
Figure 6 - Hysteresis loops for cowl lip
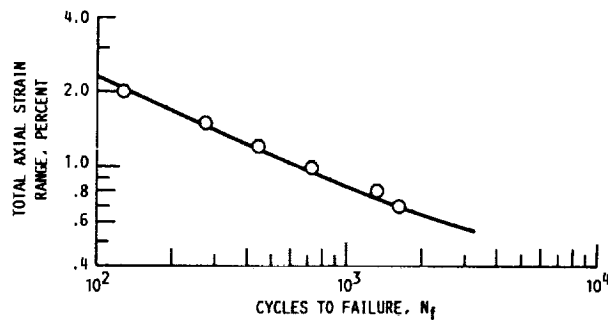
Figure 7 - Fatigue curve (taken from Conway et al [5])

COMPARISON OF HYSTERESIS LOOP CHARACTERISTICS

A comparison of hysteresis loop characteristics (total strain range, stress range, elastic strain range, plastic strain range and the approximate creep strain range) is presented for three different (elastic, elastic-plastic and elastic-plastic-creep) analyses in Table I. Using the total strain ranges shown in this table and fatigue curve of Fig. 7, the elastic, elastic-plastic and elastic-plastic-creep analyses are shown to predict the cyclic crack initiation lives as 2300, 1000 and 800 cycles, respectively. Since the elastic-plastic-creep analysis is judged to give the most realistic structural analysis results, the corresponding life of 800 cycles to failure is also judged to be the most realistic estimate of expected life time of cowl lip.

Table I - Comparison of Hysteresis Loop Characteristics

Analysis	Effective Stress at Maximum Temperature, MPa	Effective Stress Range, MPa	Total Mechanical Strain Range	Elastic Strain Range, $\Delta\varepsilon_{el}$	Plastic Strain Range, $\Delta\varepsilon_{pp}$	Creep Strain Range, $\Delta\varepsilon_{pc}$	Cycles to Failure, N_f
Elastic	-554.4	726.7	0.0062	0.0062	----------	----------	2300
Elastic-plastic	-9.7	60.7*	0.0085	0.0005	0.0080	----------	1000
Elastic-plastic creep	-9.0	60.0*	0.0092	0.0005	(»)0.0080	(»)0.0007	800

Strain range between points A and B of hysteresis loop of Figure 6.

CYLINDRICAL THRUST CHAMBER LINER
(Unified Creep-Plasticity or Viscoplastic Analysis)

To demonstrate the development and application of a finite element solution technology pertaining to viscoplastic models, the problem of a cylindrical thrust chamber is presented. Two types of channel geometries, rectangular and circular, were analyzed. The latter configuration is more thermally compliant. The finite element models for these geometries together with the number of elements and nodes are shown in Fig. 8. The thermal and pressure loading cycles are shown in Fig. 9.

Thermal Analyses: Steady-state heat transfer analyses were performed for the two channel geometries using MARC program. The temperature values thus obtained were linearly interpolated to obtain the temperature distributions for the two geometries over the complete loading cycle. The plots of these temperature distributions may be found in Arya, et al (Ref. 6).

RECTANGULAR   CIRCULAR

532 ELEMENTS,
601 NODES

552 ELEMENTS,
615 NODES
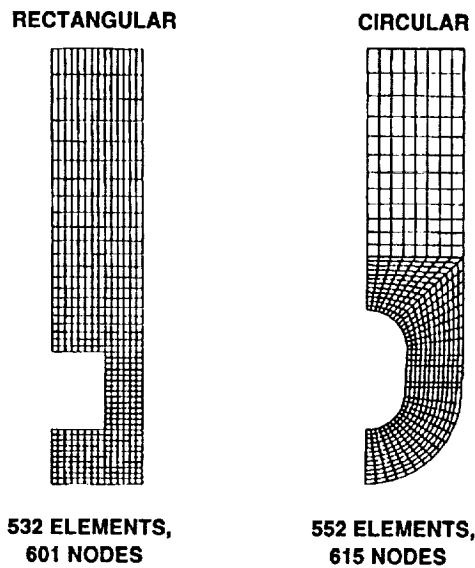
Figure 8 - Finite element models for two channel geometries

TYPICAL CYCLE HISTORY

HEAT TRANSFER
COEFFICIENT,
TEMPERATURE, OR
PRESSURE

COLD PHASE   HOT PHASE

.10   .90   .80   .45   1.25

TIME, sec
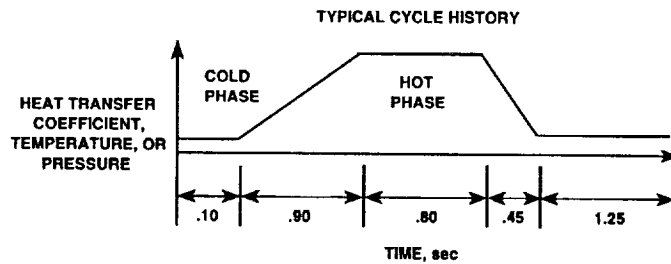
Figure 9 - Cyclic thermal and pressure loadings

STRUCTURAL ANALYSES FOR THRUST CHAMBERS

A viscoplastic model put forth by Freed (Ref. 2) was employed to conduct the nonlinear structural analyses. The model was implemented in MARC program through user subroutine HYPELA. Complete details of implementation are given in Arya and Kaufman (Ref. 7). The material of the segments is copper. The values of material constants taken from Freed (Ref. 2) were utilized in numerical computations. Figure 10 depicts the deformed geometries of channels after five loading cycles. To facilitate visual interpretation, the deformations are magnified by a factor of 1000. The figure shows significant deformation of rectangular channel. The circular channel shows little apparent deformation.

RECTANGULAR   CIRCULAR

(MAGNIFICATION FACTOR = 1000)
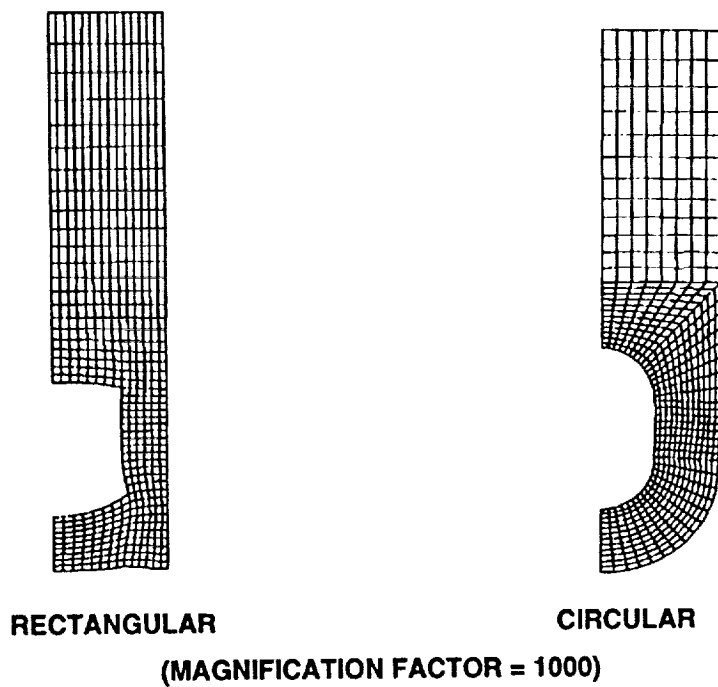
Figure 10 - Deformed shapes of the channels after five loading cycles.

160

THINNING OF COOLANT CHANNEL WALLS

Figures 11 and 12 show the thinning of coolant channel walls after different loading cycles in x and y directions, respectively. These figures show that the rectangular channel wall thins more rapidly than the circular channel wall in both the x and y directions. The circular channel geometry may thus have a greater cyclic ratcheting lifetime than the rectangular channel geometry.
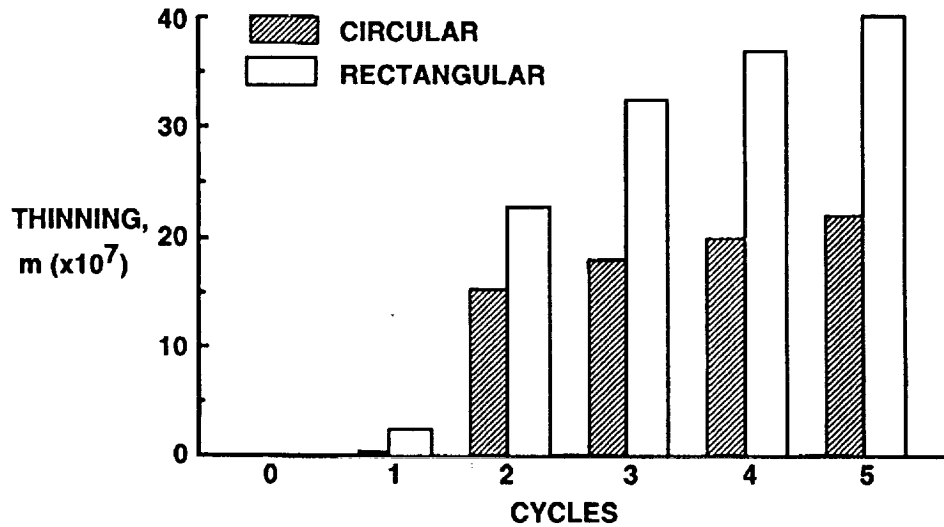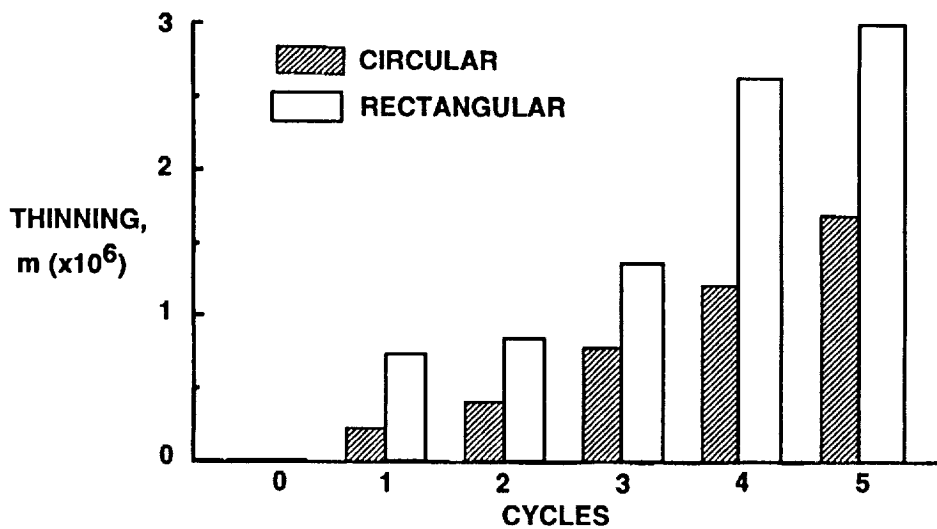

Figure 11 - X-Direction

Figure 12 -Y-Direction

LIFE ANALYSES OF THRUST CHAMBERS

As in the case of the cowl lip problem, the 'critical' locations were determined for the rectangular and circular geometries. By calculating the total strain ranges at these critical locations and using the fatigue curve of Fig. 7, the cyclic lives for rectangular and circular geometries can be estimated. The lower total strain range for the circular channel geometry is the evidence of its greater thermal compliance. The results are summarized in Table II. Complete details of life analyses may be found in Arya et al (Ref. 6). It is seen from this table that the circular channels have significantly higher cyclic lives than the rectangular channels for identical loading cycles. Also, keeping in view the uncertainties associated with life prediction and approximations used therein, it is seen from this table that the predicted lives for two channels are in fair agreement with their observed lives.

Table II - Calculated and Observed (Experimental) Lives of Thrust
Chambers (Viscoplastic Analysis)

Channel Geometry	Total Strain Range	Cycles to Failure	
		Calculated	Experiment
Rectangular	2.6%	75	200
Circular	1.05%	600	>637

CONCLUSIONS

The finite element solution technologies for time-dependent inelastic analyses are described. These include classical (non-unified) creep-plasticity and unified creep-plasticity (viscoplastic) analyses. The classical creep-plasticity analysis is applied to a hypersonic inlet cowl lip problem and the unified creep-plasticity analysis to a cylindrical rocket engine thrust chamber problem. The stress-strain responses calculated from these analyses are used to assess the cyclic lives of these components. It is concluded from the results presented in this paper that the assessments of cyclic lives based on inelastic finite element analyses are realistic (cowl lip) and in fair agreement with the observed lives (thrust chamber).

REFERENCES

1. *MARC General Purpose Finite Element Program*, MARC Analysis Research Corporation, Palo Alto, CA, 1988.

2. Freed, A. D. and Verrilli, M. J., *A Viscoplastic Theory Applied to Copper*, NASA TM-100831, 1988.

3. Melis, M. E. and Gladden, H. J., "Thermostructural Analysis with Experimental Verification of a High Heat Flux Facility of a Simulated Cowl Lip," in 29th Structures, Structural Dynamics and Materials Conference, Part 1, American Institute of Aeronautics and Astronautics, New York, 1988, pp. 106-115.

4. Arya, V. K., Melis, M. E. and Halford, G. R., "Finite Element Elastic-Plastic-Creep and Cyclic Life Analysis of a Cowl Lip," *Journal of Fatigue Fracture Eng. Mater. Struct.*, Vol. 14, No. 10, 1991, pp. 967-977.

5. Conway, J. B., Stentz, R. H. and Berling, J. T., *High Temperature, Low-Cycle Fatigue of Copper-Base Alloys in Argon; Part I-Preliminary Results for 12 Alloys at 1000 F (538 C)*, NASA CR-121259, 1973.

6. Arya, V. K., Jankovsky, R., Halford, G. R. and Kazaroff, J. M., unpublished paper, 1992.

7. Arya, V. K. and Kaufman, A., "Finite Element Implementation of Robinson's Viscoplastic Model and Its Application to Some Uniaxial and Multiaxial Problems," *Journal of Engineering Computations*, Vol. 6, No. 3, 1989, pp. 537-547.

PAGE _____ INTENTIONALLY BLANK

Life Prediction Systems for Critical Rotating Components

Susan E. Cunningham
United Technologies Pratt & Whitney
West Palm Beach, FL

INTRODUCTION

With the advent of advanced materials in rotating gas turbine engine components, the methodologies for life prediction of these parts must also increase in sophistication and capability. This talk presents Pratt & Whitney's view of generic requirements for composite component life prediction systems, discusses efforts underway to develop these systems and solicits industry participation in key areas requiring development.

ADVANCED MATERIAL ROTOR APPLICATIONS

Advanced monolithic materials such as single crystal nickel and composite materials including metal matrix, ceramic matrix and polymer matrix composites are either currently in use or under development and more components are being identified for their potential application in Pratt & Whitney gas turbine engines. Extensive use of composite materials is part of P&W's commitment to producing higher thrust-to-weight engines for military aircraft of the future. Examples of some of the components designated for advanced material technologies are listed here. Because of their low weight and high durability, polymer matrix composites are now being considered for use as fans and fan blades. PMC material technology developments recently have resulted in greater durability and impact absorption and these new forms of PMC's show potential for fan blade applications. In addition to PMC fan components, titanium matrix composite fan blades are being developed and boron aluminum composites have been investigated for use in rotor reinforcement and fan blades. Resistance to impact damage, rather than temperature, is a key driver in fan component development and these metal matrix composites offer benefits in this area. The compressor requires high strength, high temperature, high creep strength and relatively ductile materials. Weight reductions in the compressor can be accomplished by reinforcing the rotor with titanium matrix composite materials, and using metal matrix reinforcements in spacers, coverplates and shafts. Finally, in the turbine, basically, two different advanced material systems will be used. Single crystal nickel blades are currently in use in engines for their extremely high temperature, high strength capability. Single crystal nickel is highly anisotropic and its strength can be directionally controlled, leading to the ability to withstand high axial stresses present in the turbine blades. The second material system is that of ceramic matrix composites which, because of their high temperature and relatively low weight, are ideal for use as heat shields and coverplates. Using them in conjunction with monolithic materials makes them viable as reinforcements in the turbine rotor.

Fan
Lightweight MMC Rotor
PMC Blades

Compressor
Ti MMC Rotors and Spacers
MMC Coverplates and Shafts
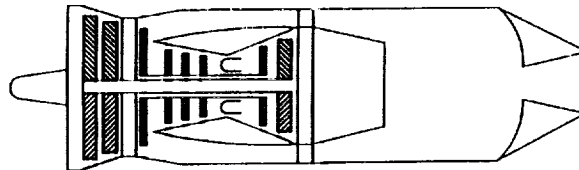
Turbine
S/C Nickel Blades
CMC Reinforced Rotor
CMC Heat Shields and Coverplates

LIFE SYSTEM REQUIREMENTS

The goal of a life prediction system is to accurately evaluate the remaining life of a component given its stress state, geometry, environment, existing damage and any other factor which might contribute to the part's demise. The cost to develop such a system for conventional materials is significant. Gas turbine engine environments operate at high temperatures for extended periods of time under high inertial loads and vibratory stresses. These loadings may also interact in a nonlinear manner. In laboratory testing, the complex in-service conditions are seldom reproduced to give accurate assessment of a component's damage tolerance. We rely on tests which intentionally isolate damage and damage progression modes in order to develop simple mechanistic models for assessing the life of a part. It is important that these modes be mechanistic, or physically-based, since their use is required over a wide range of conditions and it is impossible to reproduce all conditions in the laboratory. We therefore need models which can be interpolated and linearly combined to yield predictions of behavior at any service condition. Further, the Engine Structural Integrity Program (ENSIP) requires that all components classified as safety critical and made from composite materials must be capable of sustaining specified damage and continue to function without requiring repair for their design service lives. This means that we must be able to show that when a part is damaged, it will be able to continue operating with that damage until the design service life is reached. In conventional materials we take a fracture mechanics approach to determine if the stresses are below a threshold value or, if higher than this, if the stresses are within the range that a flaw will grow at a controlled rate. For advanced materials to satisfy ENSIP, we need to show that either the materials will contain no defects, or if they do, that the predicted behavior of the material will not lead to damage propagation such that part rupture will occur during a specified maintenance-free operational period.

- Mechanistic

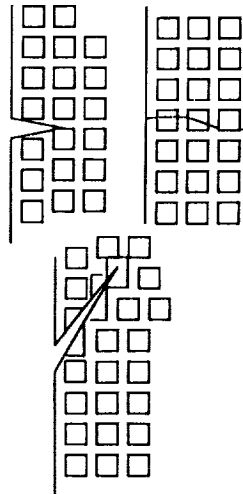- Satisfy ENSIP Requirements

LIFE SYSTEM ADVANCEMENTS NEEDED

Damage propagation predictions in conventional monolithic materials are accomplished through classical fracture mechanics approaches where a single crack dominates, controls the component's capability to withstand load and propagates according to a growth rate law which is a function of the crack tip stress intensity. The approach is primarily dependent on the geometry of a crack and has been shown to yield good predictive capability when used for component life from a specimen database. Damage in advanced materials, however, is not limited to self-similar or even mixed-mode single cracks and fracture mechanics approaches may not lend themselves to an advanced material life system. Take, for example, the case of cracking in single crystal nickel alloys. The microstructure of these alloys contains cuboidal, ordered precipitates which exhibit different properties than the matrix material. In a way these alloys are two-phase composites and to predict their fracture behavior we must transcend conventional fracture mechanics wisdom and instead relate the fracture mode, not just to geometry, but to the energy state required to move dislocations across precipitate boundaries and along active slip planes. Metal matrix composites also show different fracture behavior depending on temperature, material, ply layup and stress level. Take, for example, three crack geometries which have been observed in titanium matrix composites. In each case, fiber bridging has been observed to some extent. If we are to predict lives of components with this kind of fracture behavior, we must not only consider the effects of crack tip stress reduction due to shear lag but we also need to be able to predict crack geometry based on constituents and conditions. All these are advancements which need to be made if these materials are to be used in fracture-critical parts.

Multiple Discrete Damage Modes
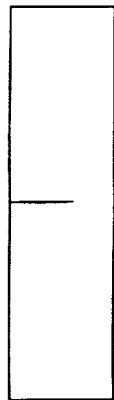

Monolithic   Single Crystal Nickel   MMC

LIFE SYSTEM ADVANCEMENTS NEEDED

Ceramic and polymer matrix composites exhibit even different damage behavior. The damage associated with these materials no longer can be simply associated with a single dominant or pair of discrete cracks. We must now consider damage that is not always distributed uniformly or periodically within a damage zone. As an example, we can consider crack density, rather than crack length, as a damage parameter and address the probability of fiber failure. The variation of these parameters and the influence drivers such as stress state, temperature, and environment have on the parameters will have to be characterized. In addition, CMC and PMC engine components will require more sophisticated architectures than unidirectional plies so models describing damage in these complex systems will be required.

Distributed Damage Modes Require Methods which Combine Mechanics and Stochastics
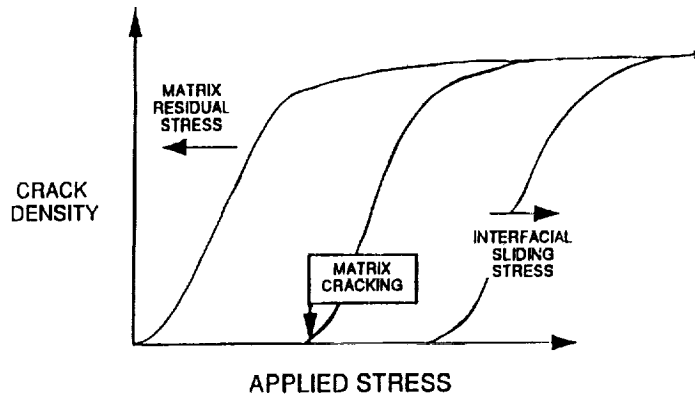
LIFE SYSTEM ADVANCEMENTS NEEDED

A further complication in the life prediction of ceramic matrix composites for high temperature applications is related to the heat conduction properties of the components. Heat transfer is especially important in the structural analysis of these components. When damage occurs in a CMC structure under high thermal loading, aberrations in the local heat transfer characteristics occur and cause severe local temperature gradients and high thermal stress states. These high stresses lead to greater damage and the cycle continues in a highly coupled manner. This interaction must be accounted for in a CMC life system.

CMC Behavior Highly Coupled System

STRESS

HEAT TRANSFER

DAMAGE (LIFE)

172
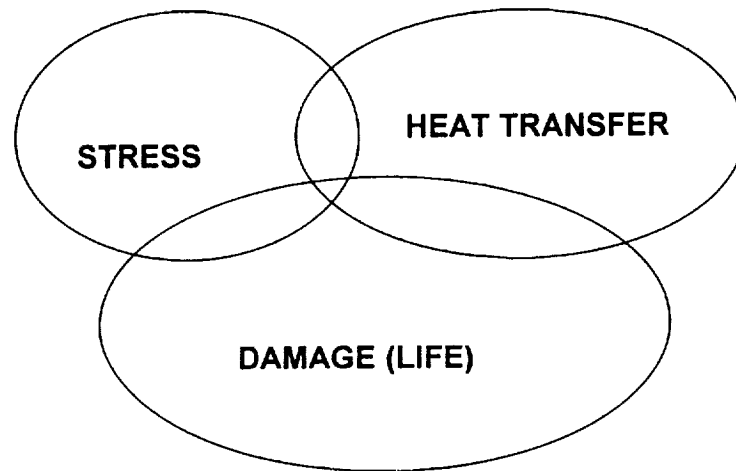
ELEMENTS OF A LIFE SYSTEM

Basically, we can identify three elements which contribute to a life prediction system. First we need to determine the stress state of the component by way of a numerical stress analysis. Once this state is known we can identify the mode of damage most likely to occur based on the constituents of the material, the loading configuration and the material properties. The damage mode will determine which analytical models for damage propagation are relevant for use in determining life and this decision point is the most distinct difference between a conventional life system and a system for advanced materials. Finally, the life calculations are performed using analytical models which predict damage initiation, propagation and failure. Each of these three elements will be described in more detail in the next three slides.
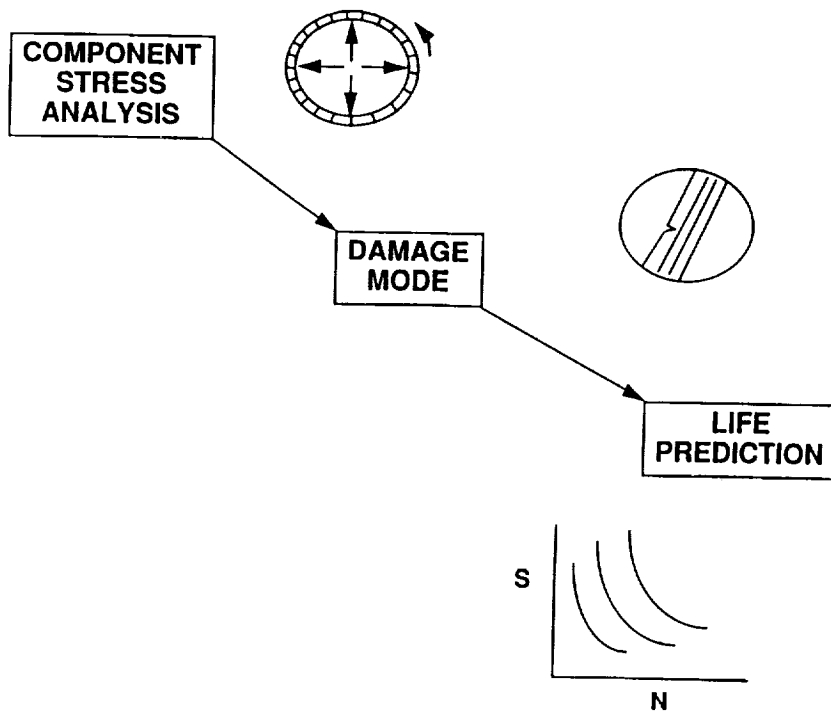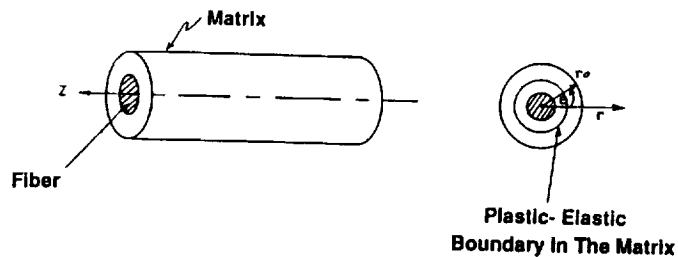
ELEMENTS OF A LIFE SYSTEM

The component stress analysis is a global analysis that incorporates composite behavior through constitutive modeling at a local level. This means that a good description of stress-strain behavior at the microlevel is required to give a good description of what happens at the laminate level. Several factors play important roles in the micro and macro level mechanics. These include thermal effects (since properties change as functions of the temperature), operating conditions, laminate response, constituent properties and the constitutive behavior, and environmental effects. This last factor is especially important in CMC high temperature applications since oxidizing atmospheres can lead to fiber degradation if exposure by matrix cracking occurs. It is important to understand how each of these factors interact if accurate stress analysis is to be performed.

```
                    OPERATING
                    CONDITIONS
                                                    THERMAL
  CONSTITUENT                                        EFFECTS
  PROPERTIES

                    COMPONENT
                     STRESS
                    ANALYSIS
                                                    LAMINATE
                                                    RESPONSE

  ENVIRONMENTAL
    EFFECTS

                    CONSTITUTIVE
                     BEHAVIOR
```
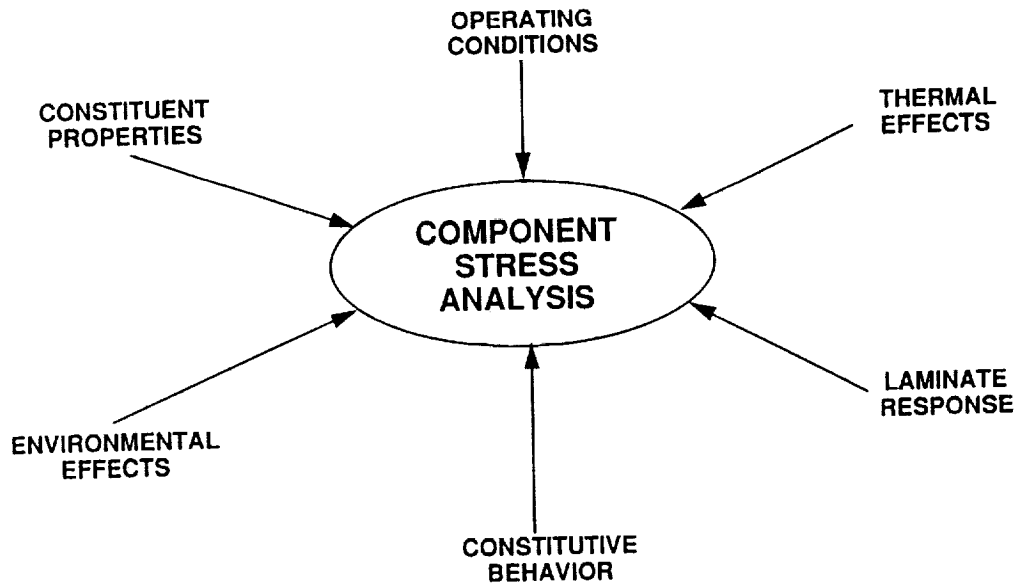
STRESS ANALYSIS REQUIREMENTS

The stress analysis requires micromechanical stress/strain behavior models in order to incorporate the behavior at the local level into the global behavior predictions. Current available models rely on concentric cylinder approaches. Often these approaches inaccurately model the interface conditions or the matrix outer radius boundary condition. Models are being developed, for example, that of Naik and Crews, which better approximate the tractions on the matrix outer edge boundary and these can be readily implemented in existing component stress analysis codes. Requirements for such models include the ability to model imperfectly bonded interfaces to account for friction and wear at the fiber/matrix interface, multiaxial loading to account for transverse, shear, tension and compression conditions, temperature dependent materials properties which are important in TMF and thermal residual stress calculations, and yielding in the matrix.

Need Good Micromechanical Stress/Strain Behavior Models

Plastic- Elastic
Boundary In The Matrix

Assumptions:

- Imperfectly bonded interfaces

- Elastic transversely isotropic fiber

- Multiaxial loading

- Temperature dependent materials properties

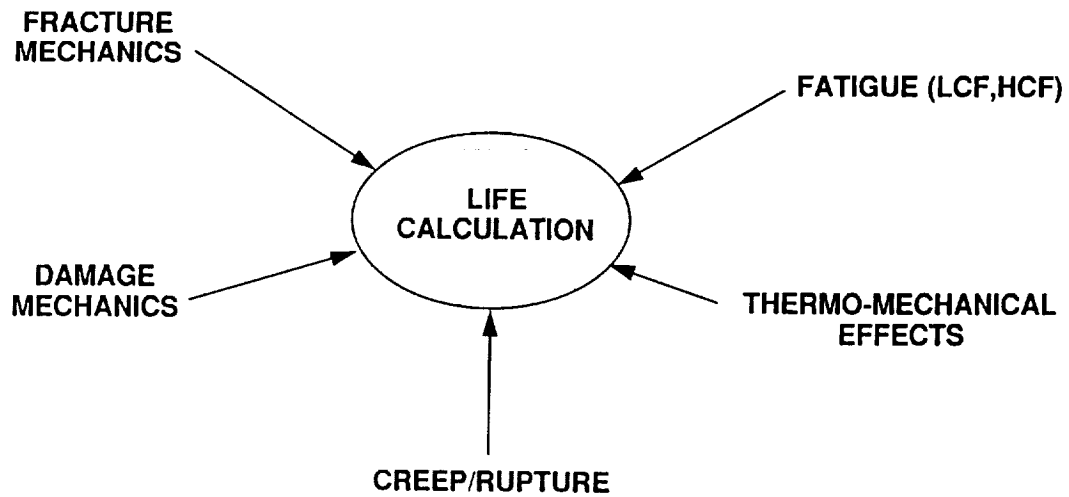- Elastic-plastic isotropic matrix

175

ELEMENTS OF A LIFE SYSTEM

Before a life system can be established, failure criteria are needed. Depending on the needs of the component, these could be on a global scale (for example, through-thickness cracking of a component or laminate), or on a local level (for example, multiple fiber fracture, matrix cracking or small-scale laminate failure). In addition, because different material systems yield different types of damage, the material system and the failure criteria are the inputs to a map which enables identifying the relevant damage mode or modes which may lead to failure. This failure mode map is a key part of a composite life prediction system and the development of it will rely heavily on parametric experimentation.

GLOBAL
FAILURE
CRITERIA
(COMPONENT OR
LAMINATE)

LOCAL
FAILURE
CRITERIA
(MATRIX/FIBER
OR
LAMINATE)

IDENTIFY
RELEVANT
DAMAGE
MODE (S)

MATERIAL
SYSTEM
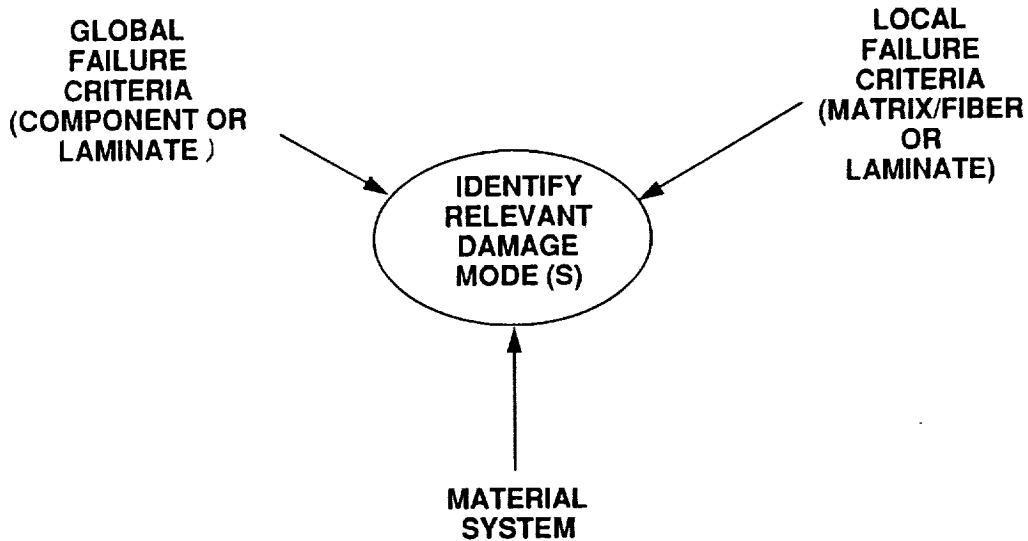
ELEMENTS OF A LIFE SYSTEM

The final elements of a composite life system are the individual models which estimate the rate of damage progression. These elements can be treated as individual modules addressing several different modes of damage. Fracture mechanics based models will be used for cases where discrete damage leads to failure. These are appropriate for MMC materials that fail by a limited number of dominant matrix cracks, for fiber matrix separation due to shear loading, or for delamination caused by interlaminar shear. Fracture mechanics based models have advantages over other model types since they have a large experience base, are easily incorporated in existing life systems for conventional materials and they, to a great extent, rely on material properties of the matrix alone, reducing the number of tests required on the composite materials. Damage mechanics approaches are being considered for cases where distributed damage controls fail. CMC and PMC materials are candidates for this type of model. It is noted that incorporating damage mechanics into life systems will require a change in philosophy from current life analysis methods. Initiation lives are important to predict and so high and low cycle fatigue models will be incorporated as will TMF and creep models. This latter damage mode is especially important in some composite materials applications, for example, the High Speed Civil Transport, where the design service life is 18,000 hours. It is noted that characterizing material behavior for these long exposures will require accelerated test techniques and better extrapolation modeling.

FRACTURE
MECHANICS

FATIGUE (LCF,HCF)

LIFE
CALCULATION

DAMAGE
MECHANICS

THERMO-MECHANICAL
EFFECTS

CREEP/RUPTURE

TMF AND DAMAGE INITIATION MODELING

Several damage models have already been investigated at P&W. The Smith-Watson-Topper model for predicting stress-strain response has been used to evaluate LCF and TMF data obtained in tests of Ti-15-3/SCS-6. LCF isothermal loading and TMF in-phase and out-of-phase loading were analyzed. Stress-strain states in the fiber matrix for each of these loading modes were calculated from a concentric cylinder constitutive model. The resultant stress-strain data were reduced to a single parameter, effective stress as shown here. It is noted that an additional parameter which accounts for thermal residual stresses induced by cooling from composite consolidation has recently been developed and is being studied.

Stress-Strain Response from Fatigue Data
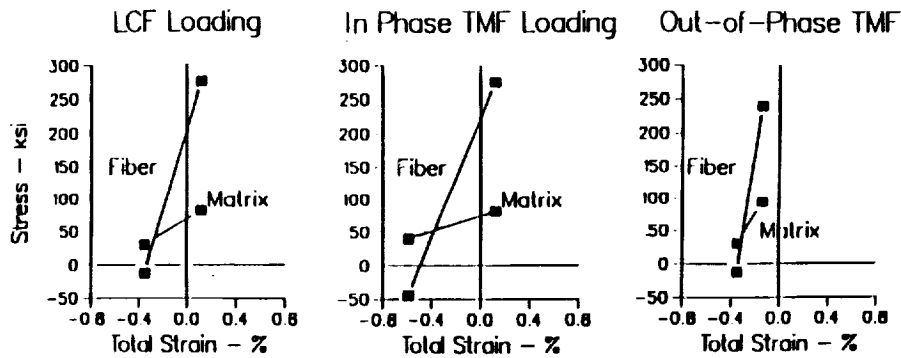
Smith-Watson-Topper Parameter
Effective Matrix Stress

$$\sigma_{eff} = \sqrt{\sigma_{max} \frac{\Delta \varepsilon}{2} E}$$

178

TMF AND DAMAGE INITIATION MODELING

The results of the SWT analysis are shown here. The parameter effectively collapsed the longitudinal fatigue data to a single line relating life to effective stress. More work will be performed to assess this model's ability to accurately predict fatigue lives of different materials under different loading conditions.

Longitudinal Fatigue Life
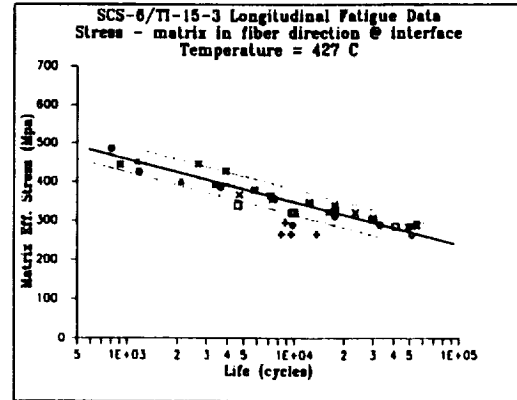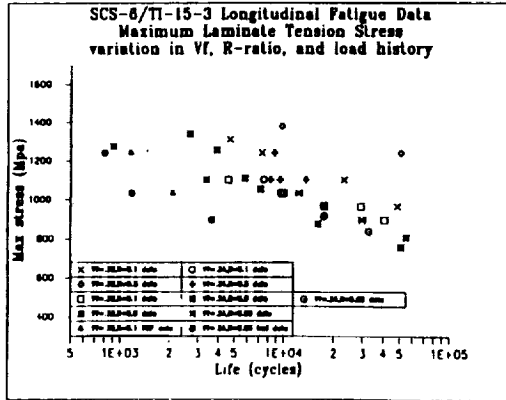
CRACK GROWTH MODELING

Fracture mechanics modeling for predicting the crack growth rates when dominant cracks exist has included the evaluation of large-scale bridging models first presented by Marshall, Cox and Evans and by Budiansky, Hutchinson and Evans for monotonic loading and later developed for cyclic loading by McMeeking and Bao. Our evaluation has included the use of TiMC crack growth data from outside sources. It appears that the fiber bridging models, which depend to a large extent on the frictional shear stress (τ) at the fiber - matrix interface, have a useful place in the analysis of crack propagation in composites that fail by fiber-bridged cracks. The use of the figure, developed by W. S. Johnson and associates, is gratefully acknowledged.

Mode I Fatigue Loading with Fiber Bridging (McMeeking, Evans, Bao)
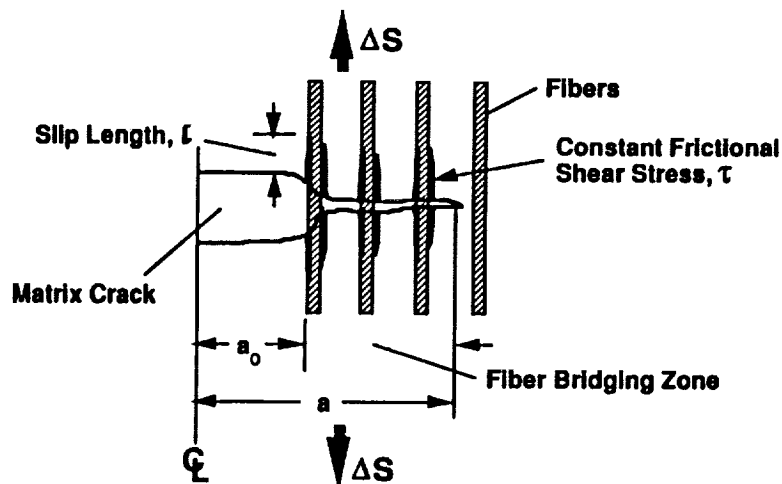
CRACK GROWTH MODELING

An advantage of the McMeeking and Bao work is that it uses τ to predict fiber failure caused by fiber overstress. Onset of fiber breaking leads to rapid crack propagation, shown here by the data of Walls and Zok, and could be used as a failure criterion. Disadvantages of this approach relate to the difficulty in characterizing τ and the observations which suggest that τ is not a constant. Rather, τ changes with number of fatigue cycles and varies as a function of position along the fiber. It is expected that the shear lag models which use τ to predict crack propagation will incorporate it as an empirical fitting parameter rather than a material property.

Mode I with Fiber Bridging (Walls and Zok, UCSB)
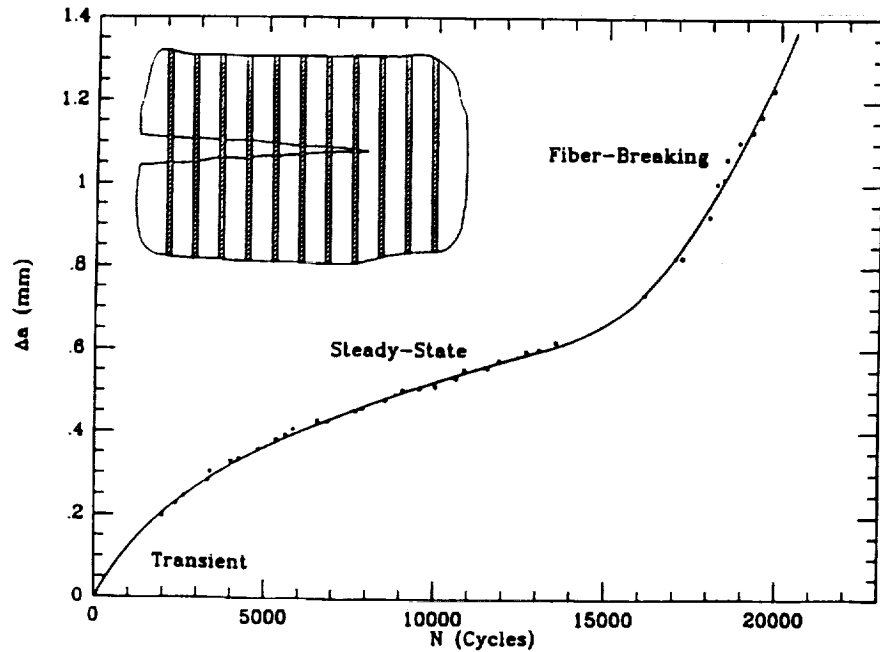
CRACK GROWTH MODELING

Fracture mechanics approaches depend to a great extent on the geometry of the crack. In order for these models to be viable for component durability assessment, solutions for appropriate flaw geometries must be established. For the case of a ring reinforced with a metal matrix composite, several flaw geometries are anticipated. These include penny-shaped cracks embedded in the composite reinforcement, surface flaws starting in the monolithic casing and propagating into the MMC core, and case-core bond line separation in both Mode I and Mode II. These are not simple problems. Current crack bridging models have not transcended the two-dimensional edge- and center-crack geometries and techniques for either extending current solutions to three-dimensional approximations or using numerical schemes for three-dimensional modeling will have to be developed.

Specific Geometry Requirements

- Bond Line Separation (Mode I) and Surface Flaw

- Embedded Flaw

Monolithic Casing

MMC Reinforcement

Bond Line Separation (Mode II)

Surface Flaw
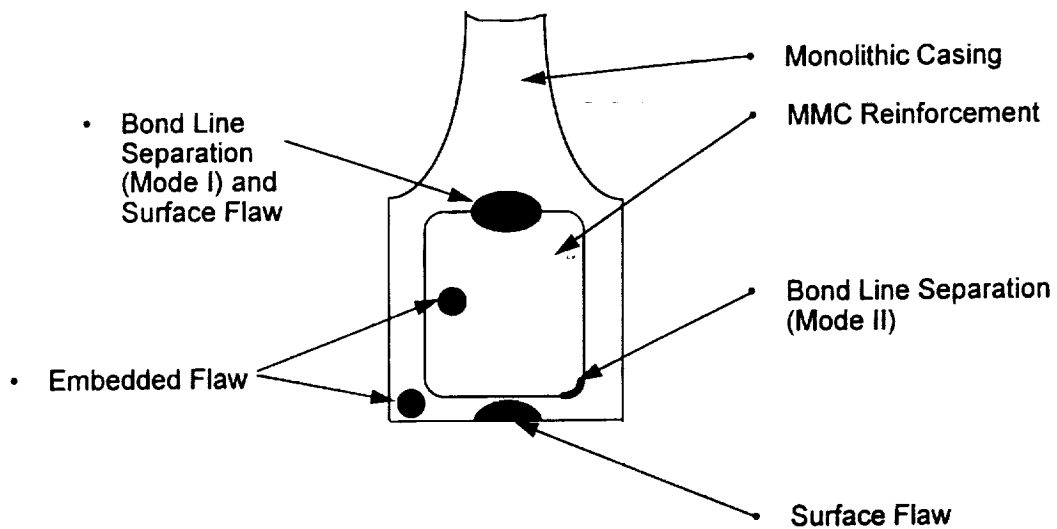
DAMAGE MECHANICS MODELING

Damage mechanics modeling is a new concept in component life analysis but may be required for predicting life of new materials that exhibit distributed damage. Instead of characterizing damage by a crack length, damage mechanics models use parameters that are degraded by accumulation of damage, such as stiffness, strength, or coefficient of thermal expansion. These models are appropriate for CMC's, PMC's and IMC's. An issue to be addressed before this approach can be successful is the question of the rank of tensor that is appropriate for these materials. In other words, how directionally dependent are the parameters on the damage, or, how directionally dependent is the damage progression on material anisotropy and loading configuration? In addition, the damage parameter itself will have to be established, bearing in mind that inspection requirements and parameter measurement will be important in the life analysis development and calculation. For example, if composite strength is the damage parameter, the number of specimens required to characterize the model will be significant compared to a parameter which can be characterized nondestructively.

Accumulation and Evolution of Distributed Thermomechanically Induced Microstructural Defects

- Continuum Damage Mechanics (CDM) - Macro representation of micro damage

- Appropriate for CMC's , IMC's, PMC's through tensorial CDM

- Model Form : $D = f(1 - \frac{\dot{A}}{A})$ for $\dot{A}$...measured property
  A...property of undamaged state

- Damage parameters: stiffness, strength, CTE, etc.

Remaining Life (%) vs Damage Parameter, D
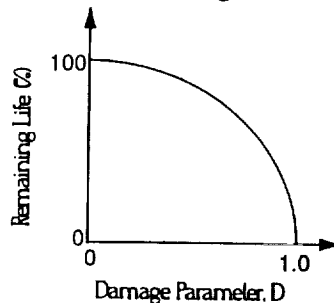
PRIMARY DEVELOPMENT NEEDS

In conclusion, P&W is committed to the development of a life prediction system for advanced composites. However, there are several key areas requiring substantial development and industry cooperation for their solution. P&W has been successful with other cooperative efforts such as the one recently with NASA Lewis Research Center in which three composite rings were fabricated and tested and we look forward to future efforts in our quest for a state-of-the-art life prediction system. Specifically, I leave the following list of some critical areas requiring development. Of high priority is the incorporation of interface element layers and matrix plasticity in micromechanical models for stress-strain behavior. Also important for the near-term is the ability to track and predict damage progression in the complex fiber architectures anticipated for CMC and PMC components. Experimental characterization and related computational efforts are needed to develop failure mode maps for all composite materials under investigation. Accelerated test and analytical techniques are required to relate long-term behavior in service environments to shorter-term behavior in the laboratory. Finally, before PMC components can be used in engine applications, significant effort must be expended to understand damage progression and material behavior in these materials.

- Stress-Strain Micromechanical Behavior

    - Interface element layer to simulate imperfect fiber/matrix bond

    - Capability for modeling Elastic-Plastic matrix

- PMC Materials Behavior and Modeling

- Ability to Track Distributed Damage/Different Fiber Architectures

- Experimental/Computational Damage Mode Mapping

- Accelerated Test and Analysis Techniques

184

N94-22616

Recent Advances in Computational Structural Reliability Analysis Methods

Ben H. Thacker, Y.-T. (Justin) Wu, Harry R. Millwater,
Tony Y. Torng, and David S. Riha
Southwest Research Institute
San Antonio, Texas

PAGE_____ INTENTIONALLY BLANK

INTRODUCTION

The goal of structural reliability analysis is to determine the probability that the structure will adequately perform its intended function when operating under the given environmental conditions. Thus, the notion of reliability admits the possibility of failure. Given the fact that many different modes of failure are usually possible, achievement of this goal is a formidable task, especially for large, complex structural systems. The traditional (deterministic) design methodology attempts to assure reliability by the application of safety factors and conservative assumptions. However, the safety factor approach lacks a quantitative basis in that the level of reliability is never known and usually results in overly conservative designs because of compounding conservatisms. Furthermore, problem parameters that control the reliability are not identified, nor their importance evaluated.

This paper presents a summary of recent advances in computational structural reliability assessment. A significant level of activity in the research and development community has been seen recently, much of which has been directed towards the prediction of failure probabilities for single mode failures. The focus of this paper is to present some early results and demonstrations of advanced reliability methods applied to structural system problems. This includes structures that can fail as a result of multiple component failures (e.g., a redundant truss), or structural components that may fail due to multiple interacting failure modes (e.g., excessive deflection, resonate vibration, or creep rupture). From these results, some observations and recommendations are made with regard to future research needs.

PROBABILISTIC STRUCTURAL ANALYSIS METHODS (PSAM) PROGRAM

The methodologies presented in this paper have been developed by the Southwest Research Institute (SwRI) under sponsorship from the NASA Probabilistic Structural Analysis Methods (PSAM) Program [1,2]. The objective of the NASA/PSAM program is to develop probabilistic structural analysis methods for critical space shuttle main engine (SSME) components such as turbine blades, transfer ducts, piping systems, and liquid oxygen posts. These components are considered critical because of the severe consequence of failure. A major accomplishment of the PSAM program is the development of the NESSUS computer program, which integrates advanced reliability methods with general structural analysis capabilities. Rocketdyne (Rockwell Corporation) has and is currently applying NESSUS to critical SSME components [3].

The methodologies developed by PSAM are applicable to a wide range of applications. Under several other projects, SwRI is applying PSAM technology to geomechanics, nuclear waste, rotordynamics, industrial design and optimization, biomechanics, and numerous other structural and mechanical reliability problems [4, 5, 6].

- **Ten-Year Research and Development Program**
  - Phase 1: Probabilistic Structural Response Analyses of the Space Shuttle Main Engine Components (1984-1989)
  - Phase 2: Structural System Risk Assessment, Qualification, Certification, and Health Monitoring (1990-)

- **Simulate Uncertainty/Variability in Loads, Material Properties, Geometries**

- **Computer Code NESSUS Integrates Reliability Methods with Structural Analysis Methods (FEM, BEM)**

- **PSAM Methodology and Code are General Structural Risk Assessment and Reliability Design Tools**

Prime Contractor: Southwest Research Institute
Project Sponsor: NASA Lewis Research Center

SUMMARY OF NESSUS 6.0 CAPABILITIES

The probabilistic structural analysis methods used in this paper are implemented in the NESSUS[tm] probabilistic computer program [7]. NESSUS couples numerous advanced probabilistic algorithms with general-purpose structural analysis capabilities to provide a very efficient means of computing probabilistic results for complex applications. Thus, the key feature of NESSUS is its ability to establish the cumulative distribution function (CDF) for complex structures with a minimum number of response resolutions. Figure 1 summarizes the capabilities in NESSUS Version 6.0.

Random Variables

Loads

- Forces
- Pressures
- Temperatures
- Vibrations (PSD)

Material properties

- Moduli
- Poisson's ratio
- Yield stress
- Hardening parameters
- Material orientation

Geometry
User-defined

Probabilistic Methods

Fast Probability Analysis

- Advanced Mean-Value
- First and Second-Order
- Fast Convolution

Sampling

- Standard Monte Carlo
- Latin Hypercube
- Adaptive Importance

Probabilistic Fault Tree

Probability of Creep Rupture

1.0

0

360 3D Solid Elements
810 Nodes, 2100 DOF

Service Life

Probabilistic Results

- Full probability distribution
- Component reliability
- System/multi-failure-modes rel.
- Probabilistic sensitivities
- Probability-based risk/cost

Performance Functions

- Structural responses:
  stress, strain, disp., freq., etc.
- Fatigue and fracture life
- Creep rupture life
- User-defined subroutines
- External analysis programs
  (requires custom-made interface)

Analysis Types

Static
Transient dynamics
Buckling
Vibrations
Nonlinearities

- Plasticity
- Large displacement

Element Library

Beam
Plate
Plane strain
Plane stress
Axisymmetric
3D solid
Enhanced solids

Operating Systems

Mainframes

- CRAY
- VAX

Workstations

- HP
- SUN
- APOLLO

Figure 1. Summary of NESSUS Version 6.0 Capabilities.

One of the challenges in computational structural reliability is the development of efficient and accurate probabilistic analysis algorithms for analyzing structures where the computations of the performance and its sensitivities are very time-consuming. Recently, probabilistic methods based on the limit state approach have been developed and successfully integrated with finite element and boundary element methods. In these methods, the primary computational effort is typically spent on locating the most probable point (MPP) for a limit state function, $Z = z_i$, as illustrated in Fig. 2. Once the MPP is identified, the probability of failure can be estimated. Several approaches are available to search for the MPP. One efficient method, developed and implemented in NESSUS, is the advanced mean value method (AMV), which has been shown to be extremely efficient [8]. One of the limitations of the limit state approach is that the probability estimate is based on a low-order polynomial approximation. The adaptive importance sampling (AIS) method provides a quick way to check the AMV solution by sampling in the most likely failure region [9].

- **Input Variables Defined Using Probability Distributions**

- **Fast Probability Integration Estimates MPP on Response Surface**

- **Advanced Mean Value (AMV+) Iteration Computes Converged MPP and Estimates Probability of Failure (p_f)**

- **Adaptive Importance Sampling (AIS) Can be Used to Check p_f Calculation**
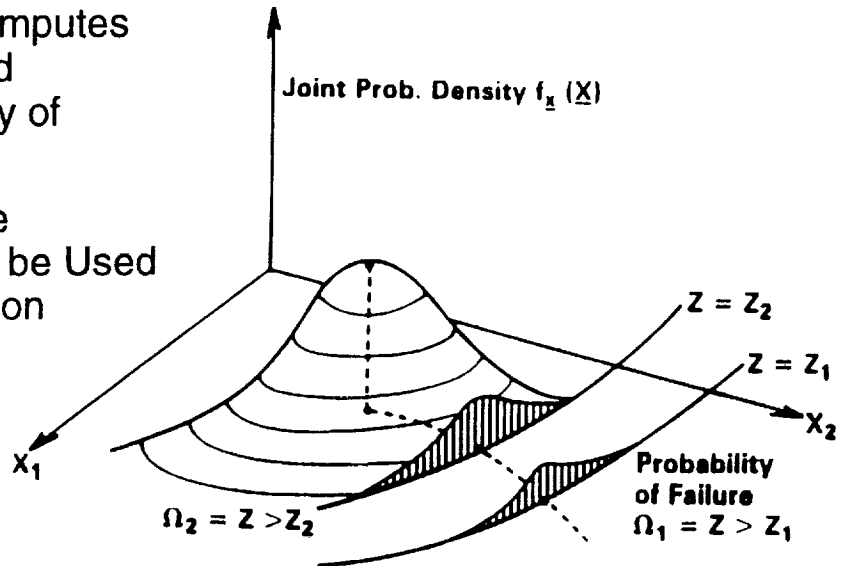
Figure 2. Joint Density Function and Most Probable Point (MPP) for Two Random Variables.

RELIABILITY ANALYSIS USING COMPONENT STRESS AND MATERIAL RESISTANCE CURVES

The example shown in Fig. 3 considers a circular disk subjected to two equal and opposite point loads. The disk is assumed to fail when the equivalent stress at the center of the disk exceeds the material yield stress, which is a function of temperature. Random variables considered include the loading, thickness of the disk, and the temperature. A simple relationship is used to describe the degradation of yield stress as a function of temperature.

Using NESSUS, the distribution functions for stress and strength were computed. The reliability analysis, also performed with NESSUS, then computed the probability of strength being less than stress, which was considered failure. The probabilistic analysis was verified using both AMV and Monte Carlo with the circular disk modeled in closed-form and with finite elements.

Component Stress

Maximum von
Mises Stress in
Disk Under Load

Thin Disk
Modeled Using
Finite Elements

Material Resistance

Yield Stress Modeled as
Function of Thermal Cycles

$$\sigma_y = \sigma_{y0}\left(\frac{T_F - T}{T_F - T_0}\right)^n$$

Probability of Failure Computed Using NESSUS

Strength Variable
Yield Stress
Mean=35.4 ksi
Std=1.8 ksi

Stress Variable
Equivalent Stress
Mean=23.0 ksi
Std=3.23 ksi

$p_f = 0.00291$
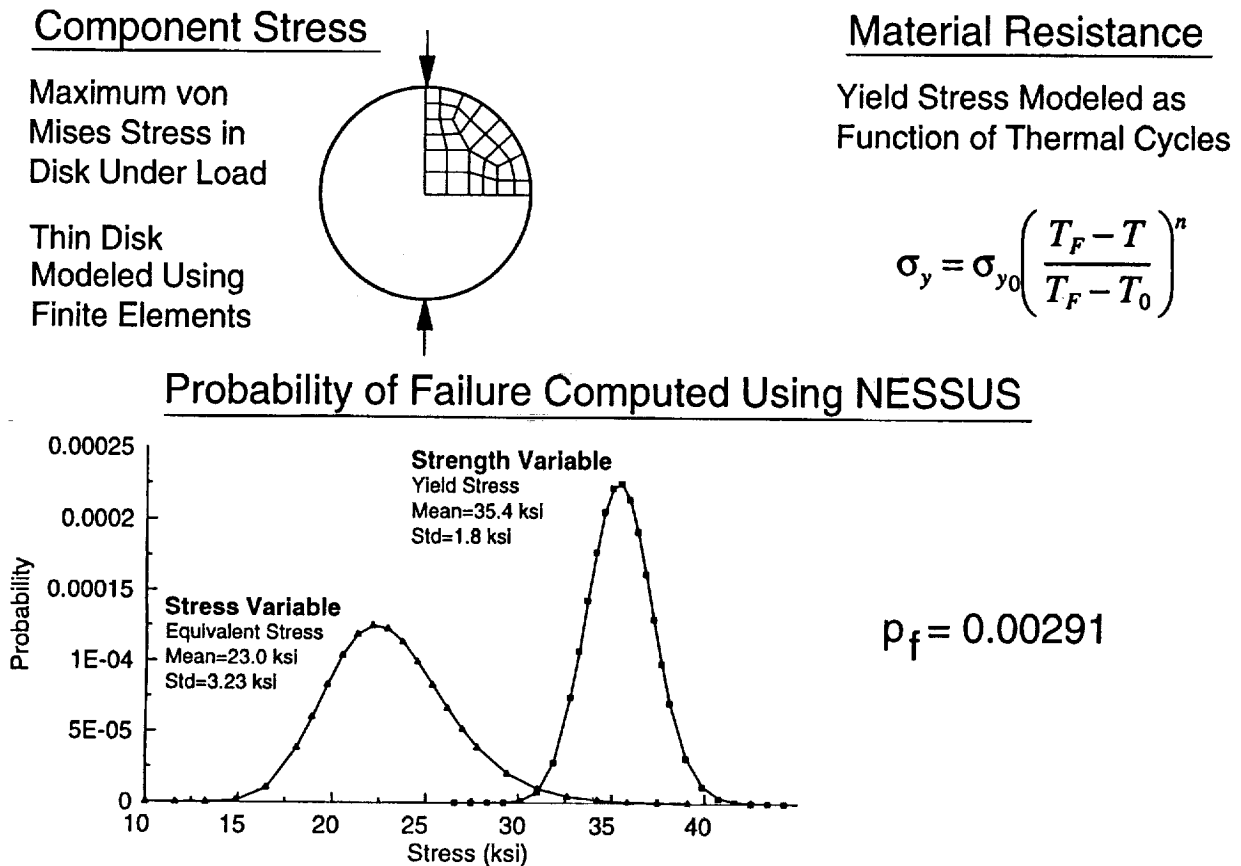
Figure 3. Component Reliability Analysis Demonstrated for Simple Example.

ROCKET ENGINE TURBINES SUBJECT TO SEVERE CONDITIONS

Representative of a more real world component reliability problem, a model of an SSME component was considered. The high-pressure fuel turbopump blade, shown in Fig. 4, represents a critical component in the SSME engine in that failure of a blade can result in loss of the complete engine. Stringent limitations on size and weight coupled with the hot hydrogen enriched steam turbine fluid and the cold hydrogen cooling fluid results in a very severe thermal environment. Probabilistic methods are ideally suited for the SSME turbine blade analysis where the lack of available local measurements results in significant uncertainty in loads such as thermal response. The lack of data is attributed to the difficulty in making measurements in the extreme environments and operating conditions within the engine.

- Severe Design Requirements
  - Comparatively Short but Severe Service Life
  - Strict Limitations on Size and Weight
  - High Energy Content of Fluids
  - High Specific Work Output
  - Rapid Start and Short Run Duration
  - Severe Thermal Shock Conditions
  - High Stage Loading and Stress
- Blades Prone to High Cycle Fatigue Cracking
- Operating Stresses and Deflections Must be Closely Controlled
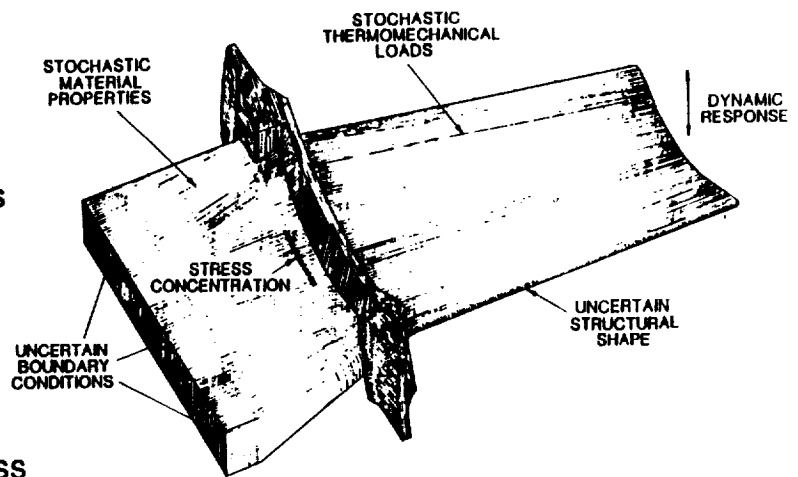
Figure 4. Space Shuttle Main Engine (SSME) Turbine Blade.

TURBINE BLADE RANDOM VARIABLE INPUT

Several methods exist for modeling uncertainty, such as probability distributions, fuzzy sets, convex models, bounding, etc. The probability distribution approach is used here to model each engineering variable in terms of its statistical parameters, namely its mean, standard deviation and distribution type. The standard deviation characterizes the magnitude of the scatter in the data and the distribution describes how the scatter is distributed about the mean. The variables listed in Table 1 were used for the demonstration analyses presented in this paper.

Table 1. Random Variable Definitions Used for the Turbine Blade Analysis.

Variable	Symbol	Mean Value	Standard Deviation	Distribution
Crystal Orientation about z	θ_z	+3°	3.9°	Normal
Crystal Orientation about y	θ_y	-2°	3.9°	Normal
Crystal Orientation about x	θ_x	+5°	3.9°	Normal
Young's Modulus	E	18.38E6 psi	0.46E6 psi	Normal
Poisson's Ratio	v	0.386	.00965	Normal
Shear Modulus	G	18.63E6 psi	.47E6 psi	Normal
Material Parameter	B_0	86.0	0.086	Normal
Density	ρ	0.805E - 3 lbm/in³	0.493E - 5 lbm/in³	Normal

TURBINE BLADE CREEP RUPTURE RELIABILITY ANALYSIS

A component reliability analysis of the turbine blade considering failur by creep rupture was performed. The turbine blade is modeled using the finite element model shown in Fig. 5. The blade is composed of a single crystal material described by three elastic constants, and three orientation angles. In the analysis, the blade is rotating at a constant speed and operating at a constant temperature. The failure mode being studied is creep rupture due to operation of the blade under elevated temperature. The temperature, stress and rupture life are related using a Larson-Miller relation, given by $P = T(C + \log t)$ where P is the Larson-Miller parameter; T is the absolute temperature; and t is the rupture life. More detail of this analysis is given in Ref. [10].

Possibly one of the most valuable products of the probabilistic analysis are the probabilistic sensitivity factors (PSF), shown by the bar chart in Fig. 5. The PSF's provide an important ranking of the problem variables with respect to the total *uncertainty* in the response. Therefore, since the statistics of the input variables are contained in these sensitivity data, the PSF data provide a more realistic and useful ranking of the variables.

Loads:
Pressure
Thermal
Centrifugal
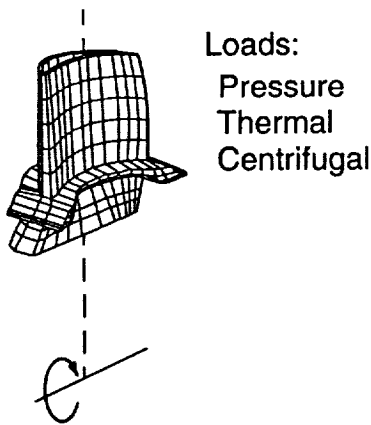
● Turbine Blade Operating
at High Speed in High
Temperature Environment

● Failure by Creep Rupture
Possible if Operated Past
Critical Time

● AMV+ Procedure Used to
Assess Reliability
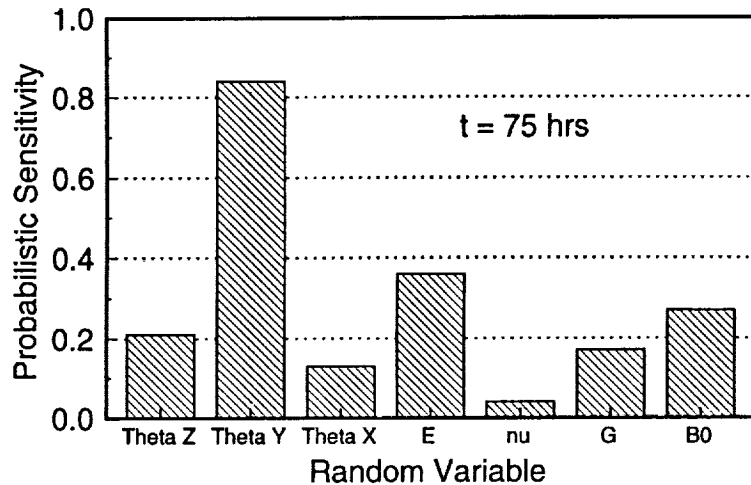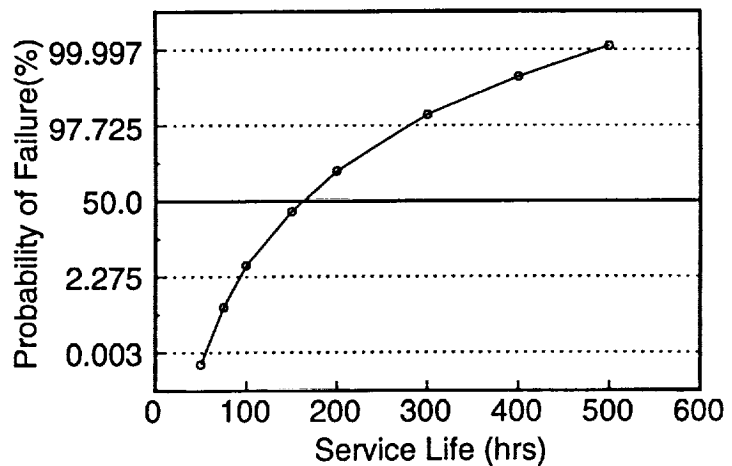
Figure 5. Creep Rupture Reliability Analysis of the Turbine Blade.

194

PROBABILITY OF EXCEEDING 60 KSI EFFECTIVE STRESS

Another component reliability analysis of the turbine blade considers stress exceedance. Figure 6 shows the probability of the von Mises stress exceeding 60 ksi. The plot was obtained by computing the probability of exceeding 60 ksi stress at each node using the NESSUS program and plotting the results using a general-purpose finite element graphics program.

The probabilistic information was obtained from a mean-based sensitivity analysis and must therefore be interpreted accordingly. The contours indicate where the high failure probability regions are located and where more refined analyses should be directed. It should be noted that the high probability regions may not be the same as the high stress regions from a deterministic analysis. This is because the standard deviation in stress varies from location to location in the mesh. For example, although the mean stress at some location (A) may be lower than the mean stress at some other location (B), the standard deviation may be higher at A than at B (i.e., more variation in stress). Thus, the *probability* of exceeding a certain stress level could be higher at A than at B even though the mean stress is lower at A than at B.
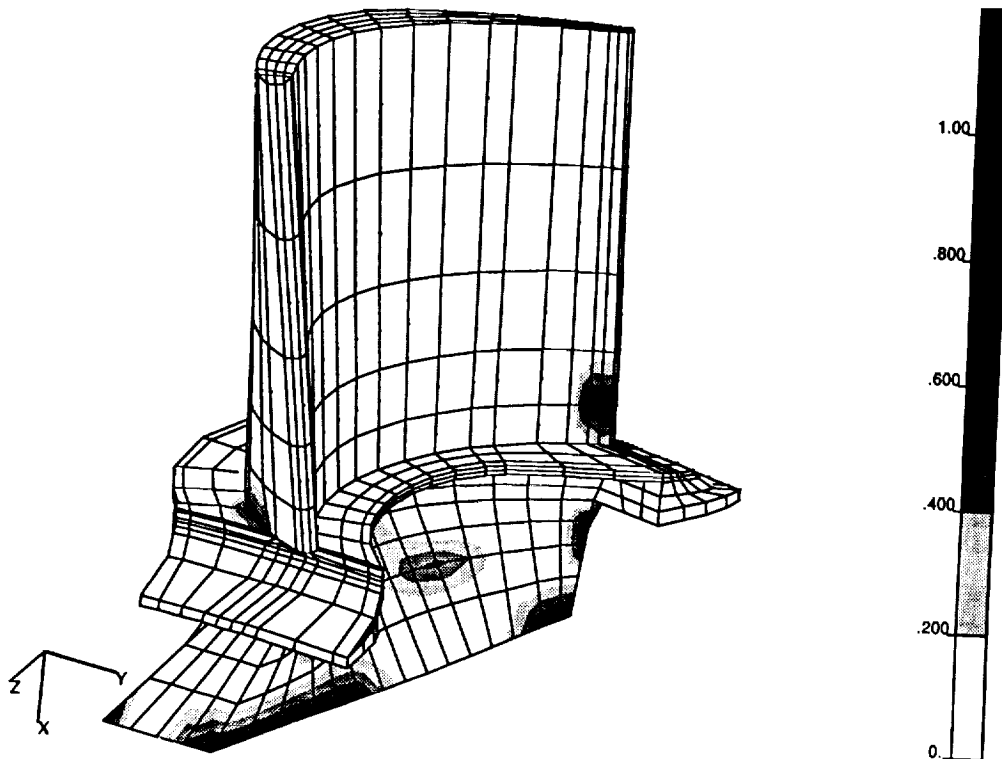
Figure 6.   Probability of Exceeding 60 ksi Effective Stress.

NESSUS PROBABILISTIC FAULT TREE ANALYSIS METHODOLOGY

What dictates failure in real structures, as previously described, will usually be a sequence or interaction of individual component failure modes. A popular method for modeling system failure as a function of component failures is with a fault tree. A fault tree provides a systematic way to deal with multiple, possibly complicated, failure paths composed of multiple components or multiple failure modes (bottom events). In traditional fault tree analysis, probabilities are assigned to the bottom events, and propagated through gates (AND, OR, etc.). For typical structural reliability analysis problems, however, the failure events will often times be correlated due to common problem variables. To account for this dependency, it is necessary that the limit state functions, rather than simply the probabilities, be used to define the bottom events. In addition, conditional limit state functions must be established that represent updated structural system configurations as a result of sequential failures (for modeling redundancy or progressive fracture for example). Figure 7 shows how failure modes and sequential failure can be modeled using a fault tree. Sequential failures can be modeled using the PRIORITY AND gate. A sequence of limit state functions corresponding to a sequence of updated structural configurations with load redistribution, must be generated during the analysis. This fault tree methodology has been developed and is implemented in NESSUS [9].
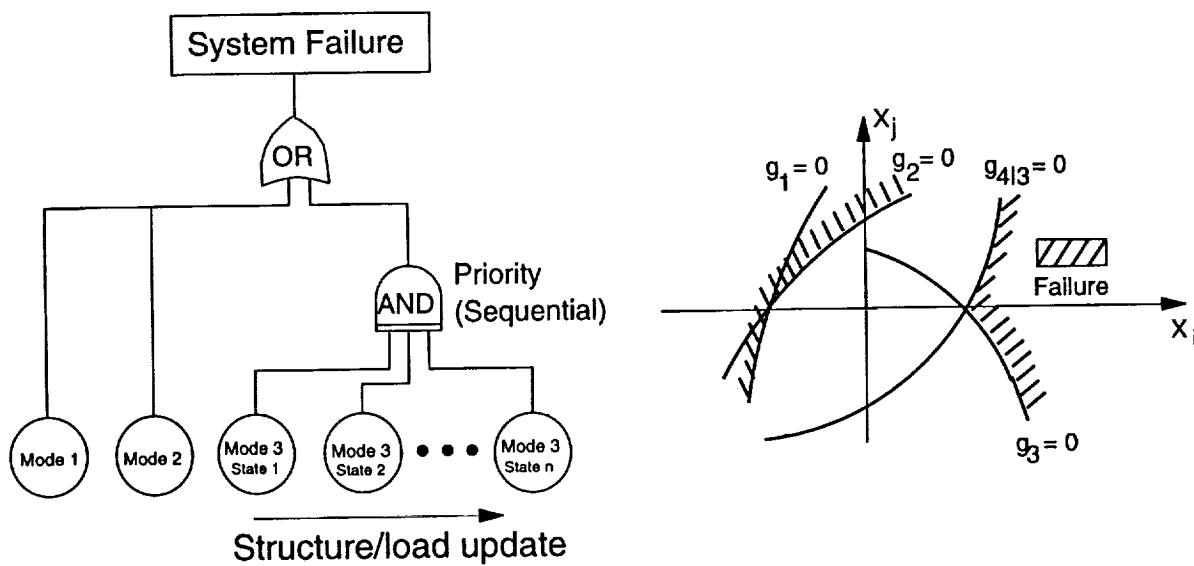
- Fault tree used for modeling multiple failure modes and paths
- Bottom events modeled using FEM model, approximate response surface, analytical equation
- Dependencies between bottom events accounted for
- Reliability calculated by adaptive importance sampling

Figure 7. NESSUS Probabilistic Fault Tree Analysis Methodology.

196

NESSUS SYSTEM RELIABILITY ANALYSIS EXAMPLE

Figure 8 shows a simple fault tree for a simple structural component. The hypothetical structure has three failure modes: vibration, stress and fracture. The structure is considered failed if any of the three failure conditions are satisfied. This is represented with the "OR" gate. Failure is defined as the first natural frequency being within a certain range, the stress exceeding a stress limit, and the mode I stress intensity factor exceeding the fracture toughness. For vibration, a two-sided limit is used to define failure and is represented in terms of an "AND" gate. As indicated, three of the bottom events are modeled analytically and one is given by finite element model.

Probability of system failure was obtained using several sampling methods; conventional Monte Carlo and adaptive importance sampling (AIS) using the exact limit state functions, and AIS on an approximate limit state. The approximate limit state consists of a closed-form approximation to the finite element model computed using the AMV+ procedure described earlier. The results indicate that the AIS method achieved results comparable to those obtained using Monte Carlo at 1/78 the computational cost. As also indicated, good agreement is obtained using the approximate limit state also, with further reductions in calculation cost. This example indicates the practical application of structural system reliability using a fault tree approach with advanced probabilistic methods.
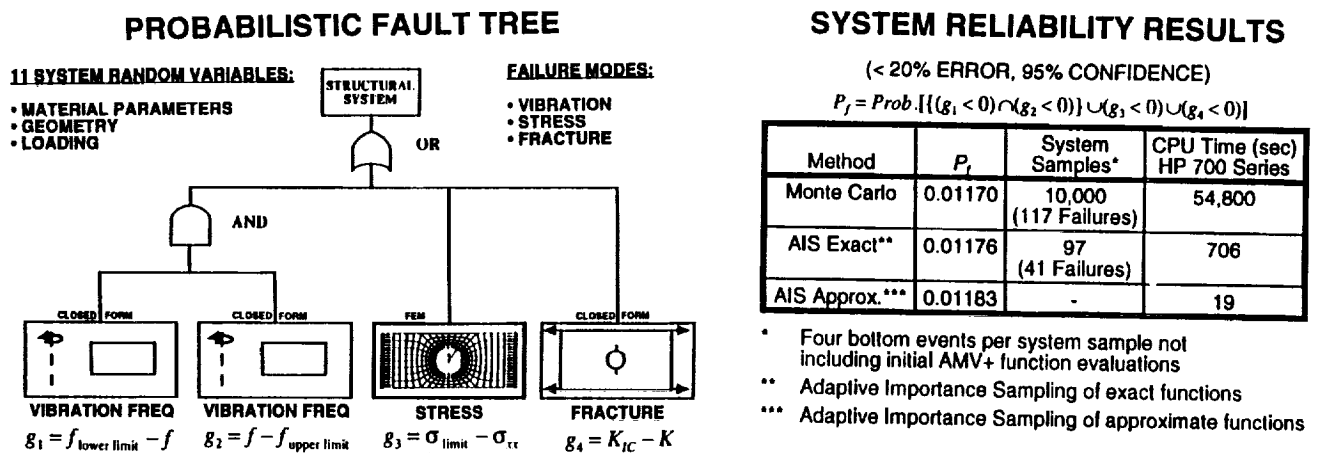
Figure 8. NESSUS System Reliability Analysis Example.

SYSTEM RELIABILITY ANALYSIS OF THE TURBINE BLADE

To demonstrate the computational system reliability methodology on a realistic-sized problem, the turbine blade was analyzed probabilistically considering three modes of failure: frequency, yield, and rupture. The procedure employing approximate limit states for the component modes is recommended for this level of deterministic modeling. Each mode of failure is first analyzed using the AMV+ procedure to establish the approximate limit state. The computational effort required for this step is given in each bottom event box in Fig. 9. Next, the system failure is computed using AIS. This procedure is automated in NESSUS. This example demonstrates that system reliability assessment is now possible for complex structural systems.

Structural Failure

OR

AND

FEM Model Used for All Bottom Events

1456 3D Solid Elements
2454 Nodes, 5946 DOF

Vibration
$P_f = 0.0053$
CPU = 40 min

$g = f_{low} - f$

Vibration
$P_f \approx 0$
CPU = 40 min

$g = f - f_{up}$

Yield
$P_f = 0.00233$
CPU = 24 min

$g = S_{lim} - S$

Creep
$P_f = 0.00978$
CPU = 36 min

$g = P_1 - P_2$
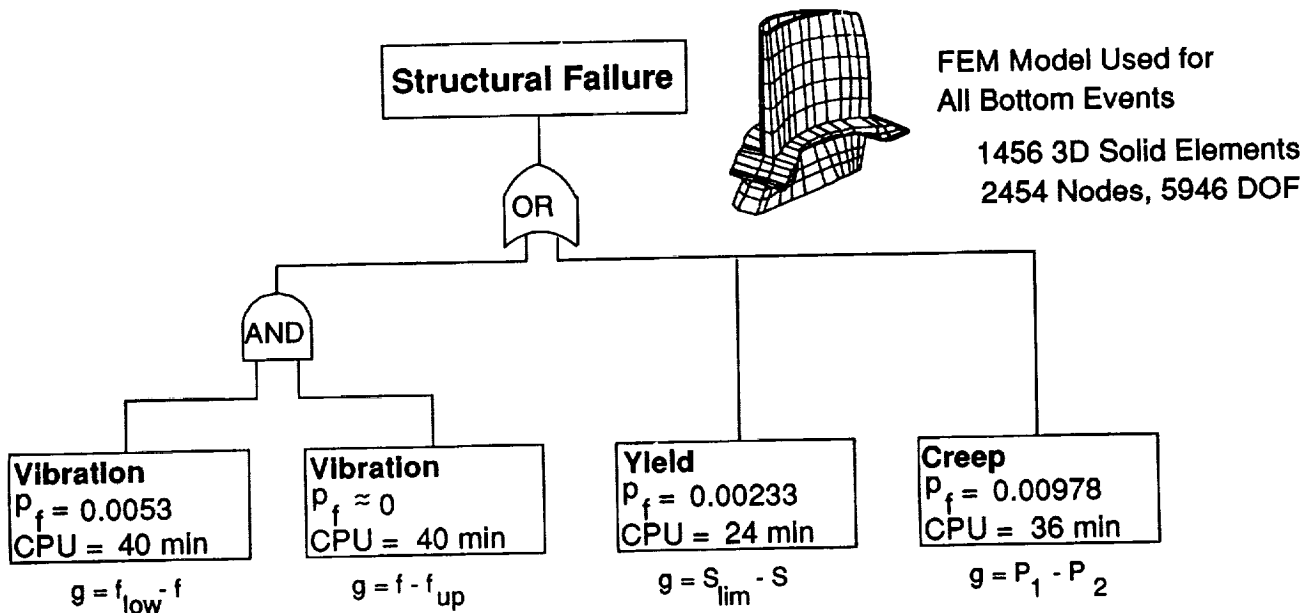
Probability of Structural Failure: 0.01711

Total CPU Time Required: 2.5 hours

CPU Times for HP Series 750 Workstation (64Mb RAM)

Figure 9. System Reliability Analysis of the Turbine Blade.

SYSTEM RELIABILITY ANALYSIS IDENTIFIES
CRITICAL FAILURE MODES AND RANDOM VARIABLES

As in the component reliability analysis procedure described earlier, the system reliability analysis also provides a probabilistic ranking of the inputs. The inputs for the system analysis are the component failure modes, whereas the inputs for the component analysis are the problem variables. Thus, not only are the problem variables ranked by importance, but the dominate failure modes are also identified. As shown in Fig. 10, for example, the creep rupture mode is seen to contribute the most to the overall system probability. The bar chart on the right shows the problem variable ranking for each failure mode. This type of information is required to establish a reliability based design procedure.
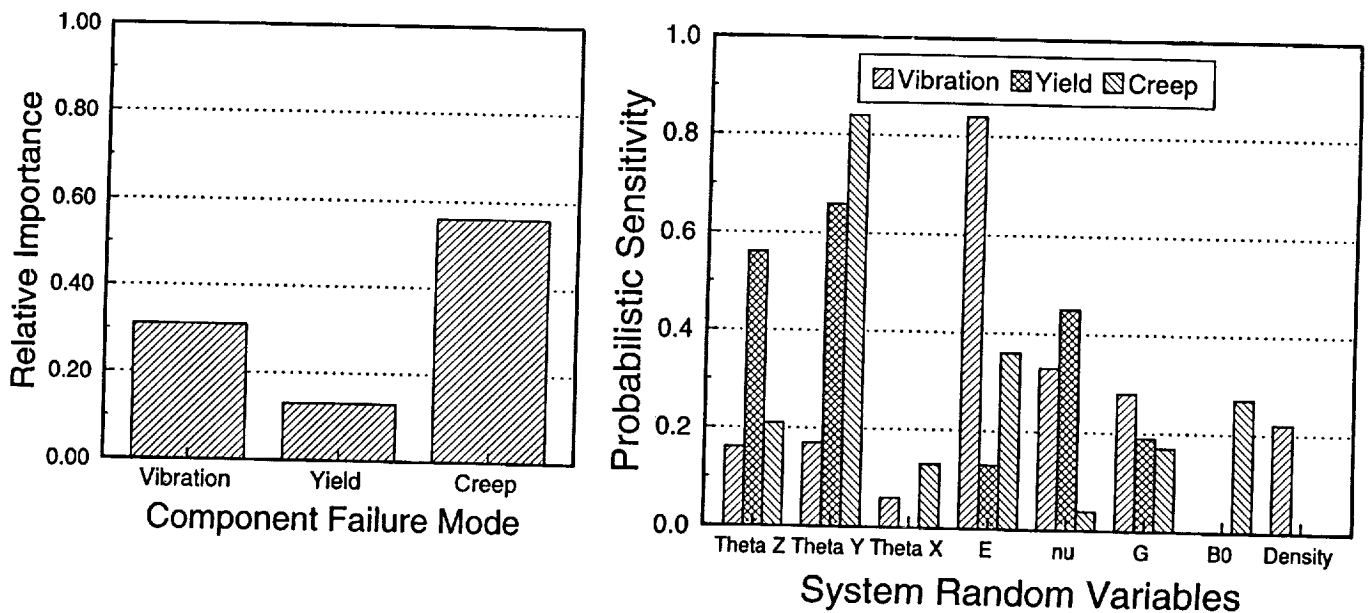
**Figure 10. Dominate Failure Modes and Problem Variables are Identified
in the System Reliability Analysis.**

RELIABILITY ANALYSIS AND DESIGN PROCEDURE

How the probabilistic methodologies presented here would fit into a typical design procedure is shown in Fig. 11. The shadowed boxes indicate the position of the component and system reliability analyses in the overall design cycle. The first step in the process is to identify all of the physical variables and sources of uncertainty. How these physical variables affect the problem variables comprises the next step. For example, in the SSME, the fuel mixture ratio (a physical variable) effect s the pressure, thermal, and centrifugal loading (problem variables) on the turbine blade. In the next steps, the individual failure modes are identified and analyzed both deterministically and probabilistically. Next, the overall system failure and dominate failure modes and problem variables are identified, which are used in subsequent steps to alter the design subject to the design requirements (e.g., cost, weight, reliability).
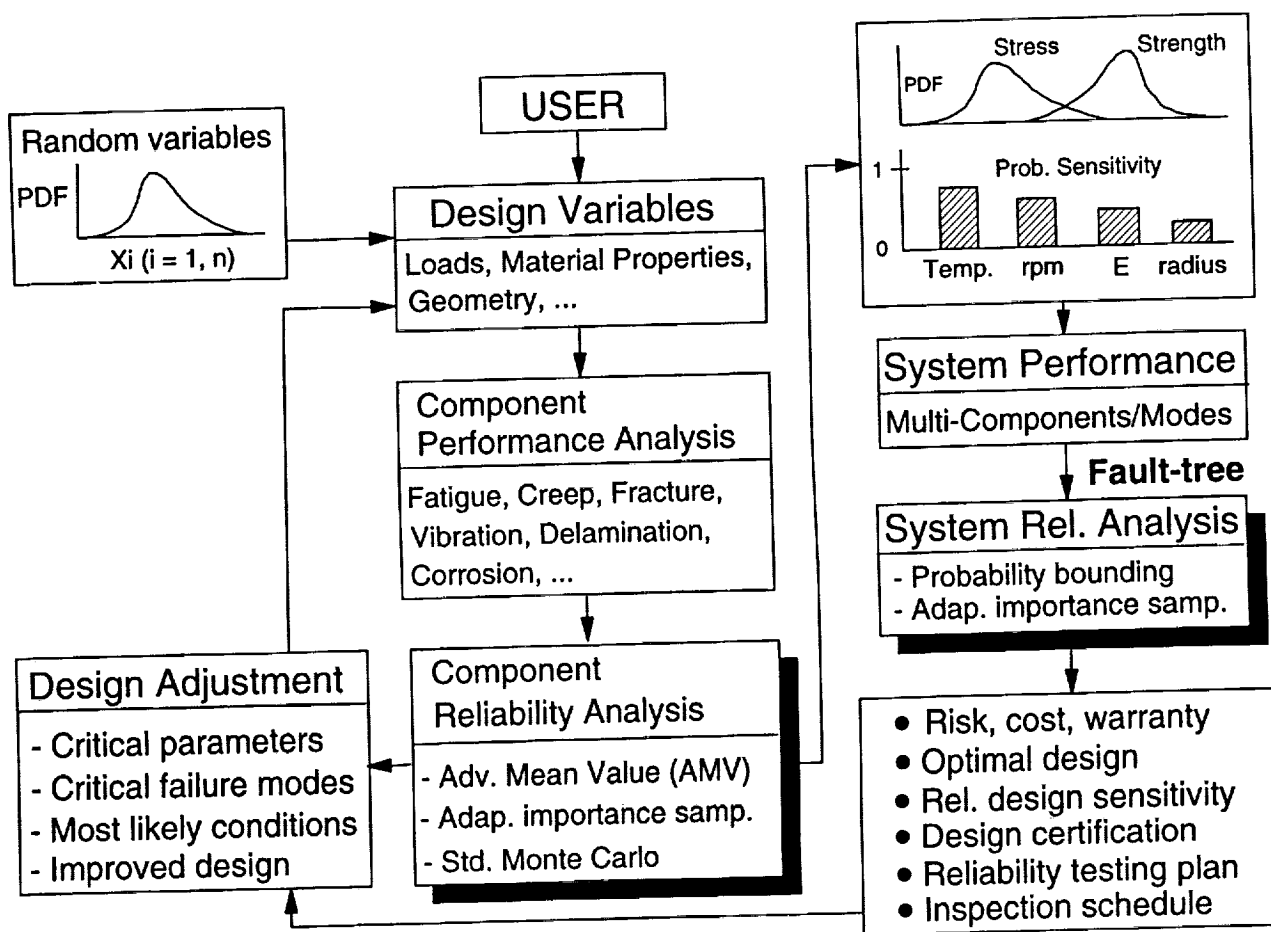
Figure 11. Component and System Reliability Analysis Integrated Into The Design Procedure.

STATE-OF-THE-ART TECHNOLOGY IN COMPUTATIONAL STRUCTURAL RELIABILITY ANALYSIS

It must be recognized that probabilistic structural analysis methods are not as well developed as deterministic design methodologies. Computational tools, such as those described in this paper, are just recently becoming available and have only been applied to limited numbers of problems. Moreover, training and experience are required to conduct a probabilistic analysis, neither of which are easily acquired at the present time. Consequently, before probabilistic methods can be successfully integrated into the current design cycle, several challenges, such as those listed in Fig. 12, must be overcome.

● What is Possible Now:
- Moderately Detailed Component Reliability Analyses (10,000 DOF)
- Simplified System Reliability Analyses (< 5 Modes)
- Simplified Integrated Risk/Reliability Analyses

● Current Challenges:
- Awareness, Comprehension and Acceptance
- Identification of Uncertainties or Randomness
- Probabilistic Data Bases
- Robustness and Validation of Recently Developed Computational Tools

Figure 12. State-of-The-Art In Computational Structural Reliability Analysis.

APPLICATIONS WILL SUPPORT (DRIVE) FUTURE RESEARCH AND DEVELOPMENT

The requirement for a probabilistic approach is dictated by need, and current application needs will certainly impact the future research directions. A few of these application areas are listed in Fig. 13. One of the more promising areas is probabilistic fracture mechanics. This is because fracture usually results in sudden catastrophic failure of the system. Both progressive fracture and multi-site damage are of current concern and will require probabilistic methods.

- **Probabilistic Progressive Fracture**
- **Multi-Site Damage (Linkup)**
- **Parallel Processing**
- **Certification**
- **Health Monitoring**
- **Multi-Disciplinary Reliability Assessment**
- **Optimum Inspection Scheduling and Retirement**
- **Human/Modeling Error**
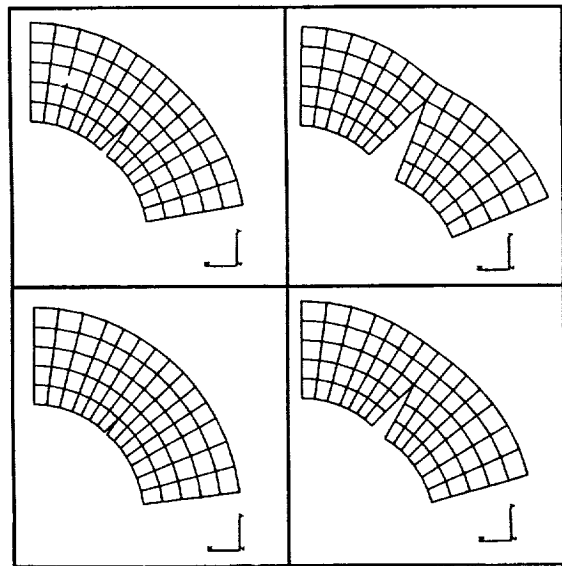
Figure 13. Some Current Application Areas That Will Require Probabilistic Methods.

REFERENCES

1. Chamis, C. C., "Probabilistic Structural Analysis Methods for Space Propulsion System Components," *Probabilistic Engineering Mechanics*, Vol. 2, No. 2, 1987.

2. Cruse, T. A., Burnside, O. H., Wu, Y.-T., Polch, E. Z., Find, P. K., Dias, J. B. and Rajagopal, K. R., "Probabilistic Structural Analysis Methods for Select Space Propulsion System Structural Components (PSAM)," *Computers and Structures*, Vol. 29, No. 5, 1988, pp. 891-901.

3. Cruse, T. A., Chamis, C. C. and Rajagopal, K. R., "Probabilistic Structural Analysis, Reliability and Risk of Critical SSME Components," NASA-MSFC Conference on Advanced Earth-to-Orbit Propulsion Technology, May 1990.

4. Thacker, B. H. and Senseny, P. E., "Probabilistic Structural Analysis of Deep Tunnels," *Probabilistic Methods in Geomechanics*, A. F. Fossum (ed.), AMD Vol. 134, American Society of Mechanical Engineers, NY, 1992, pp. 1-13.

5. Wu, Y.-T., Journel, A. G., Abramson, L. R. and Nair, P. K., Uncertainty Evaluation Methods for Waste Package Performance Assessment, NUREG/CR-5639, U.S. Nuclear Regulatory Commission, Jan. 1991.

6. Wu, Y. T., Torng, T. Y., Millwater, H. R., Fossum, A. F. and Rheinfurth, M. H., "Probabilistic Methods for Rotordynamics Analyses," SAE-911110, April 1992.

7. Millwater, H. R., Wu, Y.-T., Torng, T. Y., Thacker, B. H., Riha, D. S. and Leung, C.-P., "Recent Developments of the NESSUS Probabilistic Structural Analysis Computer Program," AIAA-92-2411, April 1992.

8. Wu, Y.-T., Millwater, H. R. and Cruse, T. A., "An Advanced Probabilistic Structural Analysis Method for Implicit Performance Functions," *AIAA Journal*, Vol. 28, No. 9, Sept. 1990, pp. 1840-1845.

9. Wu, Y.-T., "An Adaptive Importance Sampling Method for Structural System Reliability Analysis," ASME Winter Annual Meeting, Nov. 1992.

10. Thacker, B. H. and Wu, Y.-T., "A New Response Surface Approach for Structural Reliability Analysis," AIAA-92-2408, April 1992.

An Overview of Computational Simulation Methods for Composite Structures Failure and Life Analysis

Christos C. Chamis
NASA Lewis Research Center
Cleveland, OH

PRESENTATION OUTLINE

• Background

• Objective

• Progressive Fracture in Polymer Composite Structures

• Hierarchical Simulation of Failure/Life in High Temperature Composite Structures

• Probabilistic Evaluation of Composite Structural Failure/Life/Reliability

BACKGROUND

Computational simulation methods for composite structures integrity, durability, failure and life analysis have been an on-going activity in the Structural Mechanics Branch at Lewis over the past two decades.

Recent activity focus is on three parallel methods to simulate structural failure, life and reliability:

   • Progressive fracture - polymer composite

   • Hierarchical simulation - high temperature composites

   • Probabilistic evaluation - polymer composites

OBJECTIVE

Provide a brief overview of these recent activities with some typical results.

CODSTRAN ANALYSIS CYCLE

Progressive fracture in composite structures must include simulation of the (1) composite behavior in all its scales and respective failure modes (14 per ply and its adjacent interplies), (2) complex structural configurations with various loading conditions and boundary conditions, (3) hygrothermal environments, (4) synthesis of the composite structural behavior from micromechanics to global response, and (5) decomposition of the composite global structural response. All of these are incorporated in CODSTRAN as illustrated in Fig. 1.

Reference: Minnetyan, L., Chamis, C. C. and Murthy, P. L. N., "Damage and Fracture in Composite Thin Shells," NASA TM 105289, October 1991.
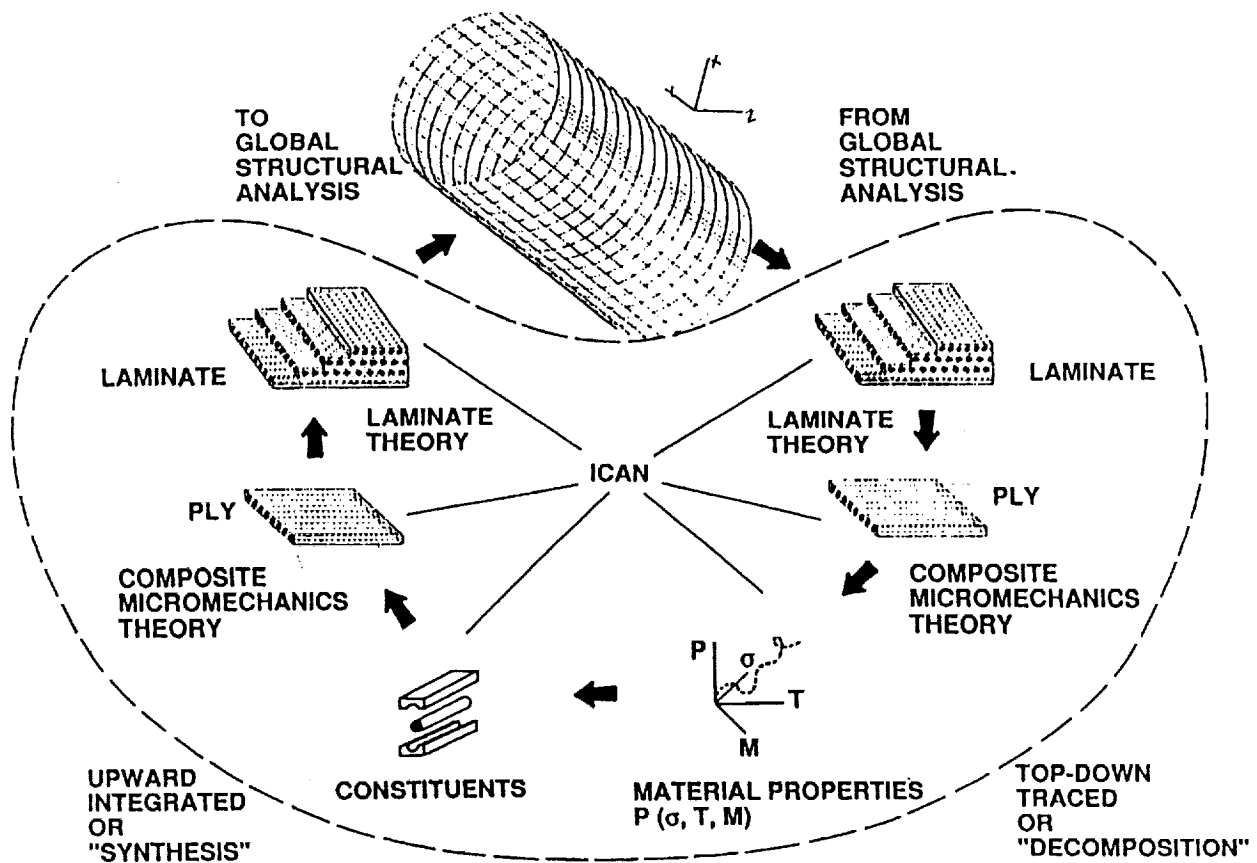
Figure 1 - Codstran Analysis Cycle Schematic

CODSTRAN LOAD INCREMENTATION

An incremental progressive fracture strategy is employed in CODSTRAN as illustrated in Figs. 2 and 3. Thermal and hygral loads are handled the same was as are cyclic and dynamic loads. Imposed displacements are also handled the same way.
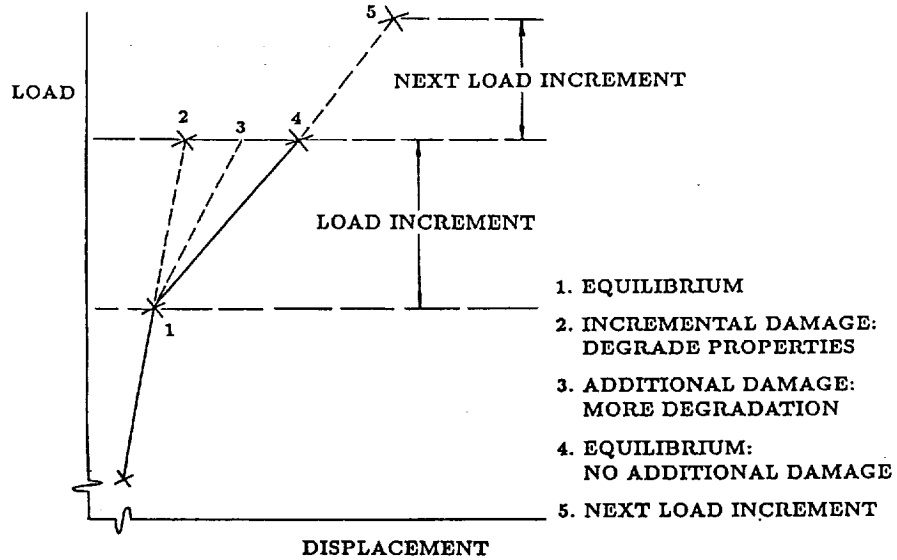
Figure 2 - Codstran Load Incrementation Schematic
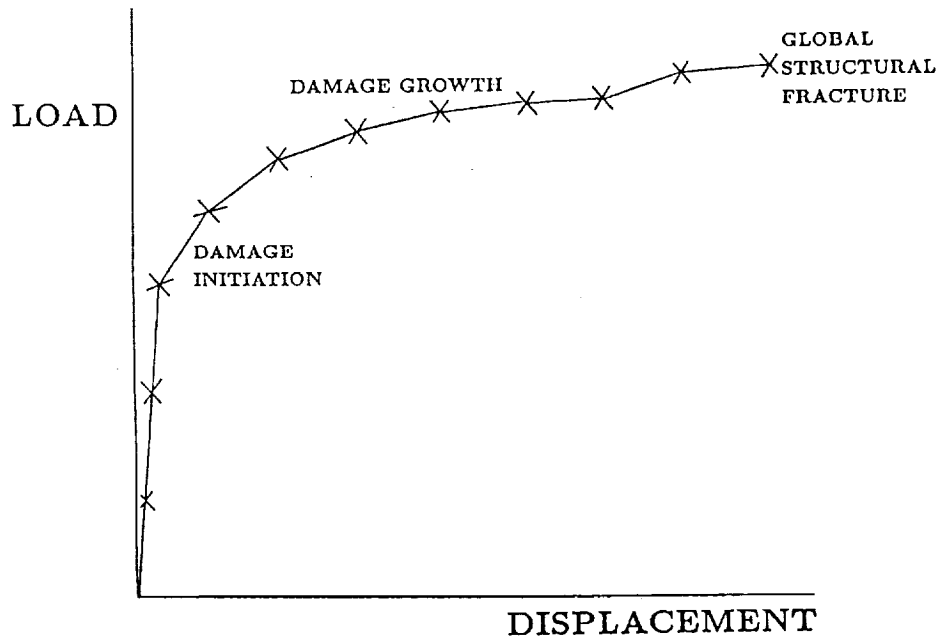
Figure 3 - Overall Codstran Simulation Displacement

SHELL STRUCTURES EVALUATED

An illustrative example of CODSTRAN's effectiveness is the composite shell shown in Fig. 4. This composite shell has surface and mid-thickness defects (cut plies) as shown in Fig. 5. The progressive fracture results obtained for internal pressure are presented in Fig. 6. The shell with surface defects exhibits the most progressive damage to fracture. The shell without defects exhibits some progressive damage to fracture while the shell with the mid-thickness defects exhibits no progressive damage and has the lowest burst pressure. These three cases demonstrate that CODSTRAN can readily be used to evaluate defect-location effects on composite structural fracture.
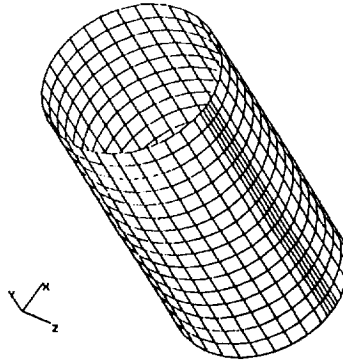
Composite Shell T300/Epoxy[90_2/±15/90_2/±15/90_2/∓15/90_2]

shell diameter = 40 in. length = 80 in.

612 nodes, 576 quadrilateral elements

initial fiber defect in 2 adjacent hoop plies

defect extends 5 in. along axial direction of shell

Figure 4 - Shell Structures Schematic
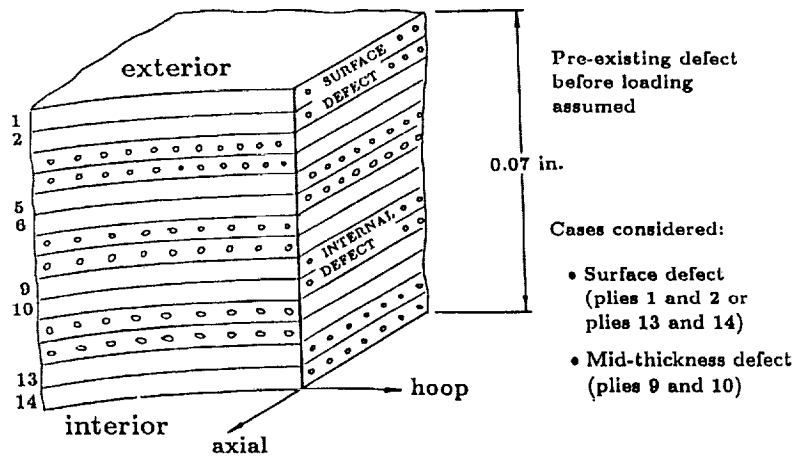
Figure 5 - Composite Shell T300/Epoxy[90_2/±15/90_2/±15/90_2/∓15/90_2]
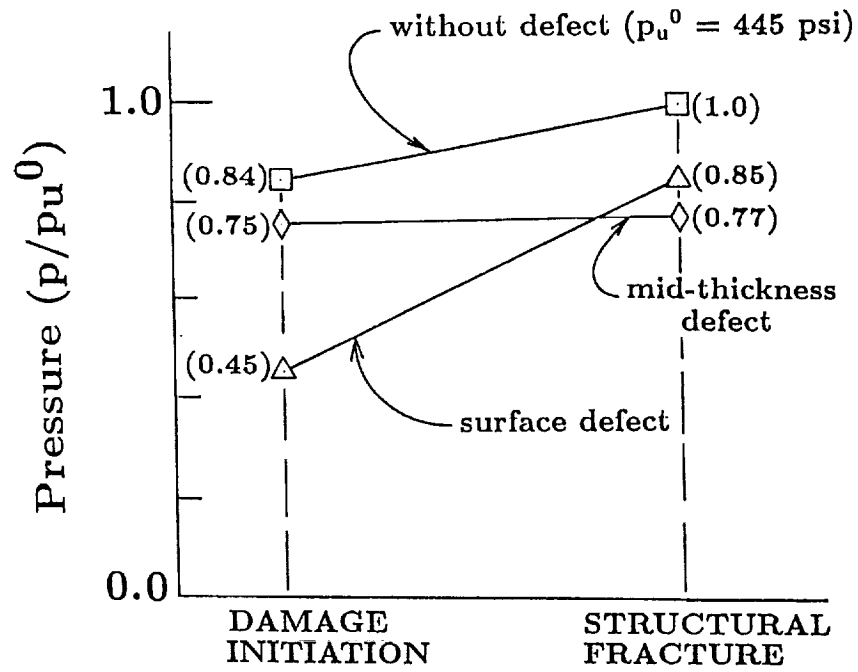
Figure 6 - Summary of Results for Composite Shell
Composite Shell T300/Epoxy[$90_2/\pm15/90_2/\pm15/90_2/\mp15/90_2$]

STIFFENED COMPOSITE CYLINDRICAL SHELL PANEL

Another illustrative example is the application of CODSTRAN to built-up composite structures depicted in Fig. 7. The laminate configuration is shown in Fig. 8. The progressive fracture results obtained for different loading conditions are summarized in Figs. 9 and 10. This composite structure exhibits the most extensive damage when subjected to tensile load and the least when subjected to combined loads. Internal pressure increases the load as well as the extent of the progressive damage.

This illustrative example demonstrates that complex composite structures subjected to different loading conditions can be evaluated for progressive fracture and up to structural fracture by using CODSTRAN.
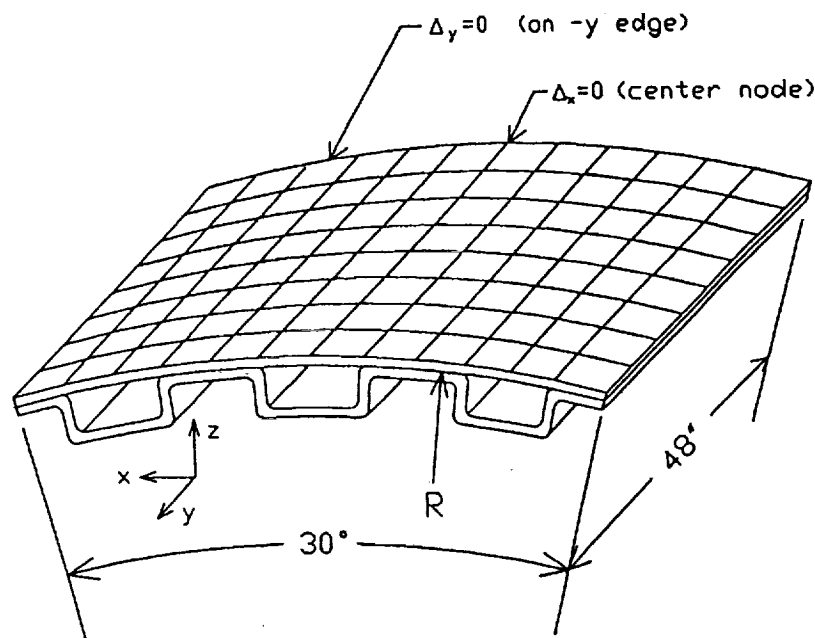
NOTE: $\theta_y = 0$ (all edge nodes)

$\Delta_{radial} = 0$ (all edge nodes)

Figure 7 - Stiffened Composite Cylindrical Shell Panel Schematic

outer shell $[90_2/\pm15]_s$ (50 plies)

$90°$ hoop plies

$\pm15°$ angle plies

stiffener web
toe extension
bonded to outer shell

stiffener web
$[\pm45]_s$ (20 plies)

stiffener flange $[0_{10},\pm45_{20}]$ (50 plies)

Figure 8 - Schematic of Laminate Structure

□ = tension only
○ = tension and shear
△ = tension, shear, press.

Tensile Load (MN/m)
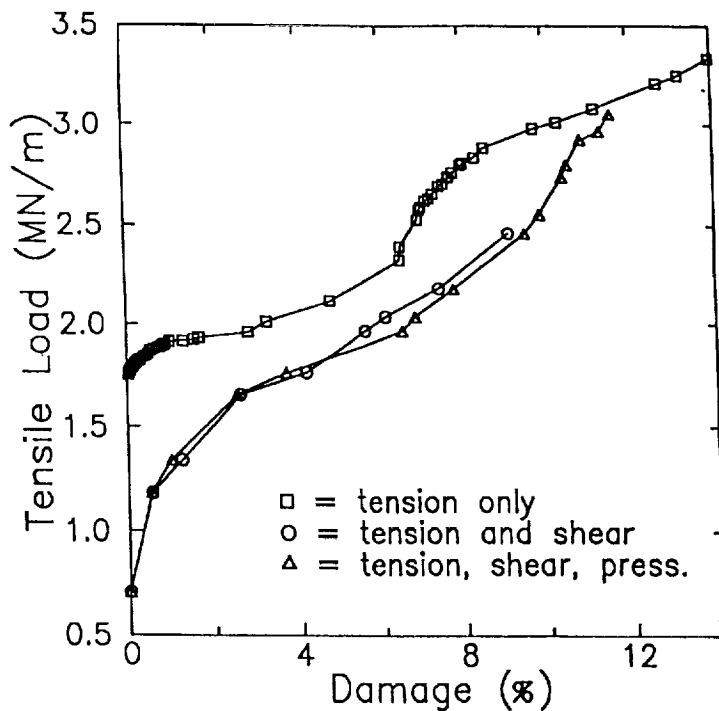
Damage (%)

Figure 9 - Axial Tension Load and Damage Progression

213

Figure 10 - Axial Compression Load and Damage Progression

GENERALIZATION

The general procedure to simulate progressive fracture in composite structures by using CODSTRAN is outlined in Fig. 11. Progressive fracture provides information for (1) detrimental defect size, (2) qualification inspection and retirement-for-cause criteria, and (3) developing and implementing fracture control plans.
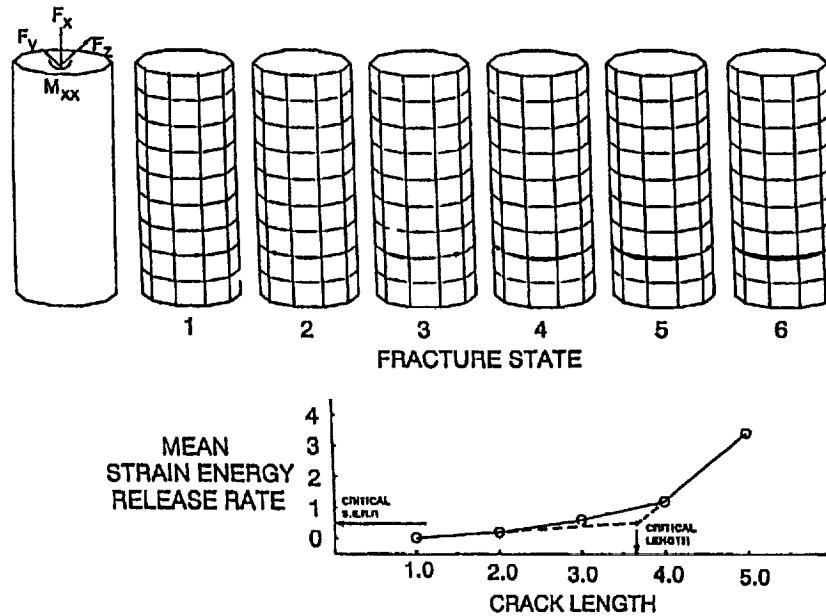
Computational simulation of structural fracture

• Develop global finite element structural/stress analysis model

• Apply spectra loads

• Identify hot spots for spectra loads

• Introduce flaws

• With spectra loads on structure grow flaws

• Monitor structural performance degradation versus flaw growth

• Identify flaw size for unacceptable performance degradation

• Set qualification, inspection and retirement-for-cause criteria

Figure 11 - Generalization Procedure

HIERARCHICAL COMPUTATIONAL SIMULATION/TAILORING
OF HOT COMPOSITE LAMINATES/STRUCTURES

The hierarchical simulation/tailoring of hot composite laminates and structures is performed by the use of several function-specific computer codes summarized in Fig. 12, where the computational capabilities, general input, code names and specific objectives are described.

Reference: Chamis, C. C., Murthy, P. L. N. and Singhal, S. N., "Computational Simulation of Hot Composite Structures," NASA TM 103681, January 1991.
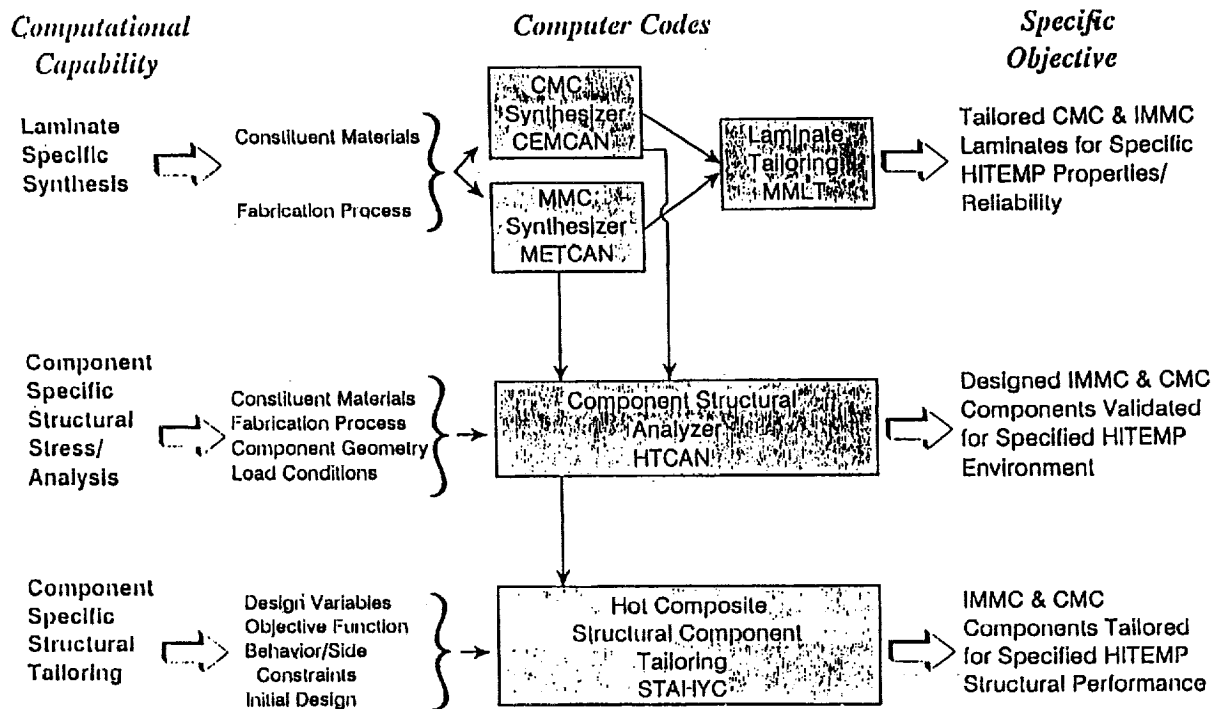
Figure 12 - Hierarchical Computational Simulation/Tailoring of Hot Composite
Laminates/Structures (Computer Codes - Description)

216

HITCAN: AN INTEGRATED APPROACH FOR HOT COMPOSITE STRUCTURES

A block diagram of the HITCAN computer code is shown in Fig. 13. It includes two independent computer codes: (1) METCAN (Metal Matrix Composite Analyzer) for the nonlinear metal matrix composite mechanics, and (2) MHOST, a dedicated finite element computer code for nonlinear finite element structural analysis. The nonlinear material behavior in HITCAN is represented by a multifactor relationship described in Fig. 14.

Reference: Singhal, S. N., Lackney, J. J., Chamis, C. C. and Murthy, P. L. N., "Demonstration of Capabilities of High Temperature Composite Analyzer Code HITCAN," NASA TM-102560, March 1990.
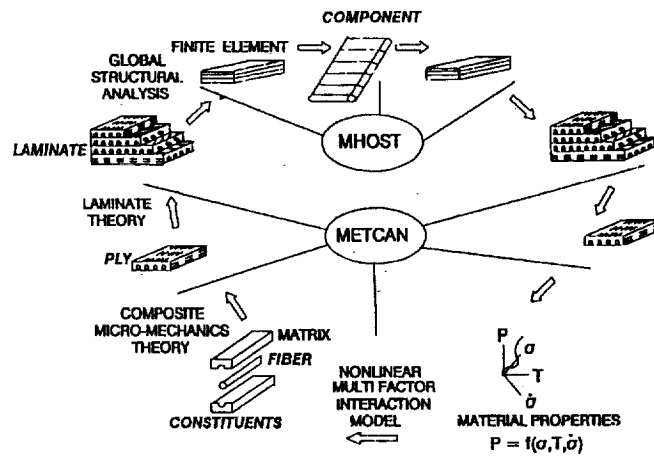
Figure 13 - HITCAN: An Integrated Approach for Hot Composite Structures

$$\frac{S_n}{S_o} = \left[\frac{T_C - T_u}{T_c - T_o}\right]^n \left[\frac{S_F - \sigma_M}{S_F - \sigma_o}\right]^m \left[\frac{N_{MF}S_F - N_M\sigma_{Mc}}{N_{MF}S_F}\right]^p \left[\frac{N_{TF}S_F - N_T\sigma_{Tc}}{N_{TF}S_F}\right]^q \left[\frac{t_FS_F - t\sigma_M}{t_FS_F}\right]^r$$
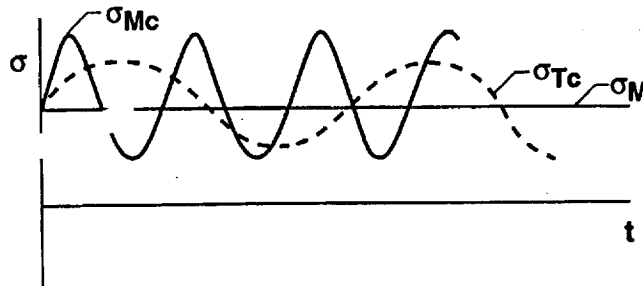
Figure 14 - Multifactor Relationship for Estimating Life

217

DEMONSTRATION: ACTIVELY COOLED HOT-COMPOSITE PANEL BUCKLING

Application of HITCAN to determine the buckling resistance of an actively-cooled panel is shown in Fig. 15. Fiber degradation (interaction with the matrix at high temperatures) decreases the buckling resistance of the panel as would be expected. Combined thermomechanical loading decreases the buckling resistance as well. This type of hot composite structure evaluation is only possible by the kind of hierarchical simulation integrated in HITCAN.

**Simply Supported-Free Actively-Cooled Structure under axial & uniform Temp. Load
for (SiC/Ti-15-3-3-3, Top:[90,0]$_s$ Bottom:[90]$_s$, Spars:4[0]$_s$); 0.4 FVR**
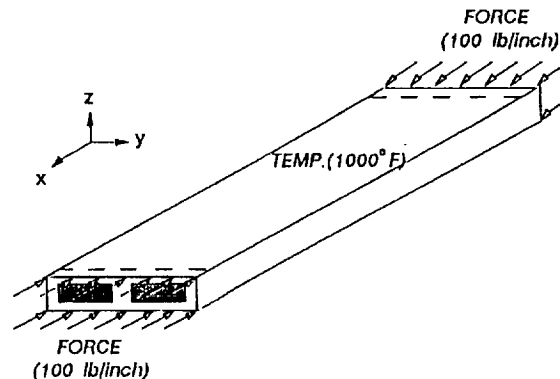
CRITICAL BUCKLING FORCE

(i) UNDER MECHANICAL LOADING ONLY = 2950 lb/inch

(ii) WITH FIBER DEGRADATION, UNDER MECHANICAL LOADING ONLY = 2850 lb/inch

(iii) UNDER THERMO-MECHANICAL LOADING = 2720 lb/inch

Figure 15 - Demonstration: Actively Cooled Hot-Composite Panel Buckling
(Without and With Combined Loads)

218

DEMONSTRATION: ACTIVELY COOLED HOT-COMPOSITE PANEL - RESULT

The corresponding displacements and micro-region stresses in the actively-cooled hot-composite panel (Fig. 15) are shown in Fig. 16. The fiber stress increases as the load increases while the matrix stress decreases and the stress in the interphase remains about the same. The fibers are the main load carrying members at these high temperatures which is the primary purpose for putting them there in the first place.
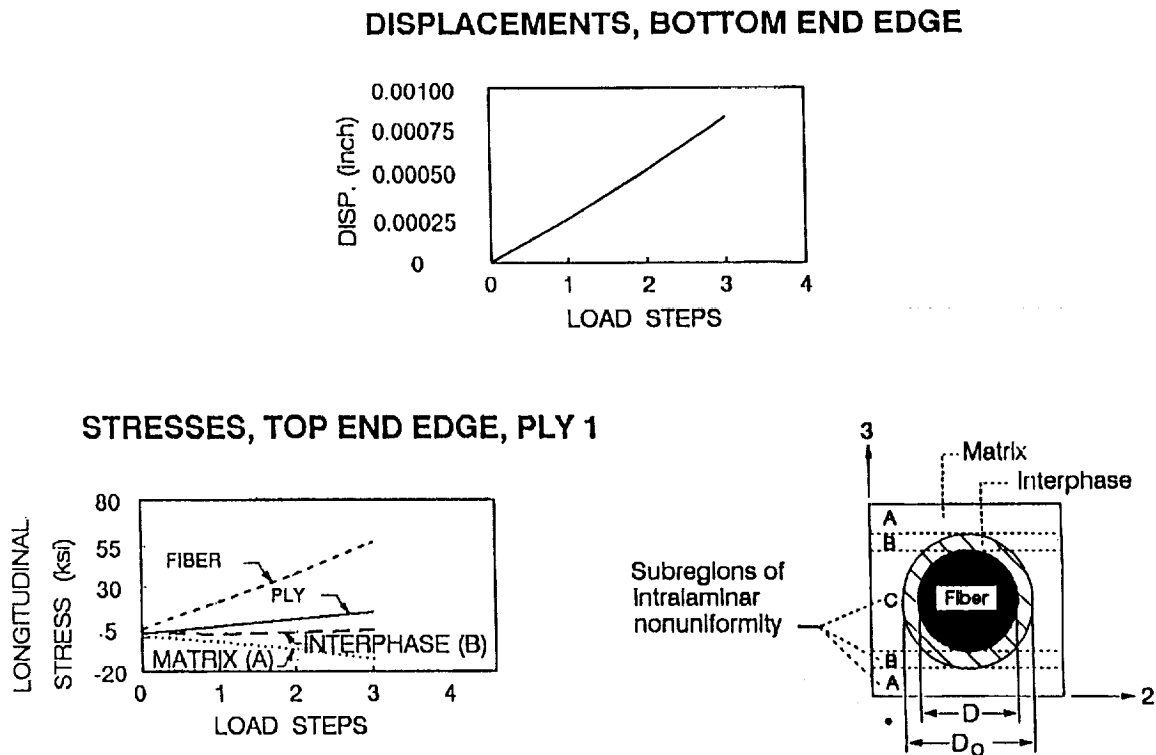
DISPLACEMENTS, BOTTOM END EDGE

STRESSES, TOP END EDGE, PLY 1

Figure 16 - Demonstration: Actively Cooled Hot-Composite Displacements and Microstresses

APPROACH: INTEGRATED PROBABILISTIC ASSESSMENT OF COMPOSITE STRUCTURES

The computer code IPACS (Integrated Probabilistic Assessment of Composite Structures) is depicted schematically in Fig. 17. It consists of combining two different codes: Probabilistic composite mechanics and probabilistic finite element structural analysis. The combination of these two codes provides the capability to simulate various uncertainties associated with composite structures from constituent material properties to structural description.

Reference: Shiao, M. C. and Chamis, C. C., "Probabilistic Evaluation of Fuselage-Type Composite Structures," NASA TM-105881, November 1992.
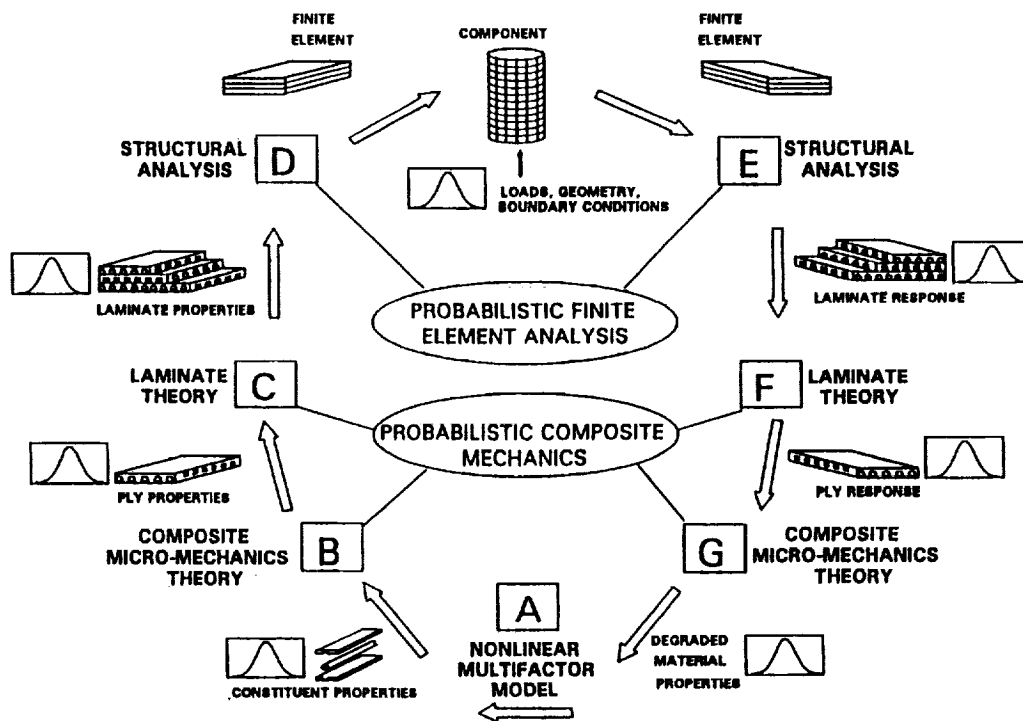
Figure 17 - Approach: Integrated Probabilistic Assessment of Composite
Structures Simulation Diagram

IPACS ASSESSMENT OF A COMPOSITE WING

The composite structure shown in Fig. 18 is selected as a sample case to illustrate application of the IPACS computer code. The various uncertainties included are summarized in the figure.
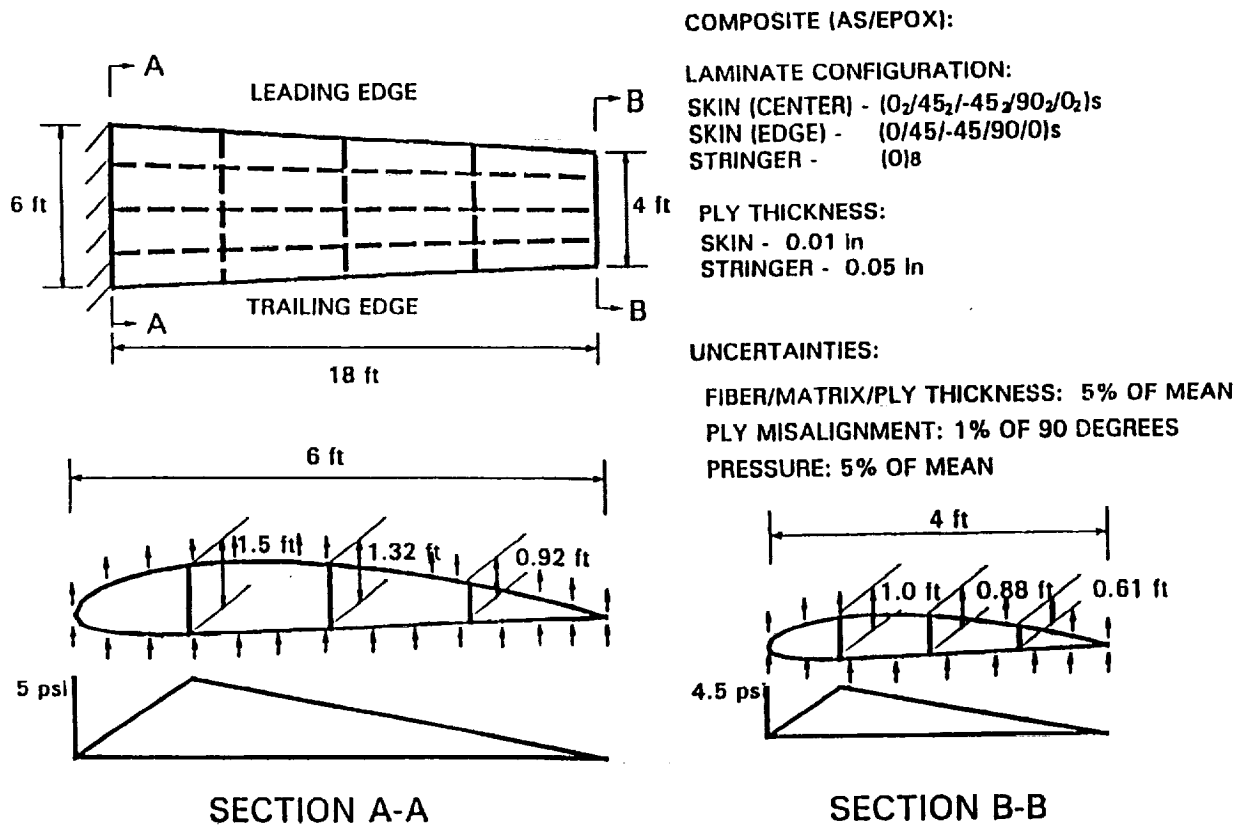
COMPOSITE (AS/EPOX):

LAMINATE CONFIGURATION:
SKIN (CENTER) - $(0_2/45_2/-45_2/90_2/0_2)s$
SKIN (EDGE) - $(0/45/-45/90/0)s$
STRINGER - $(0)8$

PLY THICKNESS:
SKIN - 0.01 In
STRINGER - 0.05 In

UNCERTAINTIES:

FIBER/MATRIX/PLY THICKNESS: 5% OF MEAN
PLY MISALIGNMENT: 1% OF 90 DEGREES
PRESSURE: 5% OF MEAN

LEADING EDGE

TRAILING EDGE

6 ft

4 ft

18 ft

6 ft

1.5 ft   1.32 ft   0.92 ft

5 psi

SECTION A-A

4 ft

1.0 ft   0.88 ft   0.61 ft

4.5 psi

SECTION B-B

Figure 18 - Geometry and Loading for a Composite Wing

221

COMPRESSIVE FATIGUE LIFE OF A COMPOSITE WING

The fatigue life results obtained by using IPACS for the composite wing are shown in Fig. 19. The sensitivity factors that influence the fatigue life are also shown. The probability of fatigue failure increases exponentially with fatigue cycles. Two wings in ten thousand will fail in one-hundred-thousand fatigue cycles. Another important aspect of the probabilistic assessment is the evaluation of the sensitivity factors. These are shown in the lower part of Fig. 19. Only eight of the about one-hundred factors influence fatigue life.

This multitude of sensitivity factors illustrate the difficulty associated with predicting fracture in composite structures by using classical or traditional approaches. The composite wing probabilistic assessment demonstrates that the development of IPACS has matured sufficiently to be effectively used in aeronautics composite structures of practical significance.
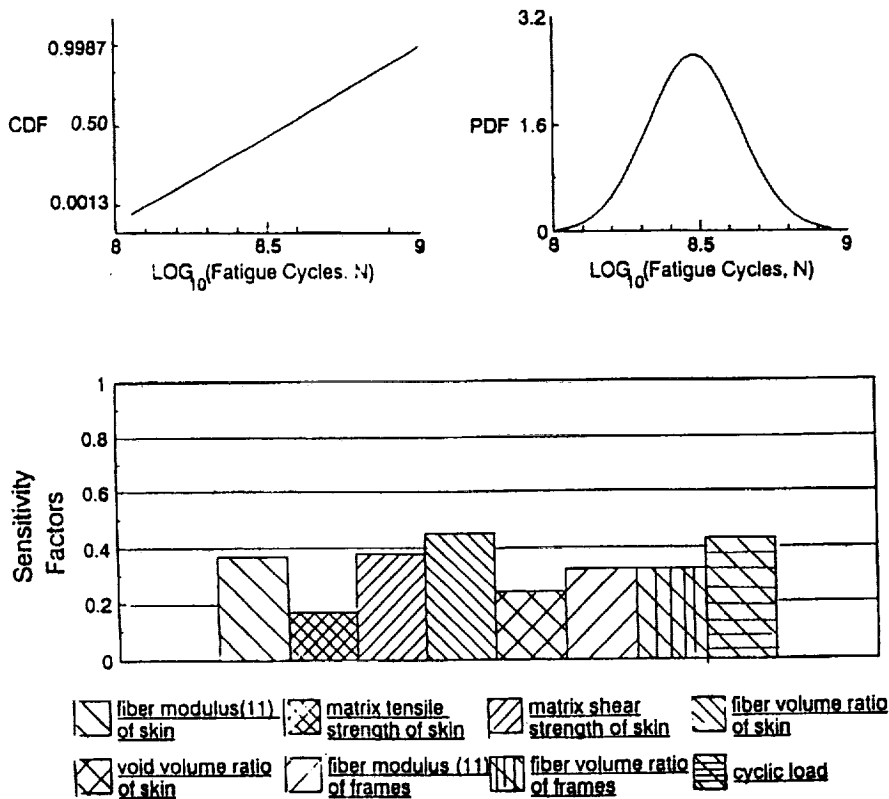
Figure 19 - Compressive Fatigue Life: Probabilistic Distributions and Sensitivity Factors

SUMMARY OF RESULTS

- Composite shells with internal defects and subjected to internal pressure exhibit no damage growth prior to fractures.

- The hierarchical simulation for high-temperature composite structures behavior accurately simulated fracture in a SiC/Ti ring.

- The IPACS computer code simulates uncertainties/sensitivities in evaluating life/reliability of composite wing-type structures.

CONCLUSION

Three parallel computational simulation methods are being developed at the LeRC SMB for composite structures failure and life analysis:

- Progressive fracture CODSTRAN

- Hierarchical methods for high-temperature composites

- Probabilistic evaluation

Results to date demonstrate that these methods are effective in simulating composite structures failure/life/reliability.

PAGE_____INTENTIONALLY BLANK

N94-22618

Analysis of Thermal Mechanical Fatigue in Titanium Matrix Composites

W. Steven Johnson and Massoud Mirdamadi
NASA Langley Research Center
Hampton, VA

INTRODUCTION

Titanium metal matrix composites are being evaluated for structural applications on advanced hypersonic vehicles. These composites are reinforced with ceramic fibers such as silicon carbide, SCS-6. This combination of matrix and fiber results in a high stiffness, high strength composite that has good retention of properties even at elevated temperatures. However, significant thermal stresses are developed within the composite between the fiber and the matrix due to the difference in their respective coefficients of thermal expansion. In addition to the internal stresses that are generated due to thermal cycling, the overall laminate will be subjected to considerable mechanical loads during the thermal cycling. In order to develop life prediction methodology, one must be able to predict the stresses and strains that occur in the composite's constituents during the complex loading. Thus the purpose of this presentation is to describe such an analytical tool, VISCOPLY.

COMPOSITE CONSTITUENT PROPERTIES

The mechanical properties of the fibers and the matrix materials at room temperature are shown in Table I.

Table I. Mechanical Properties

FIBERS	MATRIX
Silicon-carbide (SCS-6)	Ti-15V-3Cr-3Al-3Sn (Ti-15-3)
E = 400 GPa	E = 93 GPa
ν = 0.25	ν = 0.36
σ = 3.6 x 10^{-6} mm/mm/^{o}C	σ = 8.2 x 10^{-6} mm/mm/^{o}C
Diameter = 0.14 mm	σ_{ys} = 690 MPa

THERMOMECHANICAL FATIGUE TEST SETUP

The schematic diagram of the thermomechanical fatigue test setup is shown in Fig. 1. Liquid nitrogen is used in conjunction with induction heating to allow for precise specimen cooling rates.
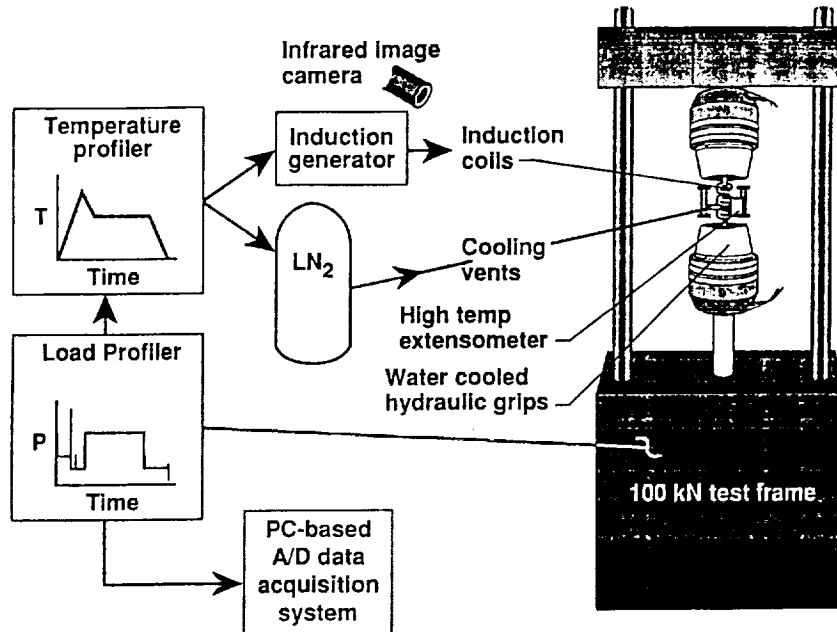
Figure 1. Thermomechanical fatigue test setup.

VISCOPLY PROGRAM DESCRIPTION

The VISCOPLY program is a two-dimensional symmetric laminate analysis code that can account for thermoviscoplastic response of both the fiber and/or the matrix material. The program combines the vanishing fiber diameter (VFD) model, a thermoviscoplasticity theory, and laminated plate theory. The program is based on the constituent properties of the fiber and the matrix. The fiber and matrix properties can both be nonlinear with time and temperature. VISCOPLY accepts any combination of in-plane normal and shear loading, out-of-plane normal loading and temperature change and can load in stress or strain control. Sequential jobs which allow any order and rate of load and temperature can be performed. The VISCOPLY program predicts the average stresses and strains in the fiber and matrix, and determines the overall laminate response.

THERMOVISCOPLASTICITY THEORY

The VISCOPLY program is based on the viscoplasticity theory of Eisenberg and Yen (1981), which was modified by Bahei-El-Din (1990). The theory assumes an existence of a rate-independent equilibrium stress-strain response. Inelastic deformation takes place if the current stress state is greater than the equilibrium stress state. The uniaxial constitutive equation, $\varepsilon_{in}=k\ R^p$, is a power law relationship requiring only two experimentally determined parameters, k and p. These parameters are determined from two monotonic, uniaxial tests performed at each temperature of interest. A strain-controlled test is conducted to determine the equilibrium curve and a load-controlled test is conducted to determine the overstress, R, and the inelastic strain rate, ε_{in}. The equilibrium curve and the load-controlled test results are then used to determine k and p as described in the following sections.

EQUILIBRIUM CURVE

The equilibrium curve is established by conducting a strain-controlled relaxation test. The test specimen is loaded to a predetermined strain level. The strain is then held constant to allow for stress relaxation. This sequence is repeated and the end points of the maximum relaxation events are joined to form the equilibrium curve for a given temperature. This is schematically shown in Fig. 2.
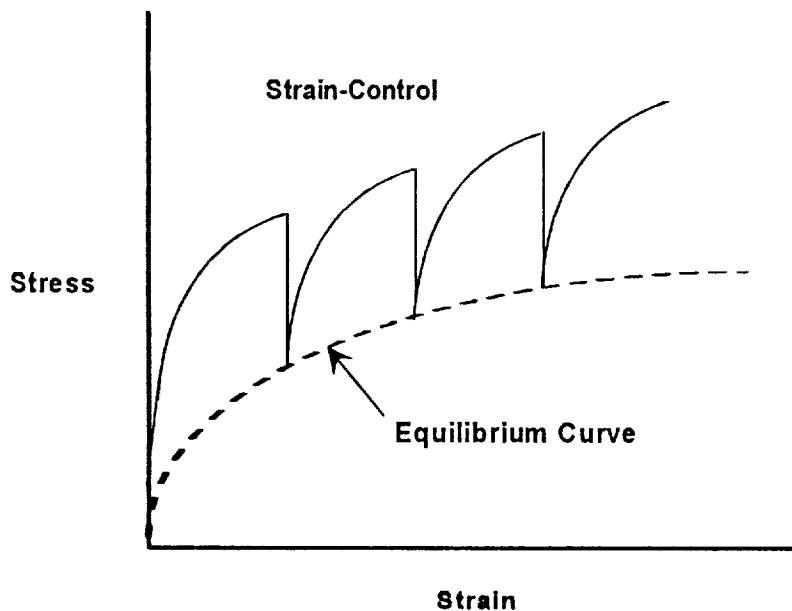

Figure 2 - Determination of equilibrium stress-strain response

CONSTANTS FOR THE EISENBERG-YEN MODEL

The constants k and p for the Eisenberg-Yen model are derived as shown by the schematic diagram in Figs. 3 and 4. The solid line on the stress-strain plot in Fig. 3 is a constant load rate test. The distance between the equilibrium curve and the constant load rate curve is the overstress, R. The amount of overstress is then plotted against the instantaneous strain rate as shown in Fig. 4. The k and p are then determined from the intercept and slope.
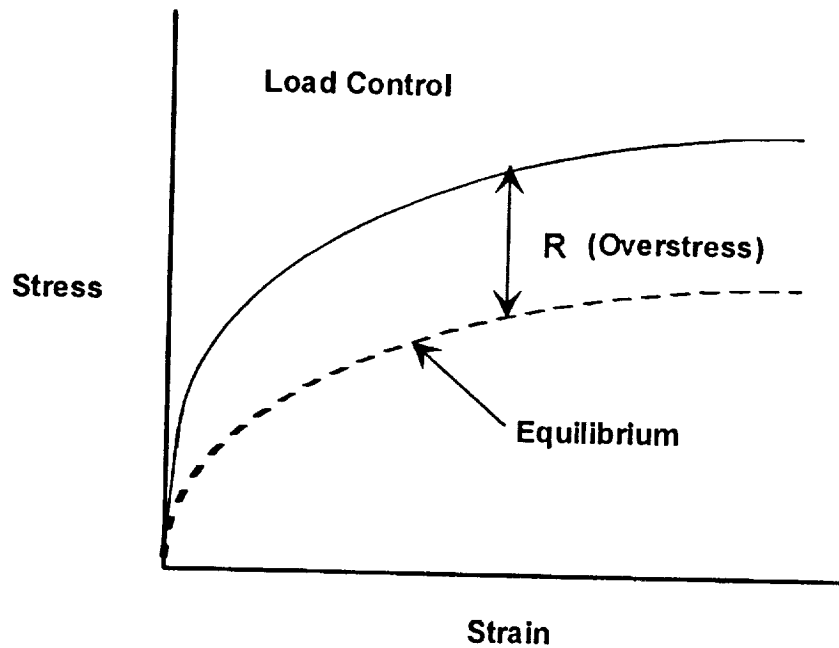

Figure 3 - Determination of overstress, R.
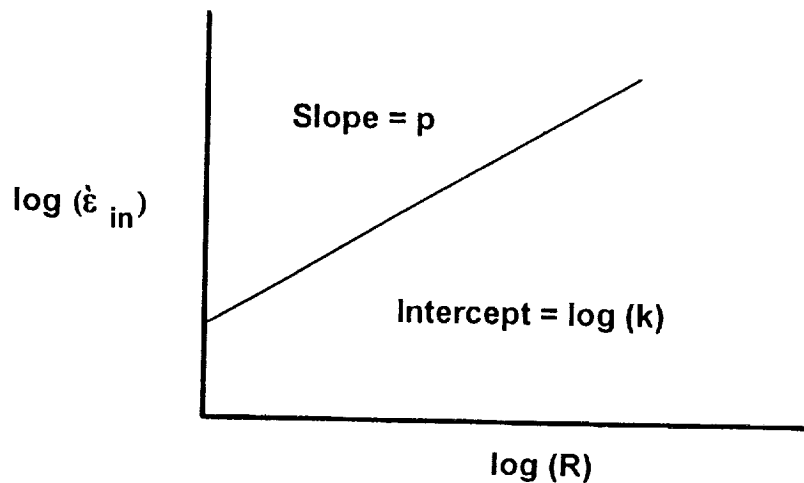
Figure 4 - Determination of the constants k and p.

MODEL CHECK ON THE MATRIX MATERIAL

Figure 5 shows an example of the model fit to the matrix data alone. These material constants will be used in all subsequent predictions.
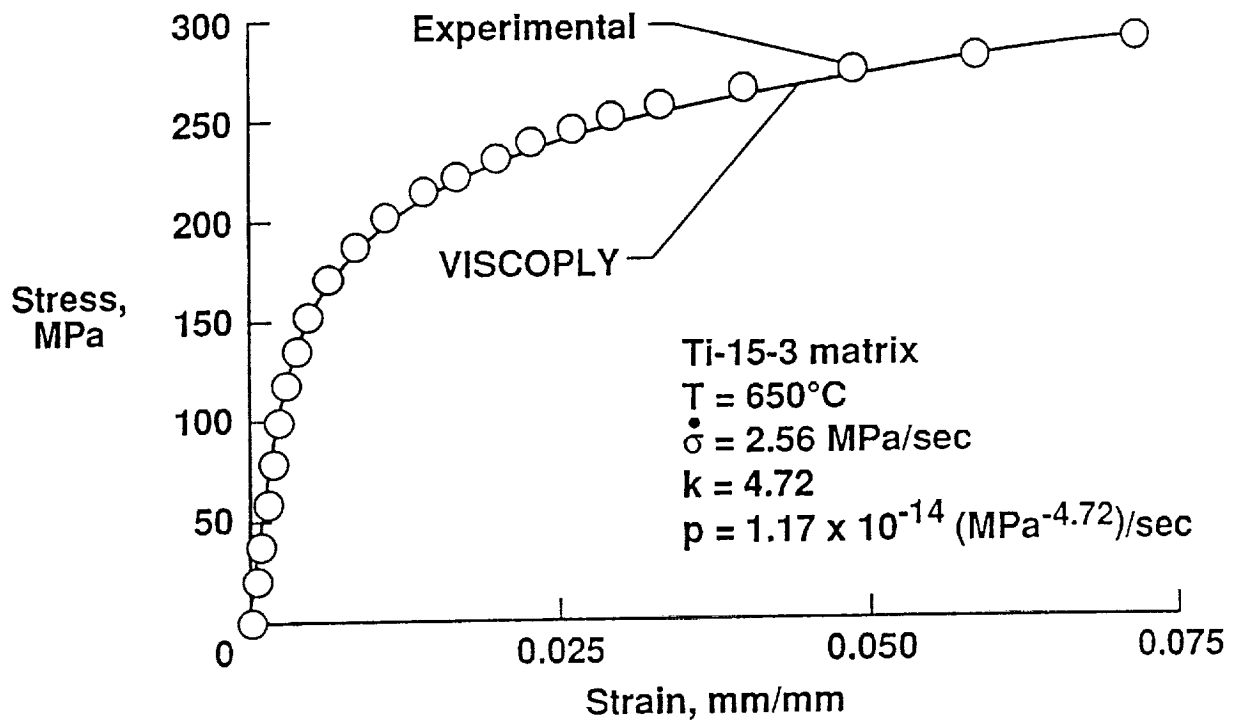
Figure 5 - Best fit approximation to the experimental data.

PREDICTION OF MATRIX RESPONSE

Figure 6 shows a comparison of measured and predicted time-dependent matrix response to a loading and relaxation test. Very good agreement between the model and experimental results was found.
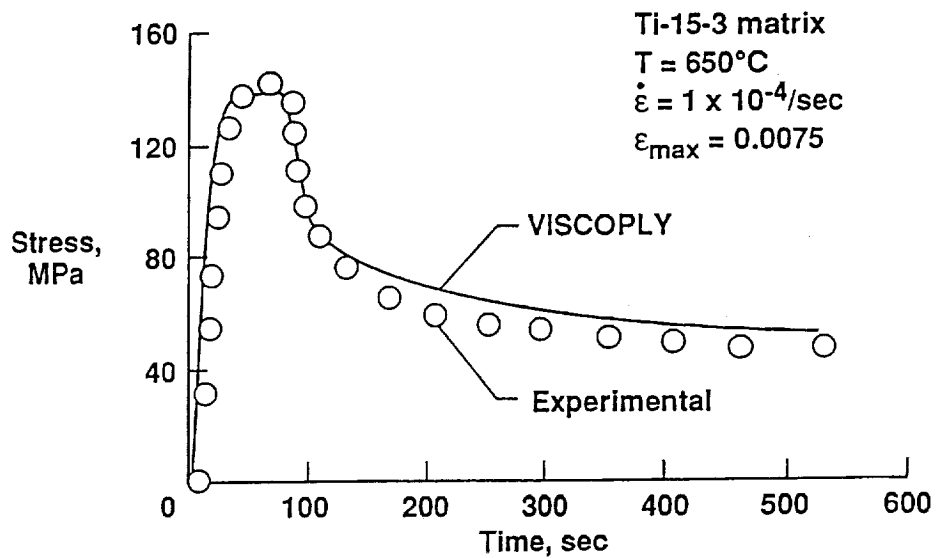

Figure 6 - Prediction of time-dependent matrix response.

PREDICTION OF A UNIDIRECTIONAL COMPOSITE RESPONSE

The predicting loading - unloading response of a unidirectional composite at elevated temperature is shown in Fig. 7. The VISCOPLY prediction was based only on those parameters determined from the constituent tests. As seen in the figure, VISCOPLY captured the essence of loading, unloading, and the permanent deformation of the composite.
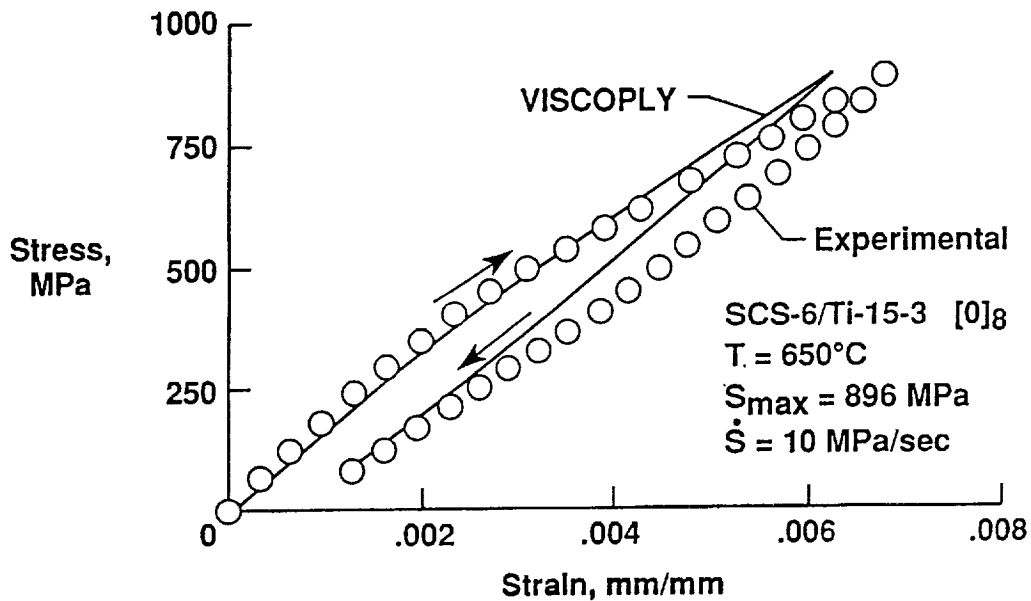

Figure 7 - Prediction of composite response.

234

ACCOUNTING FOR INTERFACE FAILURES IN 90° PLIES

In the VISCOPLY program the transverse modulus of the fibers in the 90° plies is reduced to simulate the fiber/matrix interface failures that have been shown to occur at very small load levels. It was determined that by multiplying the transverse modulus by 0.1 gave the best fit to the experimental data as shown in Fig. 8. This factor will be used in all future predictions of composite response above the fiber/matrix separation stress level at all temperatures.
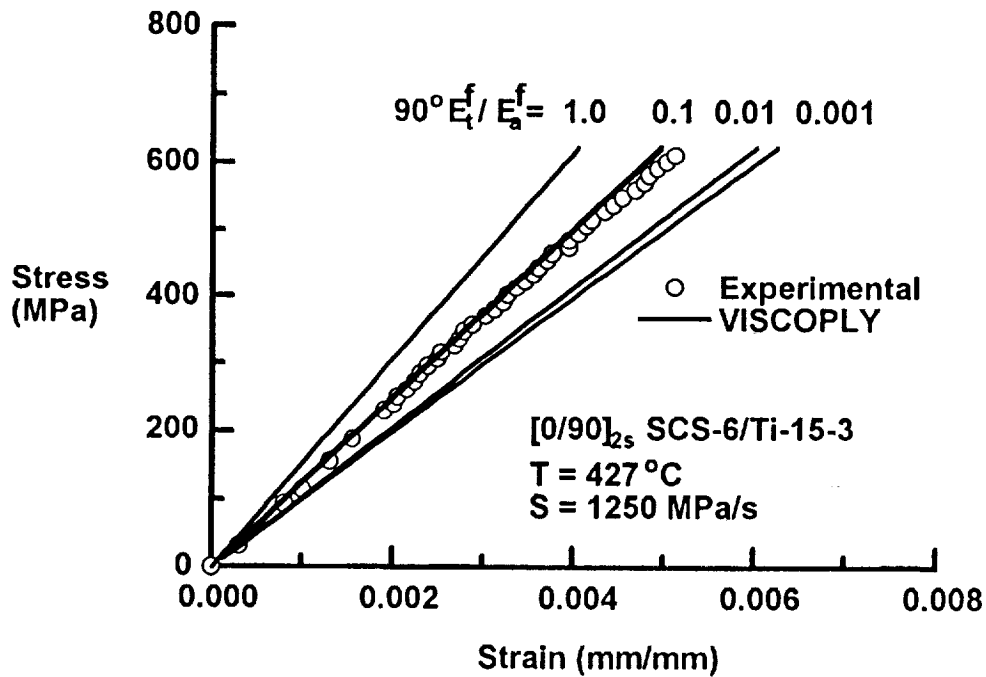

Figure 8 - Effect of reducing fiber transverse modulus on VISCOPLY predictions.

FLIGHT SIMULATION PROFILE

The flight profile shown in Fig. 9 was applied to actual specimens and the overall laminate stress-strain response was measured.
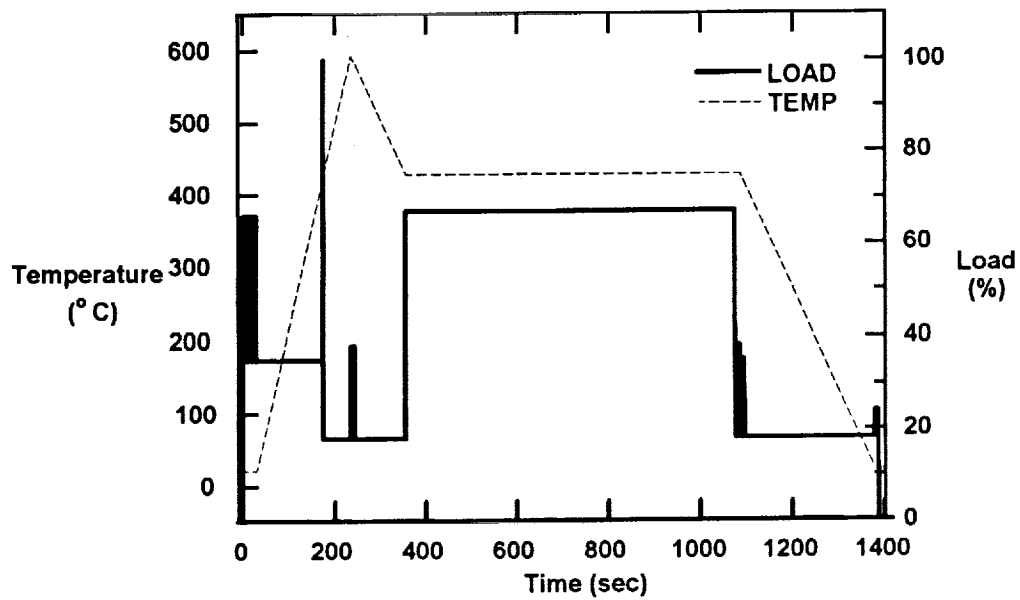

Figure 9 - Generic hypersonic flight profile.

PREDICTED LAMINATE STRESS-STRAIN RESPONSE
TO THE FLIGHT PROFILE

As seen in Fig. 10, VISCOPLY accurately predicted the stress-strain response of the composite for the flight profile incorporating fiber/matrix interface failure of the 90° plies.
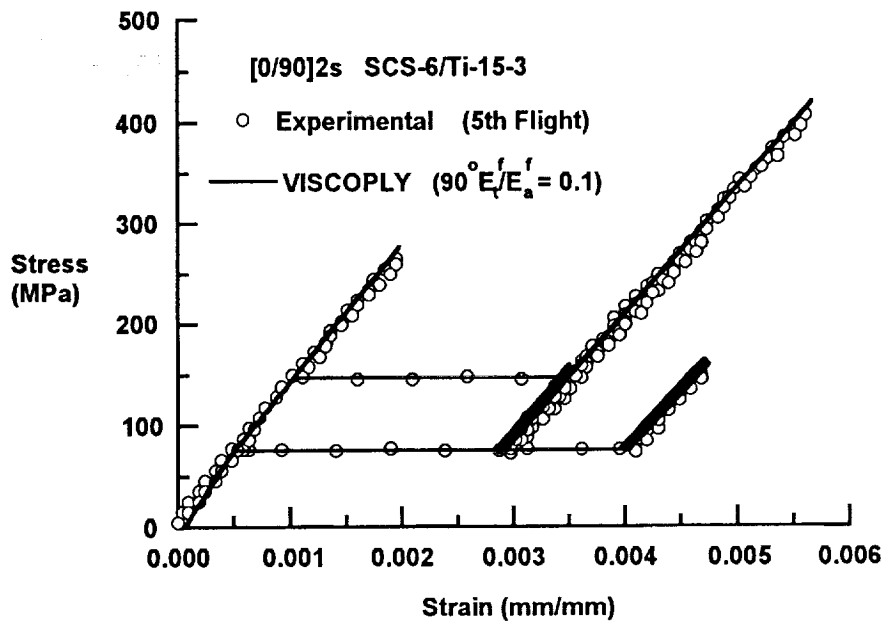

Figure 10 - Prediction of composite response under flight profile.

CONCLUSIONS

- Good characterization of constituent properties is required for accurate model predictions.
  • Matrix heat treatment should be the same as composite.
  • Rate-dependent and temperature-dependent constituent properties must be properly characterized.

- Fiber/matrix interface failure must be modeled for accurate predictions.

- VISCOPLY accurately predicted composite stress-strain response to cruise mission profile.

- VISCOPLY predictions of constituent behavior during mission profile are accurate and can be used in a failure criterion.

REFERENCES

1. Mirdamadi, M., Johnson, W. S., Bahei-El-Din, Y. A., and Castelli, M. G., *Analysis of Thermomechanical Fatigue of Unidirectional Titanium Metal Matrix Composites*, NASA TM 104105, July 1991.

2. Mirdamadi, M. and Johnson, W. S., *Stress-Strain Analysis of a [0/90]$_{2s}$ Titanium Matrix Laminate Subjected to a Generic Hypersonic Flight Profile*, NASA TM 107584, March 1992.

N94-22619

Time-Dependent Reliability Analysis of Ceramic Engine Components

Noel N. Nemeth
NASA Lewis Research Center
Cleveland, OH

ABSTRACT

The computer program CARES/LIFE calculates the time-dependent reliability of monolithic ceramic components subjected to thermomechanical and/or proof test loading. This program is an extension of the CARES (Ceramics Analysis and Reliability Evaluation of Structures) computer program. CARES/LIFE accounts for the phenomenon of subcritical crack growth (SCG) by utilizing either the power or Paris law relations. The two-parameter Weibull cumulative distribution function is used to characterize the variation in component strength. The effects of multiaxial stresses are modeled using either the principle of independent action (PIA), the Weibull normal stress averaging method (NSA), or the Batdorf theory. Inert strength and fatigue parameters are estimated from rupture strength data of naturally flawed specimens loaded in static, dynamic, or cyclic fatigue. Two example problems demonstrating proof testing and fatigue parameter estimation are given.

Designing with ceramics requires a new approach involving statistics. Inherent to this method is the realization that any component will have a finite failure probability; that is, no design is failsafe. Methods of quantifying this failure probability as a function of time and loading have been investigated and refined. These theories have been programmed into the CARES/LIFE integrated design computer program. The accuracy of the FORTRAN coding and the mathematical modeling has been verified by analytical and the available experimental data in the open literature. Using CARES/LIFE, a design engineer can easily calculate the change in reliability due to a design change. This can lead to more efficient material utilization and system efficiency.

Objective

- Develop probabilistic based integrated design programs for the life analysis of brittle material engine components

Outline

- Introduction

- CARES/LIFE program capability

- Time-dependent reliability models

- Fatigue parameter estimation techniques

- Examples

- Conclusions

Figures 1 and 2

CERAMICS FOR ENGINES

Structural ceramics have been utilized for various test engine components since the early 1970's. The high-temperature strength, environmental resistance, and low density of these materials can result in large benefits in system efficiency and performance. However, the brittle nature of ceramics causes a high sensitivity to microscopic flaws and often leads to catastrophic fracture. These undesirable properties are being overcome through material toughening strategies, improvements in processing to reduce the severity and number of flaws, and component designs that reduce susceptibility to foreign object damage. Ultimately, ceramics are envisioned to operate in small- and medium-sized automotive gas turbines operating with uncooled parts at temperatures as high as 1400 degrees centigrade.
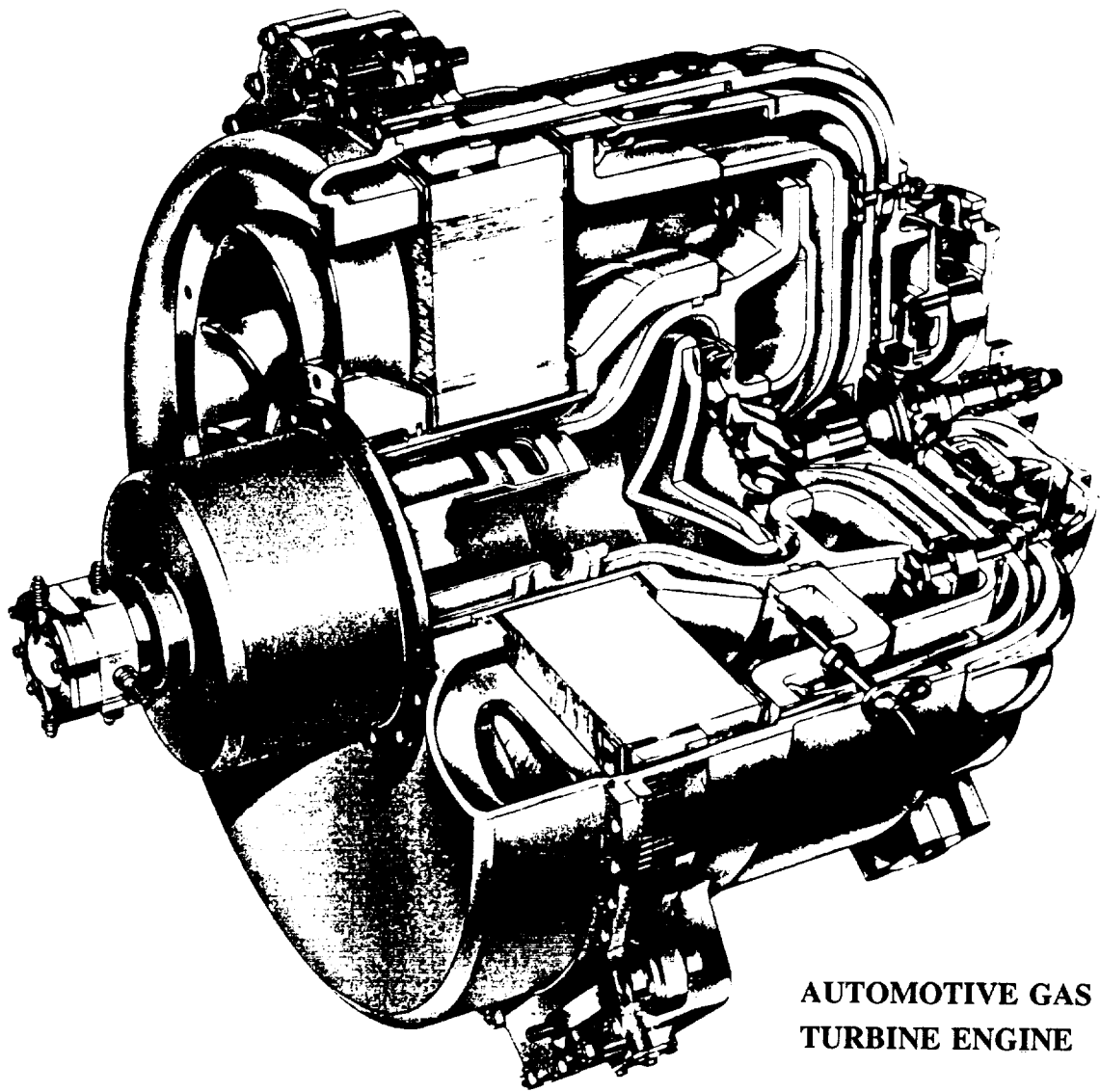
AUTOMOTIVE GAS
TURBINE ENGINE

AGT101
GARRETT TURBINE ENGINE COMPANY

Figure 3

CERAMIC TURBOCHARGER ROTORS

The first major commercial breakthrough for structural ceramics is the automotive turbocharger rotor. Over one half million vehicles in Japan incorporate this part. The reduced rotational inertia of the silicon nitride ceramic compared to a metallic rotor significantly enhances the turbocharger performance and efficiency. In the United States, the Garrett Automotive Division of the Allied Signal Aerospace Company is incorporating a ceramic turbocharger rotor in industrial diesel trucks.

Figure 4

The design of ceramics differs from that of ductile metals in that ceramic materials are unable to redistribute high local stresses induced by inherent flaws. Random flaw size and orientation require a probabilistic analysis, since the ceramic material cannot be described by a single unique strength. The weakest link theory, which analogizes the component as a series of links in a chain, accurately describes the strength response. This theory is incorporated in Weibull (1939) and Batdorf and Crose (1974) stress-volume or stress-area integrals to predict the material failure response due to thermomechanical loads. Probabilistic design is not necessarily governed by the most highly stressed location, but by the entire stress field in a component.

CERAMICS REQUIRE PROBABILISTIC DESIGN ANALYSIS

CERAMICS CONTAIN MANY MICROSCOPIC FLAWS AND SHOW SIZE EFFECT

CERAMICS ARE STIFF, BRITTLE AND HAVE NO UNIQUE STRENGTH

ANALYTICAL ULTRASONICS

HIGH RESOLUTION X-RAY

NDE MUST DEAL PROBABILISTICALLY WITH DIFFUSE FLAW POPULATIONS

ENGINE APPLICATION

WLT MODEL

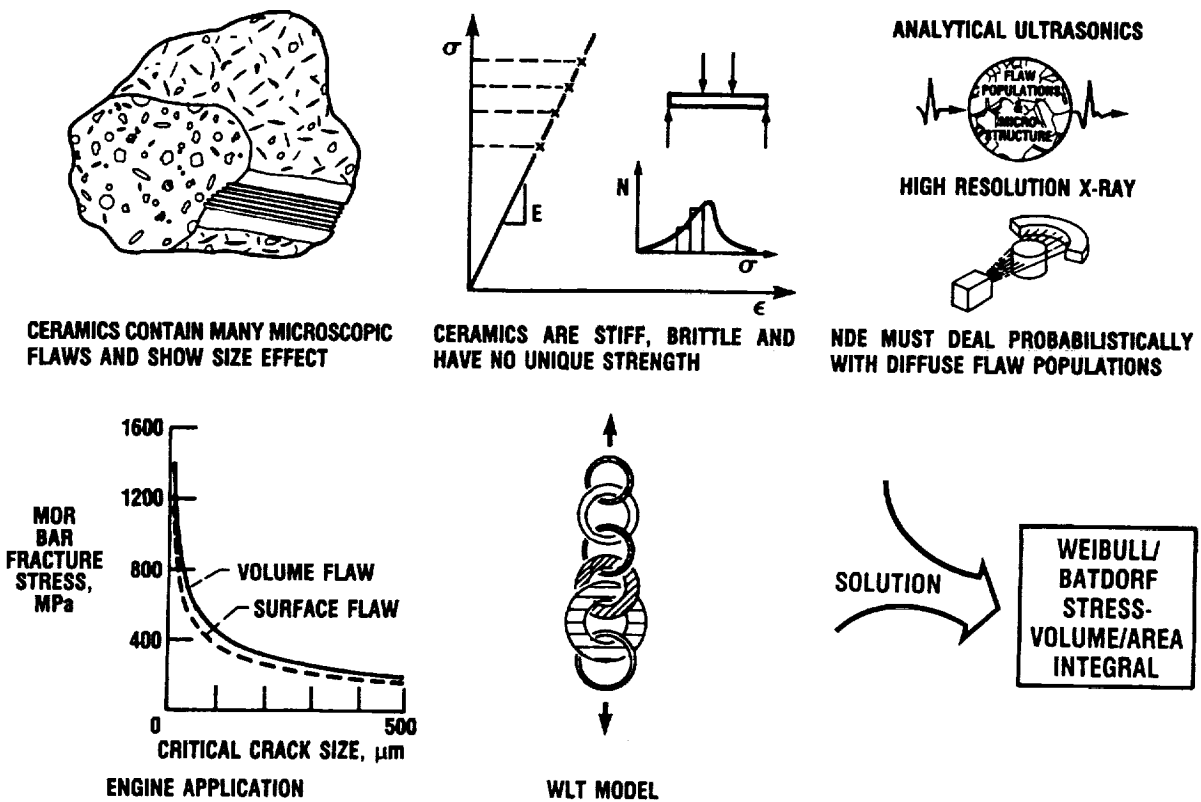SOLUTION

WEIBULL/ BATDORF STRESS- VOLUME/AREA INTEGRAL

Figure 5

STATISTICAL FRACTURE THEORIES

A common aspect of any weakest link theory is that the component volume and/or surface area of a stressed material will affect its strength, whereby larger components result in lower average strengths. This observation led Weibull (1939) to propose a phenomenological model to describe the scatter in brittle material fracture strengths in fast-fracture. To predict material fast-fracture response under multiaxial stresses, Weibull suggested averaging the tensile normal stress in all directions. As this approach is arbitrary and involves tedious numerical integration, other approaches have been subsequently introduced. The most simplistic is the Principle of Independent Action (PIA) model (Barnett (1967), and Freudenthal (1968)). The PIA theory assumes that each tensile principal stress contributes to the failure probability as if no other stress were present. Recognizing that brittle fracture is governed by linear elastic fracture mechanics (LEFM), Batdorf and Crose (1974) proposed that reliability predictions should be based on a combination of the weakest link theory and fracture mechanics. Conventional fracture mechanics dictates that both the size of the critical crack and its orientation relative to the applied loads determine the fracture stress. However, with ceramics the small critical flaw size and the large number of flaws prevent determination of the critical flaw, let alone its size and orientation. Instead, the combined probability of the critical flaw being within a certain size range and being oriented so that it may cause fracture is calculated. This model was extended to account for mixed-mode fracture by Batdorf and Heinisch (1978).

WEAKEST LINK FRACTURE MODEL	SIZE EFFECT	COMPUTATIONAL SIMPLICITY	STRESS STATE EFFECTS	THEORETICAL BASIS
WEIBULL (1939)	YES	SIMPLE	UNIAXIAL	PHENOMENOLOGICAL
NORMAL STRESS AVERAGING (1939)	YES	COMPLEX	MULTIAXIAL	PHENOMENOLOGICAL
PRINCIPLE OF INDEPENDENT ACTION (1967)	YES	SIMPLE	MULTIAXIAL	MAXIMUM PRINCIPAL STRESS THEORY
BATDORF (SHEAR-INSENSITIVE, 1974) (SHEAR-SENSITIVE, 1978)	YES	COMPLEX	MULTIAXIAL	LINEAR ELASTIC FRACTURE MECHANICS

Figure 6

FRACTURE MAP OF A HOT PRESSED SILICON NITRIDE

Creep and subcritical crack growth (SCG) are two mechanisms which cause the average strength (per unit volume or area) of ceramic materials to degrade over time. Creep is associated with high temperatures and low stress levels. Creep is due to the formation and coalescence of voids at the glassy grain boundaries of the material. SCG is associated with elevated temperatures, moderate stress levels, chemically active environments, or mechanically (cyclically) induced damage. SCG initiates at a pre-existing flaw and continues until a critical length is reached causing catastrophic propagation.
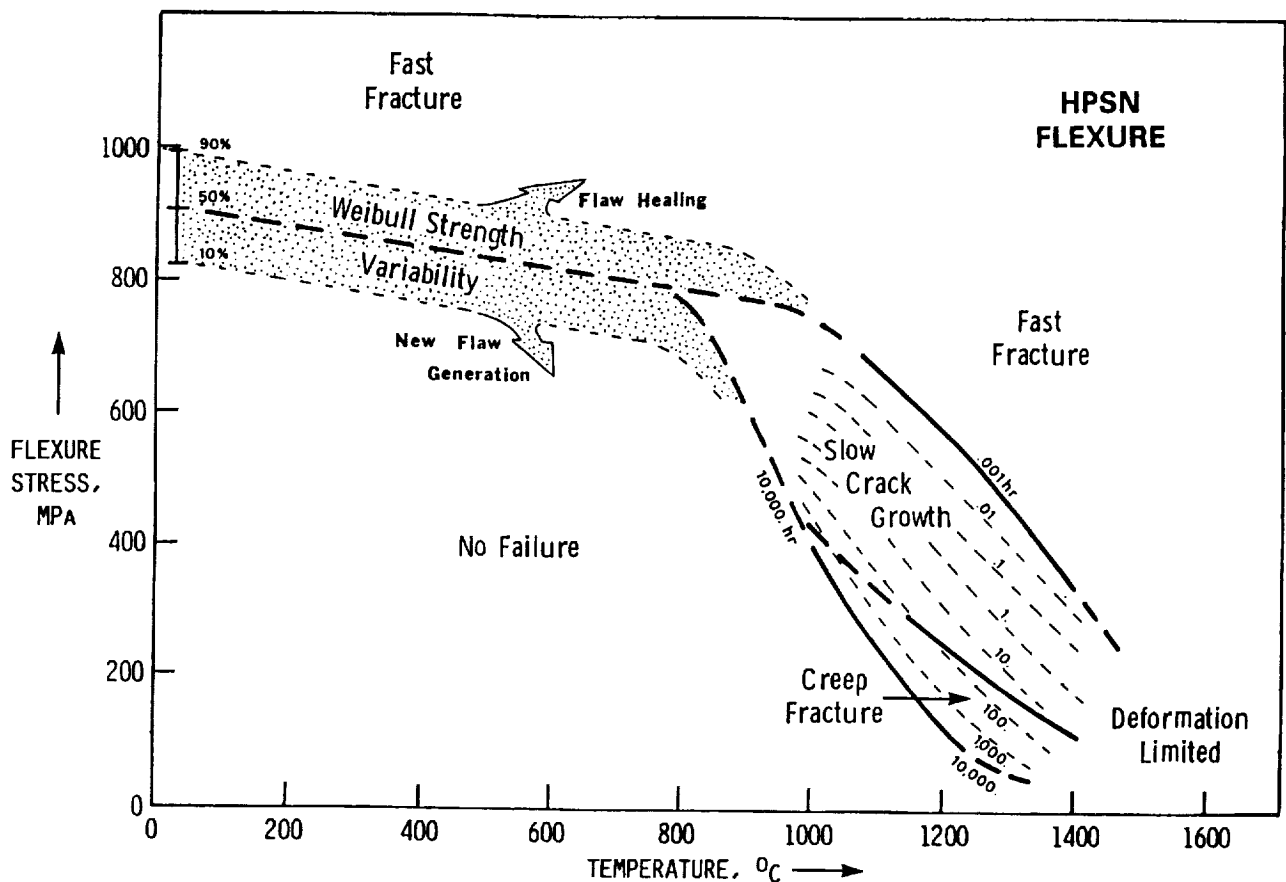

Figure 7

THE CARES/LIFE COMPUTER PROGRAM

The CARES/LIFE program is an extension of the CARES (Ceramics Analysis and Reliability Evaluation of Structures) computer program that predicts the fast-fracture reliability of monolithic ceramic components under thermomechanical loads (Nemeth, Manderscheid and Gyekenyesi (1990), and Powers, Starlinger and Gyekenyesi (1992)). CARES/LIFE predicts the probability of failure of a component versus its service life for the SCG failure mechanism. SCG operates on the pre-existing flaws in the material and therefore requires using fast-fracture statistical theories as a basis to predict the time-dependent reliability. CARES/LIFE is coupled to widely used commercial finite element analysis programs and is a public domain program.

Ceramics Analysis and Reliability Evaluation of Structures
## LIFE Prediction Integrated Design Program

- Predicts the probability of a monolithic ceramic component's failure versus its service life

- CARES/LIFE couples commercially available finite element programs to probabilistic design methodologies

Figure 8

CARES/LIFE DESIGN PROCEDURE

The first step of a probabilistic design methodology is the determination of a temperature-dependent and time-dependent fracture strength distribution from flexural or tensile test specimens. CARES/LIFE will estimate the fatigue and statistical parameters from the rupture data of nominally identical specimens. Typically this involves small specimens of simple geometry loaded in uniaxial flexure or tension. The specimens are usually cut from the component. Using these parameters the reliability of the component is calculated by integrating the stress distribution throughout the volume and area of the component. The stresses throughout the component are obtained from finite element analysis. Appropriate changes to the component geometry and imposed loads are made until an acceptable failure probability is achieved.

- **CERAMICS ARE BRITTLE AND HAVE MANY FLAWS**
- **RANDOM FLAW SIZE AND ORIENTATION REQUIRE PROBABILISTIC METHOD**
- **APPROACH:**

UNIAXIAL TENSILE STRENGTH

4-POINT BENDING

SIMPLE TESTS   **COMPLEX PREDICTIONS**
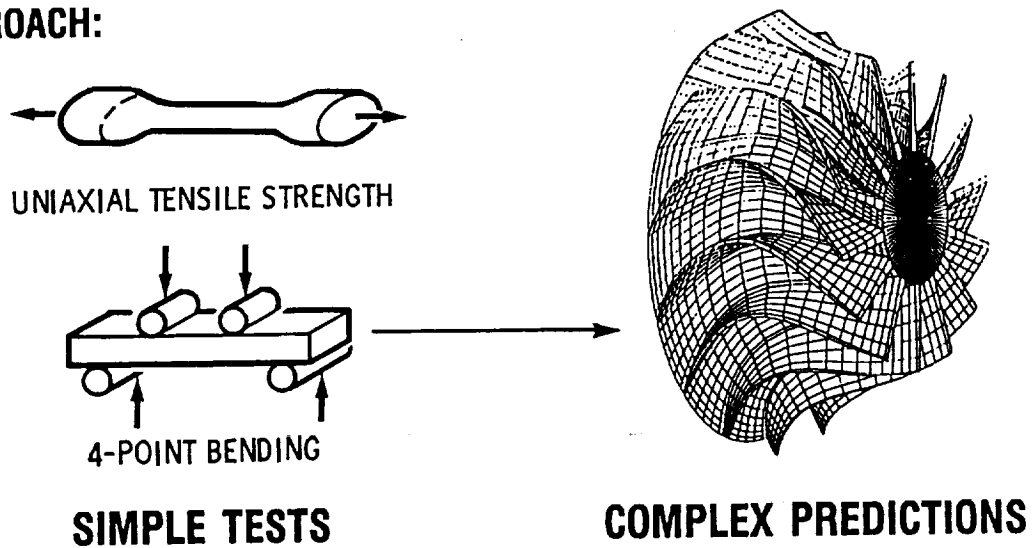
- **REQUIRES ENTIRE STRESS FIELD, NOT MAXIMUM STRESS POINT**

Figure 9

PROGRAM CAPABILITY - COMPONENT RELIABILITY EVALUATION

CARES/LIFE computes component reliability due to fast-fracture and subcritical crack growth. The SCG failure mechanism is load-induced over time. It can also be a function of chemical reaction with the environment, debris wedging near the crack tip, the progressive deterioration of bridging ligaments, etc. Because of this complexity, the models that have been developed tend to be semi-empirical and approximate the phenomenological behavior of subcritical crack growth. The CARES/LIFE code contains modeling to account for static, dynamic and cyclic loads. Component reliability can be predicted for static (nonvarying over time) and monotonic cyclic loads. In addition, for static loading, the effects of proof testing the component prior to service can be computed.

The CARES/LIFE Computer Program

● Component Reliability Evaluation

- Fast-fracture

- Time-dependent subcritical crack growth

   a) Static Fatigue
   b) Cyclic Fatigue

- Proof-testing

- Multiaxial stress states, volume flaws and surface flaws

Figure 10

CARES/LIFE incorporates proof testing methodology into the PIA, Weibull normal stress averaging, and Batdorf theories. The proof test and service loads are assumed static. The duration of the proof test and service loads are considered in the analysis. The proof test and service loads are not required to be identical. With the Batdorf theory, the two loads are allowed to be misaligned or to represent different multiaxial stress states applied in different directions. The proof test and service statistical and fatigue parameters may also be different from one another.

CARES/LIFE Proof Testing Design Methodology

- Proof test models developed for PIA and Batdorf theories

  - time-dependent

  - proof test loads need not duplicate service loads

  - off-axis (misaligned) and multiaxial loads allowed with Batdorf theory

Figure 11

In practice it is often difficult, expensive or impossible for the proof test to exactly duplicate the service condition on the component. CARES/LIFE can analyze this situation where the two loading conditions are different using two finite element analysis results files representing the stress and temperature distribution of the proof test and service condition, respectively. A typical application of this technology is predicting the attenuated reliability distribution of a turbine rotor that was proof tested with a rotational load at ambient conditions and subsequently placed into service in the hot section of a heat engine.

CARES/LIFE Can Predict Reliability When Proof Testing Does Not Duplicate The Stresses in Service
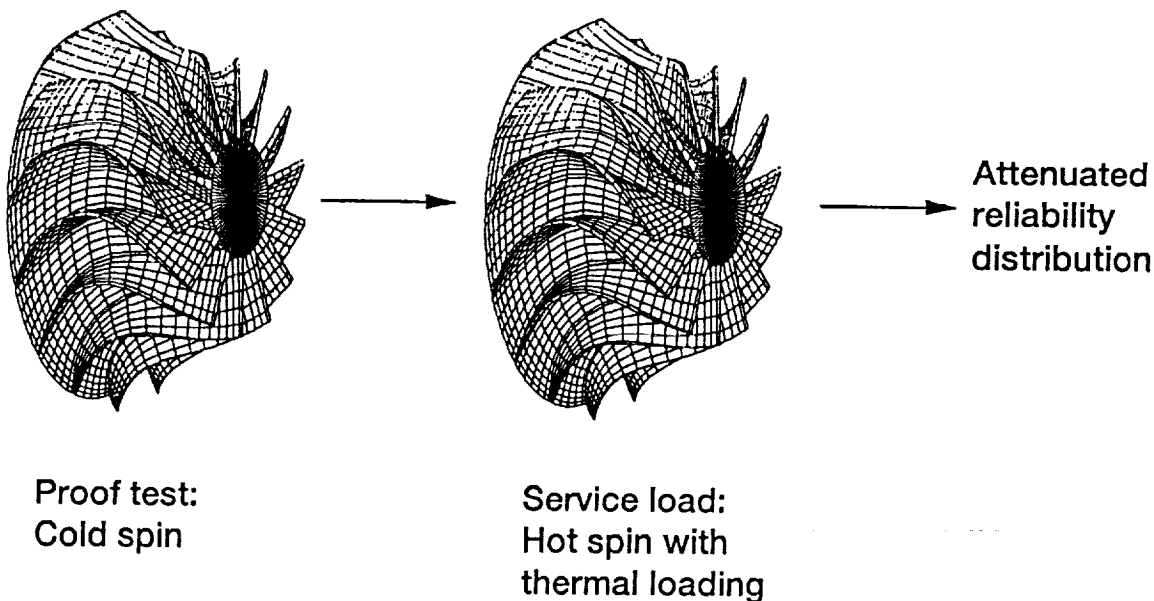
Practical
application:

Proof test:
Cold spin

Service load:
Hot spin with
thermal loading

Attenuated
reliability
distribution

Figure 12

CARES/LIFE estimates statistical and fatigue parameters from naturally flawed specimens. These parameters must be determined under conditions representative of the service environment. When determining the fatigue parameters from rupture data of naturally flawed specimens, the statistical effects of the flaw distribution must be considered along with the strength degradation effects of subcritical crack growth. CARES/LIFE is developed on the basis that fatigue parameters are most accurately obtained from naturally flawed specimens. Batdorf and Weibull statistical material parameters are obtained from fast-fracture of nominally identical specimens under isothermal conditions. Typically, these are 3- or 4-point bend bar specimens or uniaxial tensile specimens. Fatigue parameters are also measured from these same specimen geometries. CARES/LIFE can measure fatigue parameters from static fatigue, dynamic fatigue, and cyclic fatigue experiments. In addition, information regarding the statistical distribution of the flaw population is optionally obtained from the fatigue data.

The CARES/LIFE Computer Program

- Material parameter estimation from naturally flawed specimens

    - Weibull and Batdorf statistical material parameters

    - Fatigue parameters

        a) Static
        b) Dynamic (constant stress rate)
        c) Cyclic

Figure 13

CARES/LIFE has three techniques available for estimating fatigue parameters. The median value technique is based on regression of the median data points for the various discrete load levels or stress rates. The least squares technique is based on least squares regression on all the individual data points. The modified trivariant technique is based on the minimization of the median deviation of the distribution (the trivariant technique is discussed in Jakus, Coyne and Ritter (1978)). The median value technique is the least powerful estimator of the three choices; it is included in CARES/LIFE because it is a commonly used procedure.

Evaluation of Time Dependent Parameters

- ## Estimation methods to obtain fatigue parameters

    - median value

    - least squares

    - modified trivariant

Figure 14

PROGRAM STRUCTURE

CARES/LIFE is coupled to widely used finite element analysis programs such as ABAQUS and MSC/NASTRAN. An interface code to ANSYS is being prepared. CARES/LIFE is structured into separately executable modules. These modules create a neutral file database from finite element analysis results, estimate statistical and fatigue parameters, and evaluate component reliability. CARES/LIFE uses a subelement technique to improve the accuracy of the reliability solution. The subelement technique computes reliability at the element Gaussian integration points. CARES/LIFE creates a PATRAN compatible file containing risk-of-rupture intensities (a local measure of reliability) for graphical rendering of critical regions of a component.

CARES/LIFE Program Features

- ● Finite element interface program

    - - Completed for MSC/NASTRAN and ABAQUS

    - - Work in progress for ANSYS

- ● Reliability evaluation program

    - - Modular structure

    - - Subelement technique

    - - Postprocessor interface (PATRAN)

Figure 15

PIA FRACTURE THEORY

Subcritical crack growth modeling is incorporated into the PIA and Batdorf theories. The PIA theory operates on the principal stresses throughout the component. CARES/LIFE includes both the semi-empirical power law (Evans and Wiederhorn (1974)), (Wiederhorn (1974)), and the Paris Law (Paris and Erdogan (1963)), (Dauskardt, Marshall and Ritchie (1990)), (Dauskardt, et al (1992)) to describe the SCG phenomenon. The power law describes the crack growth as a function of time, t, and implies that the crack growth is due to stress corrosion. The Paris law describes the crack growth as a function of the number of load cycles, n, and implies that the fatigue is a mechanical damage process. Both models require two material/environmental fatigue parameters, N and B, that describe the strength degradation. N is the fatigue crack growth exponent and B is the fatigue constant. The degree of scatter of the fracture strengths is characterized by the Weibull modulus, m. The Weibull scale parameter, σ_o, represents a unit volume (or area) strength where 63 percent of specimens fail. Integration is performed over the volume, V (or area A) of the component. σ_i is a given principal stress component. For cyclic loading, the maximum and minimum cycle stresses, represented by the subscripts max and min, respectively, are used. For the power law, a constant called the g-factor (Mencik (1984)) can be computed such that cyclic loading can be expressed as an equivalent static load over a period, T. The fatigue constant, B, is a function of the mode I stress intensity factor, K_{Ic}, the fatigue exponent, N, the crack geometry factor, Y, and the experimentally determined material/environmental constant, A.

Component Reliability Prediction (PIA Model)

(Based on Principal Stress Distribution)

$$P_{fv}(t_f) = 1 - \exp\left[-\int_v \sum_{i=1}^{3} \left(\frac{\sigma_{i,0}(x,y,z)}{\sigma_{ov}} \right)^{m_v} dV \right]$$

Power Law :

$$\sigma_{i,0}(x,y,z) = \sigma_i \left(1 + \frac{\sigma_i^2 \, g \, t_f}{B} \right)^{\frac{1}{N-2}}$$

equivalent static time $= g \, t_f$

$$g = \frac{1}{T} \int_0^T \left(\frac{\sigma(t)}{\sigma_{max}} \right)^N dt$$

$$B = \frac{2}{A \, Y^2 \, (N-2) \, K_{IC}^{N-2}}$$

Paris Law:

$$\sigma_{i,0}(x,y,z) = \sigma_{i,max} \left(1 + \frac{\sigma_{i,max}^2 \, (1-R)^N \, n_f}{B} \right)$$

$$R = \frac{\sigma_{i,min}}{\sigma_{i,max}}$$

$$B = \frac{2}{A \, Y^2 \, (N-2) \, K_{IC}^{N-2}}$$

Figure 16

With the Batdorf theory fracture depends not only on the existence of a crack with a certain critical strength, but also on the crack shape, the far-field stress state, and the crack orientation described by the azimuthal angles α and β. A collection of random crack orientations can be described by a sphere of unit radius for volume-distributed flaws (analogously, a unit radius circle describes a collection of surface flaws). For a given flaw orientation, an effective stress, σ_e, which is a function of crack geometry, mixed-mode fracture criterion, and the far-field stress state, describes the equivalent mode I stress intensity factor on the crack. Fracture occurs when the equivalent mode I stress intensity factor exceeds the critical stress intensity factor of the crack.

Component Reliability Prediction (Batdorf)

- Requires integration of the
  projected equivalent stress
  over a unit radius sphere
  (all possible flaw orientations)

$$dA = \sin \alpha d\alpha d\beta$$
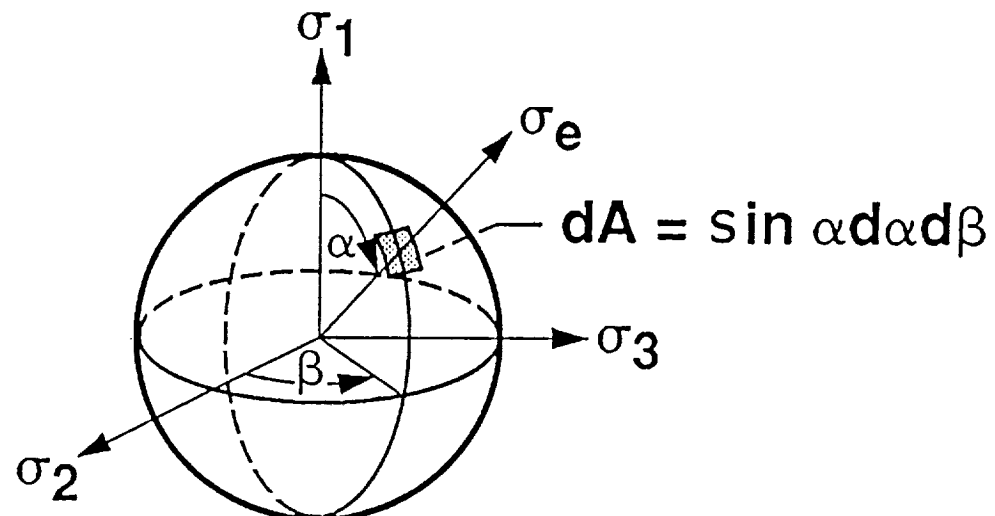
Figure 17

BATDORF FRACTURE THEORY

The Batdorf theory combines LEFM with the weakest link mechanism to achieve a mechanistic description of the rupture process. Fracture is described as a process of crack growth from randomly oriented pre-existing flaws. CARES/LIFE models SCG with the Batdorf methodology by incorporating the power law and the Paris law to account for material degradation from stress corrosion and mechanical effects such as microcracking, degeneration of bridging ligaments, and debris wedging.

Component Reliability Prediction (Batdorf Model)

$$P_{fv}(t_f) = 1 - \exp\left[-\frac{2}{\pi} \bar{k}_{Bv} \int_V \int_0^{\frac{\pi}{2}} \int_0^{\frac{\pi}{2}} \left(\frac{\sigma_{e,0}(\Psi)}{\sigma_{ov}}\right)^{m_v} \sin\alpha \; d\alpha \; d\beta \; dV\right]$$

Power law:

$$\sigma_{e,0}(\Psi) = \sigma_e(\Psi)\left(1 + \frac{\sigma_e^2(\Psi) \; g \; t_f}{B}\right)^{\frac{1}{N-2}}$$

Paris law:

$$\sigma_{e,0}(\Psi) = \sigma_e(\Psi)\left(1 + \frac{\sigma_{e,max}(1-R)^N \, n}{B}\right)^{\frac{1}{N-2}}$$

$$R = \frac{\sigma_{e,min}}{\sigma_{e,max}}$$

σ_e is a function of the mixed-mode fracture criteria and crack configuration

Ψ is a function of (x,y,z,α,β)

Figure 18

EXAMPLE PROBLEM - FATIGUE PARAMETER EVALUATION

Two example problems have been selected to demonstrate various features of the CARES/LIFE code:
(1) estimation of fatigue parameters from multiaxially stressed specimens, and (2) examination of the effect
of misalignment between a uniaxial proof test load and a uniaxial service load. In the first example, the
fatigue and statistical parameters are estimated using rupture data from 121 ring-on-ring loaded square
plate specimens made of soda-lime glass. The specimens were fractured under dynamic fatigue load
conditions in a distilled water environment. In addition, the fast-fracture strengths of 30- specimens were
measured in an inert environment of silicon oil.

Evaluation of Time-Dependent Parameters

EXAMPLE: Ring-On-Ring Loaded Square Plate Specimen
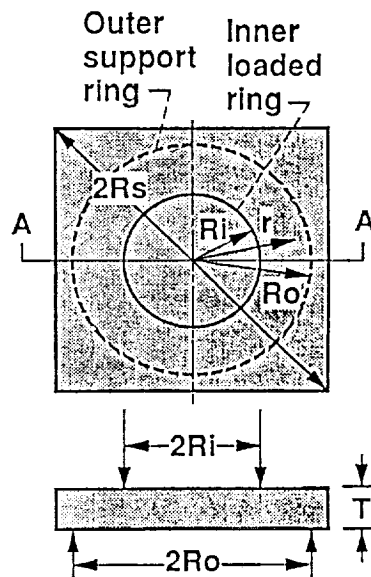
EXPERIMENT: Dynamic fatigue testing in water environment .

MATERIAL: Soda-Lime-Silica Glass

DIMENSIONS: R_i = 5.02 mm
R_o = 16.09 mm
R_s = 35.92 mm
1.42 mm $\leq$ T $\leq$ 1.58 mm

Figure 19

EXAMPLE PROBLEM - FATIGUE PARAMETER EVALUATION

This figure shows the fracture strengths, σ_f, of the 121 soda-lime glass specimens loaded at various stressing rates, $\dot{\sigma}$, and the fast-fracture strengths of the 30 specimens measured in a chemically inert environment of silicon oil. The maximum fracture stress occurs at the center of the specimen. All failures occurred at the specimen surface (surface flaws).
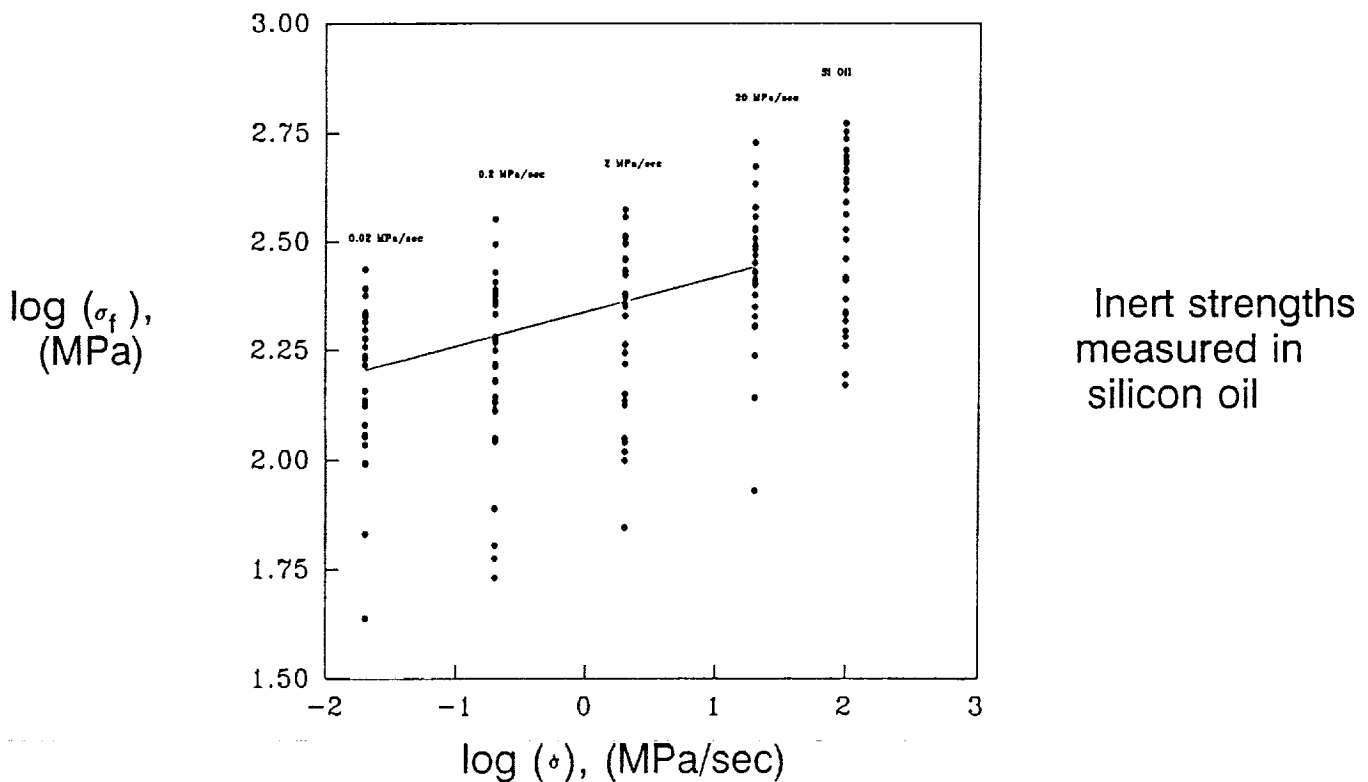
Figure 20

The median failure stress of the specimens versus the stress rate can be linearized by plotting the log of the median strength σ_f versus the log of the stress rate $\dot{\sigma}$. The slope of the line establishes the fatigue constant, N, and the intercept of the line, A_d, is used to determine the fatigue constant, B. Evaluation of the stress-area integral, A_{ef} (or the stress volume integral V_{ef} for volume flaws) is also required for the calculation of B. CARES/LIFE employs the various regression techniques previously mentioned to estimate these parameters.

Evaluation of Time-Dependent Parameters: Power Law

Variable stress rate
(dynamic fatigue)

$$\sigma_f = A_d \, \dot{\sigma}^{1/N + 1}$$
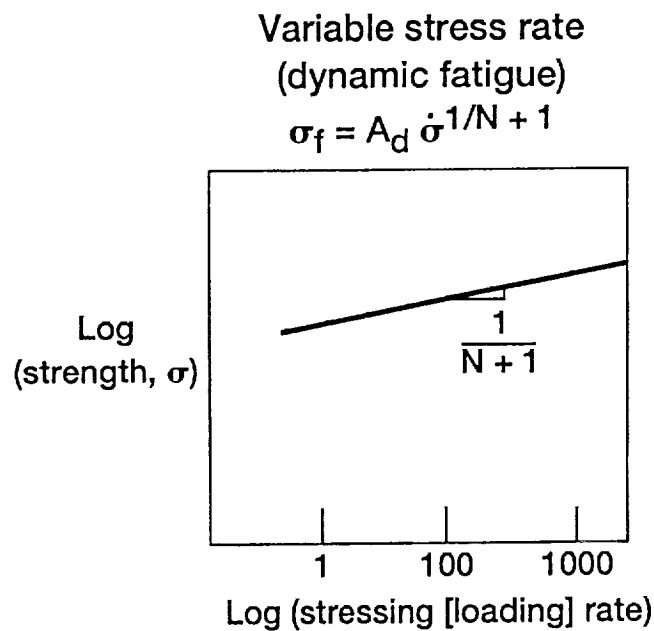
Figure 21

$$B = \frac{A_d^{N+1}}{(N+1)\sigma_{oV}^{N-2}} \left[\frac{V_{ef}}{\ell n \left(\frac{1}{1-P_{fV}} \right)} \right]^{1/m_V^{\cdot}}$$

EXAMPLE PROBLEM - FATIGUE PARAMETER EVALUATION

CARES/LIFE measures the intrinsic scatter in the fatigue data. The Weibull modulus, m, and a characteristic strength, σ_θ, representing a level of strength where 63 percent of specimens fail are estimated from the fatigue data. In this case, the characteristic strength is determined for a time to failure of one second. With these parameters the fatigue data can be transformed to an equivalent fast-fracture strength distribution. The following Weibull plot shows the ranked data failure probability versus the fast-fracture strength. The fast-fracture strengths that were measured in silicon oil are shown for comparison. As can be observed, the Weibull slope of the fatigue data derived strengths correlate well with the Weibull slope of the fast-fracture strengths measured in silicon oil.

Comparison of Inert Strengths Determined from Fatigue Data Measured in Water
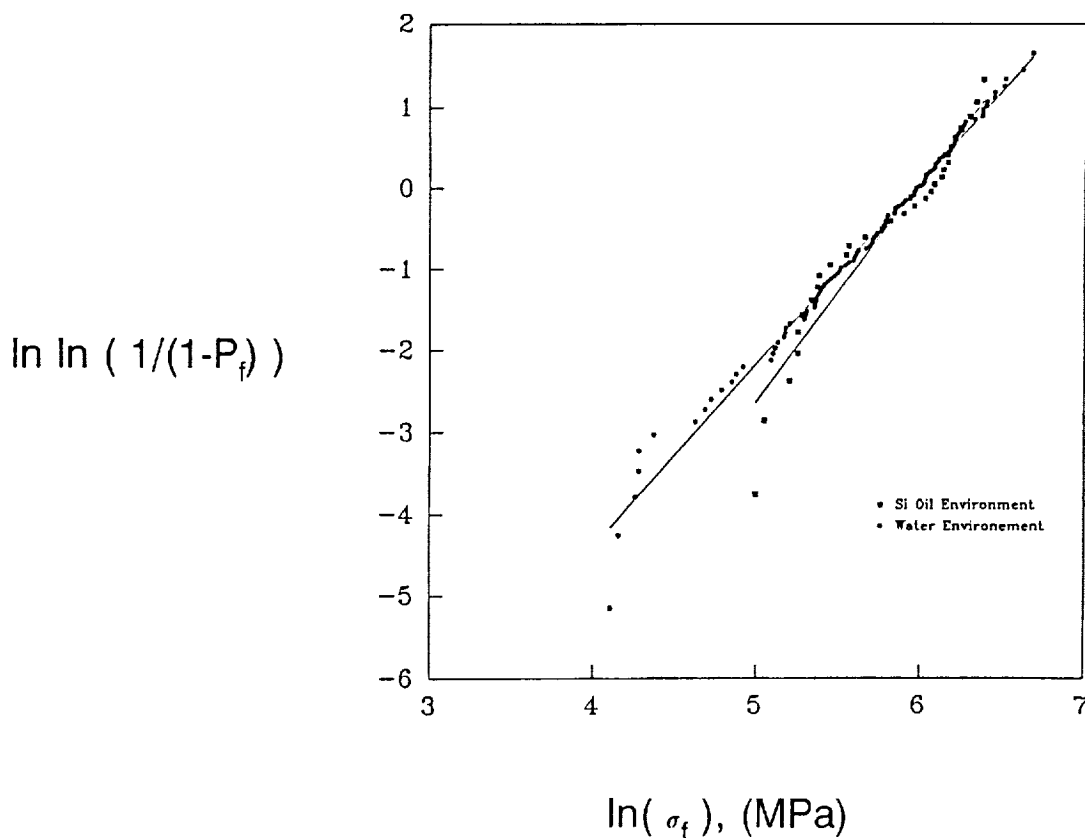## to Inert Strengths Measured in Silicon Oil

Figure 22

EXAMPLE PROBLEM - PARAMETER EVALUATION

The fatigue parameters for the soda-lime glass are estimated using the median value, least squares, and the modified trivariant techniques. For this table all parameters are obtained solely from the fatigue data. The fatigue constant B uses the subscript B to indicate that the value was obtained using the Batdorf technique.

Parameters Estimated From Soda-Lime Glass Fatigue Data

Method	Fatigue exponent, N_S	Fatigue constant, B_{BS}, $MPa^2 \cdot s$	Weibull modulus, m'_S	Scale parameter, σ'_{oS}, $MPa \cdot mm^{2/m_S}$
Median value	12.60	4 445	2.279	5 904
Least squares	11.24	6 337	2.208	6 707
Modified trivariant	11.88	5 982	2.344	5 443

Figure 23

EXAMPLE PROBLEM - PLOTTING CRITICAL REGIONS OF FAILURE

CARES/LIFE outputs the risk-of-rupture intensities of the elements into a data file formatted such that it can be read by PATRAN. The risk-of-rupture intensity is a volume or area independent measure of the potential of failure. This information enables a component to be graphically rendered such that regions on the component where failure is most likely to occur are shown. This example shows the ring-on-ring square plate specimen where the biaxially loaded central portion of the specimen shows the highest likelihood of failure.

Finite Element Model of Ring-On-Ring Specimen (1/4 Symmetry)
Risk-of-Rupture Intensities
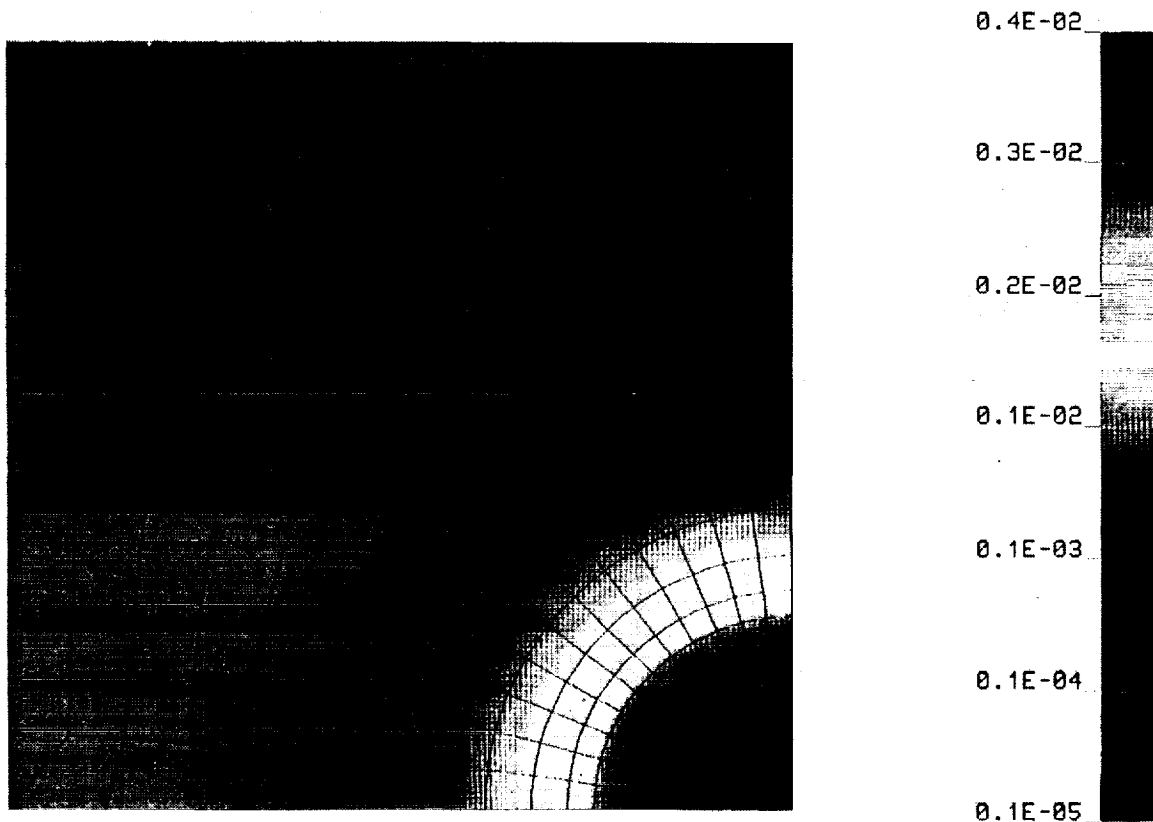
Figure 24

Proof testing screens out weak components so that the remaining components are less likely to fail in service. This attenuated failure probability, P_{fa}, is a function of the component failure probability, P_{fp}, from the proof test and the component probability of failure, P_{fi}, from the combined application of the proof test and the service load. P_{fp} is computed from the proof stress, σ_p, applied over time interval, t_p. P_{fi} is computed from the combined application of the proof stress, σ_p, over time t_p and the service stress, σ_i, applied over time, t_q. The attenuated failure probability displays a threshold stress, σ_u, and a threshold time, t_{min}, where the failure probability is zero.

Proof Testing at 650 MPa (94ksi) Truncates The Weibull Strength Distribution For Hot Pressed Silicon Nitride and Eliminates Low-Strength Specimens
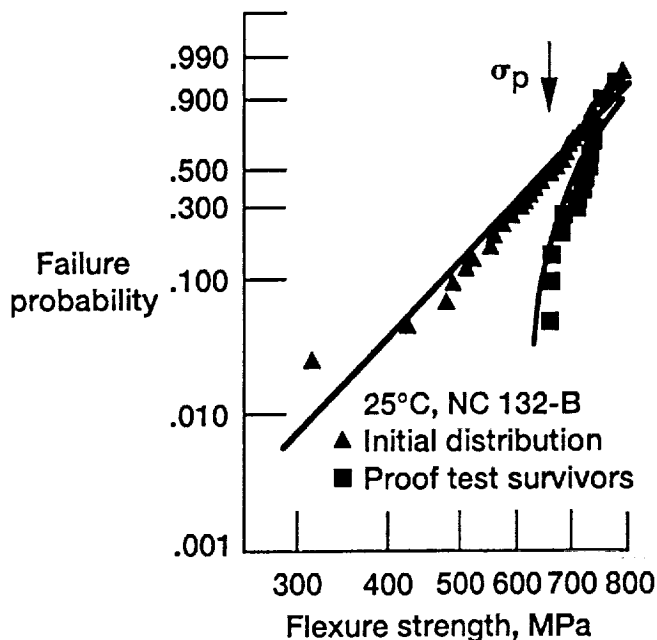
Attenuated failure probability:

$$P_{fa} = \frac{P_{fi} - P_{fp}}{1 - P_{fp}}$$

Attenuated reliability:

$$P_{sa} = \frac{P_{si}}{P_{sp}} = \exp[-(B_i - B_p)]$$

i = initial distribution
p = proof test

Figure 25

EXAMPLE PROBLEM - PROOF TESTING WITH MISALIGNED LOADS

Ideally the proof test loading exactly duplicates the service loading except that the proof load is greater in magnitude than the service load. In this example the effect of misalignment between a uniaxial proof test and a uniaxial service load is explored using the Batdorf technique with a shear sensitive and shear insensitive fracture criterion. The proof test is such that 50 percent of the components break prior to placing them in service. The failure probability is given per unit volume of material.

CARES/LIFE Proof Testing Design Methodology

EXAMPLE: Effect of misalignment between uniaxial proof test and service load

- Magnitude of proof test load, σ_p, eliminates 1 of every 2 components

Weibull parameters: $m_v = 15.0$, $\sigma_{ov} = 1000.$ Mpa $mm^{3/10}$

Fatigue parameters: $N = 40.0$, $B_w = 2000.$ MPa^2 second

Misalignment Between Proof Test and Service
Loading Effects Failure Probability
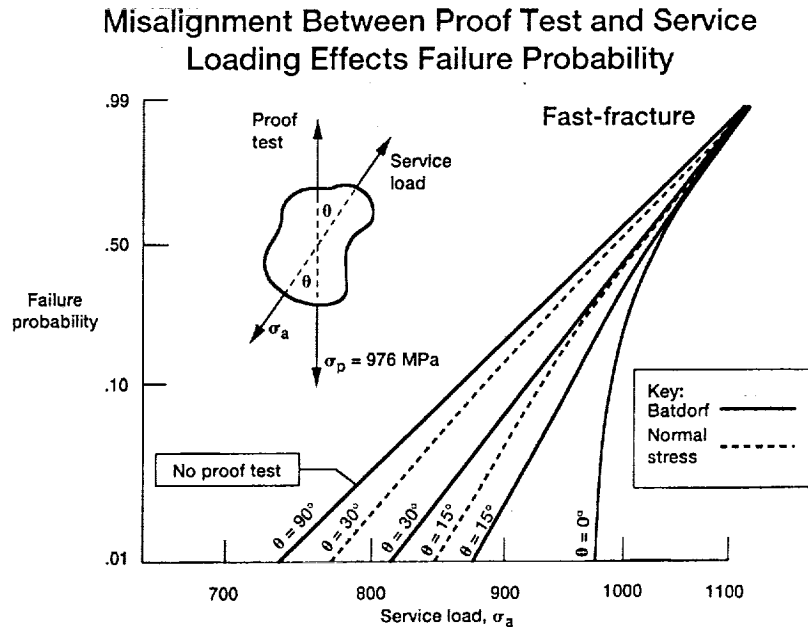
Figures 26

EXAMPLE PROBLEM - PROOF TESTING WITH MISALIGNED LOADS

For fast-fracture the effect of misalignment between the proof test and service load as a function of the angle of misalignment and the magnitude of the service load is shown. For aligned loads the classical truncated distribution is observed with threshold stress behavior. As misalignment increases, the failure distribution approaches the unattenuated (the original) distribution shown by the straight line. The effect of the fracture criterion is shown with the solid line indicating the coplanar strain energy release criteria with a Griffith crack and the dotted line showing a shear insensitive crack criteria. The effect of misalignment is more severe for a shear insensitive criteria. These same trends are observed with time-dependent loading.

Misalignment Between Proof Test and Service Loading Effects Failure Probabilty
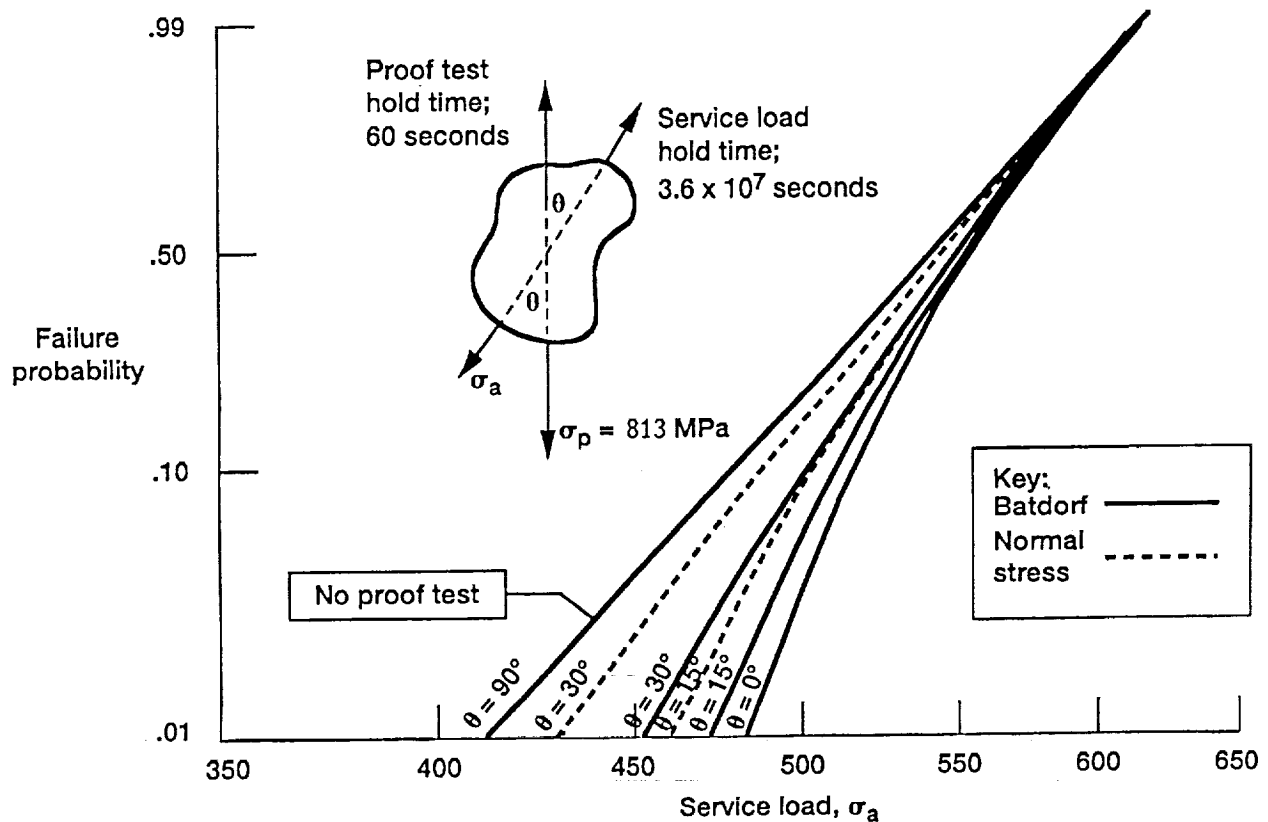
Figure 27

SUMMARY

The use of structural ceramics for high-temperature applications depends on the strength, toughness and reliability of these materials. Ceramic components can be designed for service if the factors that cause material failure are accounted for. This design methodology must combine the statistical nature of strength controlling flaws with fracture mechanics to allow for multiaxial stress states, concurrent flaw populations, and subcritical crack growth. This has been accomplished with the CARES/LIFE public domain computer program for predicting the time-dependent reliability of monolithic structural ceramic components. Potential enhancements to the code include the capability for transient analysis, three-parameter Weibull statistics, creep and oxidation modeling, flaw anisotropy, threshold stress behavior, and parameter regression for multiple specimen sizes.

- Power law and Paris law have been incorporated into the Batdorf and PIA reliability models

- Component reliability can be predicted for static, cyclic and proof test loadings

- Fatigue parameters and Weibull parameters can be estimated from static, dynamic and cyclic loading experiments on naturally flawed specimens

Figure 28

268

REFERENCES

Barnett, R. L., Connors, C. L., Hermann, P. C., and Wingfield, J. R., *Fracture of Brittle Materials Under Transient Mechanical and Thermal Loading*, U.S. Air Force Flight Dynamics Laboratory, AFFDL-TR-66-220, 1967 (NTIS AD-649978).

Batdorf, S. B. and Crose, J. G., "A Statistical Theory for the Fracture of Brittle Structures Subjected to Nonuniform Polyaxial Stresses," *Journal of Applied Mechanics*, Vol. 41, No. 2, June 1974, pp. 459-464.

Batdorf, S. B. and Heinisch, H. L., Jr., "Weakest Link Theory Reformulated for Arbitrary Fracture Criterion," *Journal of the American Ceramic Society*, Vol. 61, Nos. 7-8, 1978, pp. 355-358.

Dauskardt, R. H., Marshall, D. B. and Ritchie, R. O., "Cyclic Fatigue Crack Propagation in Mg-PSZ Ceramic," *Journal of the American Ceramic Society*, Vol. 73, No. 4, 1990, pp. 893-903.

Dauskardt, R. H., James, M. R., Porter, J. R. and Ritchie, R. O., "Cyclic Fatigue Crack Growth in SiC-Whisker-Reinforced Alumina Ceramic Composite: Long and Small Crack Behavior," *Journal of the American Ceramic Society*, Vol. 75, No. 4, 1992, pp. 759-771.

Evans, A. G. and Wiederhorn, S. M., "Crack Propagation and Failure Prediction in Silicon Nitride at Elevated Temperatures," *Journal of Material Science*, Vol. 9, 1974, pp. 270-278.

Freudenthal, A. M., "Statistical Approach to Brittle Fracture," *Fracture, Vol. 2: An Advanced Treatise, Mathematical Fundamentals*, H. Liebowitz (ed.), Academic Press, 1968, pp. 591-619.

Jakus, K., Coyne, D. C. and Ritter, J. E., "Analysis of Fatigue Data for Lifetime Predictions for Ceramic Materials," *Journal of Material Science*, Vol. 13, 1978, pp. 2071-2080.

Mencik, J., "Rationalized Load and Lifetime of Brittle Materials," *Communications of the American Ceramic Society*, March 1984, pp. C37-C40.

Nemeth, N. N., Manderscheid, J. M. and Gyekenyesi, J. P., *Ceramic Analysis and Reliability Evaluation of Structures (CARES)*, NASA TP-2916, August 1990.

Paris, P. and Erdogan, F., "A Critical Analysis of Crack Propagation Laws," *Journal of Basic Engineering*, Vol. 85, 1963, pp. 528-534.

Powers, L. M., Starlinger, A. and Gyekenyesi, J. P., *Ceramic Component Reliability with the Restructured NASA/CARES Computer Program*, NASA TM-105856, Sept. 1992.

Weibull, W. A., "A Statistical Theory of the Strength of Materials," *Ingenoirs Vetenskaps Akadanien Handlinger*, 1939, No. 153.

Weibull, W. A., "The Phenomenon of Rupture in Solids," *Ingenoirs Vetenskaps Akadanien Handlinger*, 1939, No. 153.

Wiederhorn, S. M., *Fracture Mechanics of Ceramics*, R. C. Bradt, Hasselman, D. P. and F. F. Lange (eds.), Plenum, NY, 1974, pp. 613-646.

PAGE_____ INTENTIONALLY BLANK

A High Temperature Fatigue Life Prediction Computer Code Based on the Total Strain Version of Strainrange Partitioning (SRP)

Michael A. McGaw and James F. Saltsman
NASA Lewis Research Center
Cleveland, OH

PAGE _____ INTENTIONALLY BLANK

A recently developed high-temperature fatigue life prediction computer code is presented and an example of its usage given. The code discussed is based on the Total Strain version of Strainrange Partitioning (TS-SRP). Included in this code are procedures for characterizing the creep-fatigue durability behavior of an alloy according to TS-SRP guidelines and predicting cyclic life for complex cycle types for both isothermal and thermomechanical conditions. A reasonably extensive materials properties database is included with the code.

OVERVIEW

While several computer codes have been developed and are in use for the treatment of fatigue of structural metals and alloys that operate at sub-creep temperatures, the treatment of high temperature fatigue has not shared this level of development and availability for a number of reasons. The number of high temperature applications is certainly far fewer in number and the level of development of the life prediction models is not as great. This is due to the additional complexities of material behavior above the sub-creep range, since additional damage and deformation mechanisms may become operative. The need to adequately represent material deformation behavior in order that reasonable life prediction calculations may be performed has also proved to be a significant impediment in enabling the general use of high temperature durability prediction methods as well.

- ## SRP & TS-SRP Life Prediction Approaches

- ## Code Modules Supporting TS-SRP

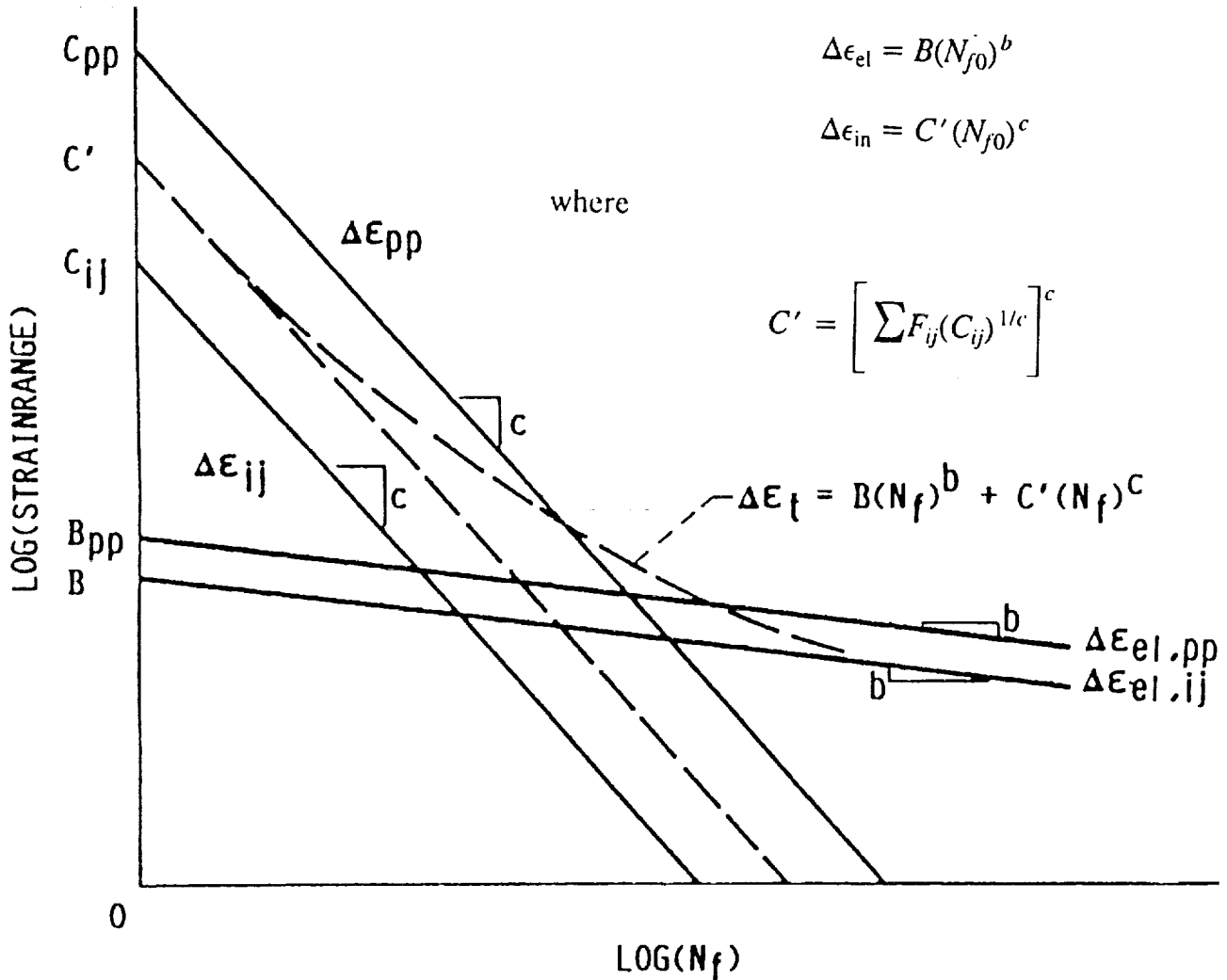- ## Overall Code Organization

- ## Summary

STRAINRANGE PARTITIONING

This paper describes a suite of computer programs that collectively implement the total strain range version of Strainrange Partitioning. Strainrange Partitioning, or SRP, was formulated on an inelastic strainrange basis, wherein the cyclic life is a function of the type and magnitude of the inelastic strainrange at a specific temperature. This approach has worked well in the high-strain, short life regime for which the inelastic strains are large enough to be determined accurately by analytical or experimental means.

$$\Delta\varepsilon_{pp} = A_1 (N_{pp})^{a_1}$$

$$\Delta\varepsilon_{cp} = A_2 (N_{cp})^{a_2}$$

$$\Delta\varepsilon_{pc} = A_3 (N_{pc})^{a_3}$$

$$\Delta\varepsilon_{cc} = A_4 (N_{cc})^{a_4}$$

$$\frac{1}{N_f} = \frac{F_{pp}}{N_{pp}} + \frac{F_{cp}}{N_{cp}} + \frac{F_{pc}}{N_{pc}} + \frac{F_{cc}}{N_{cc}}$$
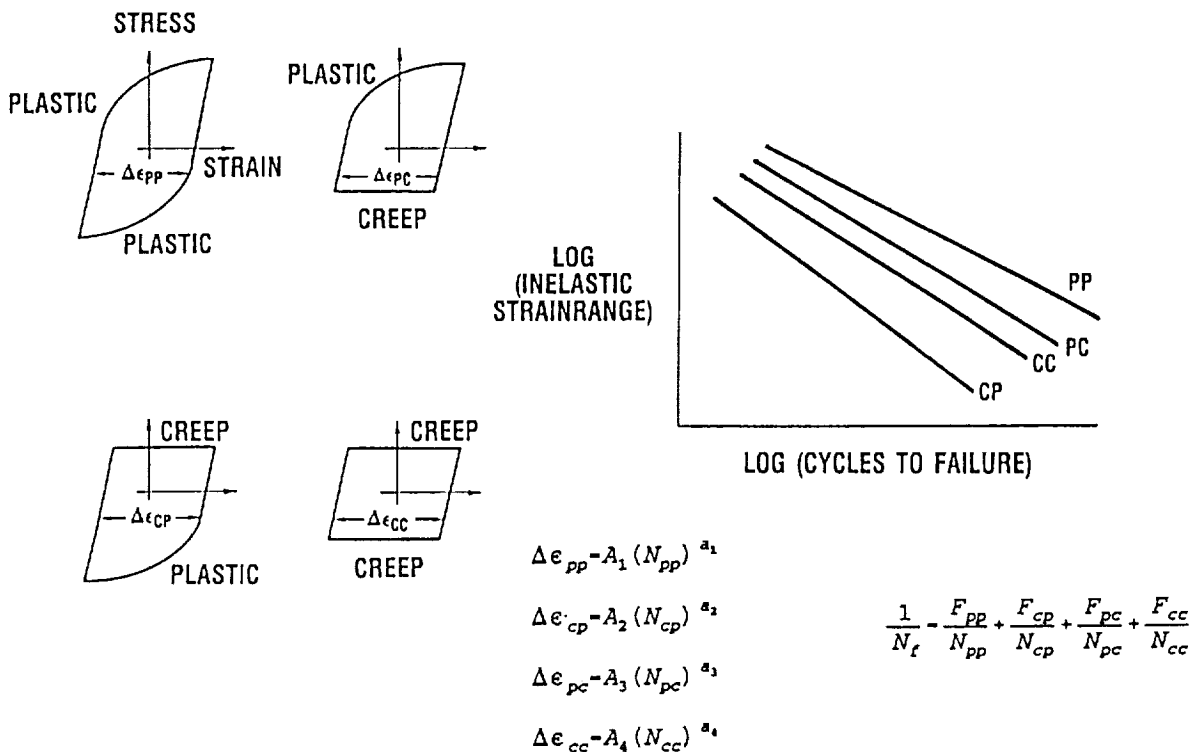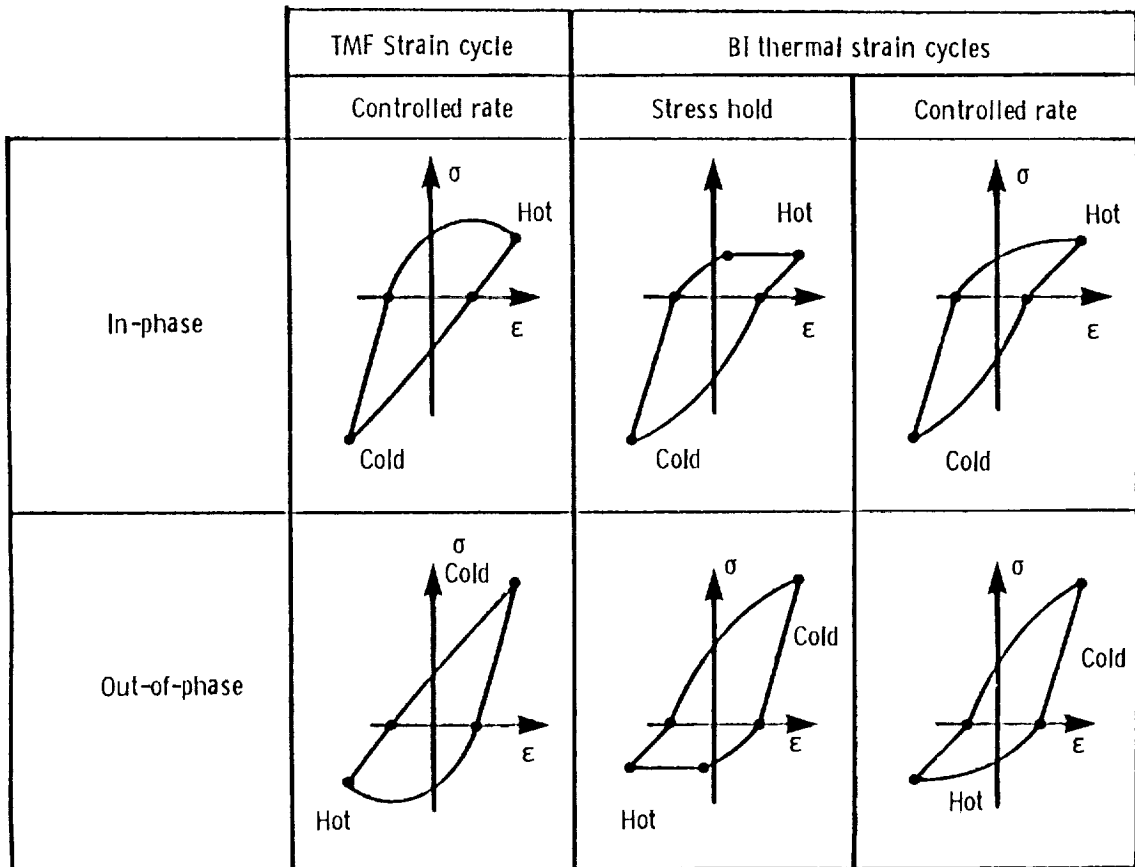
TS-SRP BASIS

In order to extend the SRP approach to address the lower-strainrange, longer-life regime, where the inelastic strains are small and difficult to determine, it was necessary to consider the total strainrange rather than just the inelastic strainrange. The method subsequently developed was termed TS-SRP, for the total strain version of Strainrange Partitioning. The computer program suite described in this paper has been developed to support the characterization of engineering alloys and prediction of cyclic life in the high temperature, long-life regime for isothermal and nonisothermal fatigue conditions using the TS-SRP life prediction methodology.

$$\Delta\epsilon_{el} = B(N_{f0})^b$$

$$\Delta\epsilon_{in} = C'(N_{f0})^c$$

where

$$C' = \left[\sum F_{ij}(C_{ij})^{1/c}\right]^c$$

$$\Delta\epsilon_t = B(N_f)^b + C'(N_f)^c$$

BITHERMAL APPROXIMATION FOR THERMOMECHANICAL FATIGUE

The application of the SRP approach to Thermomechanical Fatigue (TMF) is done through the use of the bithermal fatigue approximation to TMF. The bithermal approach has been utilized in extending the total strain version of SRP to encompass TMF, but addresses the uniform loading case. In the bithermal approach, the thermomechanical cycle (in-phase or out-of-phase) is approximated by a cycle in which the tensile portion of the loading is conducted isothermally at one temperature, while the compressive portion of the loading is performed isothermally at another temperature. The advantages of this approach include: 1) the testing requirements of bithermal fatigue are much simpler than those of TMF, 2) isothermal behavior may be related to bithermal behavior provided no new mechanisms of deformation and damage are introduced by the change of temperature, and 3) the micromechanisms of deformation and damage in the bithermal cycle should be easier to interpret and relate to isothermal behavior due to the increased contrast offered by the discrete nature of the bithermal cycle.

|	TMF Strain cycle	Bi thermal strain cycles	
	Controlled rate	Stress hold	Controlled rate
In-phase			
Out-of-phase			

TS-SRP PROGRAM SUITE ORGANIZATION

A total of five computer programs comprise the suite that has been developed for TS-SRP; their organization is as shown.

Two codes are used to manage the input and display of material properties data: INDATA and TABLE. INDATA is used to input summary data obtained from creep-fatigue experiments into a database for use by the flow and failure analysis programs. Typically, these data consist of the alloy designation and data source, and the cyclic parameters that described the material deformation and failure behavior. The programs FAIL and FLOW will be discussed in the next two figures. The program LIFE is used to predict cyclic life using the information generated by the programs FAIL and FLOW.

This program suite has been implemented on an IBM-AT running MS-DOS v. 3.10, and equipped with a numeric coprocessor, hard drive and two floppy drives. The language processors used were IBM Advanced Basic v. 3.0 for the program LIFE, and Lahey FORTRAN-77, v. 4.0 for the FORTRAN programs. The programs have been written with an emphasis on portability, and other FORTRAN-77 compilers and Basic interpreters and/or compilers (compliant with IBM Advanced Basic) may be suitable for use as well. These programs, as well as the associated database of material properties are available through COSMIC, NASA's agent for software distribution. The diskettes contain source code, executable files and sample output, as well as a cyclic creep-fatigue database for many materials (see figure that precedes Summary page). A user's manual has been developed for this program suite and is included with the software. This manual is also available as a NASA report.
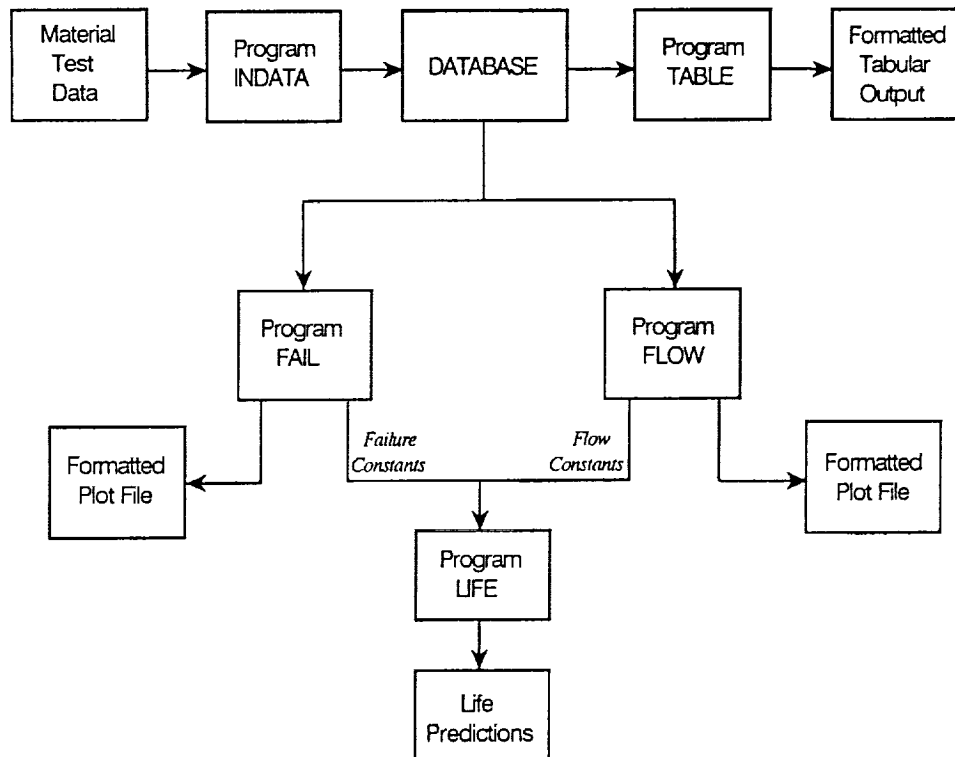
PROGRAM: FAIL

The program FAIL is used to determine the four generic SRP inelastic strainrange-life relations and the time-independent elastic strainrange-life relation for the PP cycle type. All constants in the life equations are determined through regression analysis of the appropriate data (that have presumably been entered using INDATA). The user also has the option of determining the time-dependent elastic strainrange-life relations for cycles (e.g., PC, CP and CC) with time-dependent inelastic strains. This option is typically used when the hold time per cycle is a controlled variable.

FAIL first determines the inelastic and elastic strainrange PP life relations and then proceeds to determine, in order, the PC, CP and CC strain-life relations, provided sufficiently adequate data have been previously input. As an option, the user may elect to correct data to account for mean stress effects. Upon completion of FAIL, two files are produced: the first contains the regressed constants for the SRP life relations together with the data used to make this determination.

279
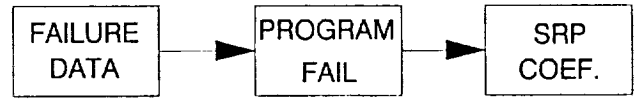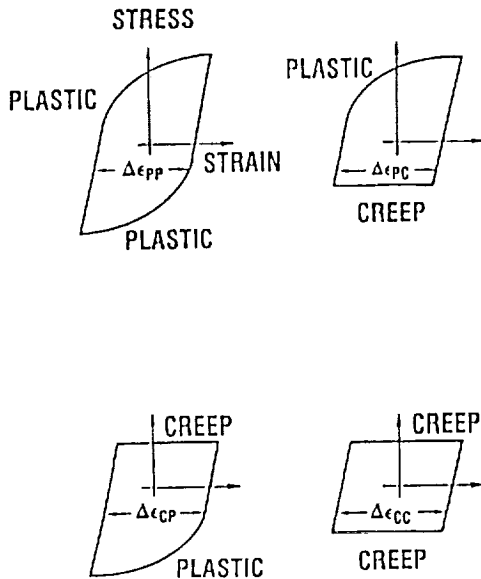
PROGRAM: FLOW

The program FLOW is used to obtain the time and waveshape dependent flow variables used to determine the constants in the flow equations, and the stress and strain values required for the mean stress correction equation. The various constants required may be determined in a number of manners, relying on a multiple regression analysis approach. Upon completion of FAIL, two files are produced: the first contains the regressed constant for the strain hardening coefficient together with the data used to make this determination, while the second contains these data in a format that is well suited for use with commercially available plotting software.
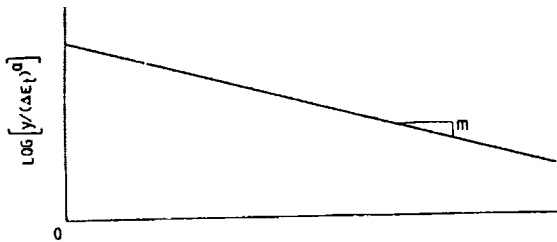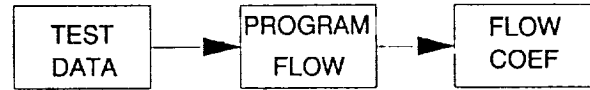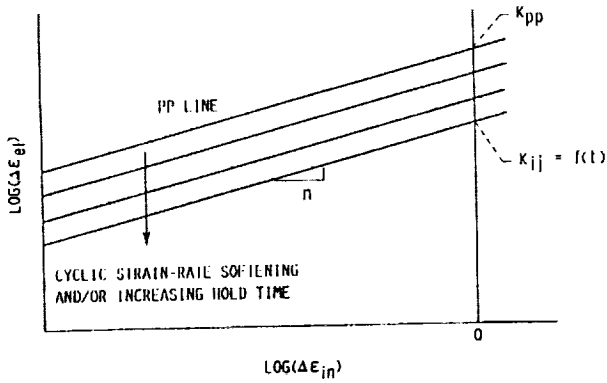
K_{ij} versus hold time
F_{ij} versus hold time
$\Big\}$ To determine B and C'

$\Delta\epsilon_{ei}$ versus hold time
$\Delta\sigma$ versus hold time
σ_c versus hold time
σ_t versus hold time
$\Big\}$ To determine mean stress correction

FORMATTED OUTPUT EXAMPLE

Once entered and verified, the data may then be printed using the program TABLE, a utility designed to provide cleanly formatted summaries of the input dataset. The figure is a sample of this output for the material AF2-1DA. Of course, the resulting database is now accessible for use in performing durability analyses using other programs in the suite.

DATE: 03/28/91

CREEP-FATIGUE DATA

LABORATORY: NASA
MATERIAL: AF2-1DA

RATE DATA & STRESSES

SPEC NO	TEST TYPE	TEMP-C TEN/COMP	RATE DATA(HALF-LIFE VALUES)					STRESSES(HALF-LIFE VALUES)					
			FREQ HZ	STRAIN-RATE-%/SEC		HOLD TIME-SEC		TEN MAX	COMP MAX	RANGE MAX	RELAXATION		
				TEN	COMP	TEN	COMP				TEN	COMP	
AF-11	HRSC	760/760	5.0E-01	2.4E-02	2.4E-02	0	0	1236.0	1336.0	2572.0	0.0	0.0	-0
AF-15	HRSC	760/760	5.0E-01	1.5E-02	1.5E-02	0	0	970.0	1021.0	1991.0	0.0	0.0	-0
AF-21	HRSC	760/760	5.0E-01	1.1E-02	1.1E-02	0	0	756.0	792.0	1548.0	0.0	0.0	-0
AF-6	HRSC	760/760	5.0E-01	1.0E-02	1.0E-02	0	0	767.0	780.0	1547.0	0.0	0.0	-0
AF-9	HRSC	760/760	5.0E-01	8.9E-03	8.9E-03	0	0	688.0	689.0	1377.0	0.0	0.0	-0
AF-33	HRSC	760/760	5.0E-01	8.2E-03	8.2E-03	0	0	674.0	676.0	1350.0	0.0	0.0	-0
AF-XX	HRLC	760/760	5.0E-01	8.4E-01	8.4E-01	0	0	689.5	689.5	1379.0	0.0	0.0	0
AF-10	HRLC	760/760	5.0E-01	8.2E-03	8.2E-03	0	0	607.0	605.0	1212.0	0.0	0.0	0
AF-3	HRLC	760/760	5.0E-01	6.6E-03	6.6E-03	0	0	564.0	560.0	1124.0	0.0	0.0	0.
AF-42	CCCR	760/760	1.7E-02	5.3E-04	5.3E-04	0	1470.0	965.0	699.0	1664.0	0.0	0.0	0.
AF-26	CCCR	760/760	1.4E-02	2.4E-04	2.4E-04	0	285.0	938.0	721.0	1659.0	0.0	0.0	0.
AF-34	CCCR	760/760	3.2E-02	7.0E-04	7.0E-04	0	428.0	983.0	626.0	1609.0	0.0	0.0	0.
AF-36	CCCR	760/760	5.0E-02	9.4E-04	9.4E-04	0	72.0	878.0	623.0	1501.0	0.0	0.0	0.
AF-40	CCCR	760/760	5.9E-02	8.4E-04	8.4E-04	0	327.0	856.0	347.0	1203.0	0.0	0.0	0.
AF-43	CCCR	760/760	3.6E-02	5.6E-04	5.6E-04	0	76.0	768.0	546.0	1314.0	0.0	0.0	0.
AF-47	TCCR	760/760	1.0E-01	2.9E-03	2.9E-03	577.0	0	701.0	1154.0	1855.0	0.0	0.0	-0.
AF-5	TCCR	760/760	1.0E-01	1.1E-03	1.1E-03	130.0	0	582.0	1028.0	1610.0	0.0	0.0	-0.
AF-27	TCCR	760/760	7.4E-02	1.1E-03	1.1E-03	46.0	0	440.0	865.0	1305.0	0.0	0.0	-0.
AF-25	BCCR	760/760	5.0E-02	1.5E-03	1.5E-03	744.0	2220.0	734.0	734.0	1468.0	0.0	0.0	0.
AF-41	BCCR	760/760	1.0E-01	2.2E-03	2.2E-03	212.0	569.0	665.0	674.0	1339.0	0.0	0.0	-0.
AF-28	BCCR	760/760	1.0E-01	1.4E-03	1.4E-03	42.0	67.0	605.0	512.0	1117.0	0.0	0.0	0.

HIGH-TEMPERATURE MATERIALS DATABASE
FOR TS-SRP

A substantial database of high temperature material properties has also been developed for use with this software, including nickel and cobalt-base superalloys, titanium, copper, and iron-base alloys and austenitic stainless steels.

RENE 80	AMZIRC	AF2-1DA
IN-100	NARLOY Z	B1900+Hf
MAR M002	TIAL64V	INCONEL 625
NIMONIC 90	2.25Cr-1Mo	INCONEL 718
WASPALLOY	HASTELLOY X	INCONEL 738
RENE 95	HAYNES 188	304 SS
		316 SS

SUMMARY

A brief overview of the TS-SRP life prediction methodology has been presented. The suite of computer programs developed to implement this methodology has been described with sample output offered to demonstrate this software capability. The program suite presented includes a materials database that is among the largest of its type available in the literature and should prove to be an attractive feature of the program suite to potential users. This database, while of clear value to the TS-SRP programs described, is also of utility in the development of alternative high temperature life prediction approaches.

- ## High Temperature Life Prediction Computer Code Based on TS-SRP

- ## Code Contains TS-SRP Constants Database for Several Materials

REFERENCES

1. Manson, S. S., Halford, G. R. and Hirschberg, M. H., "Creep-Fatigue Analysis by Strainrange Partitioning," Design for Elevated Temperature Environment, American Society of Mechanical Engineers, NY, 1971, pp. 12-28.

2. Halford, G. R. and Saltsman, J. F., "Strainrange Partitioning -- A Total Strainrange Version," Advances in Life Prediction Methods, D. A. Woodford and J. R. Whitehead (eds.), American Society of Mechanical Engineers, NY, 1983, pp. 17-26.

3. Saltsman, J. F. and Halford, G. R., "An Update of the Total-Strain Version of Strainrange Partitioning," Low Cycle Fatigue, ASTM-942, H. D. Solomon, G. R. Halford, L. R. Kaisand and B. N. Leis (eds.), American Society for Testing and Materials, Philadelphia, PA, 1987, pp. 329-341.

4. Moreno, V. et al, "Application of Two Creep Fatigue Life Models for the Prediction of Elevated Temperature Crack Initiation of a Nickel Base Alloy," AIAA Paper 85-1420, July 1985.

5. Saltsman, J. F. and Halford, G. R., Life Prediction of Thermomechanical Fatigue Using the Total Strain Version of Strainrange Partitioning (SRP): A Proposal. NASA TP-2779, 1988.

6. Saltsman, J. F. and Halford, G. R., Procedures for Characterizing an Alloy and Predicting Cyclic Life with the Total Strain Version of Strainrange Partitioning. NASA TM-4102, 1989.

7. Halford, G. R., Hirschberg, M. H. and Manson, S. S., Temperature Effects on the Strainrange Partitioning Approach for Creep-Fatigue Analysis. NASA TMX-68023, 1972.

8. Halford, G. R. and Nachtigall, A. J., "Strainrange Partitioning Behavior of an Advanced Gas Turbine Disk Alloy AF2-1DA," Journal of Aircraft, Vol. 17, No. 8, Aug. 1908, pp. 598-604.

9. Walker, K. P., Research and Development Program for Nonlinear Structural Modeling with Advanced Time-Temperature Dependent Constitutive Relations. (PWA-5700-50, Pratt & Whitney Aircraft; NASA Contract NAS3-22055). NASA CR-165533, 1981.

10. Halford, G. R., Saltsman, J. F. and Hirschberg, M. H., "Ductility-Normalized Strainrange Partitioning Life Relations for Creep-Fatigue Life Predictions," Environmental Degradation of Engineering Materials, M. R. Locthan and R. P. McNitt (eds.), Virginia Polytechnic Institute and State University, Blacksburg, VA, 1977, pp. 599-612. _____

11. COSMIC. The University of Georgia, Athens, G/

12. Saltsman, J. F., Users Manual for Computer Progri   lic
    Life Using the Total Strain Version of Strainrange

Needs
Abstract

284

NASA Langley Developments in Response Calculations Needed for Failure and Life Prediction

Jerrold M. Housner
NASA Langley Research Center
Hampton, VA

OUTLINE

- Computational methods for inserting detail in global models

    - Joining 2-D shell/plate structural regions
    - Joining 2-D shell/plate and 3-D structural regions

- Automatic adaptive refinement methods to identify areas requiring further detail analysis

- Rapid algorithms for large complex structural analysis

C.4

STRUCTURAL FAILURE ANALYSIS IN CONCURRENT ENGINEERING

Successfully competing in the aerospace world market requires significant reductions in the time to design and develop aerospace systems. Competition also requires innovative concepts for using new material systems, achieving high-performance, attaining low development and maintenance costs and long-life designs. For example, although development of composite structural concepts began some twenty-five years ago, only now are composite materials seeing significant application in commercial aircraft and spacecraft structural systems. This lag is due in large part to the inability to predict with confidence the behavior and life of composite aerospace structures under a variety of environmental conditions. Often, details which are not accounted for in the preliminary stages of design become costly and time-consuming items if addressed later in the design process. Computational tools which will allow more unified and integrated designs in a concurrent engineering environment are also needed for more efficient treatment of important system behavior. These same computational tools can also be used to reduce costs associated with development, verification and certification tests. NASA's Computational Mechanics Branch at the Langley Research Center is helping to satisfy that need by developing validated, efficient, reliable and easy-to-use computational tools to be used in assessing failure and life of structural components.

- NASA's Computational Mechanics Branch is performing research to help meet some of the goals of concurrent engineering, namely,

  - Avoid costly redesigns late in the design process

    Details ignored in early design often lead to or become sites for pre-mature failure

  - Reduce costs associated with development, verification and certification tests

- Develop validated, reliable and easy-to-use computational failure analysis tools

# ACCURACY OF INDEPENDENT REGIONAL MODELING DEMONSTRATED ON CLASSICAL EXAMPLE

New modeling technology has been developed to enhance detail global-local analysis. This modeling technology allows detail finite element models to be easily inserted within global finite element models. The salient feature of this technology, which simplifies detail insertion, is that the finite element grid points of the global and local regions need not coincide. This removes the often tedious construction of transition modeling to connect the global and local regions. The technology employs a specially developed interface element which has no width dimension. The interface element is based on hybrid variational principles of mechanics. The interface element has its own deformation shape functions and Lagrange multiplier functions which are used to impose compatibility between the regional models. From the engineer's viewpoint, the interface element is used just like any other finite element. Stiffness and mass matrices are automatically assembled including the effects of the interface connection.

Before development of this technology was initiated, it was envisioned that the interface element would need to be placed away from steep stress gradient areas, that is, in areas where the gradients are fairly benign. However, the hybrid formulation does not require such a restriction on the placement of the interface. To demonstrate that, a classical case of an isotropic plate with a central circular cutout under uniform axial tension is examined. One quarter of the plate is analyzed. The interface between the global and local regions is placed very close to the edge of the cutout. In the accompanying figure it has been placed at 80% of the cutout radius which is at a steep stress gradient location. Nevertheless, the coupled global/local analysis using the interface element gives accurate stress resultant predictions as shown in the lower left quadrant of the figure for both Nx and Ny when compared to the elasticity solution. The lower right hand portion of the figure illustrates the color contours of axial stress resultant. It reveals stresses across the interface.
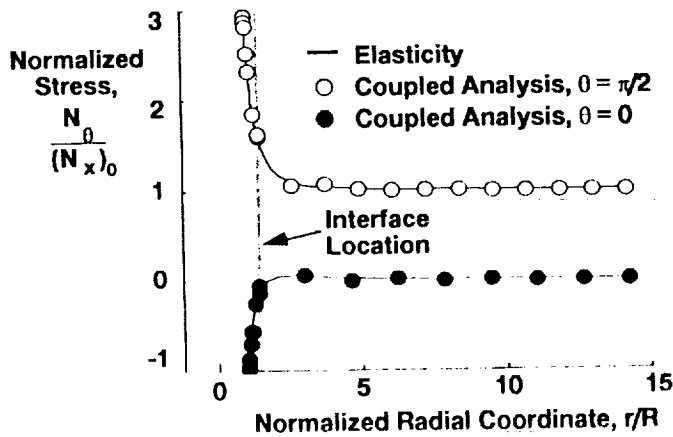

Plate with Cutout
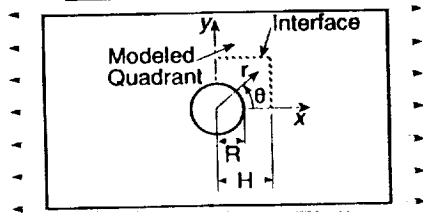
Stress Contours

Accuracy

— Elasticity
O Coupled Analysis, $\theta = \pi/2$
● Coupled Analysis, $\theta = 0$
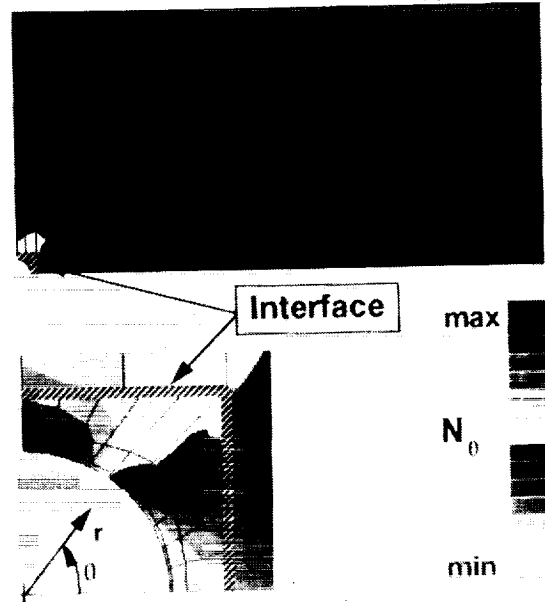
FUNCTIONAL INTERFACE METHOD ACCURATELY JOINS INCOMPATIBLE FINITE ELEMENT MODELS

The interface element can also be used to insert cracks into undamaged global models as shown. The accuracy of the method is shown by using the predicted stresses and displacement from the global/local coupled method to calculate stress intensity at the crack tip. Because no tedious transition meshing is needed to join the local and global regions, various crack lengths can easily be handled by moving the local region to the right as longer cracks are inserted or to the left as shorter cracks are inserted. Results are in excellent agreement with the reference solution for all crack lengths considered.

Cracked Plate

Quarter Model

Accuracy

Crack Length Parameter, $\frac{a}{b}$
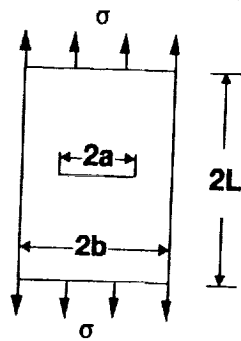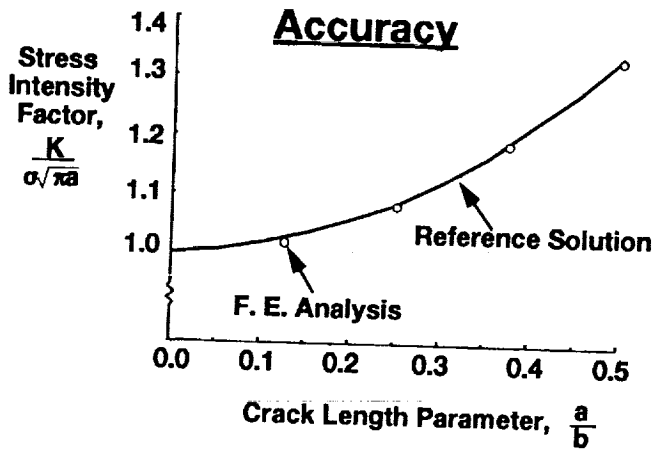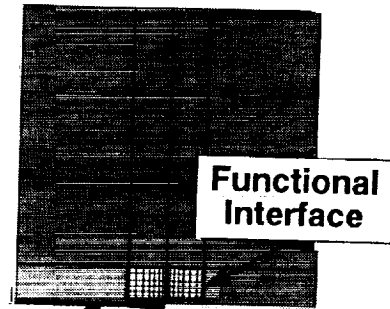
Advantages

- **No Tedious Transition Region Modeling**

- **Grid Points Along Interface Need Not Coincide**

- **Requires Fewer Degrees of Freedom than Model with Transition Regions**

- **Retains Accuracy**

290

INTERFACE METHOD FOR INSERTION OF LOCAL DETAIL MODELING EXTENDED TO CURVE PRESSURIZED FUSELAGE WINDOW PANEL

As an additional example on the utilization of interface elements, a global model of a panel in the window belt area of a fuselage is used. In order to assess the damage tolerance of the design, a crack is placed at the corner of the window. This is done by inserting a refined crack model into the global coarse model. Again, the color contours reveal the smoothness of the stresses across the interface.* Since no reference solution exists for this case, a refined finite element model was created and results from it compared with the results using the interface method. The stresses from the insertion modeling differ with the refined analysis by about 1%.
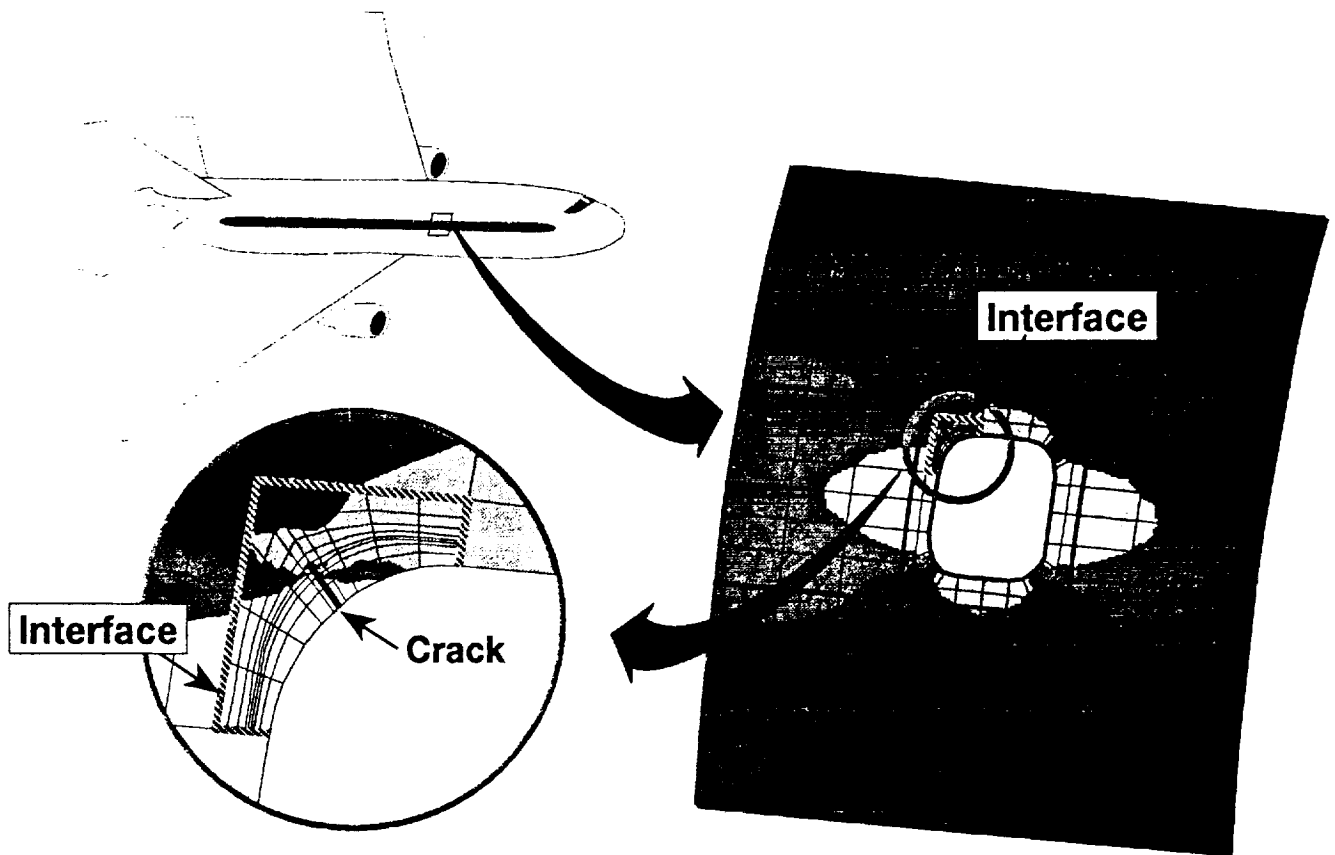
*Not shown in color.

INTERFACING CONCEPT FOR JOINING STRUCTURAL REGIONS

This chart summarizes the attributes of the interface element and regional joining technique. Basing the interface element on a hybrid variational principle is critical to the success of this technique. Other techniques, also based on variational principles, were developed and tested. These include a collocation technique (very similar to the commonly used multi-point constraints of general purpose finite element codes such as NASTRAN), and a least squares technique. In each technique a functional form, with free parameters, is laid down along the interface. In the collocation and least squares techniques this functional represents the displacements of the interface while in the hybrid technique two functionals are used, one for the displacements, and another for the Lagrange multipliers which enforce compatibility. Each region is tied to the interface using a collocation, least squares or hybrid integrated compatibility, respectively. The techniques were tried and their performance was compared on several test cases. It was found that the hybrid variational approach was consistently superior and gave accurate and reliable results. Because the regions never touch each other, except through the interface, grid coincidence is not required and models of regions or substructures can be created independently. This attribute of the method also avoids tedious-to-construct transition modeling between the refined gridded region and the coarse gridded region. This is extremely important for ease of detail refined model insertion in coarse global models and in substructuring, especially where structural components are developed independently by different individuals or organizations.

- Based on hybrid variational principles of mechanics

- Functional form for deformations and tractions is laid down along the interface

- Each structural region is joined to the interface through hybrid variational principles

  - Regional models can be developed independently of one another

  - Mesh grid points of adjoining regions need not be coincident

- Tedious-to-construct mesh transition regions between models are eliminated

- Retains accuracy while providing modeling simplification

292

MOTIVATION FOR COUPLED 2D-3D ANALYSIS

The use of composite materials for structural applications requires that detail which usually is not needed in monolithic metallic structures be considered. For example, in shell-type aerospace structures, through-the-thickness stresses are nominally small and therefore traditionally treated as a "secondary" effect in metallic structures. However, in composite materials they are no longer "secondary" in nature since through-the-thickness strengths are also small. Traditional practices may overlook these effects in the preliminary design leading to costly redesigns later or to compromises in performance. Consequently, three-dimensional analyses are often required to calculate interlaminar stresses for prediction of delamination or debonding failures at skin-stiffener interfaces. Typical critical regions are at joints, ply drop-offs in tapered skins, discontinuous stiffeners (or stiffener runout), regions of sharp stress gradient (such as near the frames in a pressurized fuselage), and in the area affected by impact damage.

Since detail 3D analyses usually require many degree-of-freedom, it is desirable to only use the 3D modeling where it is necessary and to use 2D plate and shell modeling elsewhere. This is the motivation for specialized elements that will permit 2D and 3D regions to be joined accurately.

- Interlaminar Stresses
- Delamination or Debonding Failure
- Detailed 3D Analysis

Tapered Skin

Panel with Stiffeners

Impact Damage

Pressurized Fuselage
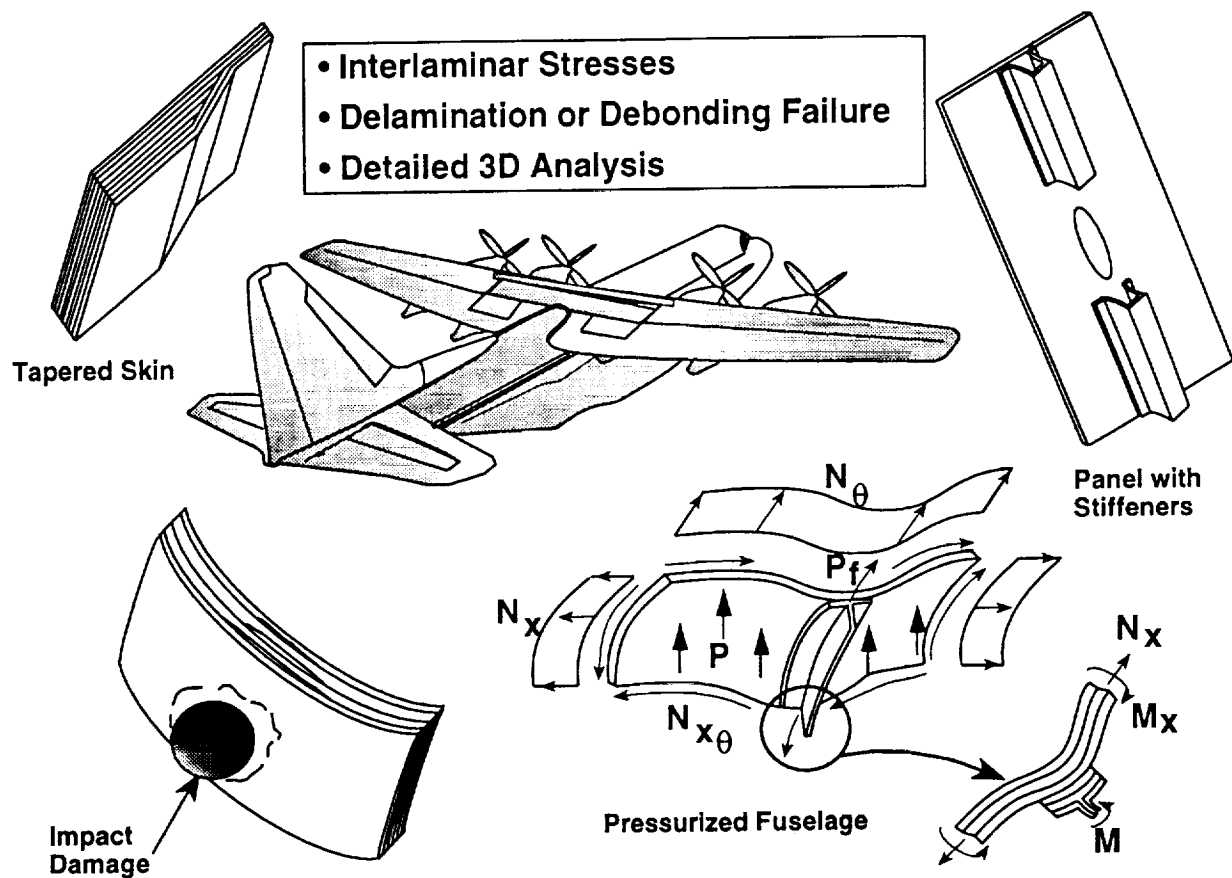
METHODS FOR COUPLING 2D MESH TO 3D MESH

Various methodologies have been proposed and experimented with to join 2D-3D regions. Among these are multipoint constraints and development of transition elements. The multi-point constraint approach requires considerable user input and is usually limited to linear constraints. The transition element approach is easy to use because it is treated like any other element and if done properly is applicable in nonlinear analysis. Recent developments in this area have led to transition elements which connect a stack of three-dimensional brick elements to a single shell or plate element. The methodology is also in place for elements which allow transition in toe directions.

- Multipoint Constraint

  - Tedious modeling

  - Usually limited to linear constraints in general purpose FEM codes

- Transition Element (Element has solid nodes and shell nodes)

  - Surana (1980, 1982): Linear and nonlinear analyses

  - Liao, Reddy, and Engelstad (1988): Geometrically nonlinear analysis of laminated composites

  - Davila and Johnson (1991): Connecting a stack of solid elements to one shell element (linear and geometrically nonlinear analyses)

15-NODE TRANSITION ELEMENT

Illustrated here is a 15 node element which allows transition in one direction. Elements which allow transition in two directions are also available. Notice that the nodes connecting to the 2D plate or shell element may lie at a location off the element. This allows a stack of transition elements to be used so that a stack of three-dimensional bricks may be connected to a 2D plate or shell element. In a nonlinear analysis, the increments in the displacement variables represent the degrees-of-freedom.

Nodes connect to plate or shell element

Nodes on this face connect to 3D element
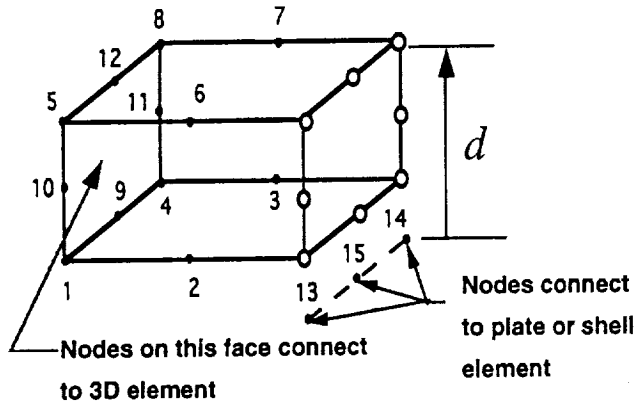
Linear Analysis

$$\begin{bmatrix} u \\ v \\ w \end{bmatrix}_{Solid} = \begin{bmatrix} 1 & 0 & 0 & 0 & d \\ 0 & 1 & 0 & -d & 0 \\ 0 & 0 & 1 & 0 & 0 \end{bmatrix} \begin{bmatrix} u \\ v \\ w \\ \alpha \\ \beta \end{bmatrix}_{Shell}$$

Nonlinear Analysis

- f_m and g_n are trigonometric functions of accumulated rotations

$$\begin{bmatrix} \Delta u \\ \Delta v \\ \Delta w \end{bmatrix}_{Solid} = \begin{bmatrix} 1 & 0 & 0 & df_1 & dg_1 \\ 0 & 1 & 0 & df_2 & dg_2 \\ 0 & 0 & 1 & df_3 & dg_3 \end{bmatrix} \begin{bmatrix} \Delta u \\ \Delta v \\ \Delta w \\ \Delta \alpha \\ \Delta \beta \end{bmatrix}_{Shell}$$

- Ref.: Davila and Johnson (1991)

HIGH-ORDER TRANSITION ELEMENTS ACCURATELY CONNECT 2D AND 3D MODELED STRUCTURAL REGIONS

In this quad-chart a benchmark case of edge delamination analysis in a composite 0/90 symmetric laminate under tensile loading is used to display the accuracy of the 2D-3D transition elements. These transition elements use high-order anisoparametric shape functions for displacements and stresses. The displacement state as well as the transverse shear and normal through-the-thickness stresses are represented by high-order polynomials. These stresses are made compatible with the assumed displacement state in a least-squares sense. The high-order behavior of these transition elements prevents a pinching phenomenon which could otherwise occur due to the lack of through-the thickness flexibility in the 2D elements. Such a pinching would overly constrain the 3D elements and lead to inaccurate results.

The 3D brick elements are placed in a region where the interlaminar stresses are desired. Even though the application case is symmetric, the bricks and associated transition elements have not been placed in a symmetric pattern about the x-axis so as to further examine the capability of the technique. As shown, predictions for the interlaminar stresses are in excellent agreement with the published solution. Also, because fewer degrees-of-freedom are required using a 2D-3D hybrid mesh rather than a full 3D mesh, the technique is efficient. The asymmetric placement of the 3D mesh indicates the flexibility of the technique to be able to place the detail 3D mesh where needed.
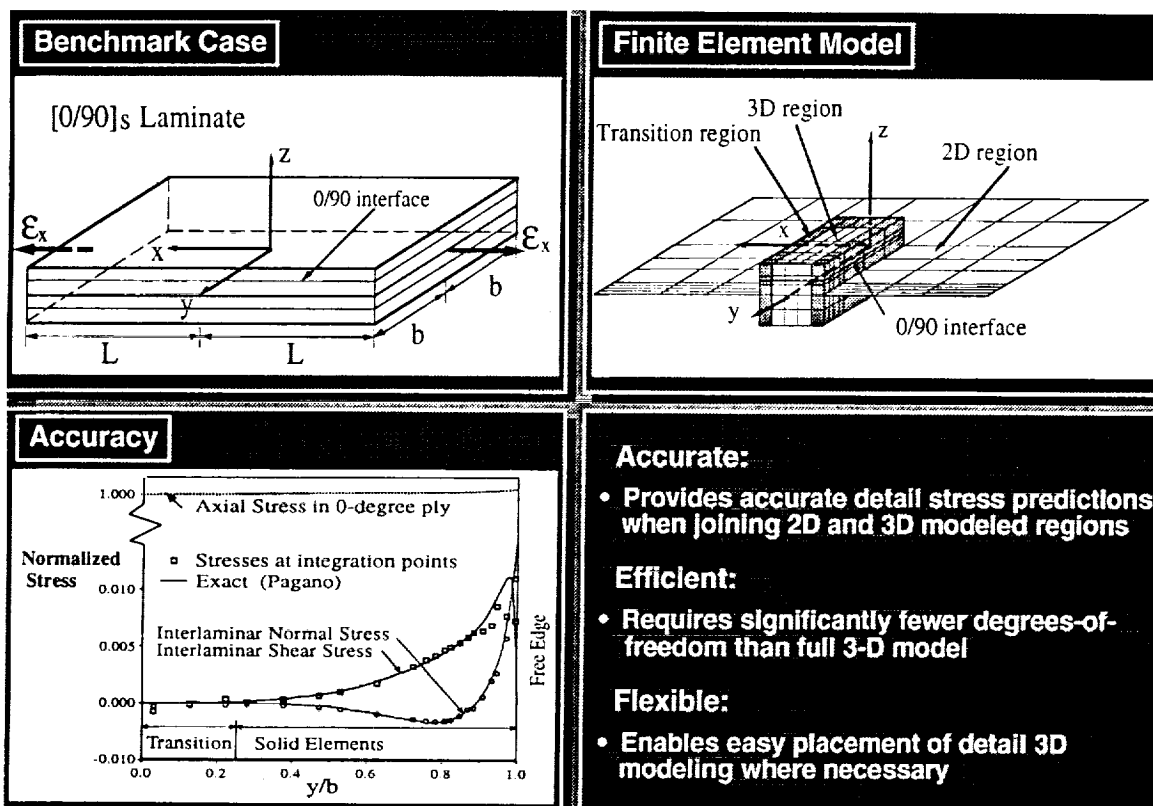
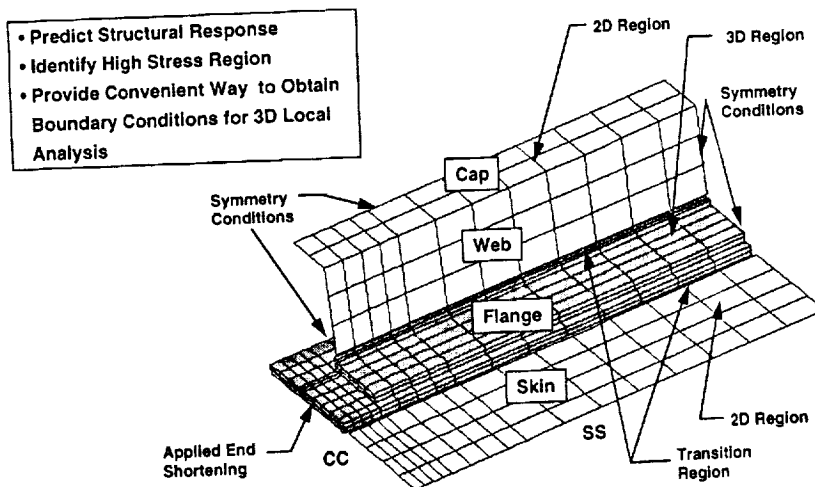# COMPRESSION PANEL WITH DISCONTINUOUS STIFFENER, COUPLED 2D-3D GLOBAL MODEL

AND

AXIAL SURFACE STRAINS AT THE MIDDLE OF THE HAT STIFFENER

Discontinuous stiffeners are often found in practice as a result of cutouts and other reasons. The stiffener termination is often referred to as runout. Because of the discontinuity, severe stress states can exist at the termination of the stiffener. Illustrated here is a discontinuous hat stiffener. To examine possible skin-stiffener debonding, it is desirable to model the skin and stiffener flange with 3D brick elements and the rest of the skin as well as the web and cap of the hat stiffener with 2D plate elements. Taking advantage of symmetry, only one quarter of the panel is shown and analyzed.

The nonlinear growth in the predicted axial surface strains with increasing applied compressive load is shown at the middle of the hat stiffener. The use of nonlinear analysis for this example becomes apparent when the axial strains at the top of the hat are examined.

COMPRESSION PANEL WITH DISCONTINUOUS HAT STIFFENER

COUPLED 2D-3D GLOBAL MODEL

297

USE OF ADAPTIVE REFINEMENT WITH MULTIPLE METHODS

The ability to embed refined detail models in global coarse models by the use of interface elements and/or transition 2D-3D elements is a powerfully attractive capability for extracting the response behavior needed for failure and life predictive analysis. These techniques may also be referred to as multiple methods since they are a hybrid of two methodologies. Moreover, the interface element and transition element capability may be combined to connect structural regions and component aerospace substructures in three dimensions: the interface elements attending to the plate or shell surface and the transition elements attending to the plate or shell thickness. This capability becomes even more powerful when it is connected to adaptive refinement capability.

The accompanying chart illustrates how adaptive refinement which uses advanced refinement indicators can identify regions requiring further refinement. The imbedding techniques can then be judiciously applied at the identified locations.

USE OF ADAPTIVE REFINEMENT WITH MULTIPLE METHODS

ADAPTIVE REFINEMENT
AND
REFINEMENT INDICATORS

STRUCTURE

IDENTIFIED STRESS AND
THERMAL "HOT SPOTS"

IMBEDDED DETAIL MODEL
USING MULTIPLE METHODS
INTERFACING TECHNIQUES

ACCURATE STRESS
STATE FOR LIFE AND
FAILURE PREDICTION
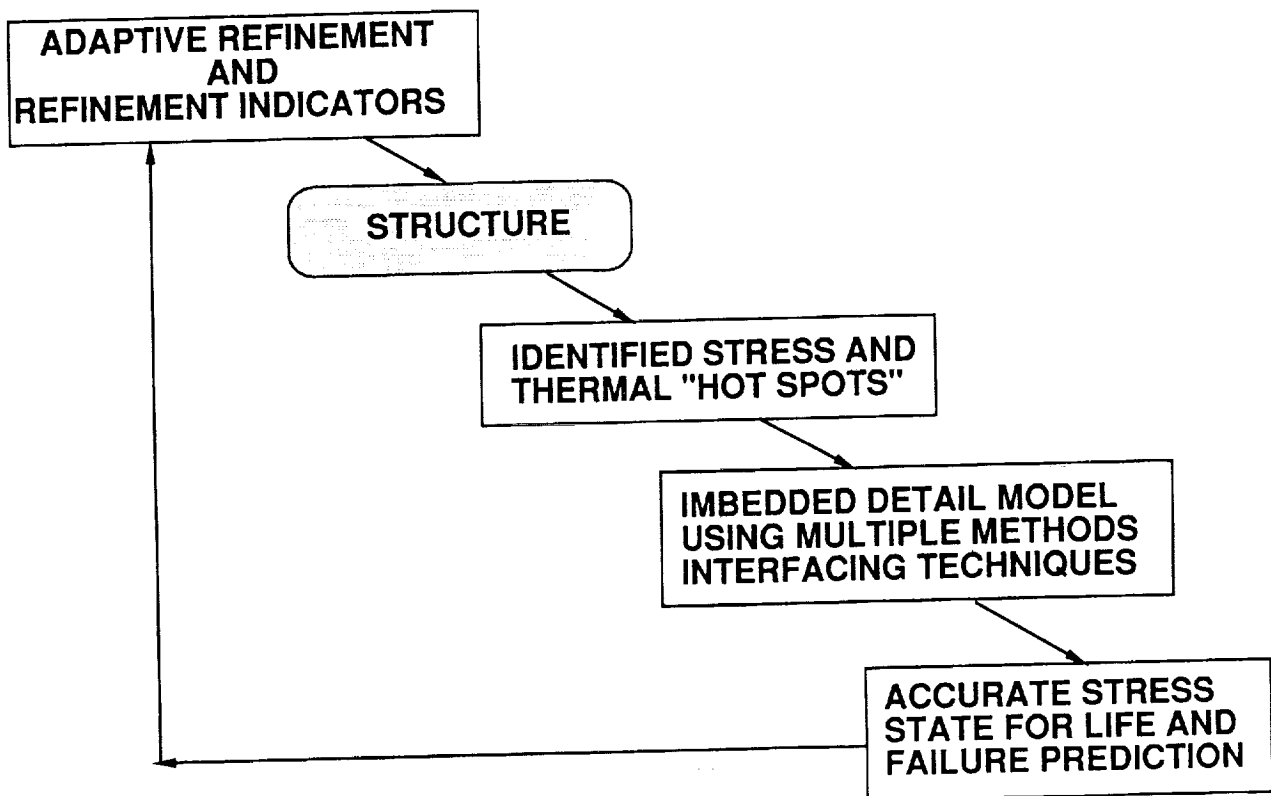
GOALS, CHALLENGES, AND APPROACH
FOR
ADAPTIVE MESH REFINEMENT TECHNOLOGY DEVELOPMENT

The goal of adaptive refinement is to provide a design tool for engineers which enhances finite element modeling by combining automation, efficiency and accuracy. Automation is brought about by the adaptivity of the mesh to highly stressed regions while accuracy and efficiency are brought about by using refined mesh only where necessary. Thus brute force global refined mesh over an entire component is avoided without the expenditure of much additional engineering time. The challenges to this technology are the treatment of (1) physical discontinuities where high stress gradients and usually stress singularities exist; (2) boundary layers; (3) components which are imperfection sensitive and hence mesh requirements can change dramatically with little change in imperfection; (4) adverse effects due to finite element distortion and element locking due to shell thinness which can require mesh refinements not driven by the physics of the response; and (5) geometric nonlinearity which requires mesh changes with increasing load and presents an enormous data handling challenge as well as procedures for mapping response from one mesh to another.

The COMET (COmputational MEchanics Testbed) code is used as a framework for developing adaptive mesh refinement capability. The modified code is denoted as COMET-AR. In this code an adaptive refinement procedure controls the code operation. The code consists of three major modules: an error estimator (or refinement indicator) module, a finite element analyzer, and a mesh refiner which operates upon certain built in rules and user-defined options. The mesh is refined until convergence is reached in accordance with a user-selected tolerance. An object-oriented data manager and database is an important feature of the code because of the intense data handling required in nonlinear adaptive refinement.
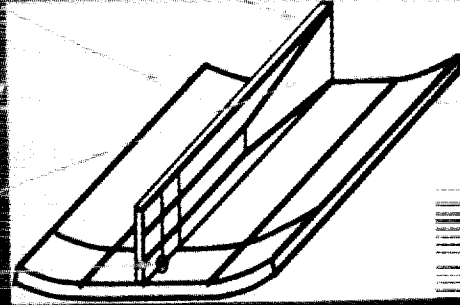
CHALLENGES

- PHYSICAL DISCONTINUITIES

- BOUNDARY LAYERS

- IMPERFECTION SENSITIVITY

- ELEMENT SENSITIVITIES
  — Distortion
  — Constraints
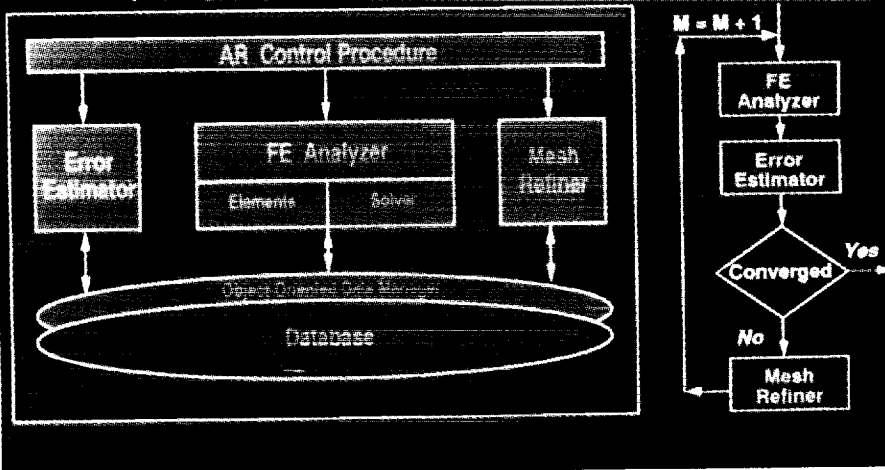 — R/t

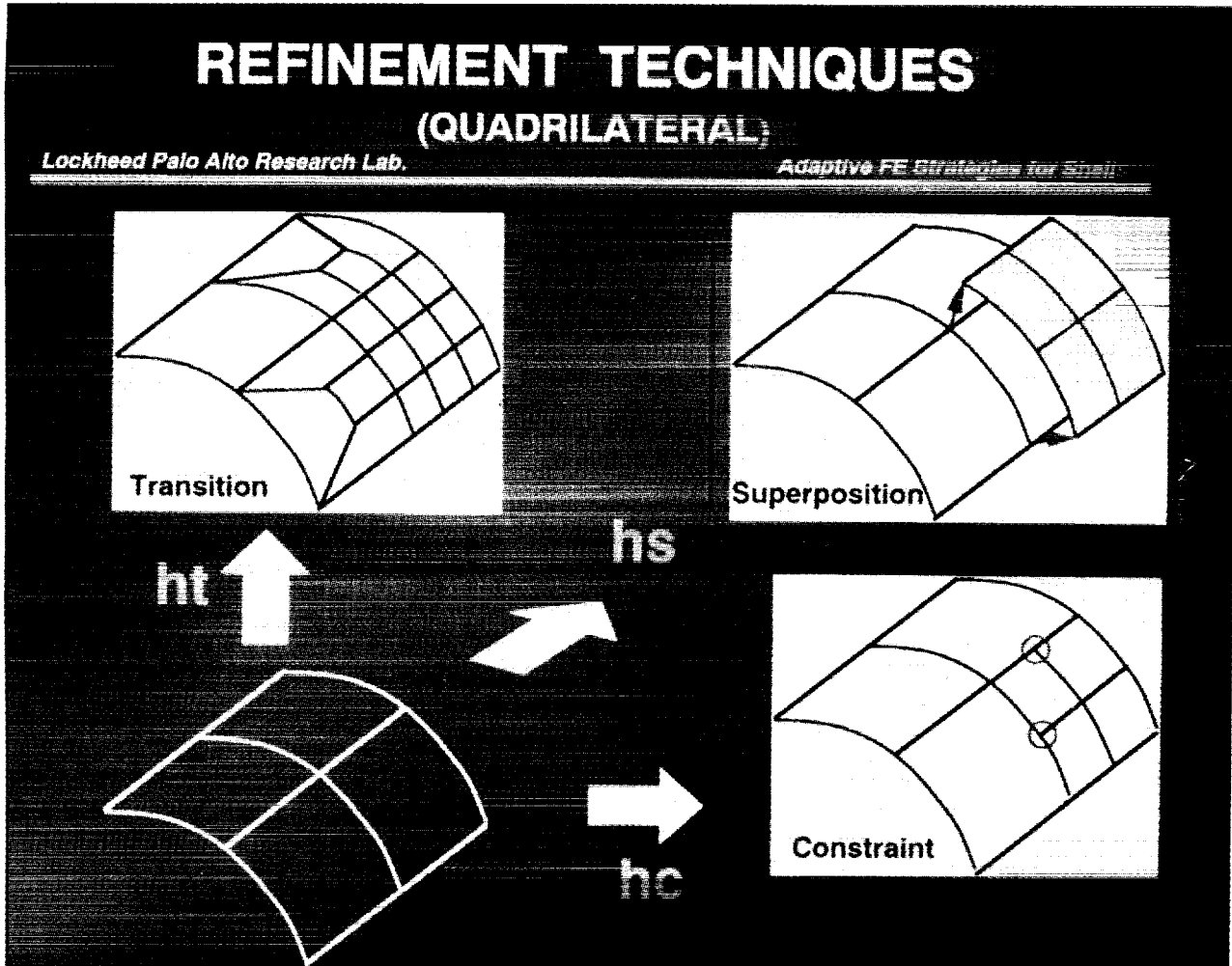- GEOMETRIC NONLINEARITY

APPROACH

COMET *(Computational Mechanics Testbed)*

M = 0

M = M + 1

AR Control Procedure

Error Estimator

FE Analyzer
Elements   Solver

Mesh Refiner

Object Oriented Data Manager
Database

FE Analyzer

Error Estimator

Converged — Yes

No

Mesh Refiner

301

REFINEMENT TECHNIQUES
FOR
ADAPTIVE MESH REFINEMENT TECHNOLOGY DEVELOPMENT

Three different techniques are being explored, namely, transition refinement (ht), superposition refinement (hs) and constraint refinement (hc). Transition refinement tends to lead to distorted quadrilateral elements whose accuracy can be unsatisfactory. Superposition refinement builds upon regions of underlying mesh by refining in a hierarchical manner. It does not suffer from distorted finite elements provided the initial user-supplied coarse mesh does not contain distorted elements. The constraint refinement technique is mathematically equivalent to the superposition technique, but leads to a different form of the governing equations.

REFINEMENT TECHNIQUES
(QUADRILATERAL)
Lockheed Palo Alto Research Lab.   Adaptive FE Strategies for Shell

Transition   Superposition

ht   hs

hc   Constraint

PERFORMANCE OF ADAPTIVE MESH REFINEMENT DEMONSTRATED ON COMPOSITE FUSELAGE-LIKE COMPRESSION PANEL

Convergence of automatic adaptive mesh refinement is displayed in the figure for a curved fuselage panel having a cutout. The panel loading is axial compression. The adaptive algorithm in the COMET-AR code zooms in by refining at the stress concentration generated by the presence of the cutout. Comparison of adaptivity results with those derived for uniform refinement, indicates the degree-of-freedom savings offered by adaptive refinement. However, the mesh refinement algorithm being used here does tend to generate distorted elements which, because of their poor accuracy can lead to over-refinement and in this case some over-prediction of the response until the mesh is further refined and convergence is reached.
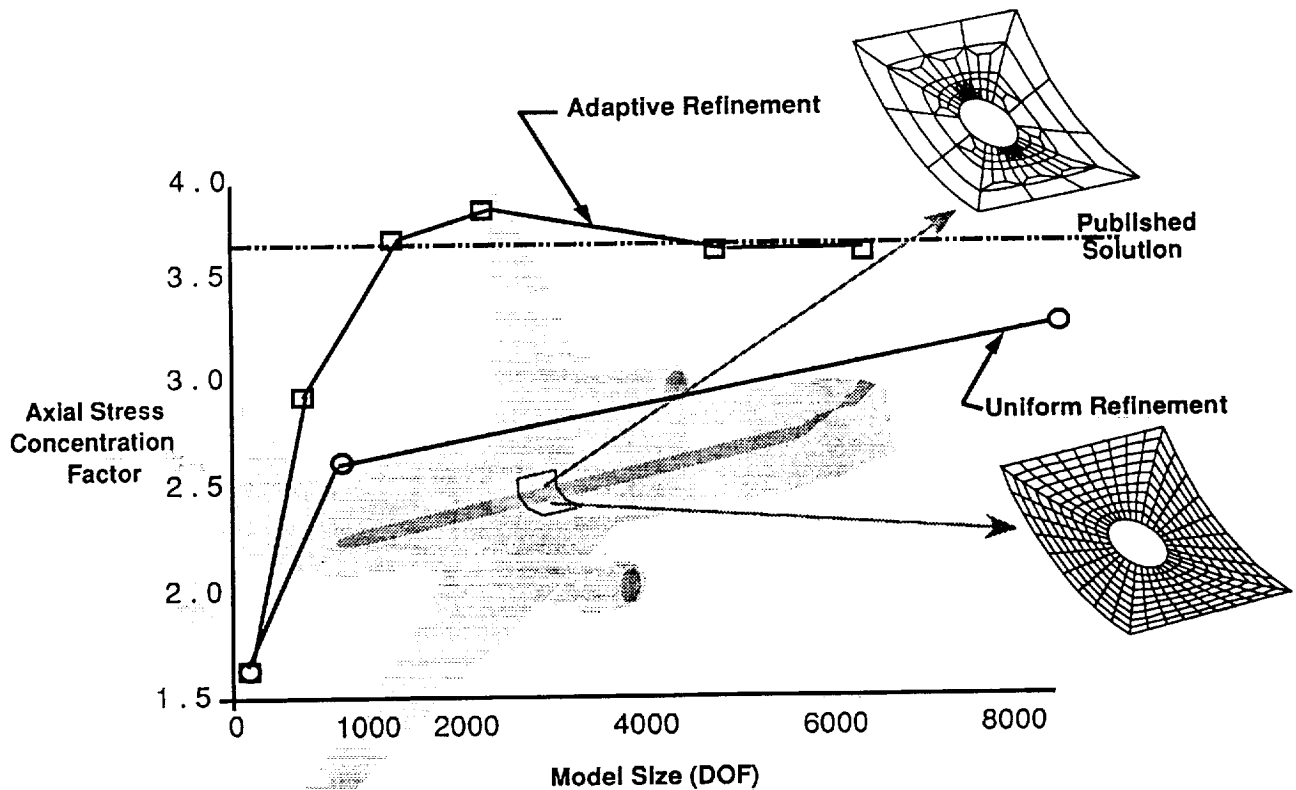
# SUPERPOSITION ADAPTIVE REFINEMENT TECHNIQUE DEVELOPED FOR BUILT-UP STRUCTURES

The advantage of the superposition technique (hs) over the conventional transitional technique (ht) is displayed in this quad-chart. The application case is a blade stiffened compression panel in which the blades are discontinuous. The ability of the adaptivity to capture the stress concentrations at the blade terminations is critical to the application of this technology to failure and life prediction. As shown by the color contours,* the axial stress concentrations at the stiffener runouts are well-captured with considerably fewer degrees-of-freedom than a uniform refinement and less than that of a conventional (ht) refinement. Notice that refinements are also taking place in the blade stiffeners as well as in the skin.
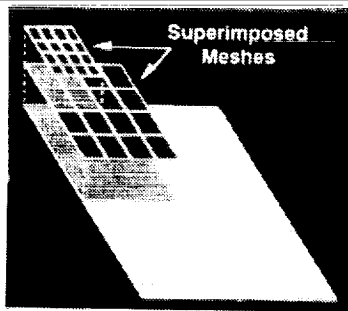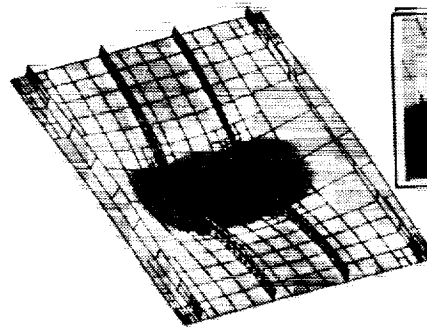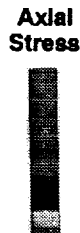

Superposition Method
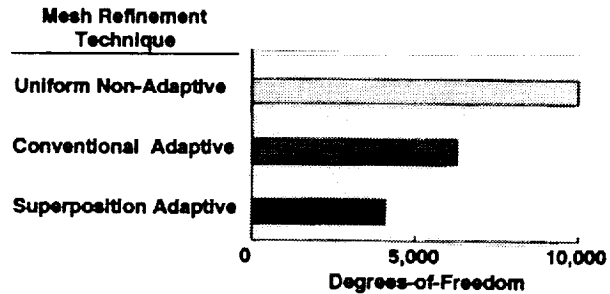
Modeling Requirements
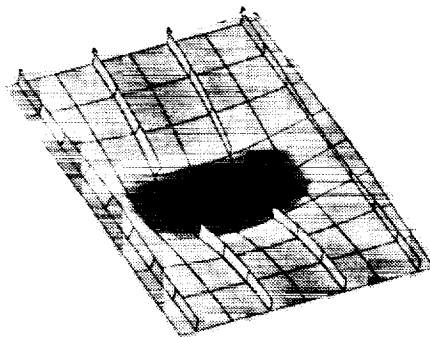

Initial Mesh

Final Mesh

Compression Panel with Discontinuous Blade Stiffeners

* Not shown in color.

STUDIES QUANTIFY EFFECT OF BOW-TYPE INITIAL IMPERFECTIONS ON RELIABILITY OF STIFFENED PANELS

A panel's reliability is the probability that it will not fail at under a specified load. That probability depends upon certain variables which vary from panel to panel. One such variable is the initial imperfection. Typically these imperfections are accounted for in design with safety factors. However, if these imperfections can be quantified statistically, then probabilistic methods can be used to calculate reliability. Understanding the factors affecting reliability can lead to improved design with lighter reliability. Studies were carried out to determine the reliability of stiffened panels assuming various reasonable probability distributions for the magnitude of a bow-type initial imperfection.

A graphite-epoxy, laminated, blade-stiffened panel having the configuration shown in the upper left-hand quadrant of the figure was designed to carry prescribed levels of combined compression and shear loads. The failure mode of the panel is buckling. The load carrying capability of each panel was calculated for various magnitudes of initial bow as shown in the upper right quadrant of the figure. The magnitude of the bow-type imperfection was then taken to be a random variable with various distributions of probability density functions as shown. Three distributions were considered: normal, maximum extreme value and minimum extreme value. Each of these distributions has a zero mean and the same standard deviation of 0.02 inches. The distributions only differ in higher moments about the mean. To simulate quality control, the distributions were truncated at plus or minus 0.04 inches. The reliability of the panel was calculated for all six distributions and all analyses were carried out using the panel sizing code, PASCO. Even though the three distributions without quality control had the same general shape, with the same mean and standard deviation, the panel reliabilities are quite different. This indicates the sensitivity of reliability to details of the probability distribution. In the case in which truncated distributions were used to simulate the effect of quality control, the reliability of the panels was not as sensitive to details of the distribution, with the reliability of all three dropping off from unity at about the same load. Moreover, for the distribution labeled Maximum, the reliability does not appear or benefit from quality control.
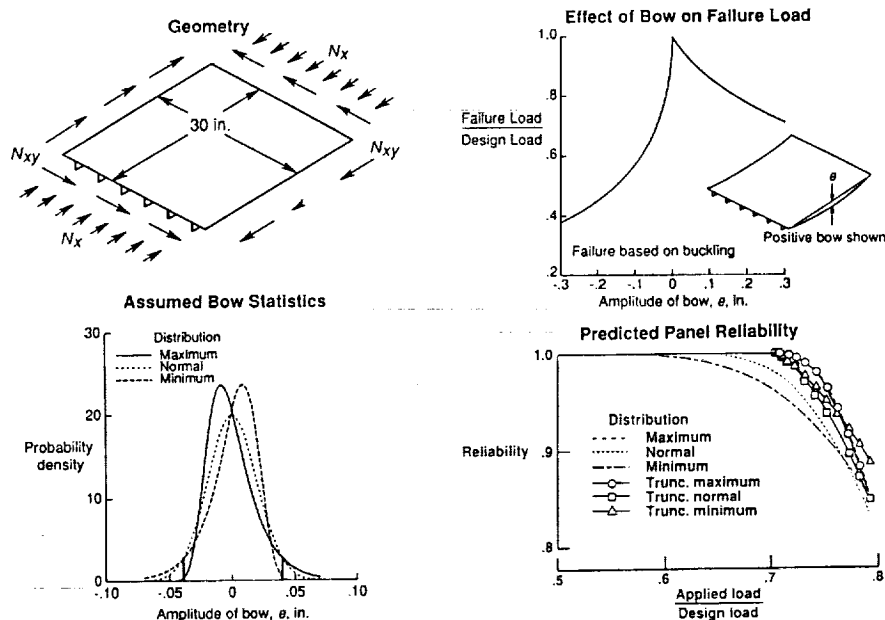
TRADITIONAL MATRIX ASSEMBLY
AND
NEW NODE-BASED MATRIX ASSEMBLY

Structural matrix generation and assembly can be a large fraction of finite element analysis time. This is especially true in design optimization and trade-off studies as well as in nonlinear analyses where generation and assembly must be performed many times. The traditional or conventional approach to generation and assembly of stiffness and mass matrices is to use an element-by-element based scheme wherein the code loops over all the elements. Such a conventional approach does not map well onto parallel computers. If the element calculations in such a scheme are assigned to separate processors, (as would be desirable in balancing the computational effort of the processors), a synchronization or communication bottleneck occurs as several processors, each of which are associated with a connected finite element, attempt to write stiffness or mass contributions to the same memory address (associated with a finite element node) at the same time.

An alternative approach, which contains no synchronization bottleneck, is to loop over the nodes rather than the elements. This requires the creation of a map showing the elements connected to a node. Once that small overhead task is accomplished there is no communication required between processors an perfect speed-ups should be achievable.

306

STRUCTURAL MATRIX GENERATOR/ASSEMBLER FOR MASSIVELY PARALLEL COMPUTERS DEMONSTRATED ON HSCT

Conventional finite element codes, executing on sequential computers, use an element-by-element algorithm to generate and assemble stiffness and mass matrices. To parallelize this conventional procedure, element stiffness calculations are distributed among different processors. However, poor performance results since synchronization of these processors is required to simultaneously add stiffness contributions from different elements connected to the same node. To overcome this, a parallel node-by-node stiffness and mass matrix generation and assembly algorithm was developed to distribute nodal, rather than element, calculations to different processors. The algorithm's parallel performance was evaluated on a finite element model of a Mach 2.4 version of a High Speed Civil Transport. The model contains over 16,000 degrees-of-freedom. Results were run on a 512-processor Intel Delta parallel computer and compared with those generated using the conventional element-by-element algorithm on the supercomputer industry standard, namely, an 8-processor Cray Y-MP supercomputer.
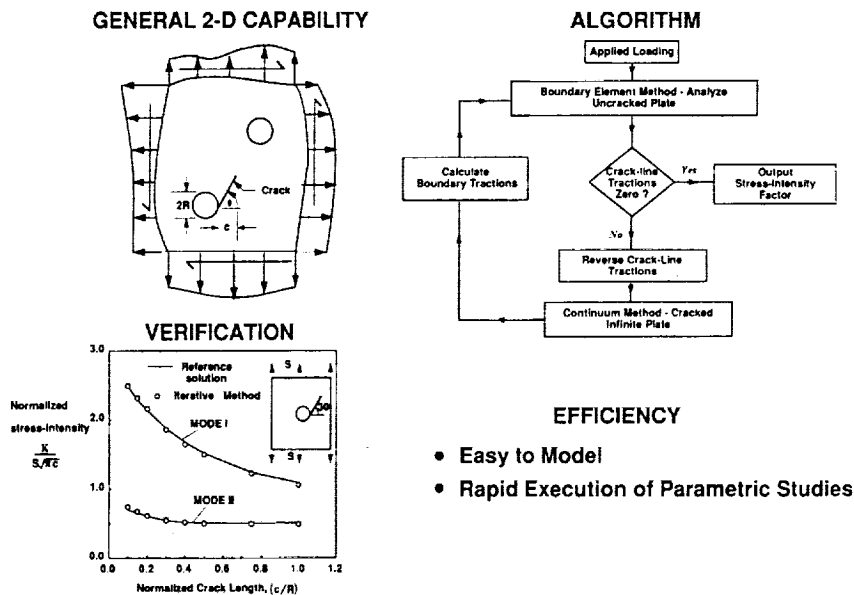
The algorithm's performance was found to be scalable, which means the computation time reduces is in direct proportion to the number of processors used. This is the highly desirable result sought, but in general is difficult to obtain on massively parallel computers due to communication time between processors. This achievement was possible by replacing the communication-intensive element-by-element algorithm with the node-by-node algorithm to eliminate interprocessor communication.
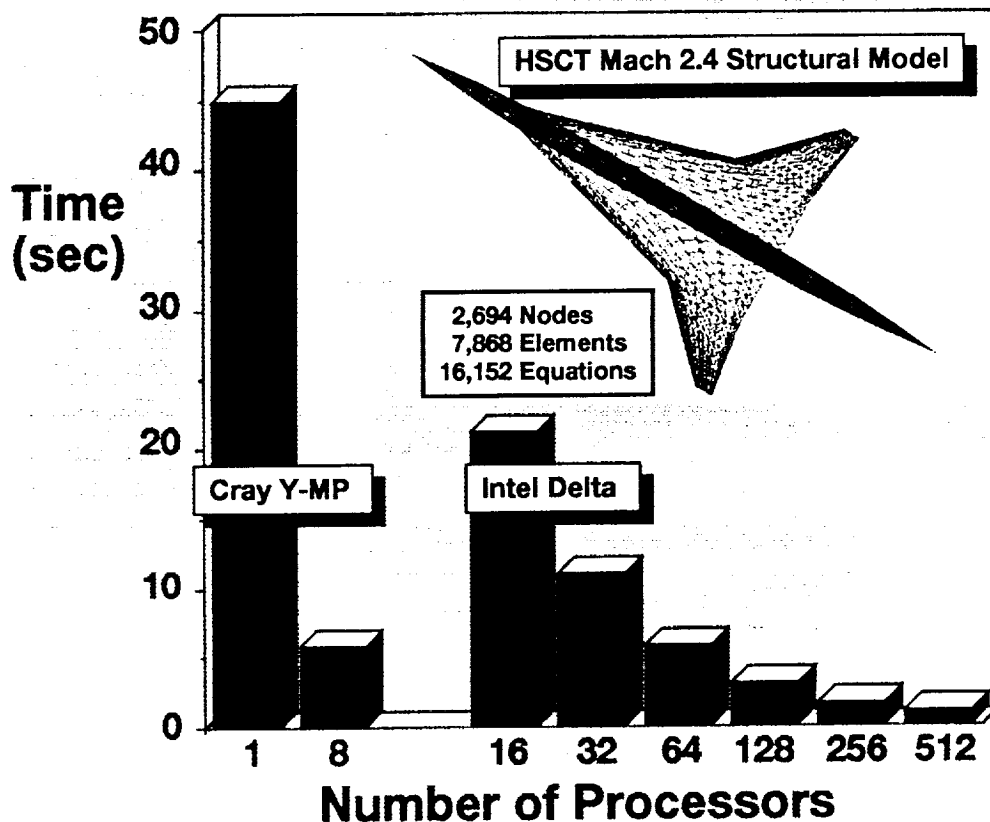
ITERATION METHOD DEVELOPED FOR EXTRACTING FRACTURE PARAMETERS

Rapid analysis tools for calculating fracture parameters are needed for predicting failure and life. Such a tool has been constructed for calculating fracture parameters (e.g., stress intensity factors) for cracks in general planar structural components. This tool uses a newly developed iterative method which combines the boundary element method (BEM) for an uncracked finite component with cutouts under general loading conditions with a continuum solution for a cracked infinite component without cutouts. A schematic illustrating the iterative method is shown in the accompanying chart. First the BEM is applied to the uncracked component. Since the BEM requires only the discretization of the component boundaries, (including cutout boundaries), the modeling is easier than with finite elements which require discretization of the entire component. Because the BEM step will not yield traction free conditions at the crack(s), the tractions predicted by the BEM step are removed by seeking the continuum solution for the equal and opposite tractions acting on the cracks of an infinite component. However, this results in unwanted tractions on the boundaries of the component. These are removed on the next iteration using the BEM. The iterative process continues until the BEM portion of the solution produces tractions on the crack surfaces which are negligibly small. The stress intensity factor for the crack is then the sum of the stress intensity factors obtained from all the iterations. Generally, only five to ten iterations are required to obtain converged solutions.

For verification, the iterative method has been applied to a plate under remote uniaxial tension having a crack emanating from a circular cutout in the plate for which accepted results appear in the literature. The variation of the stress intensity factor with crack length is shown for a crack emanating at 30 degrees from the transverse direction. Results are shown for Mode I and Mode II fracture; that is when the crack is driven by normal and shear stresses, respectively, at the crack tip. The excellent agreement with accepted results validates this new methodology which reduces modeling time and computer execution time.

GENERAL 2-D CAPABILITY

ALGORITHM

Applied Loading

Boundary Element Method - Analyze Uncracked Plate

Calculate Boundary Tractions

Crack-line Tractions Zero ?

Output Stress-Intensity Factor

Reverse Crack-Line Tractions

Continuum Method - Cracked Infinite Plate

VERIFICATION

Reference solution
Iterative Method
MODE I
MODE II

Normalized stress-intensity $\frac{K}{S\sqrt{\pi c}}$

Normalized Crack Length, (c/R)

EFFICIENCY

- Easy to Model
- Rapid Execution of Parametric Studies

308

POTENTIAL IMPROVEMENT IN ELLIPTIC BOLTED COMPOSITE JOINTS DEMONSTRATED

Composite structural components are often joined using circular bolts. These joints often fail in the composite laminate as a result of excessive bearing or shearing stresses. Increasing the bolt diameter reduces these stresses, but because it also reduces the distance from the edge of the bolt hole to the edge of the joint, it may not be practical. An alternative to reducing these stresses is to use an elliptic shaped bolt. Such a bolt may be fastened with an attached circular threaded shaft and the elliptic hole may be cut using water jet technology. To demonstrate the potential advantage of elliptic shaped bolts, analyses were performed. A closed-form approximate solution for bolt-loaded elliptical holes was formulated based on laminate theory and anisotropic elasticity. The normal load distribution on the edge of the elliptical hole was represented by a cosine series. Unknown coefficients of the cosine series were determined by a boundary collocation procedure in which the bolt is assumed to be rigid. A modified Tsai-Wu failure criterion was used to predict joint failure.

As demonstrated in the chart, two composite laminated constructions were studied. One was chosen because it is bearing-failure critical while the other is shearing-failure critical. Also, a circulate bolt diameter of a quarter inch, typical of aircraft joints, was used. The elliptic bolt was chosen to retain the 0.25 inch dimension along the minor ellipse axis with a 0.30 inch dimension along the major axis. The chart shows a 35% strength improvement for the bearing-failure critical laminate design and a 13% strength improvement for the shearing-failure critical design. These results were predicted by the closed-form approximate solution and confirmed by a detailed finite element solution.

Elliptic shape bolts can be employed in design and re-design field modifications. If a joint design using circular bolts was found to be failing on some aircraft in service, the circular bolt holes on unfailed joints could be reshaped to accommodate elliptic bolts. This would constitute a relatively inexpensive fix.
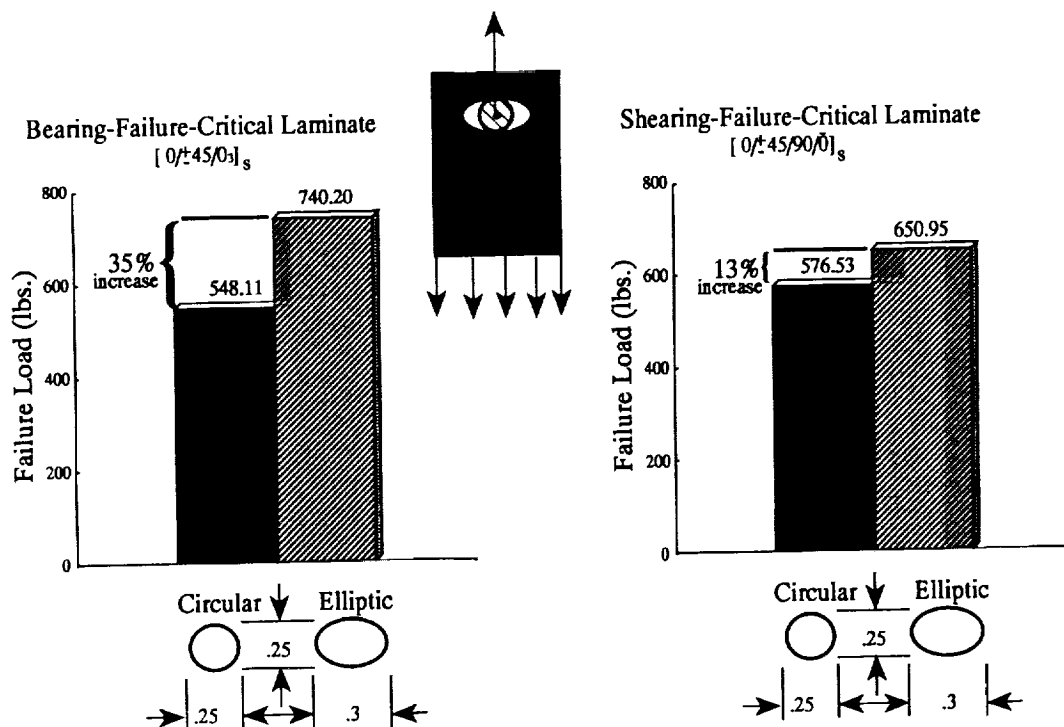
SUMMARY

- Enhance failure analysis in concurrent engineering environment

    - Automatic adaptive refinement techniques to identify potential failure sites

    - Modeling methods to simplify treatment of failure precipitating locations

- Algorithms for high-performance massively parallel computers to provide rapid performance of

    - Repetitive analysis

    - Parametric studies

- Rapid computational tools for fracture and strength analysis and design

310

Delamination, Durability and Damage Tolerance of Laminated Composite Materials

T. Kevin O'Brien
NASA Langley Research Center
Hampton, VA

PAGE _____ INTENTIONALLY BLANK

Durability and damage tolerance may have different connotations to people from different industries and with different backgrounds. In this paper, damage tolerance always refers to a safety of flight issue where the structure must be able to sustain design limit loads in the presence of damage and return to base safely. Durability, on the other hand, is an economic issue where the structure must be able to survive a certain life under load before the initiation of observable damage. Delamination is typically the observable damage mechanism that is of concern for durability, and the growth and accumulation of delaminations through the laminate thickness is often the sequence of events that leads to failure and the loss of structural integrity.

FOCUS

DAMAGE TOLERANCE - SAFETY OF FLIGHT

DURABILITY - ECONOMY OF OPERATION

DELAMINATION - DAMAGE/FAILURE MODE

Progressive failure analyses are typically based on either continuum damage models or discrete damage models. In the former, damage is treated implicitly through its influence on material parameters. The simplest and earliest example is the ply discount method used to reduce in-plane stiffness properties of a laminate to reflect the presence of damage. Recently, more sophisticated models have emerged where the complete tensoral representation of stiffness properties in a critical volume element are modified to reflect damage growth. In the discrete damage models, however, the size, shape, and orientation of damage is modeled explicitly resulting in models with internal stress free boundaries. In this paper, only examples of the discrete damage approach involving progressive delamination will be discussed.

APPROACHES TO PROGRESSIVE FAILURE ANALYSIS FOR COMPOSITE STRUCTURES

1. Continuum Damage Models - Damage treated implicitly through its influence on material parameters. Properties of critical volume elements are modified to reflect damage growth.

2. Discrete Damage Models - Damage modeled explicitly as to size, shape, orientation, creating new internal boundary conditions.

DELAMINATION SOURCES

Delaminations may arise in composite materials and structures anywhere a local discontinuity creates out-of-plane stresses. This may occur at a straight fee edge, an open hole boundary, at a terminated ply, and anywhere in the structure where a matrix ply crack forms. Furthermore, delaminations may occur due to unique configurations and loadings, such as a curved beam in bending or a flat laminate subjected to low velocity impact. Several unique configurations and loadings have been studied to determine the source of delamination and predict the structural durability of components with these features. Some of these include: (1) tapered symmetric laminates, with internal ply drops, subjected to tension and bending loads to simulate the in-board region of composite rotor hubs, (2) laminates subjected to tension and torsion loads to simulate the out-board region of composite rotor hubs, (3) curved laminates subjected to bending loads to simulate curved frames, stiffener caps, and other generic structural components, and (4) flat laminates subjected to low velocity impact.
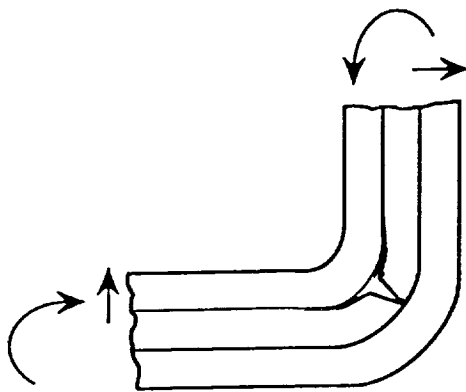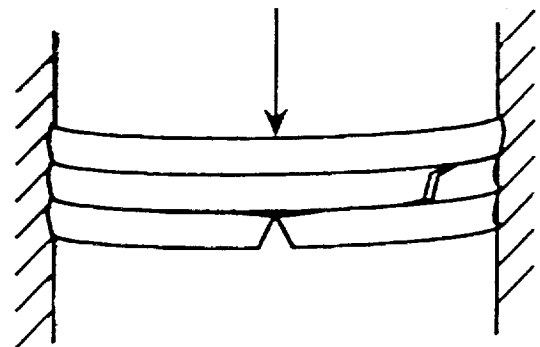
DELAMINATION IN LAMINATES UNDER COMPLEX LOADINGS
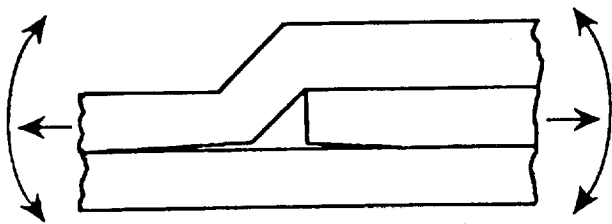
Delamination in tapered laminates
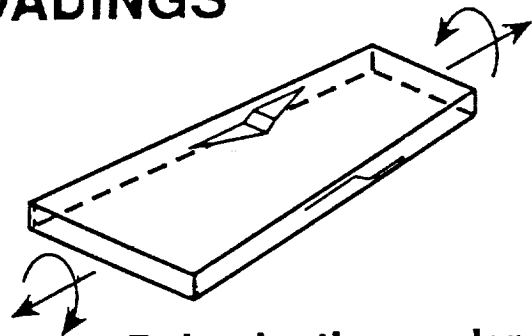
Delamination under tension/torsion loads


Delamination in curved members

Delamination from matrix cracks in bending

TAPERED LAMINATES

Stress analyses of symmetric tapered laminates subjected to tension loads indicated that interlaminar stress singularities were present at points of material and geometric discontinuities such as ply drop locations and the juncture between the flat and tapered region of the laminate. The virtual crack closure technique was used in a finite element analysis to calculate the strain energy release rate, G, for delamination growth from this juncture point. The maximum G values in these distributions were compared to delamination onset fatigue data generated using double cantilever beam specimens, and plotted as G versus the number of cycles to delamination onset, N, to predict the S-N curves for delamination onset in tapered laminates subjected to tension-tension fatigue. This technique worked well for tapered laminates with a variety of layups and materials.

## Delamination Onset Prediction in Tapered Laminates
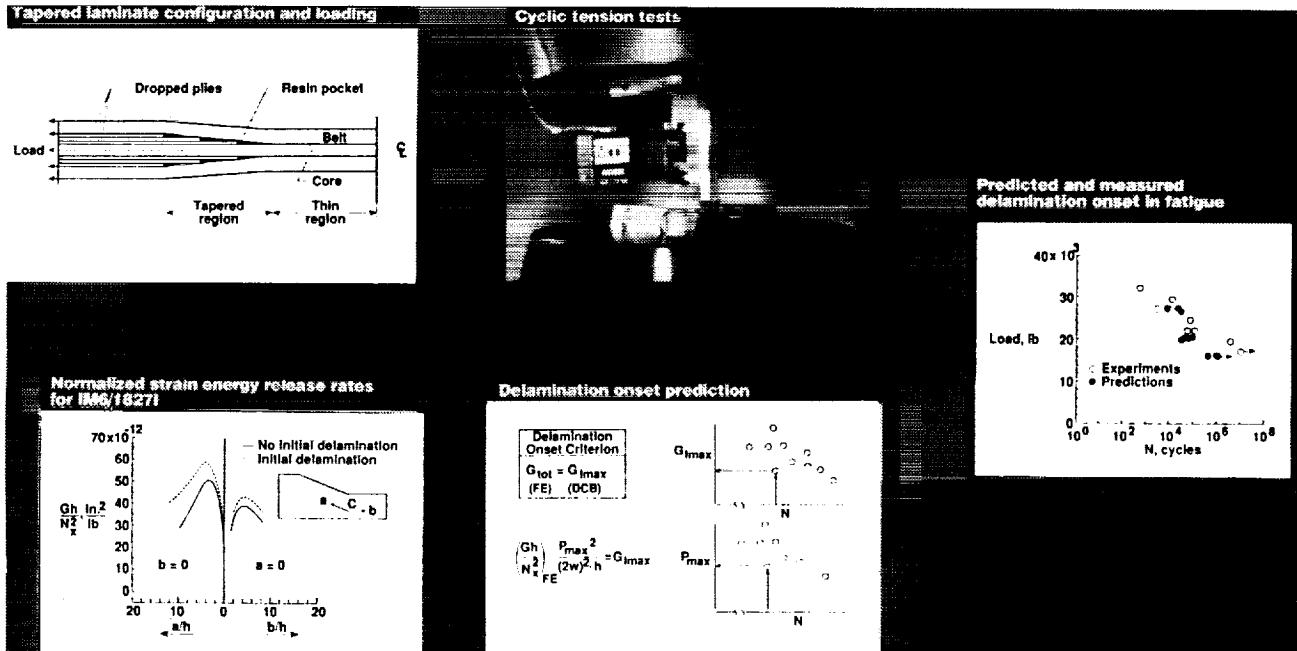
Laminates subjected to low-velocity impacts form a spiral staircase damage pattern consisting of delaminations that form between plies with matrix ply cracks. These matrix ply cracks are created by the high transverse shear stresses generated during the impact. The delaminations, however, may form and grow due to a combination of interlaminar tension and shear stresses. To illustrate this point, a two-dimensional representation of a typical impact damage mechanism was modeled using a finite element analysis. A central line loading was applied to a clamped cross-ply laminate with matrix cracks oriented at 45 degrees through the thickness and located between the central line load and the clamped boundaries. The presence of the internal stress free boundaries due to the matrix cracks yielded tensile interlaminar normal stresses at the matrix crack tips in the 0/90 interfaces in addition to the interlaminar shear stresses that would intuitively be present. The virtual crack closure technique was used in the finite element analysis to calculate the strain energy release rate, G, components for delamination growth from the tip of the matrix cracks. Both an opening mode I and a shear mode II component were always present, with the relative magnitude of the two modes depending on the material modeled (glass or graphite epoxy) and the proximity of the matrix crack tip to the load application point.

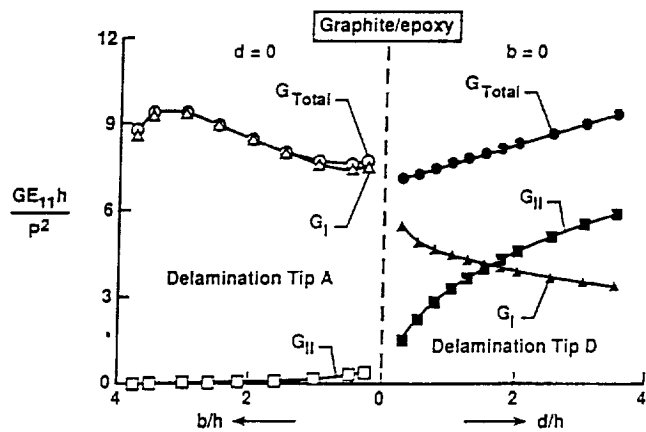# ANALYSIS OF DELAMINATION IN CROSS PLY LAMINATES INITIATING FROM IMPACT INDUCED MATRIX CRACKING
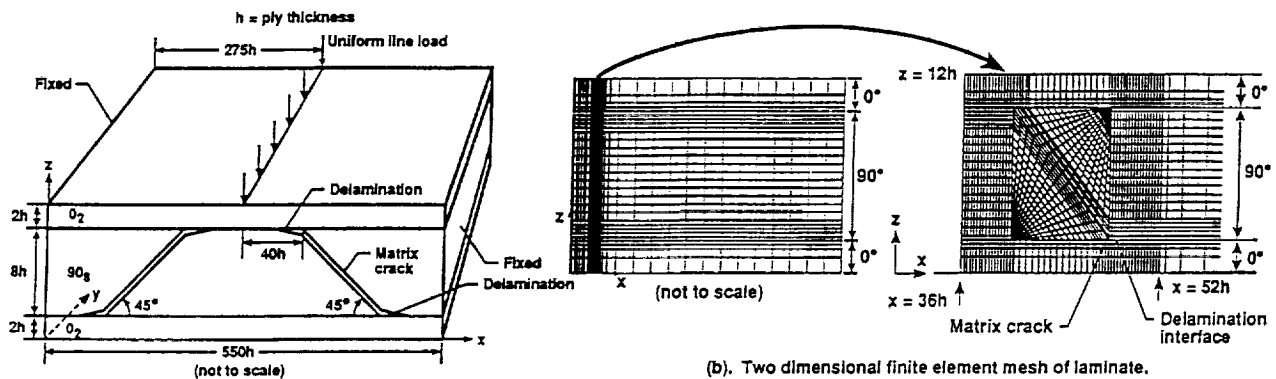
(a). Configuration and loading of a laminate containing impact induced matrix cracks.

(b). Two dimensional finite element mesh of laminate.
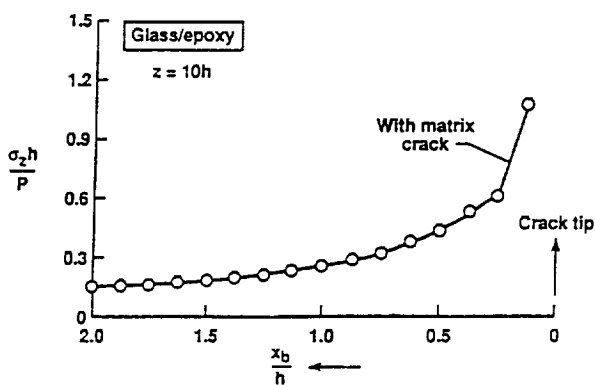
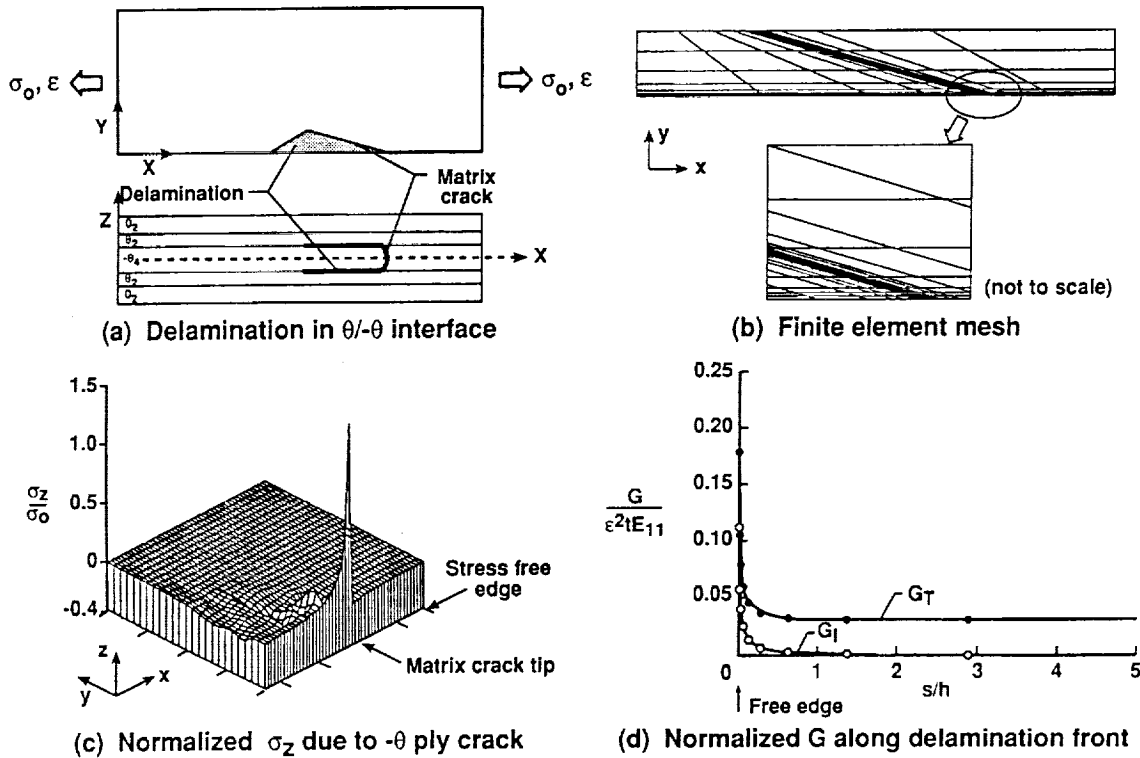(c). Interlaminar normal stress with a 45° matrix crack.

(d). Variation of G due to delamination growth on either side of the matrix crack.

LOCAL DELAMINATION

In laminates with plies oriented at an arbitrary angle to the load axis, the in-plane stresses near free edges may vary in such a way that matrix cracks form due to the tensile stress normal to the fiber direction in addition to the shear stresses along the fiber direction. This situation arises in $(0/\theta/-\theta)_s$ laminates (where θ=15 to 30 degrees) subjected to tension loads. These laminates have often been used to characterize interlaminar shear strength because of the high interlaminar shear stresses in the $\theta/-\theta$ interfaces. However, the presence of matrix cracks is typically ignored in the analyses used to determine the interlaminar shear strength of these laminates. A three-dimensional finite element analysis was performed on a $(0/15/-15)_s$ laminate with a matrix crack simulated along the -15 degree direction in the central -15 degree ply. The presence of the internal stress free boundaries due to the matrix crack yielded interlaminar normal stresses that approached a very high, and apparently singular, value where the matrix crack intersected the free edge. Hence, the local delaminations were mixed-mode delaminations that included a significant opening mode I component.

ANALYSIS OF MATRIX CRACKING AND LOCAL DELAMINATION IN $(0/\theta/-\theta)_s$ GRAPHITE EPOXY LAMINATE

(a) Delamination in $\theta/-\theta$ interface

(b) Finite element mesh

(c) Normalized σ_z due to $-\theta$ ply crack

(d) Normalized G along delamination front

318

CURVED LAMINATES

Curved composite laminates subjected to bending loads often delaminate due to the interlaminar normal stresses created in the curved portion of the beam. If the laminate has off-axis angle plies, however, the membrane stresses may cause matrix cracks to form prior to delamination. In these cases, post-mortem inspection reveals that each delamination is associated with a matrix crack. The onset of the delaminations may be influenced by the presence of these matrix cracks. The virtual crack closure technique was used in the finite element analysis to calculate the strain energy release rate, G, components for delamination growth from the tip of the matrix cracks. A significant mode I component always dominated the response. The strain energy release rate increased monotonically with delamination length, indicating that delamination onset would result in unstable delamination growth. The point of inflection in the G versus a plot was compared to delamination onset fatigue data generated using double cantilever beam specimens, and plotted as G versus the number of cycles to delamination onset, N, to predict the S-N curves for delamination onset in curved laminates subjected to bending fatigue loads. This technique worked well for a variety of layups.

DELAMINATION
IN CURVED COMPOSITE LAMINATES

CURVED LAMINATE CONFIGURATIONS AND FAILURES

LOADING APPARATUS FOR CURVED LAMINATE TESTING

LOCATION OF DELAMINATION ONSET

CHARACTERIZATION OF DELAMINATION GROWTH
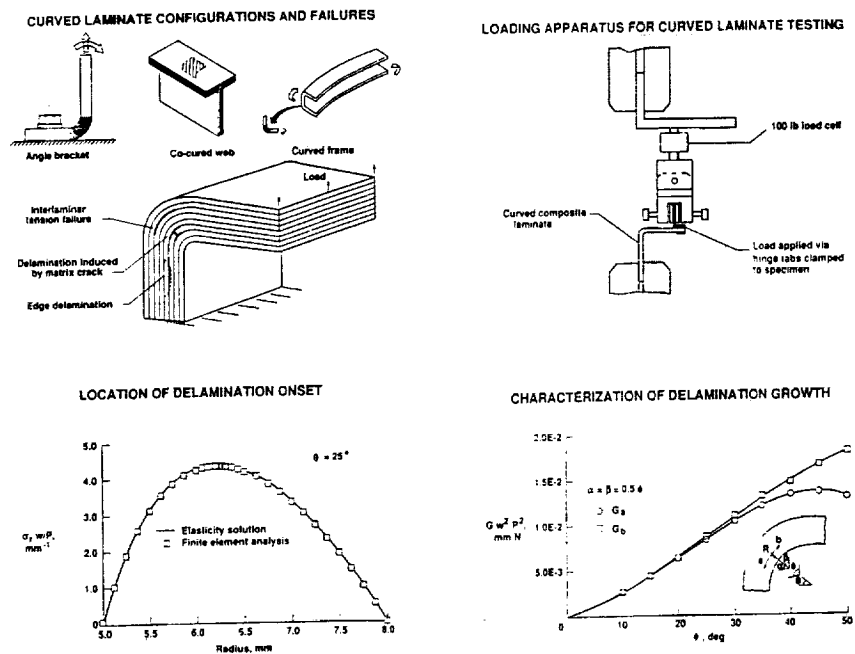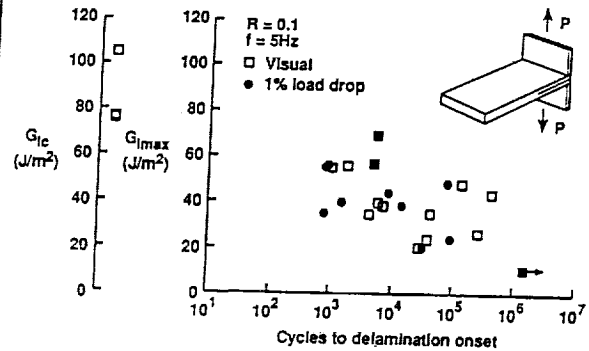
TENSION FATIGUE LIFE PREDICTION

Composite laminates subjected to tension-tension cyclic loading undergo a variety of damage scenarios prior to fatigue failure. Matrix cracks form in the off-axis angle plies and create local delaminations. These local delaminations yield strain concentrations in the primary load bearing zero degree plies. When enough local delaminations have formed through the thickness of the laminate at a particular location, the strain concentrations may be high enough to fail the zero degree plies and cause a fatigue rupture of the laminate. A model was developed to account for this fatigue failure mechanism. The strain energy release rates, G, associated with local delaminations were calculated and used to model a progression of damage starting at the top surface and working toward the laminate center. These G values were compared to delamination onset data generated from free edge delamination tests to predict the accumulation of delamination through the laminated thickness. S-N curves for a variety of layups and material combinations were predicted accurately.
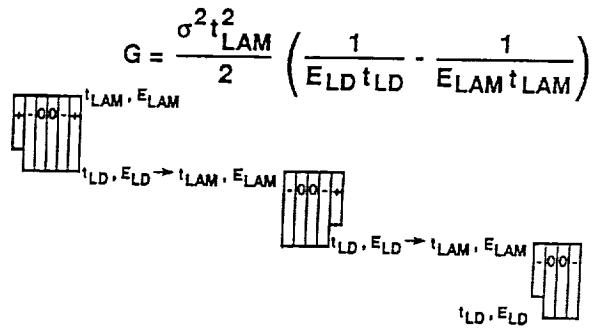
DELAMINATION-BASED LIFE PREDICTION METHODOLOGY

Schematic of Fatigue Damage in Quasi-isotropic Laminate
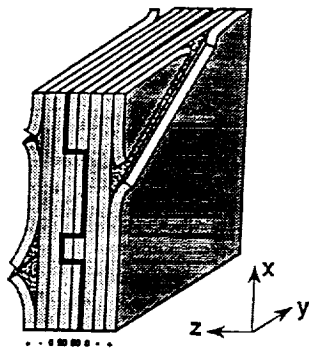
Materials Characterization

Stress Analysis of Unnotched Laminate

$$G = \frac{\sigma^2 t_{LAM}^2}{2}\left(\frac{1}{E_{LD}t_{LD}} - \frac{1}{E_{LAM}t_{LAM}}\right)$$

Typical Fatigue Life Prediction

$[\pm 45/0/90]_s$ X751/50 E-glass epoxy
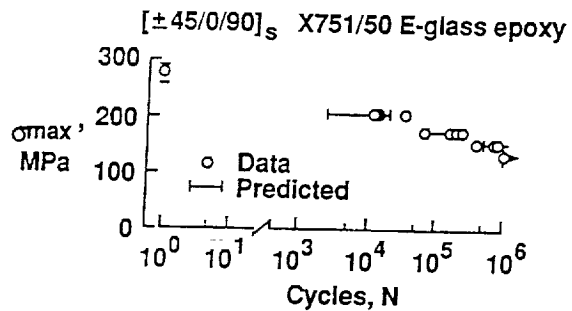
Status: Methodology must be extended to notched laminates and must include loadings typical of a built-up structure

DAMAGE THRESHOLD/FAIL SAFETY METHODOLOGY

A damaged threshold/fail safety methodology was proposed for addressing composite damage tolerance. In this procedure, matrix cracks are assumed to be present in the off-axis angle plies. Delamination onset from these matrix cracks and any other material or geometric discontinuities in the structure are predicted using fracture mechanics. Delamination growth is assessed by using either delamination growth laws along with delamination resistance curves, measuring stiffness loss, or by assuming catastrophic growth at delamination onset. The latter technique is the simplest and most conservative, and may be the only practical technique for structural components. Once a delamination is assumed to be present, however, it may not result in failure of the component even if it has grown catastrophically throughout a particular interface. An assessment of the presence of delamination on the load carrying capability of the laminate must be performed to determine the fail safety of the component. If the component is demonstrated to retain load carrying capability, the procedure must be repeated for the next source of delamination through the laminate thickness until the composite can no longer sustain the applied load.

APPROACH FOR COMPOSITES

1. Assume matrix cracks exist in off-axis plies

2. Predict delamination onset using strain energy release rate

3. Account for delamination growth

   a. Predict using growth laws and resistance curves
   b. Measure stiffness loss
   c. Assume onset corresponds to catastrophic growth

4. Assess fail safety of damaged composite

5. Repeat steps to account for accumulation of delaminations through the thickness

CONCLUSIONS

I. STRAIN ENERGY RELEASE RATE IS A USEFUL GENERIC
    PARAMETER FOR CHARACTERIZING, ANALYZING, AND
    PREDICTING DELAMINATION

II. DAMAGE THRESHOLD / FAIL SAFETY METHODOLOGY
    PROVIDES A GENERIC FRAMEWORK FOR ASSESSING THE
    DURABILITY AND DAMAGE TOLERANCE OF LAMINATED
    COMPOSITES

Needs
Abstract

Demonstrating Damage Tolerance of Composite Airframes

C. C. Poe, Jr.
NASA Langley Research Center
Hampton, VA

PAGE _____ INTENTIONALLY BLANK

INTRODUCTION

Commercial transport aircraft operating in the United States are certified by the Federal Aviation Authority to be damage tolerant. On April 28, 1988, Aloha Airlines Flight 243, a Boeing 727-200 airplane, suffered an explosive decompression of the fuselage but landed safely. A photograph of the airplane is shown in Fig. 1. This event provides very strong justification for the damage tolerant design criteria. The likely cause of the explosive decompression was the linkup of numerous small fatigue cracks that initiated at adjacent fastener holes in the lap splice joint at the side of the body. Actually, the design should have limited the damage size to less than two frame spacings (about 40 inches), but this type of "multi-site damage" was not originally taken into account. This cracking pattern developed only in the high-time airplanes (many flights). After discovery in the fleet, a stringent inspection program using eddy current techniques was inaugurated to discover these cracks before they linked up. Because of concerns about safety and the maintenance burden, the lap-splice joints of these high-time airplanes are being modified to remove cracks and prevent new cracking; newer designs account for "multi-site damage".

ALOHA AIRLINES BOEING 737-200

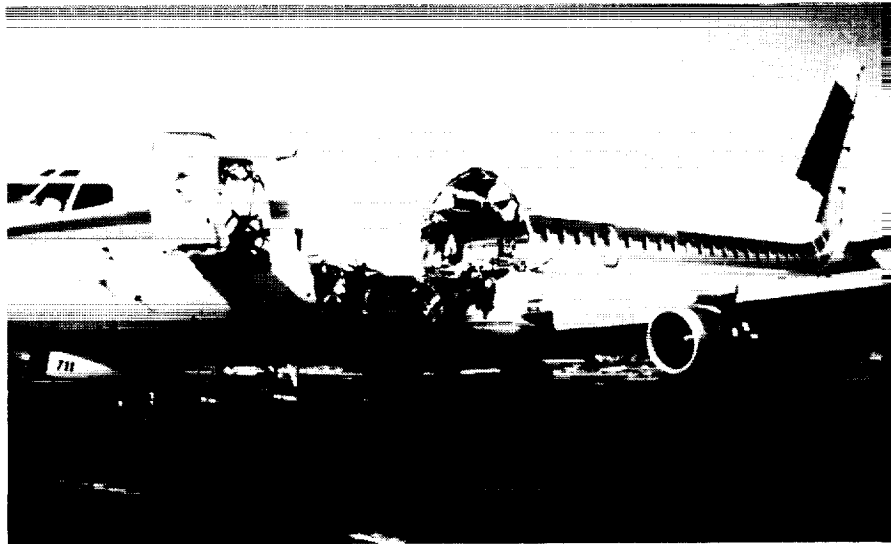Flight 243, April 28, 1988

Figure 1

APPLICATION OF REGULATIONS TO COMPOSITE AIRCRAFT

Both civil and military regulations are being adapted to composite structures. The source of damage in composite structures is more from accidental impact and lack of adhesion between plies (delamination) than from fatigue. The FAR PART 25 and MIL-STD-1530A implement the guidelines shown in Fig. 2. Both require:

1) ultimate strength and no impairment of function with undetectable impact damage and defects

2) adequate strength to return to base with discrete damage

The military requirement defines detectable impact damage as 0.10-in. or deeper dent; this or a similar requirement will likely be used for civilian airplanes. In the civilian fleet, discrete damage is usually caused by collisions with ground equipment or other airplanes at gates and failure of rotating machinery; in the military fleet, the most critical discrete damage is that caused by weapons.

Computational methodologies or strategies will be illustrated first for discrete damage and then for undetectable impact damage.

FAR PART 25
Withstand ultimate loads with following types of damage: impacts (dropped tools and runway debris), delaminations, surface damage (withstand fatigue loads without growth)
Withstand flight loads with following discrete damage: penetrations over two bays of skin, including one stringer or frame

MIL-STD-1530A
No impairment (repair or water intrusion) after 2 lifetimes with following damage:
tool drop - 0.5" dia. and 6 ft-lbf or visible damage (0.10" dent)
hail - 0.8" dia., SG = 0.9, and 90 ft/s
runway debris - 0.5" dia., SG = 3.0, and appropriate velocity
Adequate strength (consistent with inspectibility) after 2 lifetimes with following damage:
scratch - 0.02" deep and 4.0" long
delamination - equiv. to 2.0" dia. circle with critical shape and location
impact - 1.0" dia. hemispherical tup with 100 ft-lbf or 0.10" dent
Contain battle damage

Figure 2

TENSION DAMAGE TOLERANCE FOR AS4/3501-6

Failing strain is plotted against cut length in Fig. 3 for three structural configurations:

1) a plain composite skin

2) a skin with stiffeners

3) a skin with integral S-glass buffer strips

For the stiffener and buffer strip configurations, respectively, the cut length is equal to two bays of skin and one cut element. The cut length associated with two bays of skin is two times the centerline spacing of stiffeners or two times the centerline spacing of buffer strips less the width of one buffer strip (distance between inside edges rather than between the centerlines). A cut element is a cut stiffener or buffer strip. Cuts can generally be used to conservatively represent discrete damage for uniaxial tension loading. The curves were calculated using linear elastic fracture mechanics and a generalized fracture parameter based on a point strain failure criterion (Refs. 1-7). These predictions are accurate as long as the size of matrix cracks and delaminations at the ends of the cut are small compared to the cut length, much as plastic zone size in homogeneous metals. For long cuts, the curves are linear in the log-log plot with a negative slope of one half. With decreasing cut length, the curves approach the failing strain of the fibers ε_{tuf}, which was calculated as the ratio of unnotched tension strength of the laminate F_{tu} to the Young's modulus in the loading direction E_x. A maximum strain failing criterion is usually quite accurate for laminates with fibers in the loading direction that do not delaminate significantly at the free edges. The two curves, which were calculated for each configuration, represent the range of results for all laminates in the family $0°/\pm45°/90°$ where half of the plies are $\pm45°$. Although the range of failing strains is small, the range of strengths are much larger.

The curves for buffer strips are the highest and those for a plain skin are the lowest; the curves for stiffeners are about midway between. The buffer strips and stiffeners are quite beneficial. The buffer strips are unidirectional strips of S-glass that replace the AS4 fibers in the $0°$ plies. They can be manufactured economically by weaving a largely unidirectional fabric with alternating strips of S-glass and carbon (Ref. 6). The calculations in Fig. 3 were made assuming that the S-glass material has the same thickness as the $0°$ AS4 ply and that the spacing of the buffer strips was five times the width. The failing strain can be increased even more by increasing the thickness and width of the buffer strips. The most effective buffer strip material has the largest product of strength and failing strain. The effectiveness of the stiffeners will be discussed more subsequently.

(See next page for Figure 3)

Design points that represent the regulations in Fig. 2 are also plotted in Fig. 3 for undetectable impact damage and for discrete damage. A design ultimate strain of 0.004 is assumed. The design point for undetectable impact damage is arbitrarily plotted at a cut length of 1 in., which should conservatively represent a 0.10-in. dent caused by an impact; even then, a plain skin is nearly acceptable. Two design points are shown for discrete damage, one for a wing skin and one for a fuselage skin. For a wing, two bays of skin would be about 12 inches (2 × stringer spacing) and, for a fuselage about 40 inches (2 × frame spacing). Following a discrete damage event, FAA Advisory Circular No. 25.571-1A defines ultimate load as "70% of limit maneuver loads and, separately, 40% of limit gust velocity ..., each combined with maximum appropriate cabin differential pressure". Therefore, the strain corresponding to ultimate load for discrete damage would be 70% of 0.004 for the wing and 75% (100/1.33) of 0.004 for the fuselage with cabin pressure alone. For a combination of maneuver loads, gust loads, and cabin pressure, the strain would be between 70 and 75% of 0.004. Skins with buffer strips satisfy the discrete damage criteria for the wing and nearly for the fuselage. Skins with stiffeners alone will nearly satisfy the discrete damage criteria for the wing but not for the fuselage. For buffer strips and stiffeners together, the failing strains may exceed those for buffer strips alone, but that has not been demonstrated. Of course, failing strains can also be elevated by reducing stiffener and buffer strip spacing. Also, matrix cracking at the notch ends may also elevate the failing strains significantly above those plotted in Fig. 3.
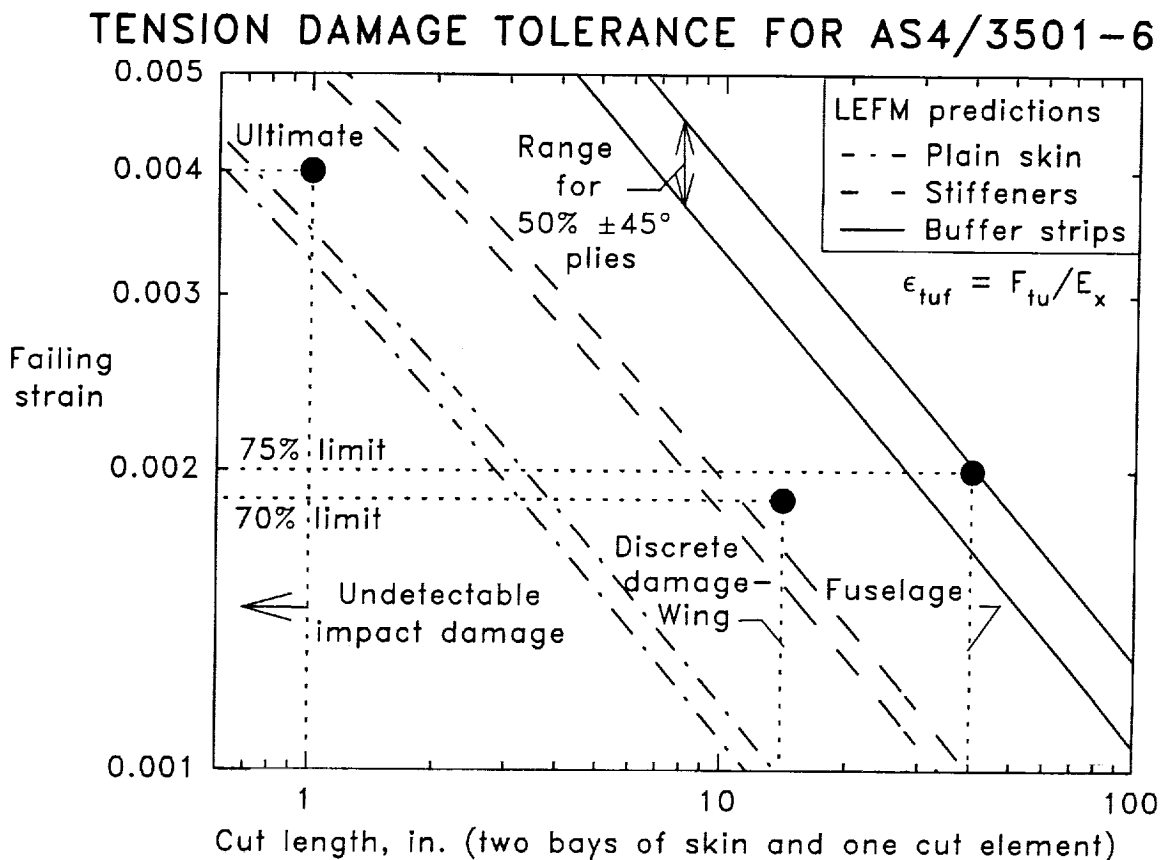
TENSION DAMAGE TOLERANCE FOR AS4/3501-6

Figure 3

DISCRETE DAMAGE - TOUGH AND BRITTLE RESINS

Strengths normalized by unnotched strengths are plotted against cut length in Fig. 4 for quasi-isotropic laminates made of T300/BP-907 and T300/5208 prepreg tape. The tension strength and failing strain of BP-907 epoxy is more than twice that of 5208, and the matrix damage at the notch tip is accordingly much less. The strengths of the T300/5208 laminates are elevated somewhat relative to those of the T300/BP-907 laminates by the greater matrix damage. The curves are predicted using the same method used in Fig. 3 except that for the T300/5208 laminates, the distance d_0 in the point strain criterion is assumed to increase with increasing cut length to account for matrix damage at the notch tip, which also increases with increasing cut length.

The T300/5208 laminate in Fig. 4 was thin, only 8 plies. Thick (45/0/-45/90) T300/5208 laminates with cuts were shown in Ref. 8 to fail at lower stresses than thin laminates because the notch-tip damage only occurred in the outermost plies. Thus, the damage had negligible effect in thick laminates, and the strengths followed the lower curve in Fig. 4, much like the laminate with BP-907 resin. Also, in Ref. 8, strengths of (0/90) laminates with cuts decreased with increasing thickness, much like the (45/0/-45/90) laminates. On the other hand, the strengths of (0/±45) laminates with cuts increased with increasing thickness. Thus, the predicted strengths in Fig. 3 could be conservative or unconservative due to notch tip matrix damage, depending on layup and thickness. More sophisticated analyses are required to account for notch tip matrix damage.
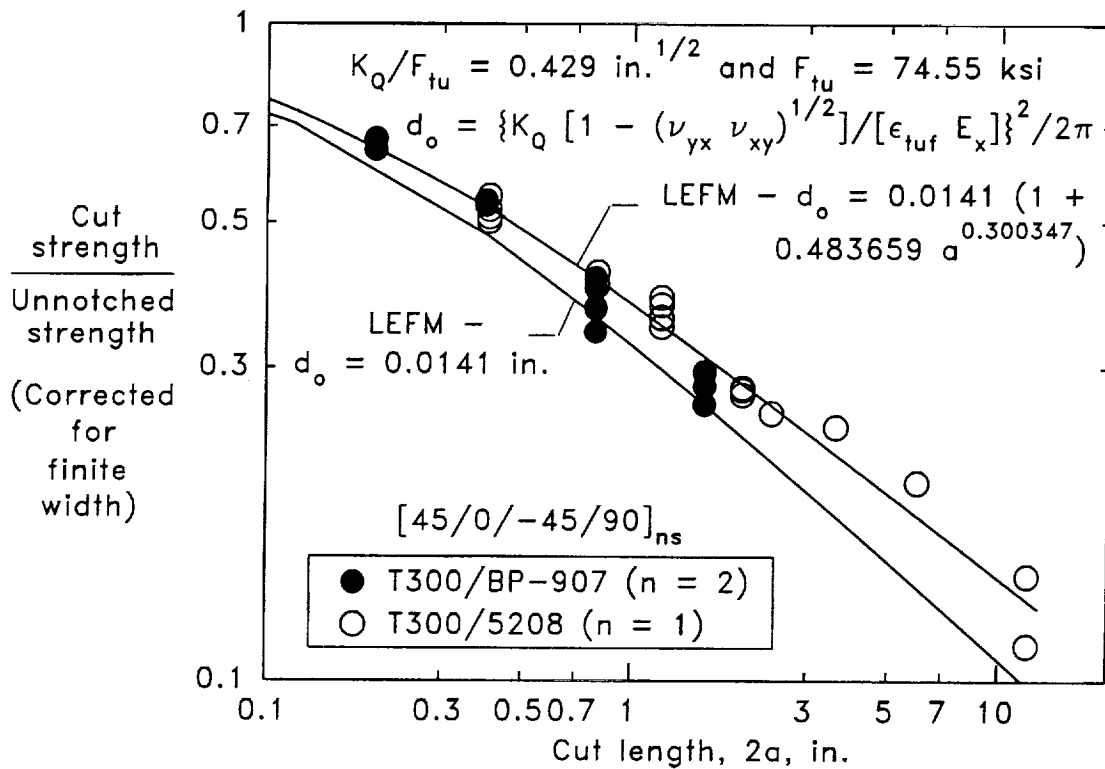

Figure 4

329

COMPRESSION DAMAGE TOLERANCE FOR HOLES

Little research has been conducted for large discrete damage and compression loading. Nevertheless, some insight can be gained by considering the compression strength of open-hole specimens. Failing strains are plotted against hole diameter in Fig. 5 for 48-ply-thick quasi-isotropic laminates made of T300/5208 prepreg tape (Ref. 9). The test specimens were 5-in. wide. The failing strains were predicted using:

$$\epsilon_c = \epsilon_{cu} (1 - 2R/W) K_t^{-1} \tag{1}$$

where ϵ_{cu} is the unnotched compression failing strain, which was assumed to be 0.014; R is the hole radius; W is the specimen width; and K_t is the stress concentration factor for an isotropic sheet of finite width. For very wide specimens, $K_t = 3$ and the predicting failing strain in Fig. 5 is a horizontal line (0.014/3). For hole diameters greater than 10% of the specimen width, the local stress is elevated by the free edge (finite width effect). The predictions agree with the test data for large holes, but for small holes the test values exceed the predictions because K_t is reduced by matrix cracking at the edge of the hole, which is large compared to hole diameter. If large holes in very wide sheets follow the horizontal line in Fig. 5, failing strains would exceed 0.004. Thus, if discrete damage acts as a large open hole in a very wide sheet, the discrete damage tolerant criterion for the wing should be no more difficult to satisfy for compression loading than for tension loading where strength varies inversely with the square root of damage size. Moreover, stiffeners will have a beneficial effect in compression loading as they did in Fig. 3 for tension loading. On the other hand, buckling could be critical, but no more critical than for metal wings. In the keel area of the fuselage, the compression loads may be significant, and the discrete damage tolerant criterion may be as difficult to satisfy as in the tension case. Complex studies are currently being done in the Advance Composites Technology Program of NASA to develop fuselage and wing structure designs for commercial transport airplanes that satisfy a discrete damage tolerant criterion.
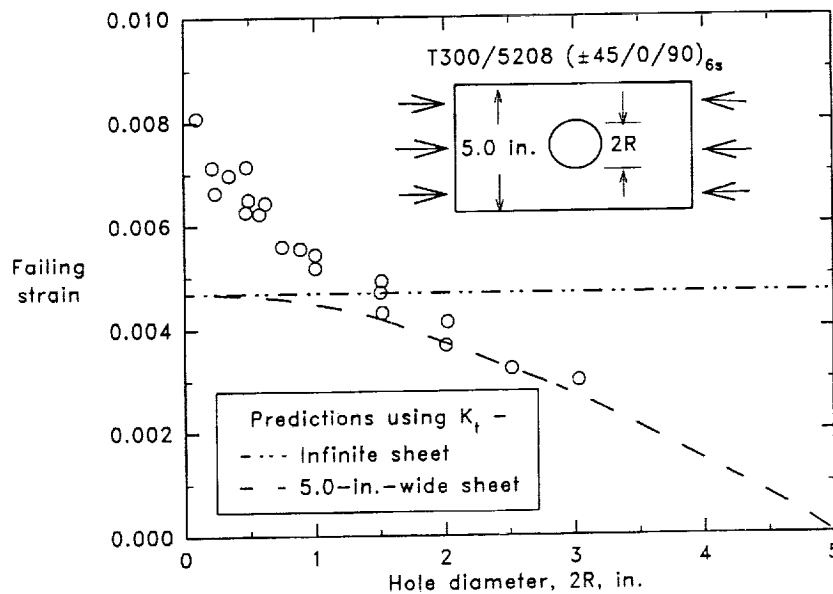

Figure 5

CONFIGURATION OF STIFFENED PANELS

Mechanically attached stiffeners are essential in metal airframe structures to provide damage tolerance with discrete damage. Stringers "pinch" skin cracks when the cracks grow past the stiffeners, reducing the crack tip stresses and elevating the strength (Refs. 10-12). The effectiveness of the stiffeners increases with increasing stiffener stiffness and with decreasing rivet spacing. Integral stiffeners are largely ineffective because the skin crack grows through the stiffener as well as across the skin (Ref. 11).

Stiffened composite panels were fabricated and tested to determine the effectiveness of cocured stiffeners in increasing the residual tension strength of laminates containing a cut (Ref. 7). In contrast to integrally stiffened metal panels, the adhesive bond between the stiffeners and skin is too weak to allow a crack to pass from the skin to the stiffener. The configuration of the panels is shown in Fig. 6. The skin or sheet was made with $(45/0/-45/90)_{2s}$ and $(45/0/-45/0)_{2s}$ layups; the stiffeners, which were unidirectional for simplicity, were made with several widths and thicknesses to give three values of μ, the ratio of stiffener stiffness to panel (total) stiffness. The panels were gripped at the ends to give uniform strain.

Material: T300/5208

Sheet layups: $(45/0/-45/90)_{2S}$

and

$(45/0/-45/0)_{2S}$

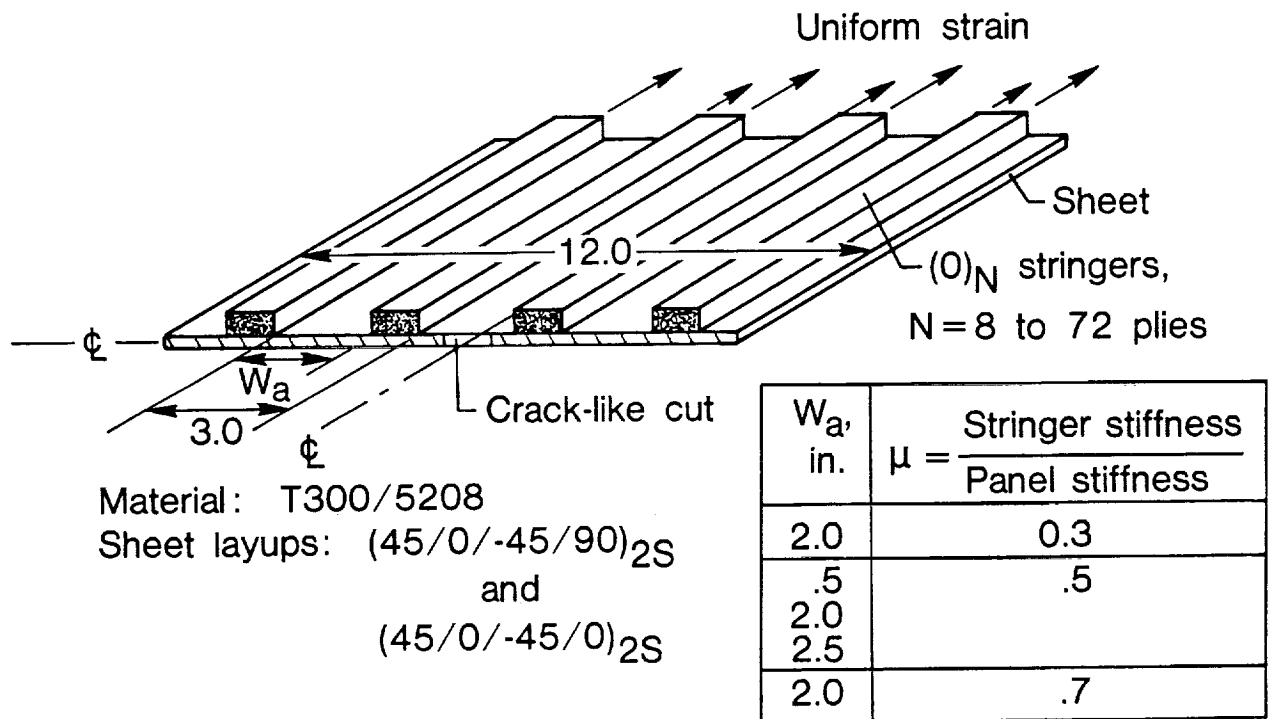| W_a, in.	$\mu = \dfrac{\text{Stringer stiffness}}{\text{Panel stiffness}}$
2.0	0.3
.5 2.0 2.5	.5
2.0	.7

Figure 6

TEST RESULTS FOR (45/0-45/90)2S PANELS WITH μ=0.5

Failing strain is plotted against half-length of crack in Fig. 7 for three of the panels in Fig. 6 with μ=0.5 and quasi-isotropic skins; the panels are labeled A, B and C. The ratio of stringer stiffness to panel stiffness μ was 0.5 for each panel. The width and thickness of the stringers were different for each panel, and the cut lengths increased with decreasing stringer width. A predicted curve is shown for the failing strain of a plain skin. Failure is represented by the small circles labeled A, B and C. Failing strains for the panels with stringers were considerably greater than those predicted for a plain skin. When the applied strains are in the neighborhood of the curve for a plain skin, the cut extends catastrophically but is arrested as the crack grows beneath the stringer. The half-length of the initial cut plus extension is plotted from the abscissa to failure. The extensions were calculated using measurements of crack opening displacement (COD) and assuming that crack length is proportional to COD. The small jumps in crack extension are probably due to damage that develops at the ends of the cuts prior to failure. One radiograph of a crack tip is shown for each panel near failure. Notice that the crack arrests at the near edge of the thinnest stringer but arrests at the far edge of the thickest stringer and arrests between the edges of the stringer with the median thickness. The growth of the cracks beneath the stringers was accompanied by a delamination of the stringers. The delamination reduces the "pinching" effect of the stringers, causing the crack to advance further beneath the stringer. The interlaminar stresses and hence the size of the delaminations increase with increasing crack length and stringer thickness.
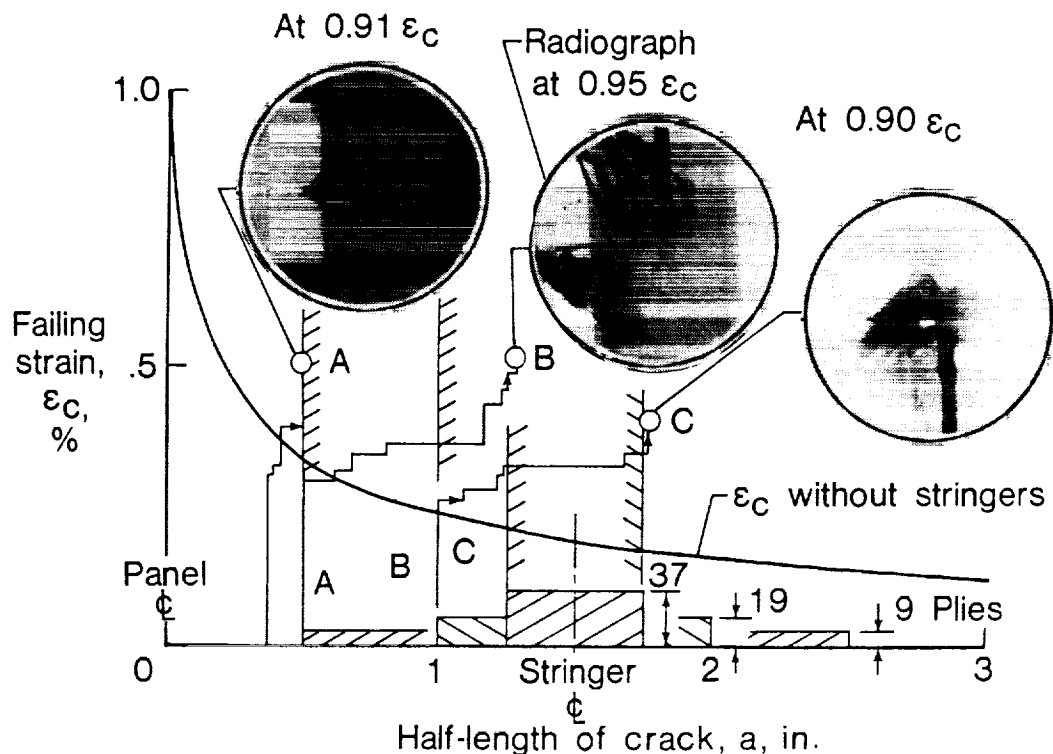

Figure 7

FAILING STRAIN VERSUS STRINGER THICKNESS

Failing strain is plotted against stringer thickness in Fig. 8 for panels in Fig. 6 with $(45/0/-45/90)_{2s}$ and $(45/0/-45/0)_{2s}$ skins. The circular symbols are test results; the solid curves were predicted for the stiffened panels; and the horizontal lines were predicted for plain skins. The predictions for the stiffened panels were made using calculations of stress intensity factors for riveted stringers where rivet spacing was equal to delamination length (Ref. 7). The tests and predictions agree for thin stringers, but the predicted strains are much too large for thick stringers. There was no benefit to increasing stringer thickness much beyond that of skin thickness. The discrepancy between test results and predictions is believed to be due to bending caused by load transferring from the skin to the stringers in the neighborhood of the crack tips. Based on the test results, an appropriate design equation was developed in Ref. 7 that limits the effectiveness of stringers due to bending; this equation was used to make the predictions in Fig. 3. More sophisticated nonlinear analyses are needed to account for bending effects.
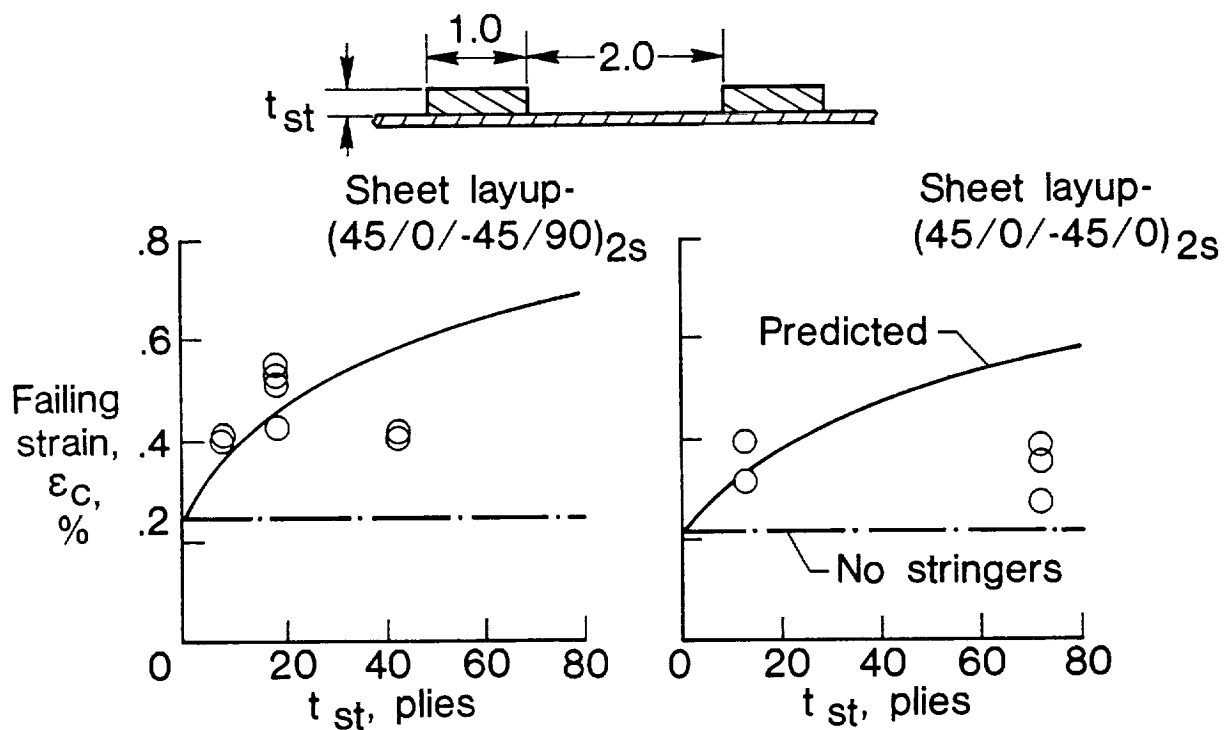

Figure 8

CROSS-SECTION OF COMPOSITE AFTER IMPACT
$(45/0/-45/90)_{6s}$ AS4/3501-6

An edge replica of a $(45/0/-45/90)_{6s}$ AS4/3501-6 laminate with impact damage from Ref. 13 is shown in Fig. 9; the cross-section of the 48-ply quasi-isotropic laminate passes through the contact site. The 10.2-lbm impacter had a 0.5-in.-diameter-hemispherical tup attached to the end; the kinetic energy was 20 ft-lbf. The visible damage consists primarily of delaminations and matrix cracks that connect the delaminations in adjacent plies.
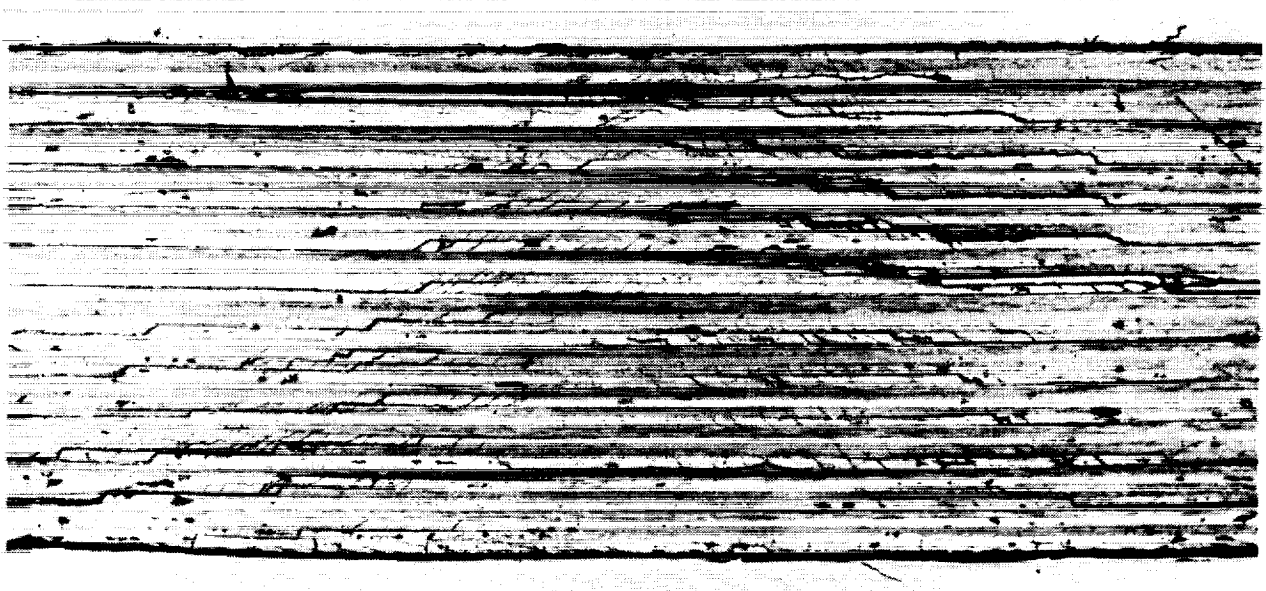

Figure 9

TYPICAL C-SCAN AFTER AN IMPACT

A C-scan of a 48-ply quasi-isotropic laminate with impact damage is shown in Fig. 10. The dark disc in the center of the image indicates delamination damage like that shown in Fig. 9. The delamination between individual interfaces is not a stack of circular discs as suggested by Figs. 9 and 10 but can be represented by spiraling flights of stairs where the stair treads represent delamination (Ref. 14). Two delaminations exist on a given interface; they resemble signal flags on opposite sides of the contact site, initiating at matrix cracks and growing only on one side of the crack (Ref. 15). The C-scan image is circular because it is an average through the thickness.

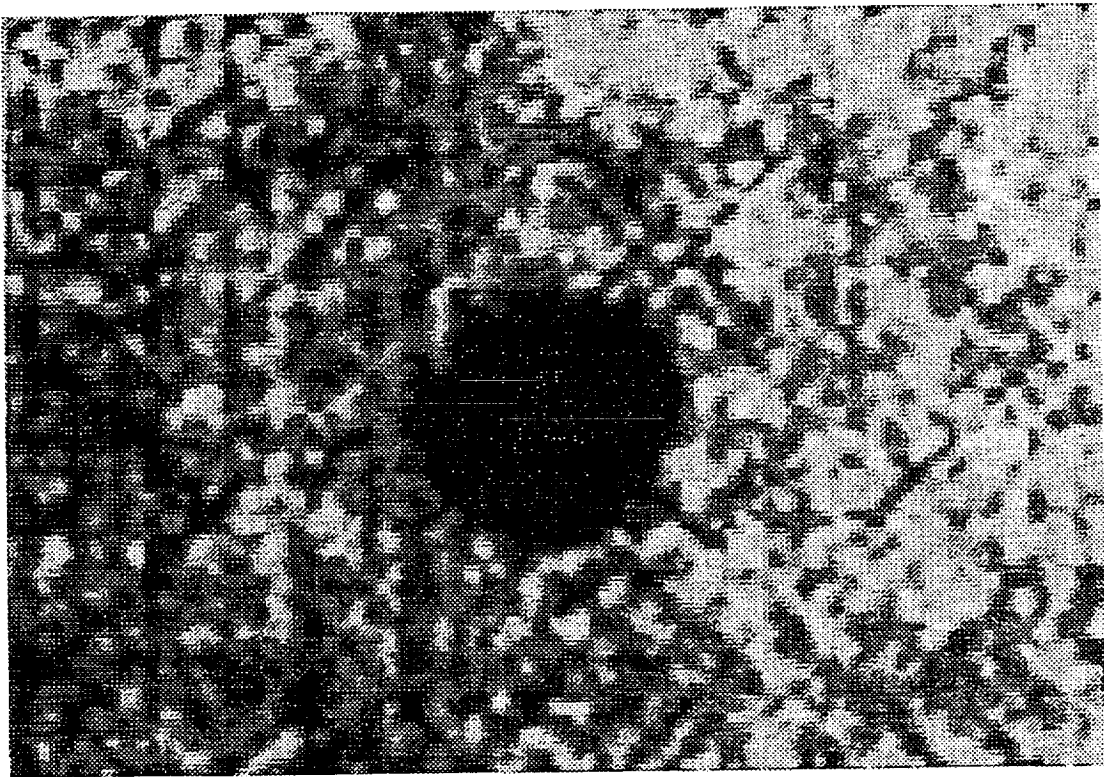## AS4/3501-6 Quasi-Isotropic Laminate

Figure 10

COMPRESSION STRENGTH VERSUS KINETIC ENERGY

Compression strengths with impact damage were measured for quasi-isotropic laminates made with AS4/3501-6 and IM7/8551-7 (Ref. 13); the 3501-6 and 8551-7 resins are brittle and toughened resins, respectively. The compression strengths are plotted against kinetic energy in Fig. 11. The strengths are divided by Young's modulus to give a far-field or remote strain. A Young's modulus of 8 Msi was used for both materials. The impacter had a mass of 10.2-lbm and a 0.5-in.-diameter hemispherical tup. The strengths are reduced dramatically by the impacts; the reduction is significantly more for the brittle resin than for the toughened resin.
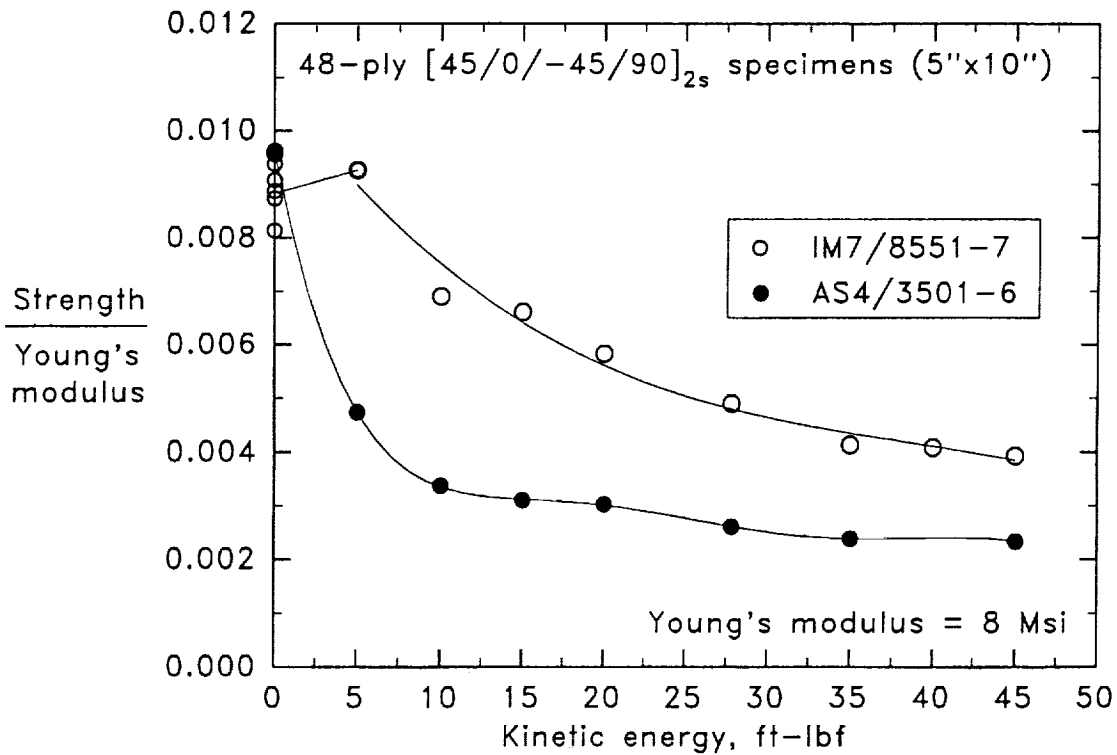

Figure 11

COMPRESSION STRENGTH VERSUS DAMAGE SIZE

The compression strengths divided by Young's modulus in Fig. 11 are replotted against damage diameter in Fig. 12. The damage diameter was calculated from areas of damage in C-scans like that in Fig. 10. For a given kinetic energy, the size of damage for the brittle resin was about two times that for the toughened resin. In terms of damage size, the strengths are nearly equal for the brittle and toughened resins. Thus, the primary difference between the compression strengths of the laminates made with brittle and toughened resins in Fig. 11 is associated with the differences between damage sizes. If damage size and strength are uniquely related, damage size would be a good metric for damage tolerance as well as damage resistance.

The damage diameter associated with the threshold for visible damage is indicated for each material. The failing strain associated with the threshold for visible damage for the toughened 8551-7 resin was significantly greater than 0.004, but that for the brittle 3501-6 resin was slightly below 0.004. The definition of visible damage was subjective and probably represents a dent significantly less deep than 0.1 inches. Thus, both materials may fail to satisfy the undetectable damage criterion for a 0.1-inch deep dent and a design ultimate strain of 0.004.
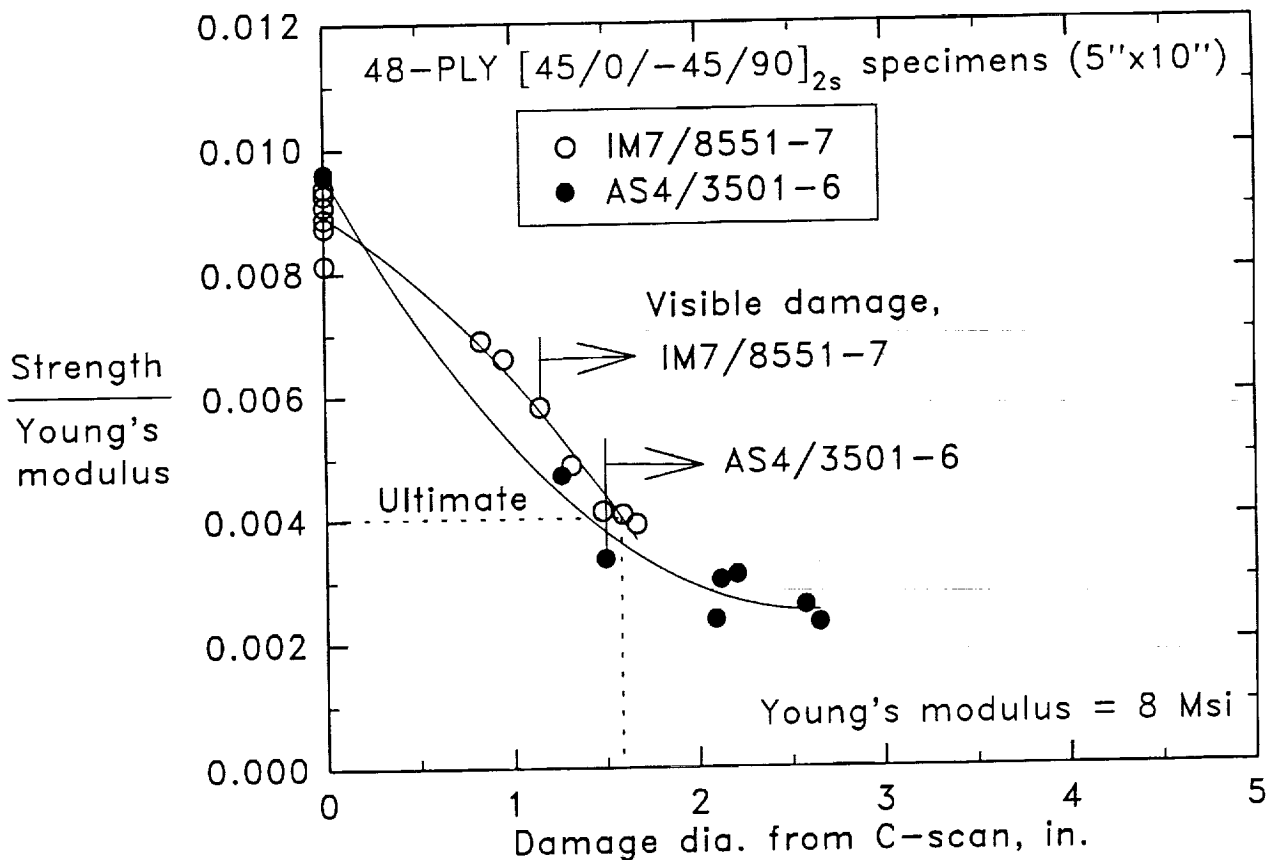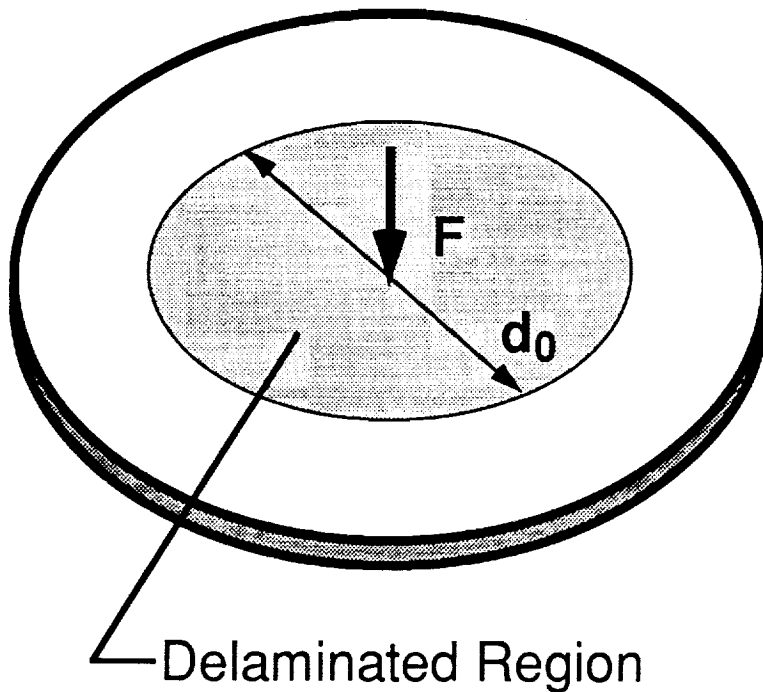

Figure 12

TRANSVERSE SHEAR FORCE

Impact force has been used by numerous investigators (Refs. 13, 15-21) to analyze impact damage like that shown in Figs. 9 and 10. A circular plate impacted at the center with a circular delamination of diameter d_0 is shown in Fig. 13. The force F is the resultant of the contact pressure, which is distributed over the contact diameter. The diameter d_0 is assumed to be large compared to the contact diameter. For an isotropic plate, the problem is symmetric in the polar sense. Neglecting inertial stresses, the transverse shear force per unit width V at the delamination front, which can be obtained solely by equilibrium, is

$$V = F/(\pi d_0)$$

(2)

Equation (2) should also be valid for a rectangular plate that is large compared to d_0.

From equilibrium:

$$V = \frac{F}{\pi d_0}$$

Figure 13

CALCULATIONS OF TRANSVERSE SHEAR FORCE

Values of transverse shear force per unit width were calculated for undamaged elastic plates using a dynamic finite element code (Ref. 20). Plate type elements were used to account for flexure of the plate, and a Hertzian spring was used to account for the indentation. The impacter was modeled as a rigid, point mass. The 48-ply-thick, quasi-isotropic square plate was assumed to be made of AS4/3501-6; impacter mass, plate size, and boundary conditions were varied. The kinetic energy and diameter of the impacter was assumed to be 13.6 J and 12.7 mm, respectively. In Fig. 14, peak values of shear force at a distance of 3.18 cm from the center of the plate are plotted against the square root of the frequency ratio $(k/m)^{1/2}/\omega$, where k is the flexural stiffness of the plate; m is the impacter mass; and ω is the first natural frequency of the plate. For a uniformly thick plate, this frequency ratio reduces to the square root of a mass ratio $\alpha(m_p/m)^{1/2}$, where m_p is the mass of the plate and α depends on the boundary conditions. The ordinate is normalized by Eq. (2), where F is the peak force calculated by the finite element code. As the mass of the plate decreases relative to that of the impacter, shear force in Fig. 14 approaches the quasi-static value from Eq. (2). Results for the large plate converge more slowly than those for the small plates and were extrapolated to the static value. These results indicate that the impact can be analyzed quasi-statically if the mass of the impacter is 150 times that of a clamped square plate or 250 times that of a simply supported square plate.
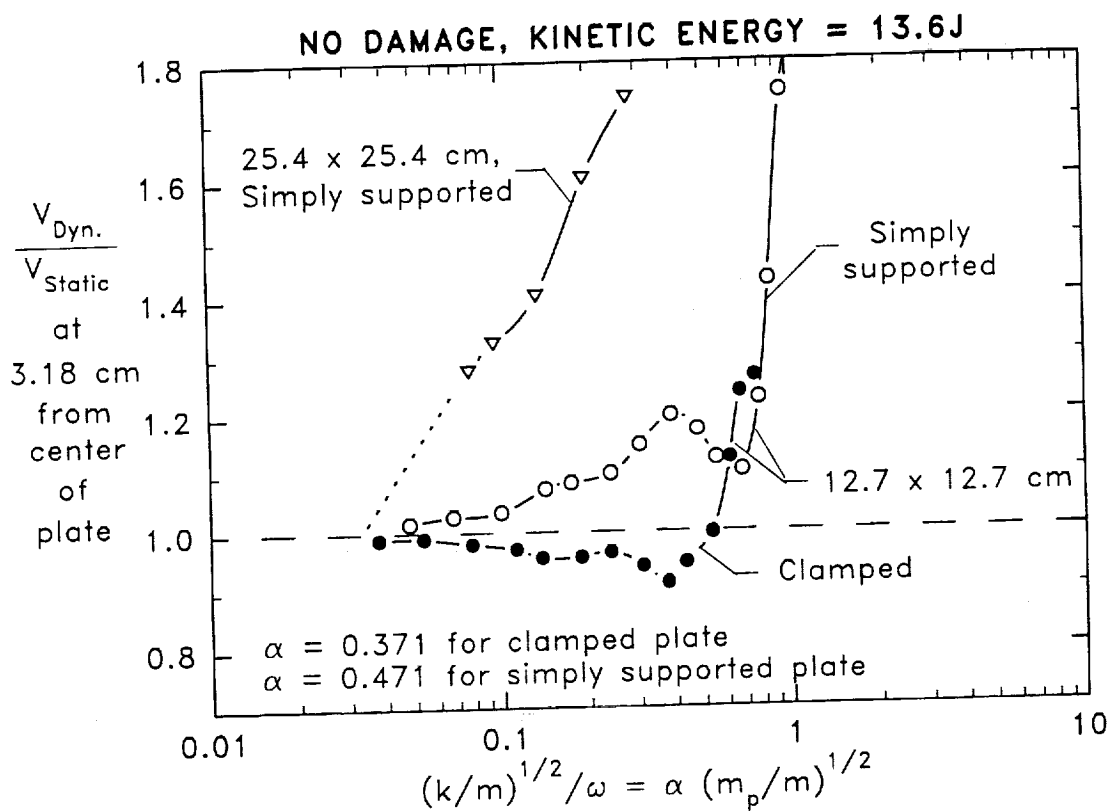

Figure 14

DELAMINATION DIAMETER VERSUS IMPACT FORCE

   Values of damage diameter from C-scans are plotted against impact force for static inde: tation tests and for dynamic impact tests (pendulum) in Fig. 15 (Ref. 21). For the static indentation tests, several plate diameters and two indenter or tup diameters were used. In all cases, the diameters increased in proportion to impact force according to Eq. (2) with V*=41.5 kN/m where the superscript * indicates a critical value of V associated with delamination growth. Thus, V* would make a good metric of damage resistance. Because the size of damage was equal for static indentation and dynamic impact tests, quasi-static behavior is indicated. The value of $\alpha(m_p/m)^{1/2}$ for a 32-ply, 5.08-cm-diameter plate is less than 0.02. Thus, the finite element results in Fig. 14 also predict quasi-static behavior.
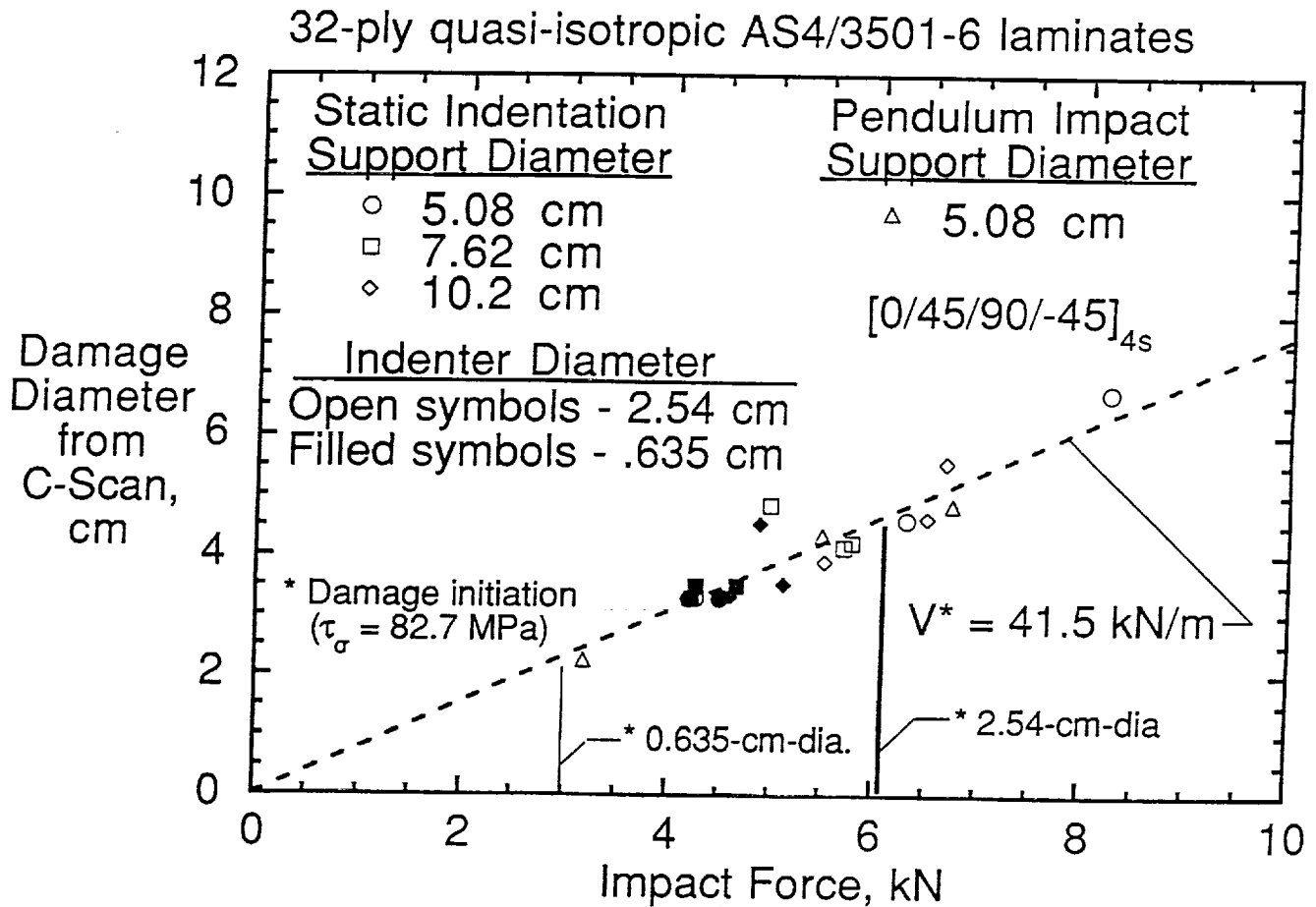
Figure 15

DAMAGE RESISTANCE FOR VARIOUS COMPOSITES

Critical values of transverse shear force are plotted in Fig. 16 for composites with various thicknesses, layups, and resins (Refs. 20 and 21). The 3501-6 epoxy is relatively brittle compared to the 8551-7 which is toughened with an elastomer. For the π/4 quasi-isotropic (QI) AS4/3501-6 laminates, the resistances for the 6.8- and 7.0-mm-thick laminates are about 85% greater than those for the 3.4- and 4.5-mm-thick laminates. For the 4.5-mm-thick AS4/3501-6 laminates, the resistance for the π/8-QI laminate is 9% less than that for the π/4-QI laminate. The resistance for the 7.0-mm-thick π/4-QI laminate made with 8551-7 is 119% greater than that of the same laminate made with 3501-6. Therefore, thickness and resin toughness had a greater effect on damage resistance than layup.
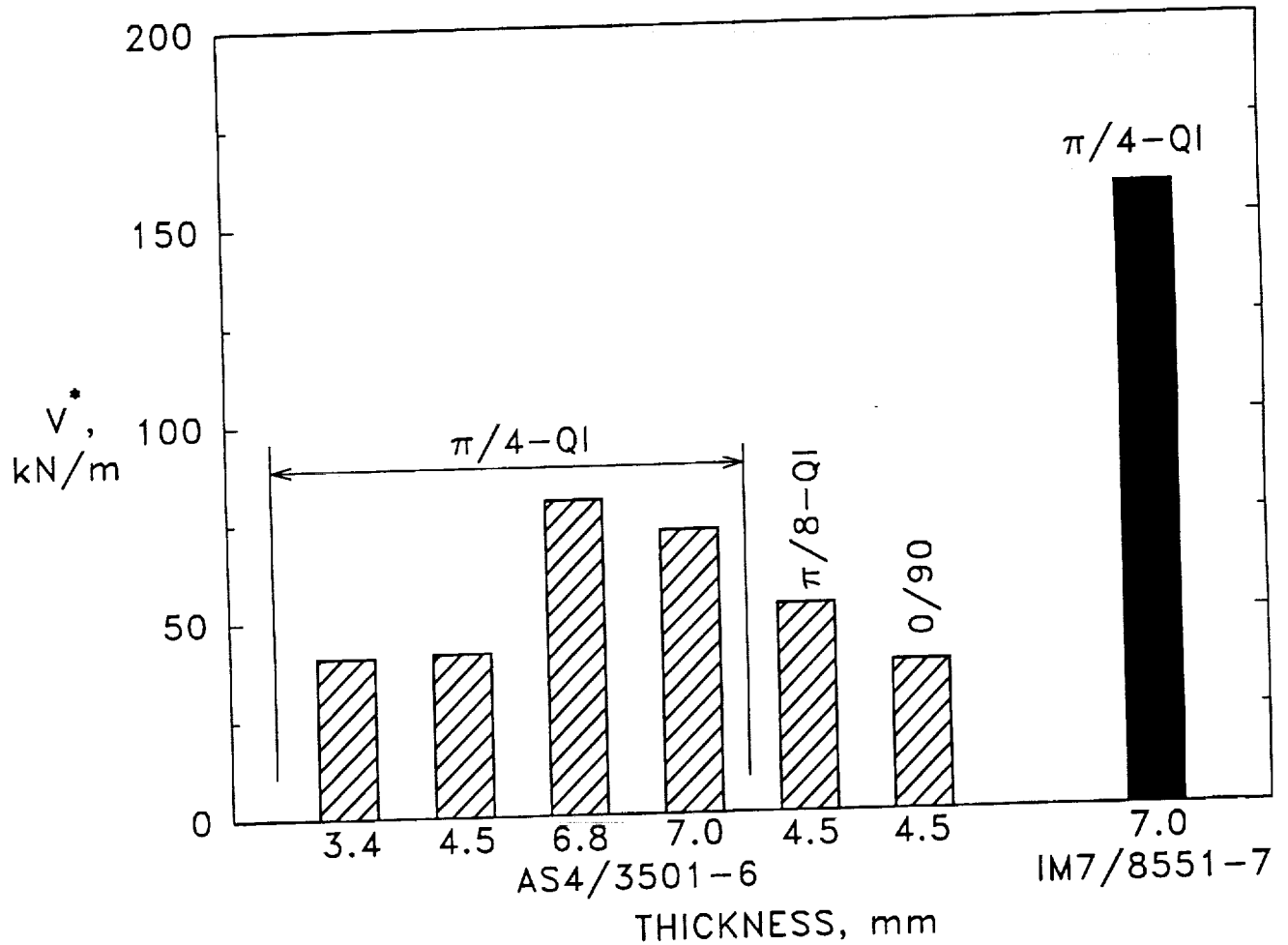

Figure 16

DAMAGE RESISTANCE PREDICTED USING MODE II
STRAIN ENERGY RELEASE RATE

Shivakumar and Elber (Ref. 18) calculated mode I and mode II strain energy release rates for a circular delamination in circular isotropic plates with impact type static loading. The contact pressure was distributed over a constant diameter, and large transverse displacements were taken into account. Mode I values were generally negligible relative to mode II values, which are associated primarily with transverse shear. Values of delamination diameter are plotted against impact force in Fig. 17 for G_{IIc} = 1.5 kJ/m2. The plate thickness was 0.1 cm, the plate radius was 1.27 cm, and the contact radius was 0.05 cm. By using the results for very small impact forces, values of G_{II} were estimated for small displacement theory; then values of delamination diameter were calculated for G_{IIc}=1.5 kJ/m2 and plotted in Fig. 17. A line for V*=53 kN/m was plotted for comparison. For both small and large displacements, the results from Ref. 18 indicate that delamination growth takes place after a critical value of impact force is exceeded. For small displacement theory, the growth is essentially unstable; but, for large displacement theory, the growth is stable as reflected in the test data in Fig. 15. Thus, the large displacement theory is essential to predict damage resistance. Accurate impact damage sizes probably cannot be predicted by modeling the impact damage as a single delamination. Thus, additional analyses are needed for multiple delaminations in anisotropic laminates with noncircular shapes.
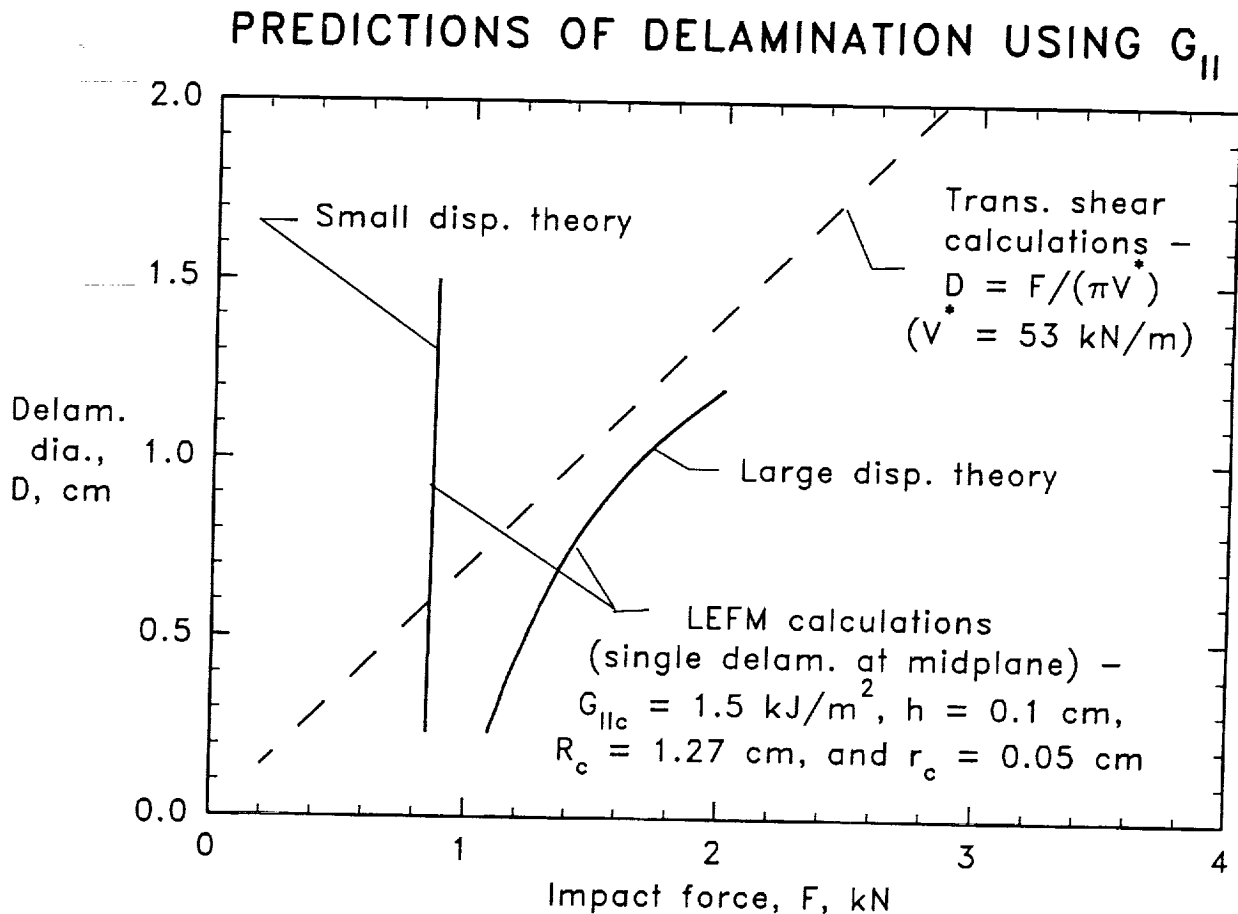

Figure 17

CONCLUSIONS

1. Damage tolerant criteria for civilian airplanes in the United States require ultimate strength with undetectable impact damage and 47 to 50% of ultimate strength (70 to 75% of limit) for discrete damage. Air Force criteria are similar.

DISCRETE DAMAGE

2. For transport airplanes, fuselage is more critical than wing because of larger stiffener spacing.

3. Buffer strips or stiffeners are required.

4. Analyses must account for bending near stiffeners and progressive damage in the skin to make accurate predictions.

5. Methodologies must be developed for compression loads.

UNDETECTABLE IMPACT DAMAGE

6. In plates of 48 plies or less, impact damage consists mostly of ply cracks and delaminations.

7. For a given damage size, compression strengths for toughened and brittle resins are nearly equal.

8. When impacter mass is 150 to 250 times that of the plate, the plate response is quasi-static.

9. Transverse shear force is a metric of damage resistance.

10. Damage resistance increases with increasing resin toughness and plate thickness.

11. Resistance to damage growth may be mostly due to large transverse displacements.

12. A 0.004 ultimate compression strain may not be attainable with a 0.10-in. dent, even for a toughened resin.

REFERENCES

1. Poe, Jr., C. C., "Fracture Toughness of Boron/Aluminum Laminates with Various Proportions of 0° and ±45° Plies," NASA TP-1707, 1980.

2. Poe, Jr., C. C., "A Single Fracture Toughness Parameters for Fibrous Composite Laminates," NASA TM-81911, March 1981.

3. Poe, Jr., C. C., "Fracture Toughness of Fibrous Composite Materials," NASA TP-2370, Nov. 1984.

4. Poe, Jr., C. C., "A Parametric Study of Fracture Toughness of Fibrous Composite Materials," *Journal of Offshore Mechanics and Arctic Engineering*, Vol. 111, No. 3, 1989, pp. 161-169.

5. Poe, Jr., C. C. and Kennedy, John M., "An Assessment of Buffer Strips for Improving Damage Tolerance of Composite Laminates," *Journal of Composite Materials Supplement*, Vol. 14, 1980, pp. 57-70.

6. Kennedy, John M., "Damage Tolerance of Woven Graphite/Epoxy Buffer Strip Panels," NASA TM-102702, Aug. 1990.

7. Poe, Jr., C. C., "Tensile Strength of Composite Sheets with Unidirectional Stringers and Crack-Like Damage - A Brief Report," NASA TM-86310, Sept. 1984.

8. Harris, C. E. and Morris, D. H., "Fracture Behavior of Thick Laminated Graphite/Epoxy Composites," NASA CR-3784, 1984.

9. Rhodes, Marvin D., Mikulas, Jr., Martin M., and McGowan, Paul E., "Effect of Orthotropy and Width on the Compression Strength of Graphite-Epoxy Panels with Holes," AIAA Journal, Vol. 22, No. 9, Sept. 1984, pp. 1283-1292.

10. Poe, Jr., C. C., "Stress Intensity Factor for a Cracked Sheet with Riveted and Uniformly Spaced Stringers," NASA TR-R-358, 1971.

11. Poe, Jr., C. C., "Fatigue Crack Propagation in Stiffened Panels," Damage Tolerance in Aircraft Structures, ASTM STP-486, 1971, pp. 79-97.

12. Poe, Jr., C. C., "The Effect of Broken Stringers on the Stress Intensity Factor for a Uniformly Stiffened Sheet Containing a Crack," NASA TM-X-71947, 1974.

13. Poe, Jr., C. C., Portanova, M. A., Jackson, W. C., Masters, J. E., and Sankar, B. V., "Comparison of Impact Results for Several Polymeric Composites Over a Wide Range of Low Impact Velocities," presented at the First NASA Advanced Composites Technology (ACT) Conference, Seattle, WA, Oct. 30-Nov. 1, 1990; NASA CP-3104, Part 2.

14. Gosse, J. H. and Mori, P. B. Y., "Impact Damage Characterization of Graphite/Epoxy Laminates," in Proceedings of the American Society for Composites, Third Annual Technical Conference, Sept. 25-29, 1988, pp. 344-353.

15. Salpekar, S. A. and O'Brien, T. K., "Analysis of Delamination in Cross Ply Laminates Initiating From Impact Induced Matrix Cracking," NASA CR-187594, Nov. 1991.

16. Greszczuk, L. B., "Damage in Composite Materials Due to Low Velocity Impact," in Impact Dynamics, L. A. Zukas, et al (eds.), John Wiley, New York, 1982, p. 55.

17. Elber, W., "Deformation and Failure Mechanics in Low Velocity Impacts on Thin Composite Laminates," NASA TP-2152, May 1983.

18. Shivakumar, K. N. and Elber, W., "Delamination Growth Analysis in Quasi-Isotropic Laminates Under Loads Simulating Low-Velocity Impact," NASA TM-85819, June 1984.

19. Sjoblom, P. O., Hartness, J. T. and Cordell, T. M., "On Low-Velocity Impact Testing of Composite Materials," Journal of Composite Materials, Vol. 22, Jan. 1988, pp. 30-52.

20. Jackson, W. C. and Poe, Jr., C. C., "The Use of Impact Force as a Scale Parameter for the Impact Response of Composite Laminates," NASA TM-104189, Jan. 1992.

21. Kwon, Y. S. and Sankar, B. V., "Indentation-Flexure Damage in Graphite/Epoxy Laminates," NASA CR-187624, March 1992.

REPORT DOCUMENTATION PAGE

Public reporting burden for this collection of information is estimated to average 1 hour per response, including the time for reviewing instructions, searching existing data sources, gathering and maintaining the data needed, and completing and reviewing the collection of information. Send comments regarding this burden estimate or any other aspect of this collection of information, including suggestions for reducing this burden, to Washington Headquarters Services, Directorate for Information Operations and Reports, 1215 Jefferson Davis Highway, Suite 1204, Arlington, VA 22202-4302, and to the Office of Management and Budget, Paperwork Reduction Project (0704-0188), Washington, DC 20503.

1. AGENCY USE ONLY (Leave blank)	2. REPORT DATE	3. REPORT TYPE AND DATES COVERED
	October 1993	Conference Publication

4. TITLE AND SUBTITLE
Computational Methods for Failure Analysis and Life Prediction

5. FUNDING NUMBERS
WU 505-63-50-17

6. AUTHOR(S)
Ahmed K. Noor, Charles E. Harris, Jerrold M. Housner, and
Dale A. Hopkins, Compilers

7. PERFORMING ORGANIZATION NAME(S) AND ADDRESS(ES)
NASA Langley Research Center
Hampton, VA 23681-0001

8. PERFORMING ORGANIZATION REPORT NUMBER
L-17321

9. SPONSORING/MONITORING AGENCY NAME(S) AND ADDRESS(ES)
National Aeronautics and Space Administration
Washington, DC 20546-0001
and
University of Virginia
Charlottesville, VA 22903-2442

10. SPONSORING/MONITORING AGENCY REPORT NUMBER
NASA CP-3230

11. SUPPLEMENTARY NOTES

12a. DISTRIBUTION/AVAILABILITY STATEMENT

Unclassified–Unlimited

Subject Category 39 and 24

12b. DISTRIBUTION CODE

13. ABSTRACT (Maximum 200 words)
This conference publication contains the presentations and discussions from the joint UVA/NASA Workshop on Computational Methods for Failure Analysis and Life Prediction held at NASA Langley Research Center, October 14–15, 1992. The presentations focused on damage, failure and life predictions of polymer-matrix composite structures. They covered some of the research activities at NASA Langley, NASA Lewis, Southwest Research Institute, industry and universities. Both airframes and propulsion systems were considered.

14. SUBJECT TERMS
Failure analysis; Life prediction; Polymer matrix composites; Computational methods; Airframes; Propulsion systems

15. NUMBER OF PAGES
362

16. PRICE CODE
A16

17. SECURITY CLASSIFICATION OF REPORT	18. SECURITY CLASSIFICATION OF THIS PAGE	19. SECURITY CLASSIFICATION OF ABSTRACT	20. LIMITATION OF ABSTRACT
Unclassified	Unclassified		

NSN 7540-01-280-5500